1949

Integrated Assessment of the Groundwater Resources of the Northwest Sahara Aquifer System: Case of the Oued Souf Valley

Thesis for the Degree of Doctor of Philosophy (PhD)

by name:

Barkat Ayoub

Supervisor:

Prof. Dr. Szabó György

Co-supervisor:

Dr. Habil. Bouaicha Foued

UNIVERSITY OF DEBRECEN
DOCTORAL COUNCIL OF NATURAL SCIENCES AND INFORMATION TECHNOLOGY
DOCTORAL SCHOOL OF EARTH SCIENCES
DEBRECEN, 2024

Hereby I declare that I prepared this thesis within the Doctoral Council of Natural Sciences and Information Technology, Doctoral School of Earth Sciences , University of Debrecen in order to obtain a PhD Degree in Natural Sciences at Debrecen University.
The results published in the thesis are not reported in any other PhD theses.

Debrecen, 4 June 2024 *Barkat Ayoub*
signature of the candidate

Hereby I confirm that Barkat Ayoub candidate conducted his/her studies with my supervision within the Landscape Protection and Climate Doctoral Program of the Doctoral School of Earth Sciences between 2019 and 2024
The independent studies and research work of the candidate significantly contributed to the results published in the thesis.
I also declare that the results published in the thesis are not reported in any other theses.
I support the acceptance of the thesis.

Debrecen, 4 June 2024 *Prof. Dr. Szabó György*
signature of the supervisor

Hereby I confirm that Barkat Ayoub candidate conducted his/her studies with my supervision within the Landscape Protection and Climate Doctoral Program of the Doctoral School of Earth Sciences between 2019 and 2024
The independent studies and research work of the candidate significantly contributed to the results published in the thesis.
I also declare that the results published in the thesis are not reported in any other theses.
I support the acceptance of the thesis.

Debrecen, 4 June 2024 *Dr.Habil. Bouaicha Foued*
signature of the supervisor

Integrated Assessment of the Groundwater Resources of the Northwest Sahara Aquifer System: Case of the Oued Souf Valley

Dissertation for obtaining a doctorate (Ph.D.) degree in the discipline of Geography

Written by Barkat Ayoub certified Hydraulic Engineer (MSc)

Prepared in the framework of the Earth Sciences doctoral school of the University of Debrecen

Landscape Protection and Climate programme

Dissertation advisor:	Prof. Dr. Szabó György
Dissertation co-advisor:	Dr. Habil. Foued Bouaicha

The official opponents of the dissertation:

Dr. Safwan Mohammed	.....
Dr. Gábor Sándor	.....

The evaluation committee:

chairperson:	Dr.	.....
members:	Dr.	.....
	Dr.	.....
	Dr.	.....
	Dr.	.....

The date of the dissertation defence: …… 20…

“The more you know, the more you know you don't know.”

Aristotle

Table of content

1. Introduction

Worldwide, water supplies are under growing pressure due to a surge in demand fueled by population increase, the necessity for more agricultural output, industrial expansion from higher standards of living, pollution from human activities, and the effects of climate change [1–3]. It is forecasted that by 2050, at least a quarter of the global population will reside in nations facing freshwater shortages, owing to water scarcity and deteriorating water quality. As a response, the United Nations has included the goal of securing available and sustainable water management within its Sustainable Development Goals, as outlined in the 2030 Agenda for Sustainable Development, titled "Transforming Our World" [4].

Climate change acts as a factor that adds further stress to the hydrological cycle by altering precipitation patterns and exacerbating extreme weather events. This, in turn, worsens water scarcity and affects both the distribution and quality of water resources, as outlined in the IPCC's report of Climate Change in 2021: "The Physical Science Basis. Contribution of Working Group I to the Sixth Assessment Report of the Intergovernmental Panel on Climate Change"[5]. These challenges underscore the urgent need for innovative and sustainable water management strategies to ensure the equitable distribution and efficient use of this precious resource. The World Resources Institute advocates for the integration of climate resilience into water resource planning to address these issues [6].

Water scarcity, particularly in arid regions, poses significant challenges to achieving the Sustainable Development Goals (SDGs), given the crucial role of groundwater. Groundwater is a key element of the hydrological cycle, found beneath the Earth's surface in a variety of landscapes, including hills, mountains, plains, deserts, and coastal areas, and even under seas and oceans. It accounts for 98% of the Earth's liquid freshwater, playing a vital role in meeting domestic and agricultural needs, especially in arid and semi-arid climates. Notably, it is the primary source of daily water for about 2.5 billion people worldwide [7–9]. As surface water supplies become increasingly strained, the importance of groundwater in meeting water demands is ever more highlighted [10]. Thus, effective groundwater management is essential for addressing both quality and quantity issues, as well as understanding its dynamics across different locations and over time [11]. However, the sustainable management of groundwater is complicated by factors such as climate change, population growth, inadequate management practices, and a lack of comprehensive understanding and coordination, leading to its gradual degradation [12].

This situation leads to numerous problems, including aquifer depletion, declining groundwater levels due to climate change-driven variations in rainfall patterns and increased evapotranspiration [13], over-extraction for agricultural, industrial, and domestic purposes [14], and increased vulnerability to contamination and pollution from various uses of groundwater [15]. These issues directly affect several sustainable development goals, such as Clean Water and Sanitation, Zero Hunger, Good Health and Well-being, and Climate Action [16]. Achieving these goals requires collaborative efforts from governments, communities, and international organizations to implement policies and practices

that ensure the sustainable use and conservation of groundwater resources in arid regions [17,18].

Groundwater serves as the primary source of drinking and agricultural water for the Saharan communities in Southern Algeria, specifically within the Oued Souf Valley, which is part of the vast Algerian Sahara. Extensive groundwater reservoirs are found as aquifers within geological layers of varying depths and thickness beneath the Oued Souf valley. The groundwater system of the Oued Souf Valley is a component of the Northern Sahara aquifer system, which comprises three groundwater aquifers, layered from top to bottom. These are the phreatic aquifer (the superficial one), the complex terminal groundwater aquifer, and the continental intercalary groundwater aquifer, with the latter two consisting of multiple water layers stacked upon each other. Notably, they collectively represent one of the world's largest hydraulic reservoirs, with mobilizable potential estimated at 5 billion cubic meters of water [19,20].

Despite the abundance of groundwater in the Oued Souf region, this has led to several issues concerning public and environmental health. Whereas, since the 1980s, driven by population growth, urbanization, and the need for economic development, local authorities have chosen to extract deep groundwater from the complex terminal and continental intercalary aquifers, in addition to the phreatic aquifer, which was the primary source for drinking and irrigation. The intensive pumping from deep aquifers and the direct discharge of this water into the environment without adequate treatment, along with the lack of a sewage network and natural outlet, have resulted in polluted groundwater near the surface. This situation jeopardizes the equilibrium and viability of the production system in the El Oued Souf region [21].

Moreover, this phenomenon has instigated rapid and disruptive changes, profoundly altering the environment and living conditions, imperiling the delicate equilibrium of the northern Saharan region, and threatening various structures, as well as harming local agriculture and eroding the traditional urban character of the city, including the Ghout system, a traditional agricultural practice. Simultaneously, serious health problems related to the emergence of polluted phreatic groundwater, including the filling of septic tanks with black, foul-smelling water mixed with waste of all kinds, have facilitated the spread of bacteriological pollution in the superficial aquifer. Additionally, water quality has degraded due to nitrates from domestic and agricultural sources. High mineralization of water has been induced, in part, by evaporation from open water bodies and salt dissolution, with Ghouts being used as impromptu landfills contributing to this issue. Stagnant water has become a breeding ground for mosquitoes, leading to an increased prevalence of waterborne and parasitic diseases such as skin disorders, leishmaniasis, malaria, and typhoid [22].

To combat this pollution and the rising phreatic groundwater, local authorities initiated a mega-project in 2005. The project was structured around four main components: a sewerage plan, a purification plan, an evacuation plan, and a drainage plan. However, due to various challenges, the project did not fully achieve its primary objective [23,24]. The failure of the vertical drainage system underscores the impact of anthropogenic activities on natural factors, which in turn

affect the spatial and temporal fluctuations of the phreatic groundwater table in the Oued Souf region. This failure continues to jeopardize the north-western Sahara aquifer system, passing through the Oued Souf Valley, in terms of water quality and suitability for drinking and irrigation, despite the natural separation of these systems. The contamination of the shallow aquifer, along with its unauthorized use for irrigation and industrial purposes, and its connection to the deep aquifer (complex terminal and continental intercalary), poses significant threats to public and environmental health in the region, necessitating an in-depth investigation into the hydrochemical and bacteriological quality of all the aquifer systems in the Oued Souf Valley to prevent adverse consequences that could impede socioeconomic activities in the region.

For these reasons, this dissertation aims to address the following scientific questions through a comprehensive investigation, employing a complex methodology for each of the aquifers comprising the Northwestern Sahara Aquifer System:

- What is the quality of the phreatic aquifer and its suitability for drinking and irrigation under the current functioning of the vertical drainage system?
- What are the physicochemical properties of the complex terminal and the continental intercalary groundwater aquifers, and are they suitable for drinking and irrigation purposes?
- How does the vertical drainage system perform, and what impact does it have on mitigating the upwelling of the phreatic groundwater table and its stability, in terms of spatial distribution and temporal variations of this aquifer, based on the data collected in the years 2008, 2009, 2014, 2016, 2018, and 2021?
- How can the shortcomings in water resource management in El Oued contribute to the persistence of groundwater upwelling?
- What is the spatial distribution of heavy metals and the extent of their contamination in the phreatic aquifer of the Oued Souf Valley?
- What are the human health and ecological risks associated with the presence of heavy metals in the phreatic aquifer?

These questions form the foundation of this thesis, which seeks to provide insights into the complex hydrogeological and environmental challenges facing the Oued Souf Valley and offer potential solutions to address them. Furthermore, the goal of this thesis is to investigate the hydrogeochemistry of the Northwest Sahara Aquifer System. This involves identifying pollutants within the aquifer to ensure the safety of its water for consumption and utilization. The research aims to comprehend the natural chemical behaviors of the aquifer to enable effective resource management. Furthermore, it seeks to develop sustainable management strategies for the aquifer, protect the environment from contamination risks, and support economic development. This is achieved by preserving groundwater as a reliable resource for agriculture, especially in water-scarce regions like the Oued Souf Valley.

2. Literature review

2.1. Groundwater

2.1.1. Quantitative aspects of groundwater

Groundwater constitutes a fundamental component of the Earth's hydrological cycle, pervading the subsurface in various geographic features, including hills, mountains, plains, deserts, coasts, and even beneath seas and oceans. A staggering 98% of the planet's accessible liquid freshwater reservoir is attributed to groundwater, making it an indispensable resource for fulfilling domestic, agricultural, and industrial water requirements. On a global scale, approximately 2.5 billion individuals exclusively rely on groundwater to meet their essential daily water needs [7,8,25]. Further underlining its significance, the United Nations Environmental Agency (UNEP) identifies 32 metropolitan areas worldwide as "megacities," each with populations exceeding 10 million, and around half of these megacities predominantly hinge on groundwater for their water supply [26]. This reliance on groundwater is accentuated as challenges in surface water availability become more pronounced over time [10]. Consequently, effective groundwater management becomes paramount to address the qualitative and quantitative challenges associated with this vital resource and to gain insights into its spatial and temporal dynamics [11]. Moreover, the continuous degradation of this natural resource is exacerbated by factors such as climate change, rapid population growth, poor resource management, and misconceptions regarding resource nature, stemming from a lack of coordination and integration of approaches [12]. This predicament has given rise to several issues, including aquifer depletion and declining groundwater levels due to climate change's association with global warming, leading to reduced rainfall and increased evapotranspiration as a result of rising temperatures, directly impacting groundwater replenishment within a region [13]. Additionally, extensive extraction of groundwater from shallow aquifers for agricultural, industrial, and domestic purposes further compounds the challenges faced [14].

2.1.2. Qualitative aspects of groundwater

Groundwater contamination is the introduction of unwanted substances into groundwater due to human activities [27]. It can result from various sources, including chemicals, road salt, bacteria, viruses, medications, fertilizers, and fuel. Nevertheless, groundwater contamination distinguishes itself from surface water contamination by being invisible and challenging to remediate with current technology [28]. Groundwater contaminants are typically colorless and odorless, and the adverse effects on human health are often insidious and hard to identify [29]. Once contaminated, cleaning it up is demanding and costly because groundwater resides in subsurface geological strata with long residence times [30,31]. The natural cleansing mechanisms for polluted groundwater may extend

over several decades or even centuries, persisting even after the cessation of the contaminant source [32].

The types of contaminants found in groundwater are rapidly increasing, but they can be broadly categorized into three main groups: chemical contaminants, biological contaminants, and radioactive contaminants [33]. These contaminants may originate from both natural and human sources [34]. Detecting and identifying pollution within groundwater poses a significant challenge. Examples of real-world, clandestine underground pollution include leaks from chemical distribution infrastructure and petrochemicals, such as pipelines and sewage collection systems like sewage tanks, urban sewage channels, and pipelines [35]. The storage and handling of mining byproducts and industrial chemicals, often without proper contamination control measures, have presented some of the most complex pollution and management issues over the past century [36]. Identifying source pollutants involves pinpointing their spatial locations, determining the duration of their activity, which indicates when they became active, and calculating the injection rate of pollutant sources, all of which influence the contaminant flow from each source [37].

2.2. Types of groundwater contaminants

2.2.1. Groundwater contamination with acidification phenomenon

Acidified precipitation is a well-established and widespread phenomenon. The concept of 'acid rain' has been recognized for more than a century and is primarily attributed to the emissions of sulfur and nitrogen oxides into the atmosphere [38,39]. The impact of acid precipitation on groundwater is generally considered to be minor. Other sources of acidity in groundwater can arise from natural water-rock interactions, contamination with industrial acids, and the breakdown of various pollutants [40–43].

2.2.2. Inorganic compounds contamination of groundwater

Nitrogen pollutants, like nitrate, nitrite, and ammonia nitrogen, are frequently encountered in inorganic contaminants commonly found in aquifers close to rural and suburban areas. Unpolluted groundwater typically contains nitrate nitrogen levels below 2 ppm. Nitrate in groundwater primarily stems from four sources: agriculture (involving the use of nitrogen-based fertilizers and animal manure), atmospheric deposition, soil cultivation, and domestic wastewater (human sewage disposed of in septic systems) [44–51].

Nevertheless, groundwater nitrate contamination has been widely documented across the globe, including the United States, where approximately 12 million tons of nitrogen-based fertilizers are used in agriculture each year, with the production of manure contributing about 7 million tons or more. In most instances, nitrogen compounds reduced in the soil undergo oxidation to form nitrate, which then migrates to groundwater, where it dissolves in water and becomes diluted, as

removing nitrate from well water is expensive. Water containing elevated nitrate levels is generally unsuitable for human consumption, especially from a public health perspective [52]. Other prevalent inorganic contaminants present in groundwater encompass anions and oxyanions, such as F^-, SO_4^{2-}, and Cl^-, as well as major cations like Ca^{2+} and Mg^{2+}. Total dissolved solids (TDS), representing the overall amount of inorganic and organic ligands in water, may also be elevated in groundwater. These pollutants commonly have a natural origin, but human activities can also elevate their levels in groundwater [53].

2.2.3. Groundwater contamination with heavy metals

Since toxic metals and metalloids pose a risk factor for the health of both human populations and the natural environment, recognition of the potential toxic effects and long-term contaminants of heavy metal pollutants has centered on the protection of soil and groundwater in recent years [54]. Metals such as zinc (Zn^{2+}), lead (Pb^{2+}), mercury (Hg^{2+}), chromium (Cr^{3+}), and cadmium (Cd^{2+}) are commonly found in groundwater, as are metalloids such as selenium (Se^{6+}) and arsenic (As^{3+}). Although several of these elements are required micronutrients at smaller amounts, large concentrations can cause serious poisoning, including respiratory difficulties and many types of cancer [55,56]. Furthermore, non-metabolization and buildup of heavy metals in soft tissues enhance their toxicity, causing organ damage, nervous system damage, and, in severe situations, death [57]. Heavy metals have negative effects that extend beyond humans; animals incur morphological, histological, and biochemical changes when exposed to environmental contaminants like heavy metals, even at low concentrations, for extended periods of time [58]. For example, exposure to hexavalent chromium (Cr^{6+}) can increase the risk of cancer [59]. Arsenic is ranked as a Group 1 human carcinogen by the US Environmental Protection Agency (EPA) and the International Agency for Research on Cancer (IARC), and As^{3+} can react with sulfhydryl (–SH) groups of proteins and enzymes to upset cellular functions and eventually cause cell death [60,61]. Toxic metals in the environment are persistent and subject to moderate bioaccumulation when they enter the food chain [55].

2.2.4. Contamination of grounsdwater by Landfills

The impact of landfills on groundwater quality hinges on an ongoing debate regarding two landfill construction approaches: "dilute and disseminate" versus "containment." To fully comprehend the effect of landfills on groundwater, it is essential to consider the composition of waste leachate [62]. Generally, the composition of leachate is influenced by factors such as the type of waste, landfill design and operations, analytical methods, and the passage of time. Many of the earlier references pertain to landfills for mixed household waste, which often contains a significant organic component, is biodegradable, and is prone to substantial long-term consolidation settling due to its low initial density and biodegradation effects. In contrast, certain industrial solid wastes are typically

disposed of in "mono-disposal" facilities, where only one or perhaps two types of waste materials are accepted [63]. Examples of such facilities include mineral deposits and waste from the mining industry (e.g., colliery shale, coal tailings, quarry fines) and pulverized fuel ash (PFA) from coal-fired power stations. There is relatively limited literature available on mono-disposal landfilling [64]. Pollution from engineered landfill sites (dumpsites) has been identified as a significant threat to groundwater resources [65].

2.2.5. Contamination of groundwater with organic pollutants

Organic pollutants have been extensively identified in drinking water, and many of these substances are recognized as potential human carcinogens or chemicals that disrupt the endocrine system. In groundwater, more than 200 organic contaminants have been discovered, and this number continues to rise [66–69]. Some of these organic contaminants are biodegradable, originating primarily from domestic sewage and industrial wastewater. Many of these organic compounds are naturally derived from carbohydrates, proteins, fats, and oils and can be converted into stable inorganic substances by microorganisms. They do not directly harm living organisms but can deplete the levels of dissolved oxygen in groundwater. Common organic contaminants encompass hydrocarbons, halogenated compounds, plasticizers, pesticides, pharmaceuticals, personal care products, and natural estrogens, among others [70–72]. A substantial portion of the halogenated compounds (e.g., chlorinated, brominated, fluorinated) persist in the environment and can accumulate in organisms, causing adverse effects on species at higher trophic levels, including humans [73,74]. Persistent organic contaminants are primarily chemicals used in agriculture, industrial processes, and human health protection [70]. Since these compounds degrade very slowly or not at all, they pose a permanent threat to the quality of groundwater intended for drinking purposes [75].

2.2.6. Contamination of groundwater with biological and microbiological pollutants

Biological contaminants encompass various entities, including algae and microorganisms like bacteria, viruses, and protozoa. When it comes to microbial contaminants, human and animal feces have been found to contain over 400 types of bacteria, along with more than 100 types of viruses [76] . While some of these microorganisms originate from natural sources, others are microscopic organisms that coexist with natural algal species and compete for available resources [77,78]. The presence of microbial contaminants in drinking water can lead to numerous human diseases, including severe diarrheal illnesses such as typhoid and cholera. Presently, the COVID-19 virus has caused a global pandemic affecting every corner of the world. Although this coronavirus primarily spreads from person to person through respiratory droplets [79], water contaminated by the virus can also pose a threat to human health [80,81]. Algal contamination is commonly observed

in surface waters like lakes and reservoirs, often due to eutrophication. However, the presence of algae at high biomass levels in groundwater is relatively rare [82].

2.3. Groundwater contamination ramifications

Contamination of groundwater poses risks to human health, environmental well-being, and socioeconomic progress. Numerous studies have highlighted the health hazards associated with elevated levels of fluoride, nitrate, metals, and persistent organic pollutants [83,84]. This concern is particularly pronounced for infants and children, who are more vulnerable to these contaminants than adults [85–91]. An illustration is the "blue baby syndrome," or infant methemoglobinemia, resulting from excessive nitrate concentrations in drinking water used for baby formulas. Groundwater contamination also affects human health indirectly through the food production system. Irrigation with contaminated groundwater can lead to the accumulation of toxic elements in crops, posing risks to human consumers [92–94]. Furthermore, contaminated groundwater can degrade land quality and negatively impact forests. High groundwater salinity in arid agricultural regions, for instance, contributes to soil salinization, affecting vegetation growth [95]. The interaction between surface water and groundwater can transport contaminants, further deteriorating surface water quality [96]. Achieving sustainable economic development necessitates a balance between natural resource renewal and human demand [97]. Freshwater, a crucial natural resource, may face depletion due to chronic groundwater contamination, disrupting the equilibrium between water supply and demand and potentially triggering socioeconomic crises or conflicts, even wars [98]. Contamination-induced water shortages could lead to conflicts among citizens, impeding a nation's socioeconomic development. Groundwater contamination transcends environmental concerns, evolving into a social issue that calls for collaborative efforts between natural and social scientists [99].

2.4. Groundwater Contamination: Detection, Prediction, and Assessment Techniques

Accurate prediction and measurement of pollutant movement are crucial for effective environmental management. This necessitates a thorough understanding of the processes governing contaminant transport. [100] identified these processes as encompassing physical, chemical, and biological reactions affecting soluble concentrations in groundwater, as well as hydrodynamic dispersion and advection. Addressing groundwater contamination issues, as outlined by USEPA (1993), involves both preventing the introduction of contaminants to aquifers and predicting and managing their movement if introduced. Protective measures often extend to safeguarding entire aquifers and surrounding areas from unintentional contamination, as highlighted in studies by [101,102] . Investigations into groundwater contamination, detailed by [103,104], cover scientific understanding of controlling processes, mathematical representation in transport models,

determination of model parameters, and the development of management models for preventing and removing contaminants.

Groundwater pollution, originating from both point and unspecified sources, further exacerbates environmental challenges. Point source pollution, as characterized by [105], allows for accurate determination and has limited spatial extent. In contrast, pollution from unspecified sources, such as agricultural practices like pesticide and fertilizer application [106], lacks a distinct origin. The detrimental impact of agricultural land, sewage, runoff from urban areas, and animal waste on water quality, particularly in increasing microorganism levels, is emphasized by studies like [107–111]. Water pollution problems arise from substances altering chemical composition, posing threats to human health and ecosystems [112]. Beyond chemical contaminants, groundwater quality is compromised by factors like pH, electrolysis, turbidity, and microbiological content [113]. Various pathways contribute to groundwater contamination, including inter-aquifer leakage, irrigation returns, leaching from soluble solids, broken sewer pipes, percolation of sprayed liquids over land, landfill leachate, and septic and sewerage effluent discharge [114]. Hence, a sequential integration of source identification models and a monitoring network design can effectively characterize pollutant sources. The crucial attributes to ascertain encompass the spatial locations of sources and the duration of their activities, elucidating when these sources became operational. Additionally, the rate of pollutant injection from each source, portraying the release of pollutants over time, is a key parameter [36].

To detect groundwater contamination, surface electrical resistivity was recently employed as a diagnostic tool. Water serves as the carrier for pollutants across both visible and imperceptible terrains. Locally, water-soluble components used in agriculture, industrial waste, dry waste sediments, etc., may be transported by water, leading to groundwater pollution. This contamination often goes unnoticed until the tainted water traverses through a local well. The repercussions of pollution may manifest downstream, particularly when river water is utilized for sensitive purposes like irrigation [115].Several assessment methods for groundwater contamination have been developed, integrated, and intensively used throughout the last decade. These methods vary depending on their purpose of identification, including statistical methods [116,117], hydrogeochemical methods [118,119], indexing methods [120–122], and spatial methods [123,124].

Statistical analysis involves the application of mathematical methods to analyze and interpret data, providing insights into patterns and relationships within a dataset. Multivariate statistical analysis extends this approach by simultaneously considering multiple variables, recognizing the interconnectedness of different factors. This enables a more comprehensive understanding of complex datasets [125,126]. Among all the statistical techniques, Hierarchical cluster analysis which can be utilized for classifying cases or variables based on their similarity or variability [127–129]. Hierarchical cluster analysis is widely applied in hydrogeochemistry studies. Its primary objective is to categorize hydrogeochemical processes in groundwater by organizing collected water samples into distinct clusters relevant to geological and hydrogeological aspects [130]. Additionally, this unsupervised approach aids in identifying similarities

among water quality variables. To create the initial clusters for the selected parameters, Euclidean distances can be employed, followed by the use of Ward's agglomeration method to link these initial clusters [120,131]. As a result, all the generated groups can be represented in a dendrogram, facilitating the visualization of the distinct groups resulting from the clustering process [132].

The hydrogeochemical analysis are very important step for the characterization of groundwater and indicating the influence of associated geology, and during the last decades several graphical plots have been devoloped for this pupose such as Stiff plot [133], Piper plot [134], Chadha plot [135], and Gibbs plot [136]. These plots are as crucial as the analytical results of the data. They not only condense the scattered hydro-chemical data but also offer numerous insights into the origin of existing groundwater chemistry through the geological conduit to study the hydrochemical facies and the controlling mechanism of all the groundwater systems [137,138].

Indexing methods are commonly employed to evaluate groundwater pollution and assess the suitability of wells for drinking, irrigation and even for pollution detection. These methods are constructed based on several key parameters that serve as representatives of the overall groundwater quality and its pollution status [139].

The water quality index serves as a valuable tool for assessing the suitability of groundwater for drinking or irrigation purposes [140,141]. It functions as a rating system, providing an overall indication of water quality by considering various parameters collectively. This approach, involving the amalgamation of detailed data to generate a score describing water quality status, proves to be a convenient and straightforward method for decision-makers to gain a deeper understanding of the quality of surface or groundwater sources [142]. The water quality index proposed by [143] stands out as one of the most powerful tools for evaluating surface/groundwater quality for drinking purposes, widely utilized by researchers [144–147].

Contaminated irrigational water negatively impacts crop yield, plant growth, soil quality, and human health. Therefore, it is crucial to assess groundwater for agricultural purposes by analyzing various ionic parameters in meq/L, using different indices [91]. Various indicators have been used intensively in the literatures [148–151] such as electrical conductivity (EC) measured in µS/cm [152], total hardness (TH) [153], and sodium adsorption ratio (SAR) representing the ratio of Na^+ ions to Ca^{2+} and Mg^{2+} ions, have been employed to evaluate groundwater for irrigation use.

The SAR value is vital in determining the potential for Na^+ accumulation in the soil due to the continuous use of sodic water. This accumulation can lead to a dominance of Na^+ ions in water flow, at the expense of Ca^{2+}, Mg^{2+}, and K^+ ions [152]. The percentage of sodium (% Na) is a key factor in classifying water sources for irrigation. Na^+ binds to soil, reducing its water transport capacity. The reaction of Na^+ with CO_3^{2-} results in alkaline soils, while its combination with chloride leads to saline soils, both of which hinder crop development [154].

In groundwater, alkaline earths like Ca^{2+} and Mg^{2+} are generally in equilibrium, playing a significant role in soil structure and crop nutrient supply. However, high

concentrations of Ca^{2+} and Mg^{2+} can increase soil pH, potentially converting the soil to a saline state and reducing phosphorus availability. Excessive magnesium can lead to alkaline soil, resulting in lower agricultural yields, referred to as "magnesium hazard" (MH) [155].

The residual sodium carbonate index (RSC) quantifies bicarbonate/carbonate and calcium/magnesium in irrigation water, affecting soil structure through precipitation reactions [150]. The permeability index (PI) assesses the long-term water transport ability of soil, influenced by the salt content and the presence of Na^+, Ca^{2+}, Mg^{2+}, and HCO_3^- ions [156]. The Kelley ratio (KR) evaluates water quality based on the Na^+ to Ca^{2+} and Mg^{2+} ratio [157]. The PS index is also one of the indicies that categorizes water for agriculture use based on the parameter values [156]. Synthetic Harmful Coefficient (K) and Irrigation Coefficient (Ka) are used to evaluate water quality [158]. Groundwater can also be classified based on the relationship between bicarbonate and calcium ions, represented by the residual sodium bicarbonate (RBSC), where an excess concentration of sodium bicarbonate has harmful effects on soil [159].

High concentrations of exchangeable sodium ions can adversely affect soil structure, causing soil aggregates to separate. Elevated sodium levels, especially with a high exchangeable sodium percentage (ESP), can lead to soil structure collapse, reduced porosity and permeability, increased soil density, and restricted root growth [91].

The assessment of water quality and pollution in various water bodies has recently advanced through the application of complex methodologies. This includes the utilization of water quality indices to detect groundwater pollution by observing visual changes in groundwater quality over time and space, relying on the selected water quality indices. One prominent index among them is the National Sanitation Foundation Water Quality Index (NSFWQI), which is considered comprehensive and widely applicable for classifying water resources based on their quality [122,160]. The NSFWQI [161]comprises nine parameters: percentage of dissolved oxygen (DO) saturation, pH, total solids (TS), five-day biochemical oxygen demand (BOD_5), turbidity, total phosphate (TP), nitrate (NO_3^-), temperature change (T), and fecal coliform (FC). Each parameter carries an individual weight proportional to its impact and significance in developing the NSFWQI model [161]. Since the introduction of the NSFWQI, numerous studies have employed this model, or its updated versions, to assess water quality in diverse water bodies [162–171]. Beside NSFWQI, the Groundwater Pollution Water Quality Index proposed by [172] which has been used widely in the literatures [124,173,174]. This index primarily assesses the relative impact of individual chemical variables, namely pH, TDS, TH, Ca^{2+}, Mg^{2+}, Na^+, K^+, Cl^-, SO_4^{2-}, NO_3^-, and F^-, on the overall quality of groundwater intended for drinking purposes [175].

Nitrate is a crucial element significantly influencing the quality of groundwater [176,177]. Globally, monitoring nitrate contamination and its impact on human health is a pressing concern, attributed to anthropogenic activities such as modern agricultural practices, the use of synthetic fertilizers, and the higher permeability of soil, which may contribute to elevated nitrate concentrations in groundwater

[121,178–181]. The Nitrate Pollution Index (NPI) serves as a valuable indicator for assessing the extent of nitrate pollution in groundwater, and it was widely used in the literatures [167].

High concentrations of heavy metals in groundwater systems pose a significant threat to human health, resulting in various detrimental effects [182]. Exposure to these harmful substances can lead to severe health complications, such as respiratory issues and various forms of cancer [56]. Moreover, the non-metabolization and accumulation of heavy metals in soft tissues heighten their toxicity, causing damage to organs, the nervous system, and, in extreme cases, even death [57]. The adverse impacts of heavy metals extend beyond humans, affecting animals with morphological, histological, and biochemical alterations when exposed to environmental pollutants like heavy metals, even at low concentrations, over prolonged periods [58]. Given these potential dangers, it is crucial to assess groundwater quality and the contamination levels of heavy metals before making any decisions. To achieve this, various quantitative indices for heavy metal pollution have been utilized in recent decades. Among these indicies, the Contamination Degree (C_{deg}) [183,184] which serves as a comprehensive representation of various water quality parameters believed to be detrimental to domestic water usage [185]. Geoaccumulation Index (I_{geo}) [186,187], as introduced by [188], serves as a tool for quantifying the extent of pollution load accumulation arising from anthropogenic or geogenic sources. This index is crucial as it offers a quantitative assessment of the levels of dissolved metals in porous media, including soil, sediments, and water [189]. To identify the origins of dissolved metals in water, soil, and sediment, and to assess the degree of contribution from anthropogenic or geogenic sources to water system contamination, the enrichment factor (EF) can be employed [190,191]. The Ecological Risk Assessment (ER) and the Potential Ecological Risk Index (PRI) represent two additional tools available for assessing the extent of contamination in the samples [173,192].

Spatial analysis is a broader field encompassing a wide array of methods and applications such as geostatistical techniques, which aims to estimate the values of a specific attribute at locations where direct measurements are not available. This estimation is achieved by leveraging information gathered from other observed points. By transforming data from these observed points into continuous fields, it becomes possible to compare the spatial patterns of the sampled measurements with those of other entities [193]. Several commonly used techniques include ordinary Kriging interpolation (OK), simple Kriging interpolation (SK), and universal Kriging interpolation (UK). Deterministic interpolation methods, such as global polynomial interpolation (GPI), inverse distance weighted interpolation (IDW), planar spline interpolation, and local polynomial interpolation (LPI), are frequently employed to generate maps of soil properties. These techniques have been extensively described in various studies [194–196]. Furthermore, these interpolation methods find application in mapping and predicting groundwater quality and contamination [197–199] as well as in mapping and predicting groundwater levels [200–205]. Ordinary Kriging (OK) [198,206–209] and Inverse Distance Weight (IDW) [210–214] are two geostatistical methods integrated with Geographical Information Systems (GIS) to qualitatively and quantitatively

analyze groundwater. OK uses a semi-variogram to measure spatial correlation and provides error estimates in unsampled areas, while IDW calculates values based on the inverse of the distance from sampled points. Cross-validation, with metrics like Root Mean Square Error (RMSE) and Mean Absolute Error (MAE), is employed to assess the accuracy of these methods and determine the most suitable one for specific applications. The strength of spatial dependency is categorized based on the variance-to-sill ratio, aiding in understanding and applying these interpolation techniques effectively [215–217].

2.5. Groundwater Quality in Arid Regions

Groundwater in arid regions serves as a critical source of water supply for agricultural, industrial, and domestic use, despite the challenges posed by the limited and variable rainfall patterns characteristic of these areas. The quality and sustainability of this vital resource have been the focus of extensive research due to the unique hydrogeological challenges these regions face [218].

One of the prevalent issues in groundwater management in arid regions is salinization, a process exacerbated by both natural conditions and human activities. [100] discuss how intensive agricultural practices, particularly irrigation, lead to the accumulation of salts in the soil profile, which eventually leaches into the groundwater system. This issue is compounded by the common use of poor-quality water for irrigation, which contributes further to the salinity [219]. The impact of irrigation on groundwater quality was particularly noted by [220], who studied the impact of agricultural runoff in North Africa and highlighted significant nitrate contamination linked to fertilizer use.

Another critical aspect is the anthropogenic contamination from industrial processes and urban development, which introduces pollutants such as heavy metals, hydrocarbons, and synthetic organic compounds into the groundwater system. [221] analyzed groundwater contamination in semi-arid areas and found that industrial pollutants tend to persist in the groundwater due to the slower hydrological cycle, which reduces the natural attenuation capacity of the aquifer systems.

Recent research continues to explore the hydrogeochemical characteristics and contamination sources affecting groundwater in arid regions. Studies such as those by [222,223] have advanced our understanding by using hydrogeochemical analysis to evaluate the evolution of groundwater composition. They focus on pollutants like fluoride and nitrate, and trace elements that pose significant risks to human health [224].

In arid regions like Wadi El-Assiuti in Egypt, recent investigations have assessed groundwater quality, emphasizing the dual challenge of ensuring suitability for both drinking and agricultural uses. This research underlines the critical impact of geological formations on water quality, with sedimentary rocks contributing to the variability in groundwater composition [225].

Another noteworthy study from the Nekor-Ghiss plain in Morocco utilizes geographic information systems (GIS) to classify groundwater quality using Piper diagrams, highlighting how geochemical interactions and human activities

influence water suitability for irrigation and consumption [226].

In the Tan-Tan region of Morocco, researchers have employed machine learning (ML) and ensemble learning (EL) models to enhance groundwater potential mapping. These models help predict groundwater levels and assess water quality, leveraging large datasets to understand complex geospatial relationships, significantly advancing groundwater management in arid areas [227].

In Egypt, specifically around the Ismailia Canal, the Water Quality Index (WQI) has been utilized to evaluate groundwater for drinking suitability. This assessment integrates environmental and hydrogeological factors, providing a comprehensive analysis of trace elements and major physiochemical parameters [228].

Studies in Egypt's Sohag region have applied deep learning time series techniques, specifically long short-term memory (LSTM) models, to forecast groundwater quality. This research uses a range of water quality parameters to create a Water Quality Index, assisting in managing groundwater resources effectively in arid regions [229].

Research has also explored how land use and cover changes affect water quality in lake basins in arid and semi-arid regions. Using models like the hybrid evolutionary algorithm, these studies examine long-term changes in land use and their impact on water quality, highlighting the importance of integrated environmental management [230].

2.6. Rising of Groundwater in arid regions

The rising groundwater levels in arid regions worldwide are influenced by multiple factors including climate change, land use modifications, and human activities such as groundwater overexploitation and inadequate water management. Climate change plays a significant role in altering groundwater recharge rates, which may contribute to increased groundwater levels in some arid zones. For instance, in Saudi Arabia, altered climate patterns have impacted irrigation water requirements, which in turn affect groundwater usage, potentially influencing groundwater levels [231].

Intensive groundwater extraction for agriculture and urban development often leads to initial depletion, followed by complex interactions that may subsequently elevate groundwater levels elsewhere. This phenomenon of overexploitation is particularly evident in regions like Libya, where it has led to seawater intrusion, thus degrading groundwater quality and altering hydrological dynamics [232].

Advancements in satellite technology, such as the Gravity Recovery and Climate Experiment (GRACE), have significantly enhanced our understanding of groundwater dynamics. A study in Alxa League, China, for example, applied machine learning techniques to improve the spatial resolution of GRACE data, providing detailed insights into the changes in groundwater storage influenced by both natural variability and human activities [233].

Groundwater management in arid areas is further complicated by socio-economic factors, including policy and governance issues. Effective management is essential in these regions to mitigate water scarcity that can intensify social and economic tensions. Changes in land use, such as increased urbanization or shifts in

agricultural practices, also impact groundwater levels by altering natural recharge areas, which can either enhance or impede groundwater infiltration. Sustainable management practices that combine scientific knowledge with community involvement are crucial to addressing the challenges posed by rising groundwater levels [234]. Moreover, rising groundwater levels can trigger environmental issues like soil salinization, which impairs land quality and reduces agricultural productivity. This problem is particularly acute in arid regions where irrigation practices elevate groundwater levels and enhance soil salinity, as documented in several studies [234].

2.7. Water resources in Algeria

Algeria possesses potential water resources amounting to 19.2 billion m^3, comprising 12.4 billion m^3 of surface water and 6.92 billion m^3 of groundwater, primarily located in the Sahara region [235]. The northern aquifers, subject to intensive exploitation, yield an annual extraction of 2 billion m^3, while certain regions face over-exploitation challenges. Extracted volumes from Saharan regions are estimated at 1.7 billion m^3 [236]. The primary source of aquifer recharge in Algeria is precipitation, characterized by irregular distribution in both time and space. Approximately 1.5 billion m^3 of water are annually extracted and utilized. Notably, 75% of Algeria's renewable resources are concentrated in just 6% of the country's territory [237,238]. Conversely, significant reservoirs are found in the southern part of the country [239]. The total usable reserves are estimated at 5 billion m^3 annually, with only 1.6 billion m^3 being utilized [19]. This available water resource satisfies about 66% of the country's annual water demand [240]. Algeria's fresh and potable water sources are categorized into three sections: surface water (rainwater reservoirs), groundwater reservoirs, and unconventional water sources [241]. Regarding water quality, Algeria's national report indicates that 44% of the collected water is of high quality, 44% is of satisfactory quality, and 12% is of poor quality, without differentiation between surface and groundwater [235].

The huge reservoir that exists in the south of Algeria and includes several Saharan regions and cities of the Algerian Great Desert such as Oued Souf Valley is called the Northwest Sahara Aquifer System (NWSAS), which ranks as the second largest reservoir globally. This aquifer system is jointly shared by three nations, namely Algeria, Tunisia, and Libya [242]. Spanning an overall area of approximately one million km^2, the distribution of this aquifer system is divided among the three countries as follows: Algeria holds 70%, Tunisia has 6%, and Libya possesses 24% [242]. Within Oued Souf Valley, the aquifer system comprises three main aquifers, each varying in terms of depth and physiochemical properties [243–245].

2.8. Rising of the Phreatic groundwater level history in Oued Souf Valley and its impact on public health and the environment

The phenomenon of rising Phreatic groundwater levels in the Oued Souf region is complex and has been occurring for almost half a century. Prior to 1956, all water used for human, animal, and agricultural purposes was sourced from the Phreatic aquifer (shallow aquifer) [246–249].

The increase in population and expansion of cultivation necessitated the drilling of the first well in the Terminal Complex to supply drinking water to Oued Souf in 1956. Between 1957 and 1969, approximately one new well per year was drilled in the Terminal Complex. From 1970 to 1980, an average of two wells per year were constructed in the Terminal Complex. Starting in 1980, the first instances of waterlogging in agricultural lands (Ghout systems) and a gradual, persistent rise of the groundwater table on the outskirts of El Oued municipality were observed, which raised concerns among the authorities in 1985 [250].

Between 1980 and 1987, around a hundred new wells were drilled in the Terminal Complex, and three wells were drilled in the Continental Intercalaire. The latter are highly artesian, with flow rates of 200 liters per second, which is 5 to 10 times higher than those of the Terminal Complex. In 1993, the groundwater had flooded the palm grove for a distance of 25 km in the Kouinine-Robbah corridor. The affected area by the rising waters covers an area of 3,000 km^2, where 380,000 inhabitants reside, distributed among 18 municipalities, including Bayadha, Robbah, Kouinine, Guemmar, Taghzout, Hassani Abdelkrim, Debila, Sidi Aoun, Magrane, Hassi Khelifa, Reguiba, Mihouensa, Oued Alenda, Ogla, Nakhla, Ourmes, and Trifaoui [21,22].

From 1993 until 2004, a series of investigations were carried out to understand the geometric and geological characteristics of the aquifer and identify the existing wells. At the end of the investigation, a series of measures were implemented, such as discontinuing new irrigation wells in the Terminal Complex and Continental Intercalary, replacing them with wells in the phreatic aquifer, reducing water supply allocations to the population, constructing new improved wells for agriculture in the phreatic aquifer, and developing new agricultural areas [251].

During that time, the region experienced severe pollution and health issues as a result of several factors such as the flat topography. Firstly, the polluted water table began to rise, filling with discolored and unpleasant-smelling water contaminated with various types of waste. This was primarily due to the flooding of septic tanks and cesspools, allowing bacterial pollution to spread throughout the shallow aquifer. Additionally, water contamination by nitrates from domestic and agricultural sources was a significant concern [252].

The water's high mineral content was another problem, resulting from intense evaporation from open water bodies and salt dissolution. Compounding the issue, the Ghouts, which were flooded areas, served as unofficial dumping sites for waste. Consequently, stagnant water created a breeding ground for mosquitoes, leading to an increase in waterborne diseases, parasitic infections, skin ailments, leishmaniasis, malaria, and typhoid among the local population [23]. For instance,

the municipal health service in the town of El Oued recorded hundreds of cases of typhoid fever during that period, highlighting the severity of the situation and its impact on public health [24,253].

In general, the Northern Sahara of Algeria, especially the groundwater quality in the Oued Souf Valley, has been the subject of research in several studies. These studies have primarily focused on the geological and hydrogeological contexts of the aquifers, exploring the Northern Sahara aquifer system [254–260]. Apart from geological and hydrogeological investigations, numerous studies conducted over the past three decades have indicated that the groundwater quality in this region is characterized by excessive total mineralization, often accompanied by high hardness and elevated fluoride concentrations. These concentrations frequently surpass the recommended guidelines of the World Health Organization (WHO) and the limits set by Algeria, assessed through conventional hydro-chemical, bacteriological, statistical, and isotopic methods [116,243,268–273,260–267]. Additionally, various studies have delved into the treatment of these groundwaters using different techniques, such as lime precipitation and electrocoagulation employing bipolar aluminum electrodes and activated natural materials [274–277]. However, no study has been conducted to assess and reveal the presence of heavy metals in the aquifers of the Oued Souf Valley.

The rising of the phreatic groundwater level and its impacts represents one of the most rare case in the history where the precipitations do not have any contribution to this phenomena since the source of precipitation in the Saharan regions varies depending on the season. In the summer, precipitation is primarily influenced by monsoon depressions, while in winter, it is associated with depressions accompanying the southward movement of polar fronts. During the transitional periods, rainfall occurs due to Sudano-Saharan depressions that cross the Sahara from the south to the north [278]. However, in the Oued Souf region, rainfall is characterized by its low, irregular, and infrequent nature [199]. Based on the climatic analysis performed on 42 years of data obtained from the Guemmar airport meteorological station (1978-2020) [279], it was revealed that the irregularity and scarcity of precipitation, high temperatures, and extremely high evapotranspiration (potential evapotranspiration- PET) have significant repercussions on surface runoff and infiltration. Throughout this research, it was also discovered that the climatic conditions in the region do not contribute to the natural recharge of the groundwater reservoirs in the Oued Souf Valley, which explains the high agricultural deficit (AD) experienced throughout the year, thus necessitating irrigation, as shown in figure 1. Furthermore, the hydrological water budget consistently indicates a deficit, which puts significant pressure on socio-economic life and may exacerbate drought and desertification phenomena.

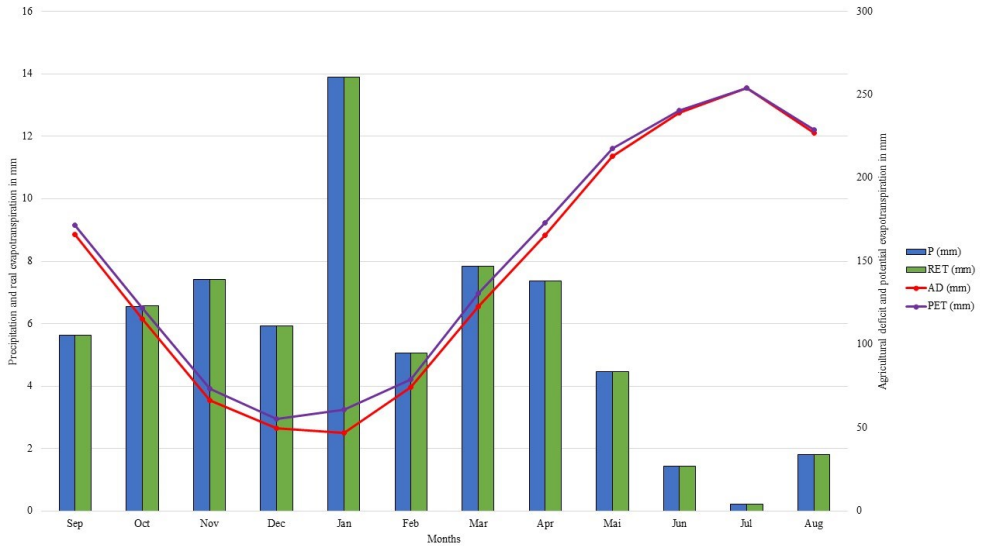

Figure 1. Water budget parameters over 42 years (1978- 2020) [279].

2.9. Vertical Drainage System of Oued Souf Valley

In an effort to address the escalating groundwater levels and pollution spread, Algerian authorities initiated a large-scale project (mega project) in 2005 via an additional drainage system (vertical drainage system) [280]. This project consisted of four plans: the Sewerage Plan, Purification Plan, Evacuation Plan, and Drainage Plan. However, despite these efforts, the project faced numerous challenges and ultimately failed to achieve its primary objective [281].

However, the implementation of the vertical drainage system involves the use of 58 drainage wells drilled at depths ranging from 21 to 40 meters. These wells are equipped with submersible pumps capable of pumping 6 litres per second. Spaced approximately 500 meters apart, the drainages are connected by 37 kilometres of pipelines to ensure the equalization of water levels in Oued Souf City. The primary objective of this system is to stabilize the water table in flooded neighborhoods, maintaining a minimum depth of 1.5 meters. Additionally, it aims to counteract the phenomenon of upwelling in other parts of the city and prevent the occurrence of new flooding areas. This is achieved through a general drawdown of 5 to 10 meters deep, which allows for autonomous sanitation in areas that cannot be connected to the drainage network [282,283].

Currently, the management of the drainage system is overseen by the El-Oued National Sanitation Office (Office National d'Assainissement d'El-Oued, ONA). The system operates on the principle of collecting all infiltration water beneath the El-Oued urban area. This water is pumped into the 58 drilled wells and utilized as much as possible for on-site irrigation of green spaces. The remaining water is collected at the pumping station and conveyed over a distance of approximately 4200 meters to the collection point of the wastewater treatment plant. There, it

undergoes treatment in aerated lagoons before being discharged at the designated discharge site (Chott Halloufa) [284]. Figure 2, represents the mega project constructed by the Algerian authorities in 2005 including the vertical drainage system.

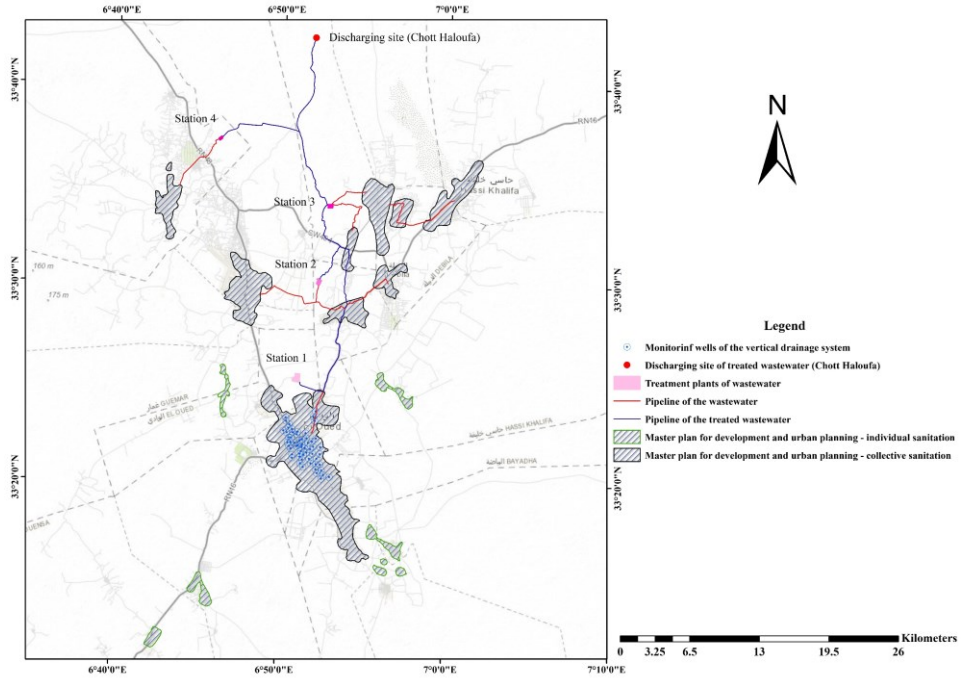

Figure 2. The mega project constructed by the Algerian authorities in 2005 modified from [284].

3. Materials and methods

3.1. General setting of Oued Souf Valley region

3.1.1. Hydrogeology of Oued Souf Valley

The uppermost aquifer in the region, known as the phreatic aquifer [285], consists of fine sands mixed with sandy clays and gypsum lenses, forming the free water table. This aquifer has a thickness of approximately 100 meters and groundwater can be found at depths ranging from 1 to 40 meters. Beneath the phreatic aquifer lies an impermeable clay layer. Groundwater extraction from the phreatic aquifer is carried out through thousands of traditionally dug wells, with the total number surpassing 35,000 in 2015. The average permeability of the phreatic aquifer is 10^{-4} meters per second, and the horizontal transmissivity and storage coefficient are estimated to be 10^{-2} meters per second and 0.2, respectively.

The natural replenishment of the phreatic aquifer occurs through the infiltration of precipitation and runoff from rock formations on the southern edge of the Great Oriental Erg. Additionally, sporadic heavy rainfall events, such as those witnessed in April 1947 and May 1967 in the region, contribute to its recharge [259,286–289]. The next aquifer, known as the complex terminal, is a deeper aquifer composed of multiple layers within various geological formations. Specifically, it belongs to the continental formations from the Cretaceous to Miocene periods. This aquifer is typically found at depths ranging from 400 to 600 meters, with an average thickness of about 400 meters. It contains fossil water that is estimated to be between 20,000 and 30,000 years old. In 2015, around 182 deep wells were drilled into this aquifer, with 28 serving irrigation purposes and 154 for municipal and drinking water supply [239,267,268]. The third deepest aquifer is referred to as the continental intercalary aquifer, consisting of continental deposits from the Middle Jurassic to the Lower Cretaceous periods, specifically the Barremian and Albian stages. The lithology of this aquifer comprises sandstones and clayey sandstones. It is situated at depths ranging from 1800 to 2200 meters, with a thickness of 200 to 400 meters. Similar to the previous aquifer, it also holds fossil water with an age of at least 20,000 to 30,000 years. Only four deep wells have been drilled into this continental aquifer, all serving the purpose of drinking water production, as the groundwater at this depth has a temperature exceeding 70°C [256,290]. Figure 3 illustrates the composition of the reservoirs within the Northwest Sahara Aquifer System (NWSAS).

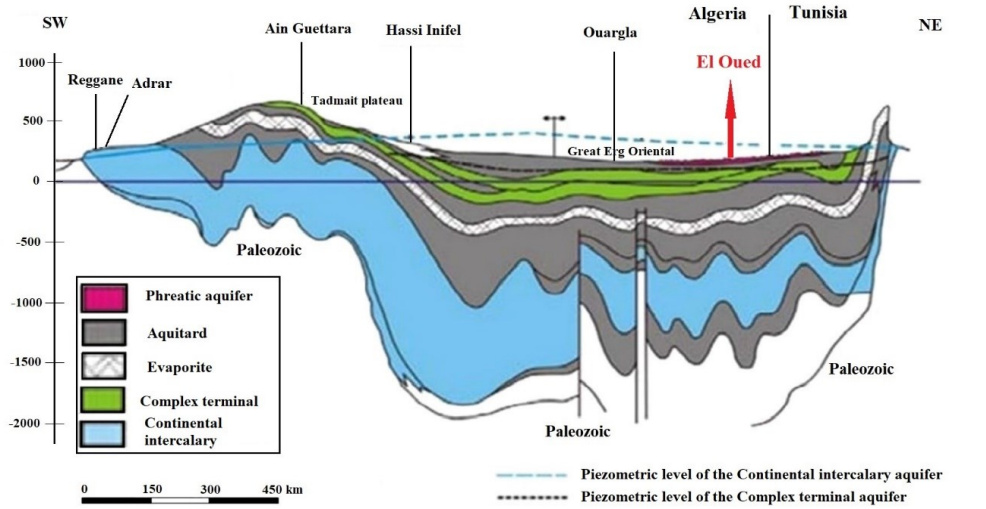

Figure 3. Hydrogeological section of the North West Sahara Aquifer System modified from [291].

The Oued Souf region, situated in the northeastern Mesozoic basin of the Sahara, is characterized by continental sand dunes formed during the recent Quaternary period. The sand dunes, composed of fine-grained, compact, and uniform sand, cover the entire region, reaching heights of up to 100 meters in the southern part. The region also features deepened plateaus known as Sahans, which are extensive and sometimes stony, with Quaternary gypsum deposits. Saline depressions, called Sebkha, are located in the northernmost part of Oued Souf Valley, occupying the lower part of the vast Saharan basin [254,258,292,293]. The Oued Souf region lies within the northeastern Mesozoic basin, also known as the Triassic basin, which is situated northeast of the Sahara platform. The region's geology comprises sediment formations ranging in age from the Lower Cretaceous to the Quaternary. The base of the sedimentary basin consists of water-rich marine formations from the Paleozoic era, overlain by layers that can extend over 2000 meters [255,294,295]. Despite the region's geology and geomorphology, the prevailing climatic conditions make the development of surface water resources challenging [278]. As a result, groundwater is the primary accessible water resource in the Souf region, serving various purposes [296]. Figure 4 provides a geological cross-section of the Oued Souf region.

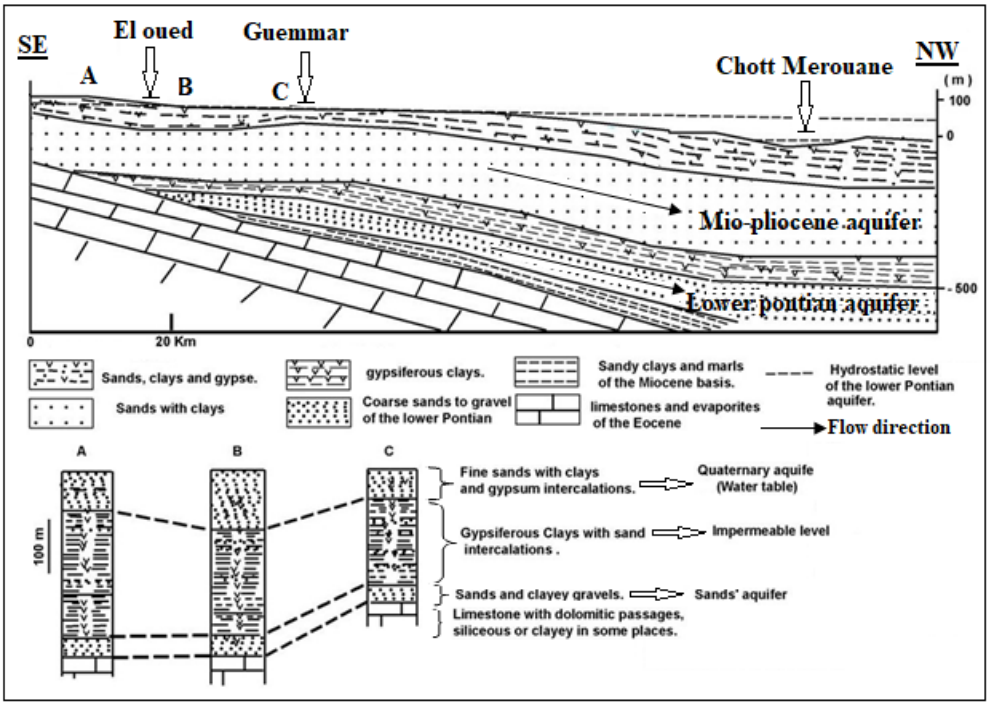

Figure 4. Geological cross-section of Oued souf valley, bottom: (A–C) are log correlation of Oued souf valley modified from [262].

3.1.2. Topography of Oued Souf Valley

Oued Souf Valley is part of the great eastern Erg, and its topographical nature is known as the lower Sahara region because of its low altitude. It is located in the Septentrional Sahara. Oued Souf Valley is characterized by a set of sand dunes of continental origin with an attitude that fluctuates from 64 to 100 meters [256]. However, the slope of the Oued Souf region is very low and oscillates between 0.03 and 0.16%, as shown in figure 5. The slope of the region is generally oriented South-North, with depressions in the city center of El-Oued.

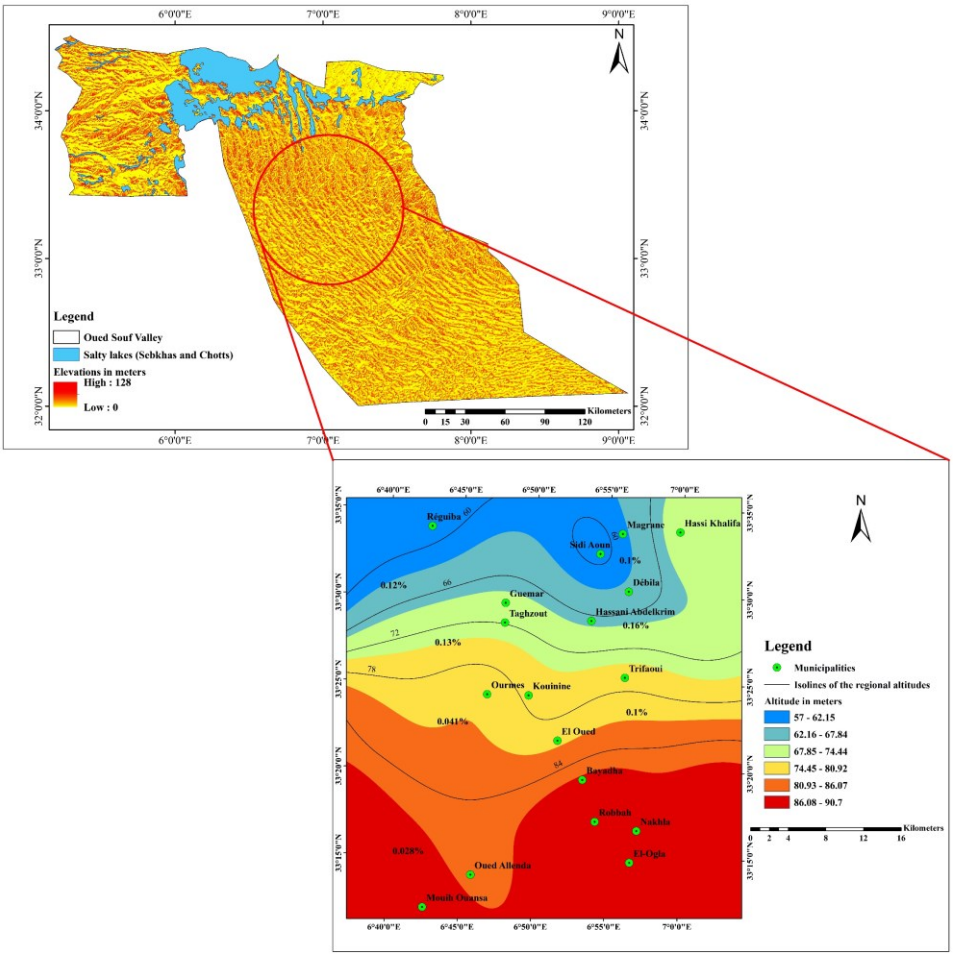

Figure 5. Integrated Topographic and Relief Map of Oued Souf region.

However, Oued Souf Valley as a term does not imply the existence of a stream of water but aims to characterize a depression where the vegetation, although thin. Hence, it can distinguish three relief forms in the Oued Souf region according to [247] such as Sahanes, Erg, and Sebkhas. The relief of Oued Souf presents itself under a double aspect, the Erg and the Sahane, in a sandy region. A form of rocky plateaus, which extends to the south with alternating dunes and rocky ridges.

- A zone of depression, characterized by the presence of a multitude of chotts which dip towards the East.
- In the South of Souf, one encounters immense and well-differentiated dunes, sometimes reaching 200 m in height; they are called the Ghroudes.

The fundamental difference to be made in the topography of the Souf is that which exists between the Erg and Sahane is that the Erg is a region where the sand accumulates in dunes; this is the most important part, it occupies 3/4 of the total surface, is relatively thick, always of the order of several tens of meters, and the

recent sinkings of wells showed a thickness a little greater than one thought 70–80 m in the southern part of Souf, 60 m at the place of El-Oued, it thins out gradually towards the north of the Souf at 30 m, and is no more than a cover at the level of the Sebkhas. It rests on impermeable clayey bedrock from the Pliocene. While, the Sahane is a flat and depressed region, sometimes stony, forming closed depressions surrounded by dunes, at the bottom of which, a few rare plants grow on a gypsum crust. However, the Sebkhas are formed When water evaporates under the effect of heat, patches of various salts are deposited on the surface forming according to the origin of their waters (phreatic or surface) the chotts and the sebkhas [297,298].

In another perspective, Sabkha is a basin occupying the bottom of a depression with high salinity and more or less separated from a marine environment, in arid regions. Nevertheless, it may still be in contact with the marine environment through a very small trickle of water (deep water basin), or on the contrary through seepage (shallow water basins). In the latter case, there may be periodic overflows of water to the basin. In both cases there will be an increase in salinity, significant evaporation, the appearance of brine and the precipitation of evaporites at the bottom of the basin if the depth is shallow, or at one end if the depth is significant [299].

3.1.3. . Agricultural and industrial activities in Oued Souf Valley

The agricultural sector is currently experiencing a boom in the Oued Souf region. Encouraging outcomes have been consistently documented over the past few decades, making Oued Souf one of the richest agricultural regions on a national scale. Agricultural activities are spread throughout the entire region, as illustrated in figure 6, indicating their dominant presence. Furthermore, Oued Souf has a total utilized agricultural area of 1,759,876 hectares of grassland that is distributed into several categories,as shown in table 1.

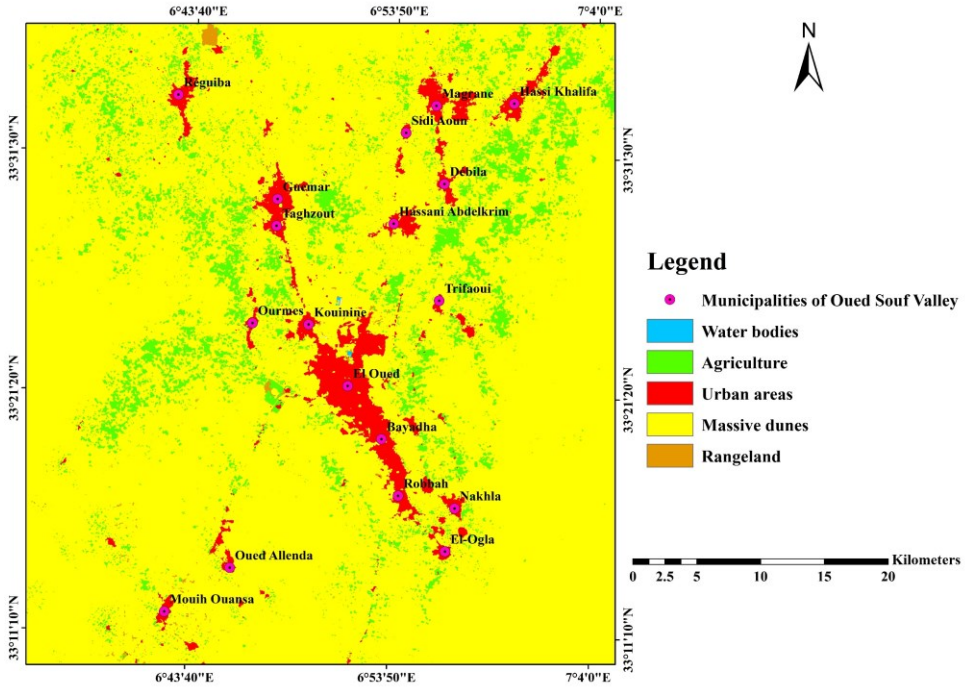

Figure 6. Land cover map of Oued Souf Valley.

Table 1. Distribution of the surface areas of land used for agriculture in Oued Souf Valley [300].

Characteristics of agricultural land	Areas in (Ha)
herbaceous crops	47 379
Fallow land	7 300
Natural grasslands	0
Vineyards	223
Fruit tree plantations	41 574
Pastures	1 410 000
Unproductive land	253 400

Phoeniciculture, referring to the cultivation of date palms, is practiced in the Saharan Ghouts, which represent a culturally significant environment of exceptional beauty and have contributed to the creation of unique landscapes in Oued Souf region [246].

The Ghout system, as a method for date production and palm tree cultivation, involves the creation of large craters dug by hand, where the palm trees are planted. Additionally, this cultivation method takes advantage of capillary action, allowing water from the phreatic aquifer to naturally rise to the roots of the date palms. This innovative approach enables farmers to avoid the expense of using traditional

irrigation systems [280]. Figure 7 illustrates the Ghout system of Oued Souf Valley.

Several types of Ghout systems exist in the Oued Souf region, depending on the soil type and the direction of the sand-carrying winds. These include circular Ghouts [301], elongated Ghouts [252], and rectangular Ghouts [302].

Figure 7. An example of the Ghout system in Oued Souf Valley.

The boundaries of the Ghouts reach the Libyan border to the south and border the Nemamchas Mountains, following a line that passes through Negrine, extends eastward to the Tunisian border, and westward to the vast oasis of Oued Righ [302].

Since the 1990s, the agricultural sector in the Souf region has experienced a significant shift in its agricultural practices, mainly due to the introduction of a new element in the Soufi landscape called the mini-pivot. Supported by the State and driven by the commitment of farmers in a participatory approach, the Saharan zone of Oued Souf has now become the country's leading region for potato production. Presently, the utilization of the mini-pivot irrigation technique is expanding throughout the Oued Souf Valley as the Ghout system [303]. As the specific utilization of fertilizers in Oued Souf is totaly related to the local agricultural practices, soil composition, crop types, and farmer preferences. However, several type of them are used in Oued Souf such as:

- Nitrogen-based fertilizers: These fertilizers contain nitrogen in various forms, such as ammonium nitrate, urea, or ammonium sulfate. They help promote leafy growth and overall plant development [304].

- Phosphorus-based fertilizers: These fertilizers provide plants with phosphorus, an essential nutrient for root development, flowering, and fruiting. Examples include superphosphate and rock phosphate [305].
- Potassium-based fertilizers: Potassium fertilizers, like potassium chloride or potassium sulfate, supply plants with potassium, which aids in overall plant health, disease resistance, and fruit quality [306].
- Organic fertilizers: These fertilizers are derived from natural sources, such as compost, manure, or plant residues. They enrich the soil with organic matter and provide a range of nutrients beneficial for plant growth [307].

Table 2. Main industries in the activity zones in Oued Souf.

Municipality	Activity field
El oued	Industrial chemistry, and food and construction materials
Kouinine	Construction materials, steel transformation and metallurgy, textiles and clothing, leathers and derived products, and industrial chemistry
Bayadha	Food and construction materials, steel transformation and metallurgy, hydraulic binders, industrial chemistry, and electrical and appliance industries
Hassi khalifa	Steel transformation and metallurgy, construction materials, and industrial chemistry
Hassani abdelkarim	Mechanical and automotive sectors, construction, and food industry
Megran	mechanical and automotive sectors, construction, and food industry
Djamaa	Mechanical and automotive sectors, construction, and food industry
Meghaiar	Mechanical and automotive sectors, construction, and food industry
Oued alenda	Electrical and appliance industries, and food industry

The industries in Oued Souf encompass various sectors, making this region one of the most significant poles of Algerian industries. However, all the existing industries in the Oued Souf Valley are spread across nine municipalities. These industries include industrial chemistry, food and construction materials, steel transformation and metallurgy, textiles and clothing, leathers and derived products, hydraulic binders, electrical and appliance industries, and mechanical and automotive sectors, as shown in table 2 [308]. Furthermore, the mining industry represents one of the most notable sectors in Oued Souf. Annually, it produces 78500 tonnes of salt from the Chotts, 5500 m^3 of sand for construction purposes, and 18930 m^3 of volcanic tuff.

3.2. Data collection, sampling and analysis

To achieve the core purpose of this thesis, several study areas have been selected based on the aquifer subject to analysis and the available data from the phreatic aquifer, the complex terminal aquifer, and the continental intercalary groundwater aquifers.

3.2.1. Analysis of the phreatic groundwater aquifer

3.2.1.1. Analysis of the phreatic groundwater level fluctuations

Research was conducted to evaluate the spatial distribution and temporal variations of the phreatic groundwater level in Oued Souf Valley. This study involved 58 monitoring wells that form part of the vertical drainage system. Among these wells, 55 are situated in El Oued, while the remaining three are located northwest of Bayadha, as illustrated in figure 8.

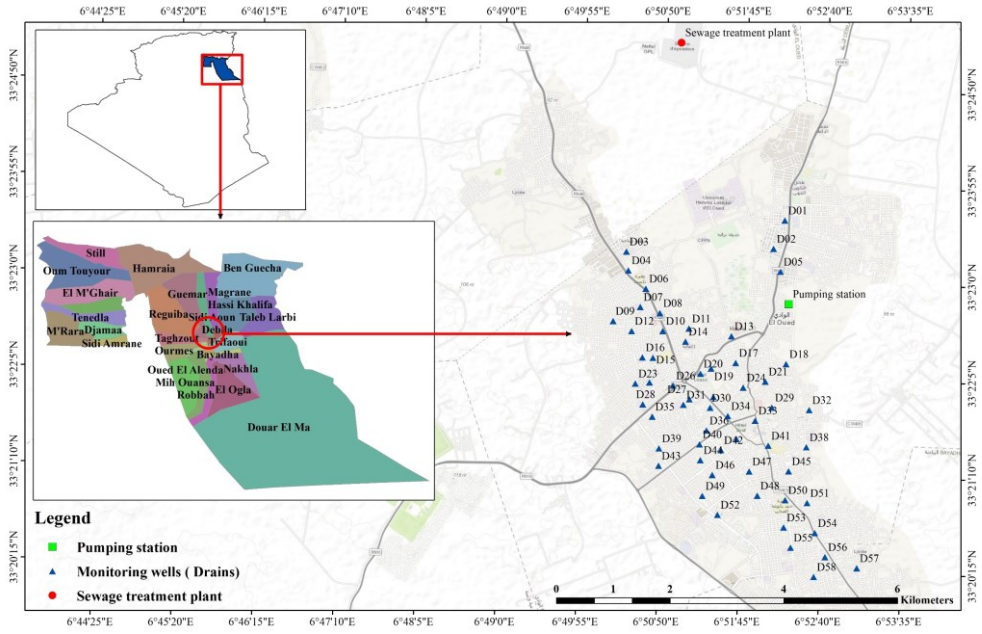

Figure 8. Location map of the study area exemplifying the distribution of the monitoring wells (drains of the vertical drainage system).

Groundwater level measurements were taken in different years, specifically in 2008, 2009, 2014, 2016, and 2018, by ANRH (Agence National des Rous sources Hydrauliques- National Agency for Water Resources) and ONA (Office National de l'Assainissement- National Sanitation Office). Additionally, data from 2021 was obtained through sampling conducted by the authors of this thesis. To ensure consistency and avoid seasonal fluctuations, all groundwater level measurements

were performed in May of each year. The depth measurements of the groundwater were collected from the ground surface using level probes and piezometers installed in each drain throughout the entire system. To minimize interference, the measurements were taken either before or after the pumping phase, allowing enough time for the groundwater level to return to its static state. Concurrently, the water flow and volumes were measured. Moreover, the geographical coordinates of these monitoring wells were determined using a Globe Positioning System (GPS).

3.2.1.2. Analysis of the physicochemical and bacteriological proprieties of the phreatic groundwater aquifer

The physicochemical and bacteriological assessment of the phreatic groundwater aquifer in the Oued Souf Valley was conducted using twenty-eight samples (22 samples from the vertical drainage system, and six samples were collected from agricultural and peri-urban areas) as shown in figure 9. The sampling area included El Oued, Bayadha, Debila, and Guemar. The sampling took place in October 2021, while all the analyses were performed in the Laboratory of Geology and Environment at the University of Constantine (Université Frères Mentouri Constantine). Temperature (T), pH, electrical conductivity (EC), and total dissolved solids (TDS) were measured on-site using a Multi–350 i multi-parameter device, while the remaining analyses were conducted using the methods of [309]. Figures 10 and 11 illustrate the practical work of the phreatic groundwater aquifer.

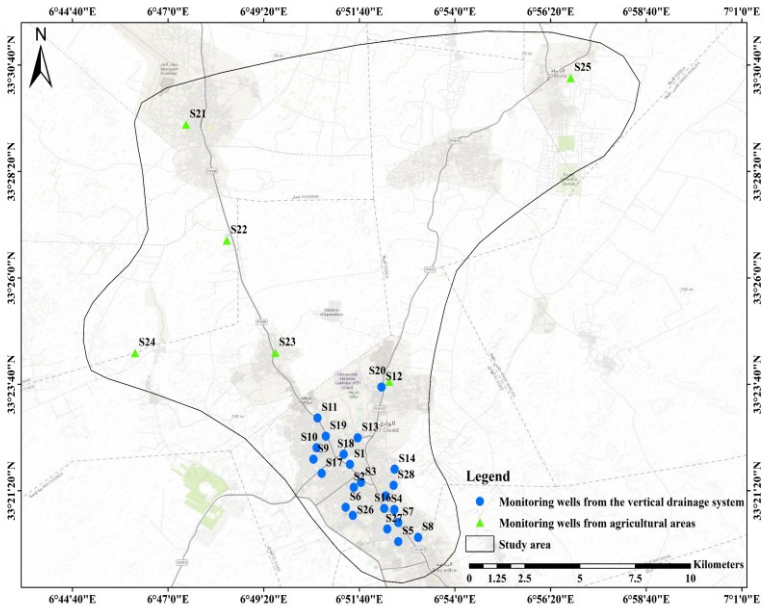

Figure 9. Spatial distribution map of the samples from the phreatic groundwater aquifer.

Figure 10. Pictures of the sampling and the on-site analysis.

Figure 11. Pictures of the lab work.

3.2.1.3. Analysis of the heavy metals in the phreatic groundwater aquifer

A research study was conducted to evaluate the presence of heavy metals in the phreatic groundwater aquifer. In November 2022, a total of 14 groundwater samples were gathered from this aquifer. Of these, 12 samples were acquired from the vertical drainage system primarily situated in the El Oued municipality, while one sample was taken from the Bayadha municipality. Additionally, two samples were collected from agricultural areas, specifically from Kouinine and Ourmes, as illustrated in figure 12. Physical parameters such as temperature, electrical conductivity, and pH were measured on-site using a Multi-350 i multi-parameters device. Subsequently, all samples were treated with 37% hydrochloric acid and transported to Hungary for comprehensive heavy metal analysis at the Laboratory of the Inorganic and Analytical Chemistry Department in Debrecen. The quantitative analysis of the elemental composition of the samples was carried out using microwave plasma atomic emission spectrometry (MP-AES 4200, Agilent Technologies). A continuous supply of plasma gas was ensured by a nitrogen generator (Agilent Technologies 4107) during the measurements. The MP-AES instrument featured a vertical torch alignment and an axial observation position. Both standard and sample solutions were introduced using an autosampler (SPS, Agilent Technologies), with a 30-second rinsing period between each sample using a 0.1 M HNO_3 solution prepared with ultrapure water. For the macro elements (Al^{3+}, Ca^{2+}, Fe^{2+}, K^{+}, Mg^{2+}, Mn^{2+}, and Na^{+}), standard solutions were prepared from the mono-element spectroscopic standard with a concentration of 1000 mg/L (Scharlau). Meanwhile, solutions for the micro elements (B^{3+}, Ba^{2+}, Bi^{3+}, Cd^{2+}, Co^{2+}, Cu^{2+}, Cr^{3+}, Li^{+}, Ni^{2+}, Pb^{2+}, Sr^{2+}, and Zn^{2+}) were prepared from the multi-element spectroscopic standard solution with a concentration of 1000 mg/L (ICP IV, Merck). In both cases, a 5-point calibration process was employed, where standard solutions were diluted using 0.1 M HNO_3 prepared with ultrapure water.

Additionally, the limit of detection (LoD) for the MP-AES method was determined following the procedure outlined in [310], a method that had been previously validated and confirmed to be appropriate.

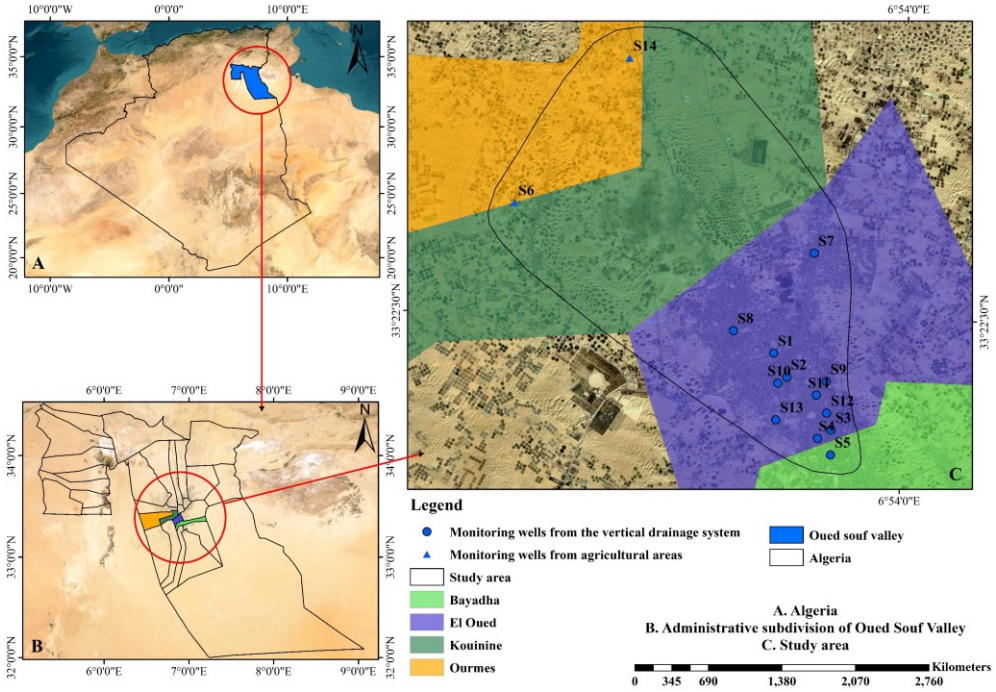

Figure 12. Study area maps illustrating the geographical distribution of the monitoring well.

3.2.2. Analysis of the deep aquifers

3.2.2.1. Analysis of the physicochemical and bacteriological proprieties of the complex terminal and the continental intercalary groundwater aquifers

To assess the complex terminal groundwater aquifer in the Oued Souf region, a total of forty-nine (49) groundwater samples were collected during March 2019 by the ANRH and Algerian of water company- Unity of El Oued (ADE- Algerriene des eaux- Unite d' El Oued). The sampling locations included El Oued, Debila, Guemar, Kouinine, Ourmas, Reguiba, and Taghzout, covering both Mio-Pliocene and Pontian aquifers. These wells are utilized for drinking and irrigation uses. Furthermore, another assessment of the deepest aquifer (the continental intercalary) has been conducted using three wells located in El Oued municipality. The utilization of three wells are for drinknig puposes, and they were used to assess the deepest aquifer is due to the shortage of the data from ANRH and Algerian of water company- Unity of El Oued (ADE- Algerriene des eaux- Unite d' El Oued). Figure 13, illustrates the spatial distribution of the analzyed samples from the complex terminal and the continental intercalary groundwater aquifers.

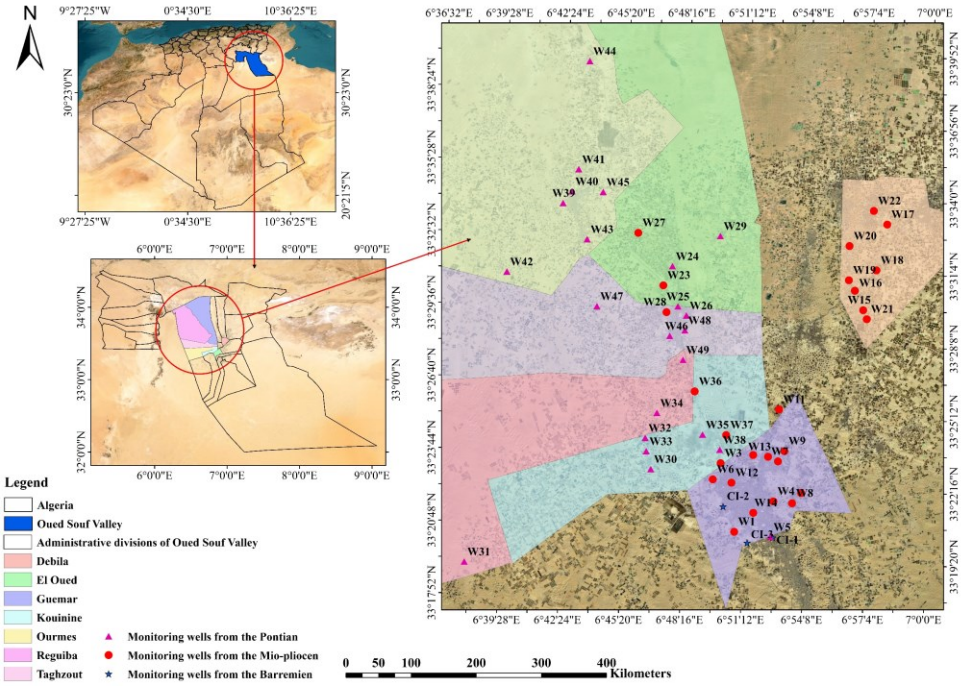

Figure 13. Location map of the study area illustrating the distribution of the monitoring wells from the complex terminal groundwater aquifer.

During the sampling process in March 2019, the groundwater was pumped briefly into polyethylene bottles for analysis. On-site measurements were taken for physical parameters like temperature, EC, and pH using a Multi–350 i multi-parameters device. For chemical analysis, elements such as Cl^- (chloride), HCO_3^- (bicarbonate), SO_4^{2-} (sulfate), Ca^{2+} (calcium), Mg^{2+} (magnesium), Na^+ (sodium), K^+ (potassium), and NO_3^- (nitrate) were analyzed using volumetry, UV-visible spectrometry, and flame spectrophotometry [309]. Table 3, summerize all informations about the number of the samples collected from each aquifer, location, dates, and the tape of the conducted analysis.

Table 3. Summary of the collected data used in this thesis

Aquifers	layers	samples	Date	Collector	Location	Utilization	Analysis
Phreatic aquifer	Quaternary	58	Oct 2021, May 2008, 2009, 2014, 2016, and 2018	Author/ANRH / ONA	El Oued, Bayadha	Irrigation of green spaces /pumping to the discharge site after being treated	Reading the static depth measurements
		28	Oct2021	Author	El Oued, Bayadha, Debila, and Guemar	Crops irrigation, and irrigation of green spaces/ pumping into the discharge site after being treated	Physicochemical/ bacteriological
		14	Nov 2022	Author	El Oued, Bayadha, Kouinine and Ourmes.	Crops irrigation/ irrigation of green spaces and pumped into the discharge site after being treated	Physicochemical/ (Heavy metals)
Complex terminal	Mio-Pliocene and Pontian	49	May 2019	ANRH/ ADE	El Oued, Debila, Guemar, Kouinine, Ourmas, Reguiba, and Taghzout	Drinking, and irrigation	Physicochemical/ bacteriological
	Mio pliocene, Pontian, and Lower	10	May 2012, 2014, 2015, 2016, 2017, 2018, 2019, and 2020	ANRH/ ADE	El Oued	Drinking, and irrigation	Physicochemical
Continental intercalary	Barremien	3	Mar2019	ANRH/ ADE	El Oued	Drinking	Physicochemical/ bacteriological
		3	May 2012, 2014, 2015, 2017, 2018, 2019, 2020, and 2021	ANRH/ ADE	El Oued	Drinking	Physicochemical

To validate the analytical results, charge balance errors (%E) were calculated, and they were found to be less than 5% with a negative value, indicating the

dominance of anions in the groundwater samples [12,127]. Additionally, ANRH conducted microbiological analyses, including parameters like total germs, total and fecal coliforms, fecal streptococci, and sulphite-reducing Clostridium, with different areas of cultivation.

3.2.2.2. Analysis of the temporal changes of the complex terminal and the continental intercalary groundwater aquifers

A comparative study of hydrochemical parameters in the complex terminal groundwater aquifer was conducted based on data from ten wells in El Oued municipality during 2012, 2014, 2015, 2016, 2017, 2018, 2019, and 2020, which were obtained from the ANRH and the Algerian Water Company - Unity of El Oued (ADE - Algerienne des Eaux). The spatial distribution of the complex terminal groundwater wells used in this comparison is represented in figure 14. Out of the ten wells used for comparison, eight wells belong to the Mio pliocene layer, one represents the Pontian, and another one the Lower Eocene. Meanwhile, another comparative study was conducted to analyze the temporal variation of the continental intercalary groundwater aquifer using hydrochemical data from 2012, 2014, 2015, 2017, 2018, 2019, 2020, and 2021, also obtained from the ANRH and the Algerian Water Company - Unity of El Oued (ADE - Algerienne des Eaux).

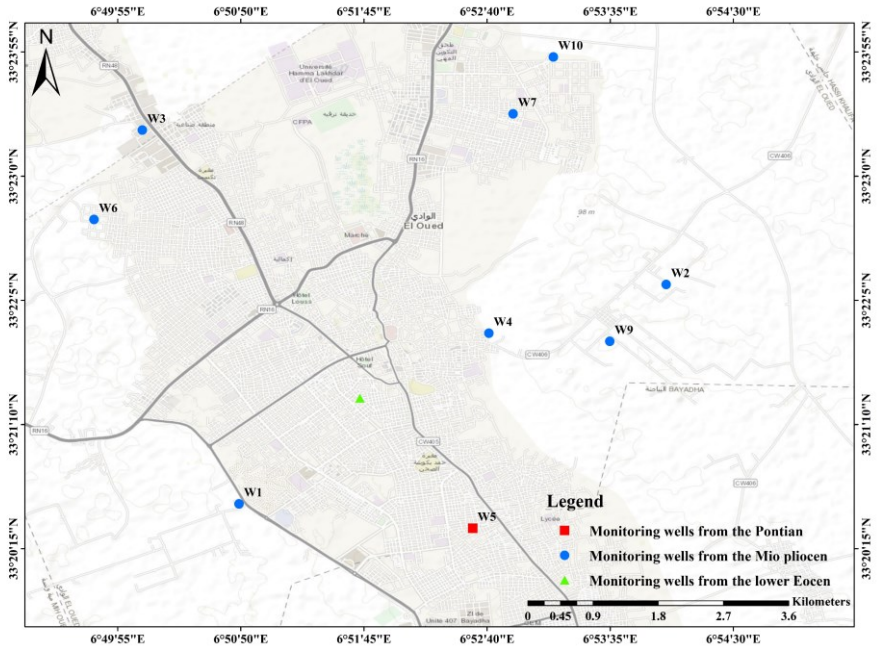

Figure 14. Spatial distribution map of the monitoring wells for temporal variation of the complex terminal groundwater aquifer.

3.3. Adopted methodology for quantitative and qualitative assessment of water resources in Oued Souf Valley

3.3.1. Statistical methods

In this thesis, hierarchical clustering analysis was conducted on each hydrochemical study of every aquifer within the entire Northwest Sahara Aquifer System of Oued Souf Valley. Q-mode, Ward's linkage, and Euclidean distance techniques were employed for this analysis. The purpose of this method was to group the groundwater samples analyzed in the laboratories and the groundwater level (static depth) to elaborate on the differences based on their similarity and identify any potential spatial patterns [311]. The hierarchical clustering analysis was performed using Origin Pro 2021 and IBM-SPSS Statistics version 26 software.

3.3.2. Hydrogeochemical methods

In this thesis, the hydrogeochemical characterization of the phreatic aquifer, complex terminal, and the continental intercalary was performed through the graphical representation of the groundwater chemistry of each aquifer system intended for the study using Stiff plot, Piper plot, Chadha plot, and Gibbs plot throughout Grapher-Golden and Diagrammes software.

Regarding the geochemical analysis of the aquifer systems, saturation indices [312], and mineral stability diagrams [313] were used in this thesis, as well as several molar ratios, such as the molar ratio in bivariate plots of Na^+-normalized Ca^{2+} and HCO_3^-, and Na^+-normalized Ca^{2+} and Mg^{2+} [118].

Chemical reactions and the determination of aqueous speciation within aquifer systems can be accomplished by assessing the equilibrium state between groundwater and existing minerals, with a particular focus on the saturation index (SI) [312]. The saturation index was calculated using the following equation:

$$SI = \mathrm{Log}\left(\frac{IAP}{K_t}\right) \qquad (1)$$

The saturation index (SI) reflects the state of a mineral, with IAP representing the ion activity product of the dissociated mineral and Kt indicating the equilibrium solubility at the mineral's temperature. If SI < 0 for a specific mineral, it suggests that the groundwater is under-saturated regarding that mineral, indicating conditions conducive to mineral dissolution. Conversely, SI > 0 indicates oversaturation of a mineral, suggesting conditions favorable for mineral precipitation. An SI value of 0 denotes an equilibrium state, where the groundwater is in balance with the mineral's solubility. On the other hand, Chloralkaline indices are one of the most used methods to comprehend the occurrence of cation exchange processes in the aquifer system, utilizing equations proposed by [314]. All chemical parameters were measured in meq/L.

$$CAI - I = \frac{Cl-(Na+K)}{Cl} \qquad (2)$$

$$CAI - II = \frac{Cl-(Na+K)}{SO_4+HCO_3+CO_3+NO_3} \qquad (3)$$

3.3.3. Indexing methods

3.3.3.1. Assessment of groundwater suitability for drinking purposes

For the assessment of the groundwater samples collected from each aquifer of the Northwest Sahara Aquifer system, the water quality index proposed by [143] was applied. The water quality index was calculated using the following formula:

$$WQI = \frac{\sum_{i=1}^{n} Q_i W_i}{\sum_{i=1}^{n} W_i} \qquad (4)$$

The quality rating for the i^{th} parameter is represented as Q_i, and each parameter is assigned a weight (W_{unit}) equal to the reciprocal of the total number of parameters (n).

$$Q_i = \left[\frac{V_i V_0}{S_i V_0}\right] \qquad (5)$$

In this given context, V_i represents the observed value of the ith parameter, while V_0 denotes the ideal value for that specific parameter in pure water. For all parameters except pH, V_0 is set to zero. Specifically, for pH, V_0 is established at 7. Additionally, S_i refers to the standard permissible value for the ith parameter. The determination of the unit weight, W_i, follows an inverse relationship with the standard permissible value, S_i, associated with water quality parameters. In simpler terms, as the standard permissible value decreases, the unit weight assigned to the parameter increases, and vice versa. This ensures that parameters with lower permissible values carry greater importance in the overall water quality index.

$$W_i = \frac{K}{S_i} \qquad (6)$$

The constant K serves as the proportionality factor, regulating the adjustment of unit weights (W_i) to establish their inverse correlation with the standard permissible values (S_i) for water quality parameters. This ensures that the unit weights properly reflect the importance of each parameter in determining the water quality index.

$$K = \frac{1}{\sum_{i=1}^{n} \frac{1}{S}} \qquad (7)$$

The threshholds values of this index are presented in table 4:

Table 4. Threshholds of drinking water quality index.

Range of drinking water quality index	Classes
<50	Excellent water
100.0-125.0	Good water
125.1-150.0	Poor water
150.1-175.0	Very poor water
175.1-200.0	Unfit for drinking

3.3.3.2. Assessment of groundwater suitability for irrigation purposes

For assessing the groundwater samples collected from the Phreatic, Complex Terminal, and Continental Intercalary groundwater aquifers for irrigation usage in this thesis, the following indices were used: PI, Kr, RSC, PS, RBSC, ESP, Ka, synthetic harmful coefficient (k), % Na, SAR, TH, and MH. The application of these indices was performed using different ionic parameters in meq/L. All these indices can be calculated using the following equations:

$$\mathrm{ESP} = \frac{100(-0.0126+0.01475\ \mathrm{SAR})}{1+(-0.0126+0.01475\ \mathrm{SAR})} \quad (8)$$

$$\mathrm{TH} = 2.5 \times \mathrm{Ca} + 4.1 \times \mathrm{Mg} \quad (9)$$

$$\%\mathrm{Na} = 100 \times \frac{\mathrm{Na+K}}{\mathrm{Ca+Mg+Na+K}} \quad (10)$$

$$\mathrm{SAR} = \frac{\mathrm{Na}}{\sqrt{\frac{\mathrm{Ca+Mg}}{2}}} \quad (11)$$

$$\mathrm{PI} = 100 \times \frac{\mathrm{Na}+\sqrt{\mathrm{HCO_3}}}{\mathrm{Na+Mg+Ca}} \quad (12)$$

$$\mathrm{KR} = \frac{\mathrm{Na}}{\mathrm{Ca+Mg}} \quad (13)$$

$$\mathrm{RSC} = (\mathrm{HCO_3} + \mathrm{CO_3}) - (\mathrm{Ca} + \mathrm{Mg}) \quad (14)$$

$$\mathrm{MH} = \frac{\mathrm{Mg}}{\mathrm{Ca+Mg}} \quad (15)$$

$$\mathrm{PS} = \mathrm{Cl} + \frac{1}{2}\mathrm{SO_4} \quad (16)$$

$$\mathrm{RBSC} = \mathrm{HCO_3} - \mathrm{Ca} \quad (17)$$

$$\mathrm{K} = 12.4 \times \mathrm{M} + \mathrm{SAR} \quad (18)$$

$$\mathrm{Ka} = \begin{cases} \frac{288}{5\mathrm{Cl}} \; if \; Na < Cl \\ \frac{288}{\mathrm{Na}+4\mathrm{Cl}} \; if \; Cl < Na < Cl + \mathrm{SO_4} \\ \frac{288}{10\,\mathrm{Na}-5\mathrm{Cl}-9\mathrm{SO_4}} \; if \; Na > Cl + 2\mathrm{SO_4} \end{cases} \qquad (19)$$

Meanwhile, the threshlods values of these indicies are illustrated in table 5:

Table 5. Threshhold values of irrigation water quality indicies.

Irrigation index	Range	Classes
Percent sodium (Na%)	< 20	Excellent
	20–40	Good
	40–60	Permissible
	60–80	Doubtful
	> 80	Unsafe
Alkalinity hazard (SAR)	< 10	Excellent
	10–18	Good
	18–26	Doubtful
	> 26	Unsuitable
Total hardness (TH)	< 75	Soft
	75–150	Moderately hard
	150–300	Hard
	> 300	Very hard
Magnesium hazard (MH)	< 50	Suitable
	> 50	Unsuitable
Permeability index (PI)	< 25	Suitable
	25–75	Moderate
	> 75	Unsuitable
Kelley ratio (KR)	< 1	Suitable
	1–2	Moderate
	> 2	Unsuitable
RSC	<1.25	Acceptble
	1.25-2.5	Slightly adapted to irrigation
	>2.5	Not suitible
Ps	< 3	Excellent to good
	> 3	Injurious to unsatisfactory
RBSC	< 5	Satisfactory
	5-10	Marginal
	> 10	Unsatisfactory
ESP	< 20	Excellent

	20- 40	Good
	40- 60	Permissible
	60- 80	Doubtful
	> 80	Unsuitable
Ka	> 18	Excellent
	18-6	Permissible
	1.2- 6	Doubtful
	< 1.2	Unsuitable
Synthetic harmful coefficient (K)	< 25	Excellent
	26–36	Good
	37–44	Injurious
	> 44	Unsuitable

3.3.3.3. Groundwater pollution assessment

The assessment of the pollution level in the groundwater aquifer systems of Oued Souf Valley in this thesis was applied throuhgt several water quality pollution indicies such as the National Sanitation Foundation water quality index (NSFWQI), Groundwater pollution index (GPI), and Nitrate pollution index (NPI). NSFWQI was computed using the following equation:

$$\mathrm{NSFWQI} = \frac{\sum_{i=1}^{n} W_i Q_i}{\sum_{i=1}^{n} W_i} \qquad (20)$$

In this equation, Q_i represents the sub-index for parameter i, W_i is the weight coefficient corresponding to parameter i, and n is the total number of water quality parameters [161].

Furthermore, GPI was used in this thesis along with the NSFWQI. Whereas, GPI assesses the relative impact of individual chemical variables, namely pH, TDS, TH, Ca^{2+}, Mg^{2+}, Na^{+}, K^{+}, Cl^{-}, SO_4^{2-}, NO_3^{-}, and F^{-}, on the overall quality of groundwater intended for drinking purposes. This index was determined based on the following steps:

- Relative Weight Assignment (RW): Each chemical parameter is assigned a relative weight (RW) ranging from 1 to 5 based on its impact on water quality. The highest RW of "5" is assigned to parameters with the most significant effects (NO_3^{-}, F^{-}, SO_4^{2-}, and Cl^{-}), while a minimum RW of "1" is given to parameters with lesser effects (K^{+} and HCO_3^{-}). Additionally, RW of "4" is assigned to pH, TDS, Na^{+}, and TH, while "2" is assigned to Ca^{2+} and Mg^{2+}.

- Weight Parameter (WP): The weight parameter (WP) is calculated as the ratio of the RW of each chemical water quality measure to the sum of all relative weights [Σ(RW)].

- Status of Concentration (SOC): SOC is computed by dividing the concentration (Cn) of each chemical variable in a groundwater sample by its respective Drinking Water Quality Standards (DWQS).
- Overall Quality of Groundwater (OQG): OQG for drinking purposes is determined, where WP represents the weight parameter, and SOC signifies the status of concentration.
- Groundwater Pollution Index (GPI): To assess the overall influence of contaminants on groundwater quality, GPI is computed by summing all OQG values. The GPI is then categorized into five classes, namely insignificant pollution (GPI > 2.5) [175,315].

The groundwater pollution index can be computed by the following equations:

$$WP = \frac{RW}{\sum RW} \quad (21)$$

$$SOC = \frac{C_i^n}{DWQS} \quad (22)$$

$$OQG = WP \times SOC \quad (23)$$

$$GPI = \sum OQG \quad (24)$$

On the other hand, the contamination level of Nitrate in the studied groundwater aquifer system was applied using NPI which was calculated using the following formula:

$$NPI = \frac{C_s - HAV}{HAV} \quad (25)$$

C_s represents the measured concentration of nitrate in the sample, and HAV is the human acceptable value of nitrate, set at 20 mg/L.

The values used as the threshholds for the utilized irrigation index in this thesis are presented in table 6:

Table 6. Threshhold values of pollution water quality indicies.

Pollution index	Range	Classes
National Sanitation Foundation Water Quality Index	91- 100	Excellent
	71- 90	good
	51- 70	moderate
	26- 50	poor
	0- 25	very poor
Groundwater pollution index	< 1.0	Insignificant pollution
	1.0– 1.5	Low pollution
	1.5– 2.0	Moderate pollution
	2.0– 2.5	High pollution

	> 2.5	Very high pollution
Nitrate pollution index	< 0	clean
	0- 1	light pollution
	1-2	moderate pollution
	2-3	significant pollution
	> 3	Very significant

3.3.3.4. Environmental and human health risk assessment

In this thesis, two diffrent approeches have been conducted in order to evaluate the environmental and human health risk throught the application of a combinition of several indicies in both of the cases. Regarding the environmental assessment, contamination degree (C_{deg}), Geo-accumulation index (I_{geo}), enrichment factor (EF), Ecological Risk Assessment (ER) and the Potential Ecological Risk Index (PRI) were computed. Meanwhile, the human health risk assessment was conducted by the computation of the chronic daily intake (CDI), hazard quotient indicies (HQ_s), and the total hazard index (HI).

The calculation for C_{deg} can be done as follows:

$$C_{deg} = \sum_{i=1}^{n} C_{Fi} \qquad (26)$$

$$C_{Fi} = \frac{C_{Ai}}{C_{Ni}} - 1 \qquad (27)$$

Additionally, C_{Fi}, C_{Ai}, and C_{Ni} represent the contamination factors, analytical value, and maximum permissible concentration of the ith component, respectively, with N denoting the 'normative value.' According to the classification proposed by [185], the contamination degree can be categorized as low when $C_{Fi} < 1$, medium when $1 < C_{Fi} < 3$, and high when $C_{Fi} > 3$. Conversely, the results for contamination degree (C_{deg}) are classified using [316] scheme, with low ($C_{deg} < 8$), moderate ($8 \leq C_{deg} < 16$), considerable ($16 \leq C_{deg} < 32$), and high ($C_{deg} \geq 32$).

The I_{geo} model is expressed by the following equation:

$$I_{geo} = \log_2 \frac{C_{HMS}}{1.5 \times GBV} \qquad (28)$$

C_{HMS} refers to the concentration of the selected metals in the groundwater sample, while the geochemical background is represented by GBV, with the World Health Organization (WHO) serving as the reference in this research [317]. Additionally, a constant of 1.5 allows for the examination of natural fluctuations in the concentration of a specific substance present in the environment. The classification of I_{geo} indices can be as follows: uncontaminated ($I_{geo} \leq 0$), uncontaminated to moderately contaminated ($0 < I_{geo} < 1$), moderately contaminated (1 to 2), moderately to strongly contaminated (2 to 3), strongly contaminated (3 to 4), strongly to extremely contaminated (4 to 5), and extremely contaminated when $I_{geo} > 6$ [188,318].

In this investigation, iron (Fe) served as the reference metal for EF computation, which can be done using the following equation:

$$EF = \frac{(\frac{Ci_{Sample}}{Fe_{sample}})}{(\frac{Ci_{reference}}{Fe\ reference})} \qquad (29)$$

Where ($C_{i\ sample}/Fe_{\ sample}$) and ($C_{i\ reference}/Fe_{\ reference}$) denote the ratio of the metal to iron in the groundwater sample and the natural background, respectively [319]. According to the classification by [320], the enrichment factor (EF) falls into six classes: minor enrichment (EF between 1 and 2), moderate enrichment (EF between 3 and 5), intermediate enrichment (EF between 5 and 10), severe enrichment (EF between 10 and 25), very severe enrichment (EF between 25 and 50), and extremely severe enrichment (EF over 50). Analyzing the EF values allows for the identification of contamination sources attributed to heavy metals present in the aquatic system. Consequently, EF values exceeding 1.5 suggest anthropogenic sources [321], while those ranging between 0.5 and 1.5 imply lithogenic sources [322].

The Ecological Risk Index is formulated by integrating the Contamination Factor (CF) with the Toxic Reaction Factor (TR):

$$ER = TR_i \times CF_i \qquad (30)$$

Where TR_i represents the toxic reaction factor for the metal, and CF_i is the contamination factor. According to [316], the standardized TR_i values for Cu^{2+}, Pb^{2+}, Ni^{2+}, Cr^{3+}, Zn^{2+}, Fe^{2+}, and Mn^{2+} are 5, 5, 5, 2, 1, 1, and 1, respectively. However, no toxic response value has been identified for Al^{3+}, B^{3+}, Ba^{2+}, Bi^{3+}, and Sr^{2+} in the literature. On the other hand, the Potential Ecological Risk Index (PERI) can be computed by summing up the total Ecological Risks (ERs) of all heavy metals dissolved in the groundwater samples [323]:

$$PERI = \sum_{i=1}^{n} ER_i \qquad (31)$$

As per the classification by [324], the categorization of ER_i and PERI can be outlined as follows: ER less than 5 indicates a low risk, 5 or more but less than 10 suggests a moderate risk, 10 or more but less than 20 signifies a considerable risk, 20 or more but less than 40 indicates a high risk, and ER greater than 40 signifies a very high risk. For PERI, the categorization is as follows: low risk when PERI is less than 30, moderate when 30 or more but less than 60, considerable when 60 or more but less than 120, and high risk when PERI is equal to or greater than 120.

As per the United States Environmental Protection Agency (USEPA), the human health risk assessment entails identifying potential adverse health effects and human exposure to chemicals in a polluted environment [325]. Three potential exposure routes are considered: direct consumption of drinking water, inhalation of air, and absorption through the skin. These simulations can be employed to calculate the dosage [326–328]:

$$\mathrm{CDI} = \frac{\mathrm{CW}\times\mathrm{IR}\times\mathrm{EF}\times\mathrm{ED}}{\mathrm{BW}\times\mathrm{WT}} \qquad (32)$$

The chronic daily intake to which a person may be exposed is known as the Chronic Daily Intake (CDI), measured in (mg/kg/day). The concentration of the selected metals in the groundwater samples is denoted as the Concentration in Water (CW), measured in (mg/l). Additionally, IR represents the ingestion rate in (L/day), EF signifies the exposure frequency in days per year, ED refers to "Exposure Duration" in years, Bodyweight (BW) is given in kilograms (kg), and (AT) is the averaging time [329,330]. The hazard quotient (HQ) for non-carcinogenic risk can be estimated as follows [331]:

$$\mathrm{HQ} = \frac{\mathrm{CDI}}{\mathrm{RFD}} \qquad (33)$$

The oral toxicity reference dose value (RFD), serving as a reference dose, signifies the daily dosage that an individual can endure at a particular level of exposure for an extended period without experiencing adverse effects, expressed in (µg/kg/day). Considering multiple toxicants, interactions are taken into account. It is assumed that the toxic risks associated with potentially hazardous substances found in the same media are cumulative. The hazard index (HI) is formed by adding all the Hazard Quotients (HQs) together collectively [332]:

$$\mathrm{HI} = \sum_{i=1}^{n} \mathrm{HQ_i} \qquad (34)$$

The non-cancer toxicity risk is considered low when both the Total Hazard Quotient (HQ) and Hazard Index (HI) values are less than 1. However, if these values exceed 1, there is a potential for health issues to arise.

In this thesis, the environmental hazards assessment of heavy metals in the phreatic groundwater aquifer, several indices were used, including the Contamination degree [185], the Geoaccumulation index (I_{geo}) [188], Enrichment factor (EF) [319], and Potential ecological risk index (PER) [324]. On the other hand, a human health risk assessment study was conducted to predict the probability and extent of hazards posed by certain activities to both human and ecosystem health over time, using the chronic risk level (chronic daily intake-CDI), hazard quotient (HQ), and hazard index (HI) indices [331]. However, for performing the human health risk assessment, the RFD values in (µg/kg/day) for Cr^{3+}, Cu^{2+}, Ni^{2+}, Pb^{2+}, Sr^{2+}, and Zn^{2+} were 3, 40, 20, 3.6, 600, and 300, respectively [333]. The considered RFD value for B was 300 (µg/kg/day) [334], while the RFD value for Fe^{2+} was considered to be 700 (µg/kg/day) [335]. In the case of Mn^{2+} and Ba^{2+}, RFD values of 24 and 200 (µg/kg/day) were considered, respectively [336]. Additionally, Al^{3+} had an RFD value of 700 (µg/kg/day) taken into consideration [337].

3.3.4. Spatial analysis and the interpolation techniques

For predicting the spatial propagation of the chemical element as well as groundwater level in the studies areas of this thesis, geostatistical modeling was used through the ordinary kriging interpolation method [209] for assessing the

phreatic groundwater level and the physicochemical elements in the phreatic groundwater aquifer complex terminal. Regarding the heavy metals, the IDW interpolation method [211] has been used due to the limited obtained samples. Additionally, to streamline the process of IDW interpolation, various simplifications and assumptions were applied. These included assuming a smooth neighborhood type, setting the smoothing factor to 1, assuming an angle of 0°, and considering the minor semi-axes as equal to the major semi-axes. On the other hand, to select the best-fitted model in both of the methods, the mean error (ME) and root mean square standardized error (RMSSE) values were considered [338].

In this thesis all the interpolation techniques were performed using ArcGIS 10.8 version.

4. Results and discussion

4.1. The Phreratic groundwater aquifer analysis

4.1.1. Assessment of Spatial Distribution and Temporal Variations of the Phreatic groundwater aquifer

4.1.1.1. Application of hierarchical clustering approach for grouping the phreatic groundwater levels

The Q-mode hierarchical clustering analysis was utilized to classify the monitoring wells (drains) from multiple years (2008, 2009, 2014, 2016, 2018, and 2021) based on their fluctuation variability. This classification was performed using Ward's linkage technique and Euclidean distance. Hierarchical clustering is a significant statistical method that assigns each case to a unique group or cluster and progressively links these clusters until only one cluster remains. By applying Hierarchical Clustering Analysis (HCA), a dendrogram representing spatial hierarchical clustering has been generated. The analysis resulted in the formation of four distinct groups, as shown in figure 15. The mean value within each group played a pivotal role in differentiating and classifying these groups. Notably, the mean values increase progressively from the first group to the fourth group, as presented in table 7.

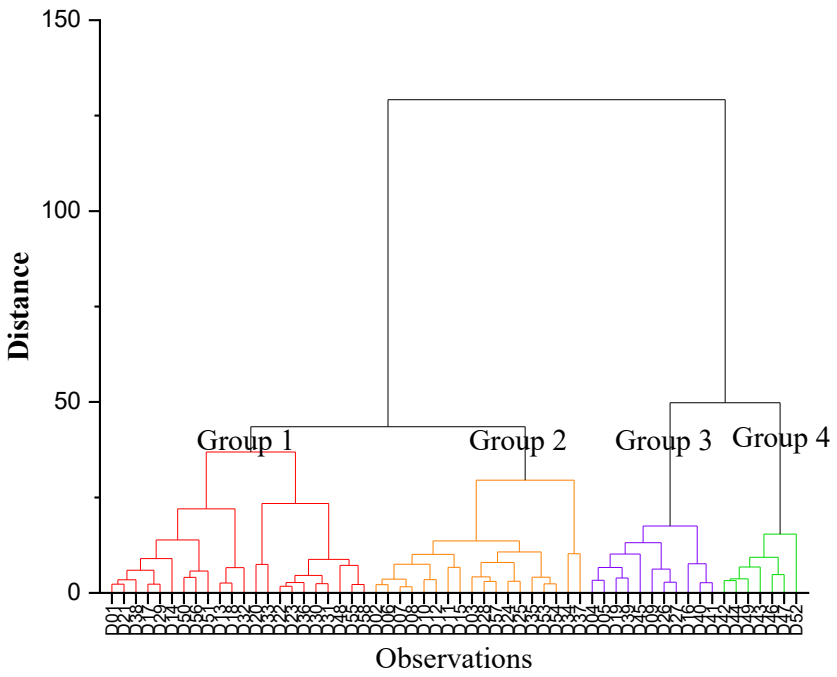

Figure 15. Dendrogram of the clustered groundwater level over the studied years.

Table 7. Statistical summary of the four main groundwater levels recorded from the drainage system in the studied period grouped by HCA.

Groups	Years	2008	2009	2014	2016	2018	2021	Mean
Group 1	N total	22	22	22	22	22	22	5.91
	Min	−0.3	−0.4	0.6	1	5.1	2.1	
	Mean	2.99	2.64	5.6	6.43	11.44	6.37	
	Max	5.92	5.46	10.36	14.48	15.8	9.5	
	Standard deviation	1.69	1.53	2.45	3.77	3.01	2.48	
Group 2	N total	18	18	18	18	18	18	7.74
	Min	2.22	2.16	4.9	1.11	10.44	8.4	
	Mean	4.62	4.34	7.18	4.95	14.31	11.07	
	Max	7.13	7.04	12.61	7.63	28.8	15	
	Standard deviation	1.43	1.3	1.74	1.94	4.51	1.74	
Group 3	N total	18	18	18	18	18	18	9.31
	Min	4.49	4.05	7.31	7.22	7.8	6.2	
	Mean	7.19	6.9	9.91	10.62	10.96	10.31	
	Max	11.3	10.51	14.02	15.1	14.4	15	
	Standard deviation	1.84	1.71	2.12	2.74	2.38	2.48	
Group 4	N total	18	18	18	18	18	18	12.98
	Min	8.5	7.86	11.2	11.7	14.46	6.3	
	Mean	12.31	11.64	14.42	15.09	15.61	8.8	
	Max	15.3	15.17	18.23	19.53	19.8	12.5	
	Standard deviation	2.15	2.26	2.56	2.38	1.87	2.37	

The spatial and temporal variations among the wells in different clusters are illustrated in figure 16. Cluster 1 comprises 22 wells that exhibit similar fluctuation patterns, with mean fluctuations ranging from 2.64 meters below ground level (mbgl) in 2009 to 11.44 mbgl in 2018. The average fluctuation for this group is shallowest, measuring at 5.91 mbgl. These wells are concentrated in the central area of the study site, expanding towards the southeast, with only one well located in the northeast. In contrast, cluster 2 consists of eighteen wells with mean fluctuations varying from 4.33 mbgl in 2009 to 14.30 mbgl in 2018. The average fluctuation in this group is deeper compared to cluster 1. The wells in this cluster are distributed across the study area, covering the southern east, the center to the northwest, and one well in the northeast. Moving on to cluster 3, the wells in this group show fluctuations in depth ranging from 6.90 mbgl in 2009 to 10.96 mbgl in 2018, with a total mean fluctuation of 9.31 mbgl. These wells are spatially distributed from the center to the northeast of the study area, except for one well in the northeast. Furthermore, cluster 4 exhibits the deepest fluctuation means, with

variations ranging from 11.64 mbgl in 2009 to 15.61 mbgl in 2018. The total mean fluctuation for this group is 12.98 mbgl. These wells are located separately in the southwest of the central part to the southwest of the study area. Notably, both the third and fourth clusters consist of the same number of wells as the second group.

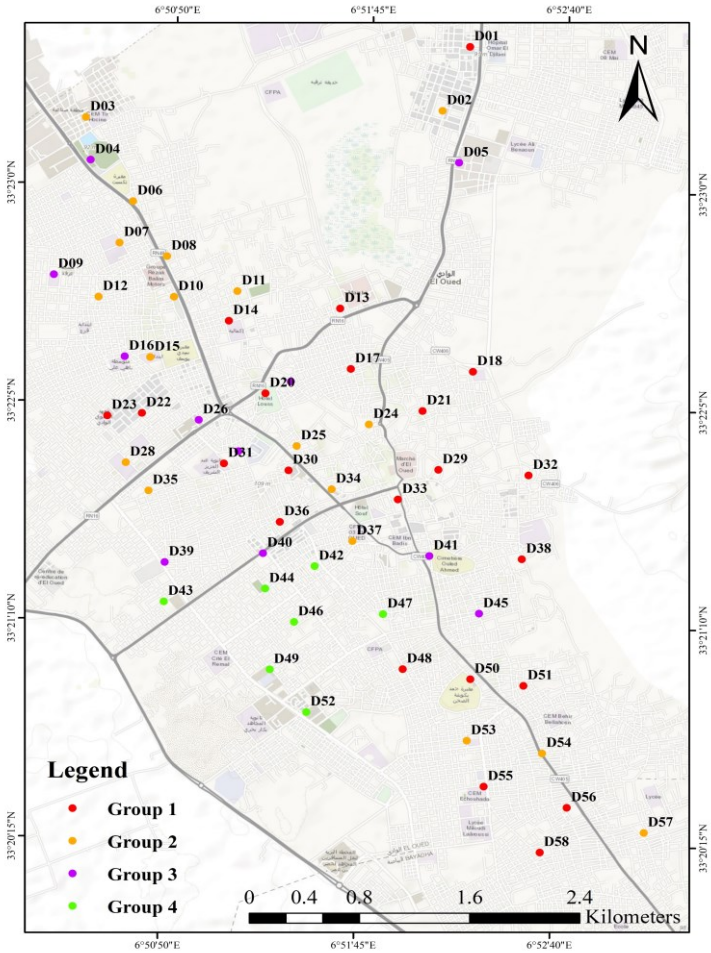

Figure 16. Map showing four clusters of drains.

4.1.1.2. Geostatistical Modelling and the phreatic groundwater level fluctuations

The initial step in statistical analysis involves the creation of frequency tables, histograms, and fundamental statistical computations. Summary statistics, such as the mean, coefficient of variation, minimum, maximum, skewness, and kurtosis values, can be found in table 8. Based on the information provided by the histograms, kurtosis, and skewness values, it can be inferred that the data for 2008,

2014, 2016, and 2021 exhibit approximately normal distribution. For the data from 2009 and 2018, a logarithmic transformation was applied before conducting the geostatistical analysis. In order to gain further insights into the upward movement of groundwater in the study area, the anisotropy of the phreatic aquifer was confirmed using semivariance analysis and ordinary kriging. In this regard, omnidirectional experimental semivariograms were generated for the groundwater levels of 2008, 2009, 2014, 2016, 2018, and 2021 in the four main directions: E-W, NE-SW, N-S, and NW-SE.

Table 8. Statistical summary of the studied groundwater levels.

Years	N tot	S.D	Mean	C.V(%)	Min	1st Quartile	Median	3rd Quar-tile	Max	Skew-ness	Kurtosis
2008	58	3.41	5.41	63.068	-0.3	3.42	4.56	6.56	15.3	1.030	0.92
2009	58	3.28	5.06	64.974	-0.4	2.75	4.15	6.53	15.17	1.073	1.07
2014	58	3.57	7.97	44.851	0.6	5.57	7.38	9.5	18.23	0.711	0.80
2016	58	4.42	7.80	56.706	1	4.94	7.13	9.73	19.53	0.510	-0.33
2018	58	3.71	12.74	29.186	5.1	10.5	12.51	14.7	28.8	1.370	5.309
2021	58	3.02	8.86	34.158	2.1	7.2	9.22	11	15	-0.341	-0.054

The analysis revealed a slight level of anisotropy, indicating that the experimental semivariograms created for different directions exhibited variations in their sills and influence ranges. However, these anisotropies were inadvertently overlooked, leading to the use of isotropic models instead. In the model selection process, mean error (ME) and root mean square standardized error (RMSSE) values were taken into account. The goal was to identify the best-fit semivariogram models, and their evaluation was primarily based on predictions. A model was considered favorable when RMSSE approached unity, and ME remained very low. The specific parameters adopted for the examined annual groundwater levels can be found in tables 9 and 10. Subsequently, hypothetical models were fitted to the more standard non-directional semivariograms, which are depicted in figure 17.

Table 9. Fitted experimental semivariogram parameters and their cross-validation results.

Year	Model	Nugget (C0)	Partial Sill (C)	Sill (C0 + C)	Range (m)	$(C_0/C_0 + C) \times 100$	Spatial Dependence
2008	Pentaspherical	2.100	13.961	16.060	3054.9	13.074	Strong
2009	Hole effect	3.639	9.239	12.878	3000.3	28.260	Moderate
2014	Gaussian	4.295	13.192	17.487	1931	24.560	Strong
2016	Circular	5.830	18.576	24.405	1865.2	23.887	Strong
2018	Spherical	1.427	13.007	14.434	702.6	9.886	Strong
2021	Stable	3.630	6.400	10.030	5062	36.191	Moderate

Table 10. Prediction errors of the selected models.

Years	Prediction Errors				
	Mean	Root Mean Square	Average Standard Error	Mean Standardized	Root Mean Square Standardized
2008	-0.033	2.559	2.520	-0.010	1.035
2009	-0.031	2.453	2.211	-0.010	1.126
2014	0.002	2.685	2.588	0.003	1.064
2016	0.042	3.185	3.579	0.004	0.913
2018	0.016	3.464	3.773	0.008	0.948
2021	-0.008	2.987	2.978	-0.004	1.002

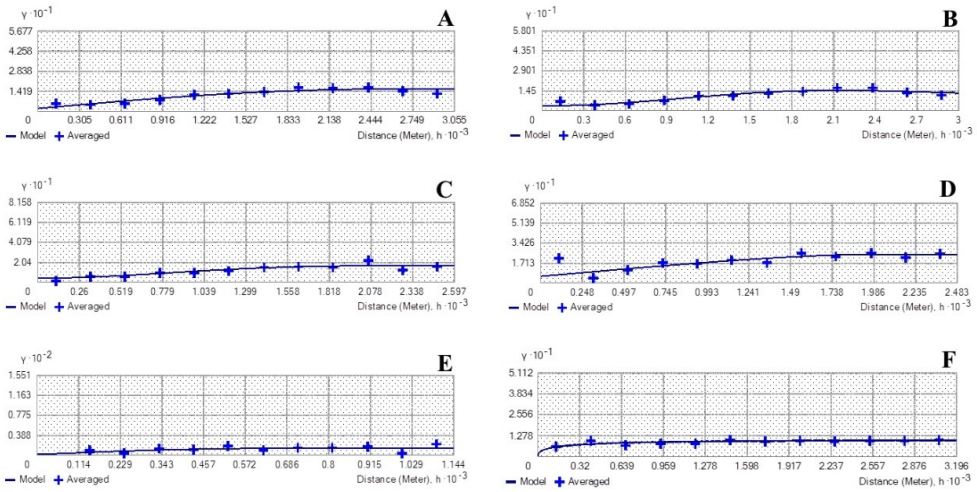

Figure 17. Fitted experimental semivariograms of groundwater level over the years: (A). 2008, (B). 2009, (C). 2014, (D). 2016, (E). 2018, (F). 2021.

The analysis of the groundwater levels for each selected year revealed that different models were the best fit for each dataset. The models used were Penta-spherical for 2008, Hole effect for 2009, Gaussian for 2014, Circular for 2016, Spherical for 2018, and Stable for 2021. These selections were based on the mean error and the root mean square standardized error.

The range of influence and the sill values of the adopted models showed significant differences. The range of influence represents the distance within which the groundwater level values exhibit spatial dependence. Notably, the minimum spatial dependence of 702.55 meters was observed in 2018, while the maximum spatial dependence of 5061.97 meters was identified in 2021. However, the presence of the nugget effect indicates variability or fluctuations across shorter distances than the spacing between observation wells, as well as other unaccounted recording errors. According to [339], the aquifer structure displays strong spatial dependence, which remained relatively constant over the years, except for 2009

and 2021 when the spatial structures showed a moderate level of dependence. Furthermore, the very low nugget effects suggest that the groundwater level fluctuations are highly time-correlated and exhibit a strong temporal structure, meaning that there is a significant connection between the groundwater levels measured at different time points.As it can be observed in the generated prediction maps of ordinary kriging for the water table status in 2008, several patterns were detected in the study area. Variations extend from the northwest to the southeast of the study area, where groundwater depths range from approximately 3 to 4 meters and upwell near the surface (1-3 meters) and even reach the surface (-0.3 meters in D20), mainly in the center of El-Oued municipality. In the southwest of the research region, the depth to groundwater was more than 6 meters below ground level and decreasing (going deeper). Another observation was that the depth was decreasing by around 2 meters near two drains, D05 (northeast) and D45 (south). In 2008, when the vertical drainage system began functioning, the groundwater levels were very shallow. Besides D20, other drains recorded very shallow levels that were close to the surface, such as D13, D17, D18, 32, and D33, where the levels ranged from 0.43 to 1.88 meters below the ground surface. On average, the depth of groundwater fluctuated by about 5.42 mbgl during 2008.

Similarly, in 2009, the groundwater level continued its upwelling from the northwest part to the southeast, where the shallowest level was recorded in D20 at -0.4 mbgl, while the deepest level was noted in the same drain as in 2008, which is D52 at 15.17 mbgl. D13, D17, D18, 32, and D33 had the same trend as in 2008, where their levels varied from 0.41 to 1.75 mbgl. The mean groundwater level in 2009 was 5.06 mbgl, which was deeper than in 2008, indicating an increase in the upwelling average in the study area during 2009, as is shown in figure 18 (A), and (B).

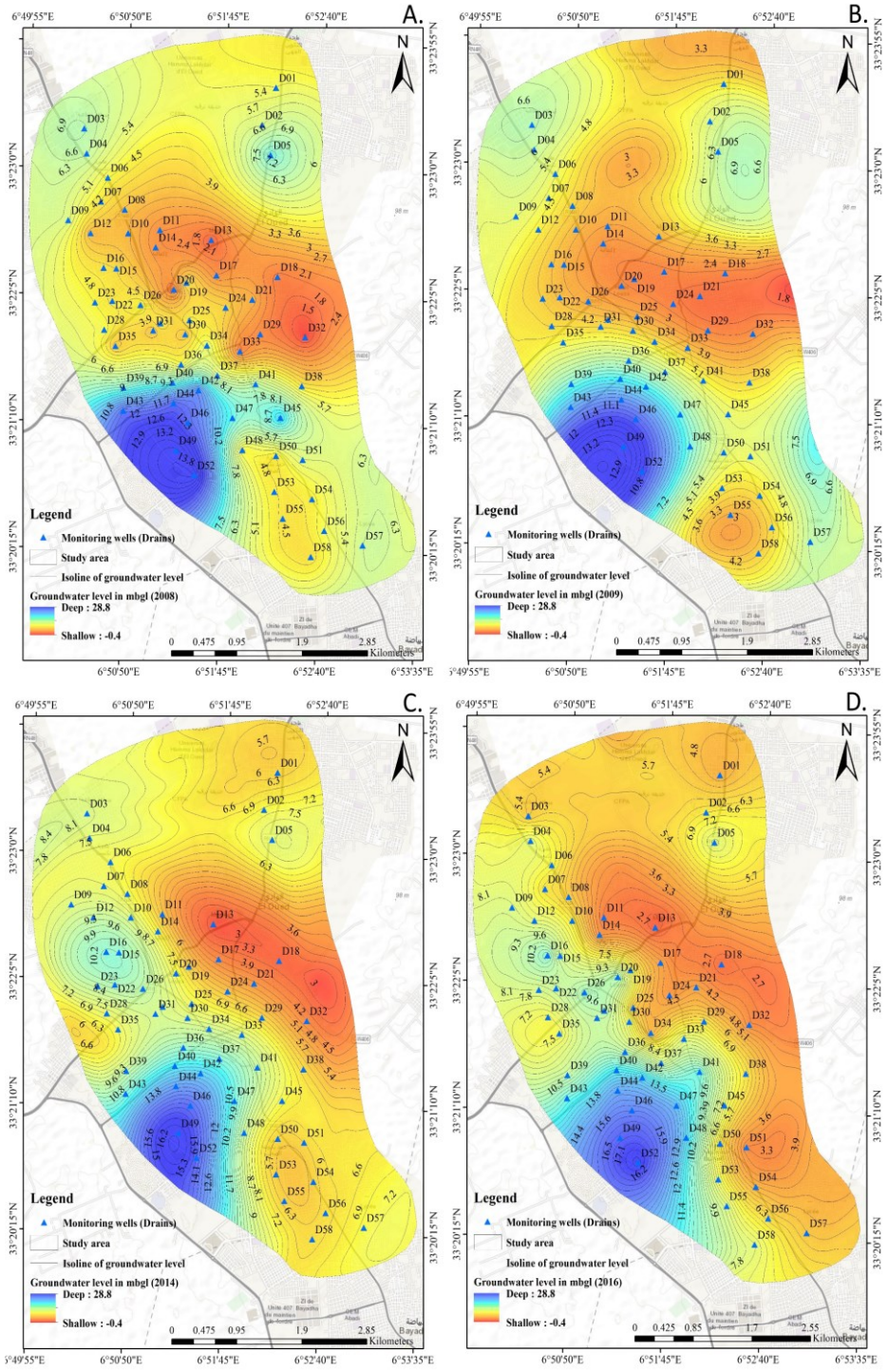

Figure 18. Evolution maps of groundwater level in the study area: (A). 2008, (B). 2009, (C). 2014, (D). 2016.

The groundwater level began its significant decline in 2014 and 2016, respectively. However, as usual, the shallowest groundwater levels were observed in a gradual upwelling state from the central northwest part to the southeast of the study area, reaching the minimum value, which was recorded as 0.6 mbgl in D13 in 2014 and 1 mbgl in 2016. The deepest levels were noted in the southwest of the study area, where the levels were more than 8 mbgl and experienced a significant decline, reaching 18.23 mbgl in 2014 and 19.53 mbgl in 2016, respectively, as illustrated in figure 18 (C), and (D). The fluctuation rates ranged from 7.97 mbgl in 2014 to 7.81 mbgl in 2016, as shown in table8. Furthermore, the minimum groundwater level in 2018 shifted to D32 at 5.1 mbgl, located in the southeast part of the city, while the deepest level shifted to D37 at 28.8 mbgl, situated in the south of El Oued city. Meanwhile, the fluctuation rate in 2018 was 12.74 mbgl. Nevertheless, when comparing the year 2008 and other years, the differences in groundwater decline and upwelling rates are predicted to be -0.36 m in 2009, 2.56 m in 2014, 2.39 m in 2016, and 7.32 m in 2018, as shown in figures 19 and 20 (E).

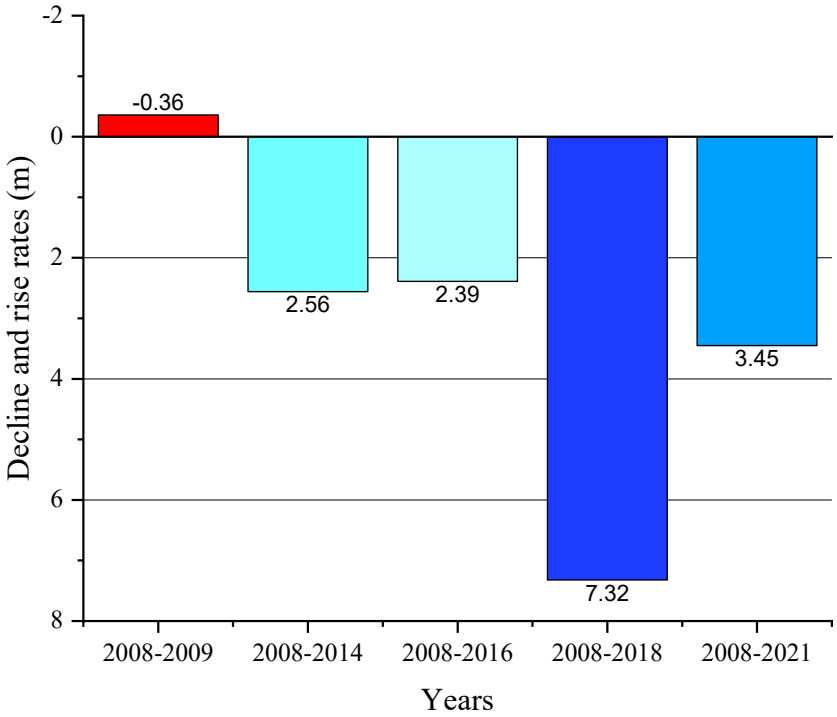

Figure 19. Decline and rise rates over the years of the observation period.

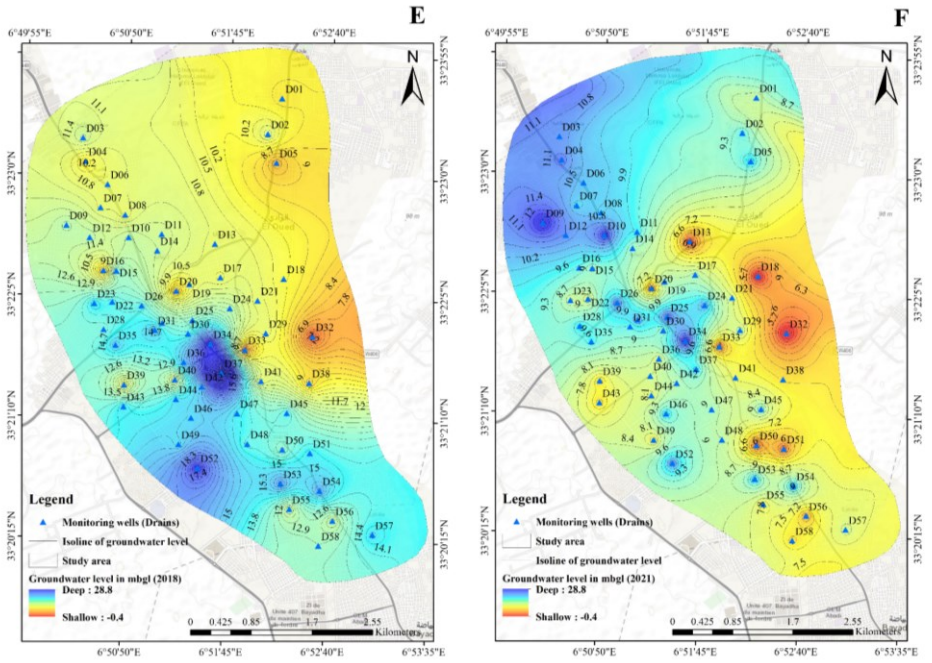

Figure 20. Evolution maps of groundwater level in the study area: (E). 2018, (F). 2021.

In 2021, a significant change in the groundwater level status was observed in the study area, particularly concerning fluctuations, decline, and rising rates. The deepest groundwater levels were found in two main regions: the center of the study area, where D34 reached a maximum depth of 15 meters below ground level (mbgl), and the northwest part, where D10 registered the same depth of 15 mbgl. Additionally, other drains like D52, D53, and D54 recorded considerable depths, as shown in figure 20 (F).

Conversely, the minimum groundwater level was observed in the central east of the study area, specifically in D32, where the groundwater level was at 2.1 mbgl. Despite experiencing a significant decline in the previous years, the depth of groundwater fluctuated by approximately 8.87 mbgl in 2021. This significant rise in groundwater levels compared to the average of 3.9 meters in 2018 indicates a notable change in the hydrological conditions of the study area, as illustrated in figure 19. These findings suggest that there have been substantial changes in the groundwater dynamics over the years, with 2021 showing a remarkable increase in the groundwater levels compared to the previous observations. The study area's hydrological balance and groundwater patterns appear to be evolving, which may have implications for water resource management and environmental planning in the region.

These observations highlight the changing patterns of groundwater levels over the years and indicate significant variations in different areas of the study area, and this is due to the fact that the water table is influenced by various factors, leading to multiple explanations for the decline of groundwater and its fluctuations during

the study period. One key factor contributing to the decline is the independent use of groundwater in the study area, which reduces the water returning to the phreatic aquifer. Based on the obtained data from ANRH and ADE in 2019, approximately 94.7% of the withdrawn groundwater from the entire aquifer system is utilized for diverse purposes. Most of this water, around 93.5%, originates from the complex terminal aquifer, with contributions from the Miocene, Pontian, and Eocene sources, along with a smaller proportion (1.2%) coming from the continental intercalary (Barrimian). The remaining 5.3% is discharged through the vertical drainage system, which handles the residual phreatic groundwater from the Quaternary period.

Notably, a significant portion of the groundwater resources is allocated to drinking water supply (40.4%) and irrigation (51.3%), possibly even more. The drainage system accounts for about 8.3% of the groundwater usage (see figure 21 A, B). The rapid expansion of agriculture and its development around the city of El Oued Souf, specifically in the agricultural areas surrounding Oued Souf city, significantly contributes to the swift decline of the phreatic aquifer through the intensive use of groundwater. This usage occurs relatively far from El Oued, reducing the return of infiltrated water to the phreatic aquifer.

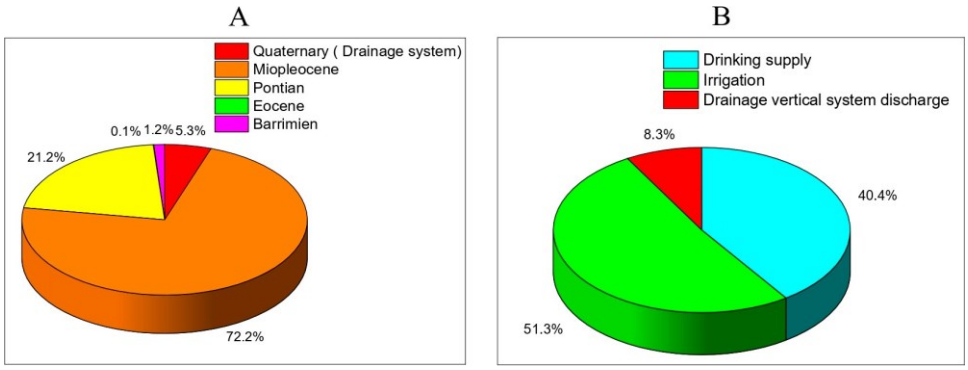

Figure 21. (A). Distribution of the extracted water in percentage from the aquifer system of the study area, (B). Distribution of the extracted water in percentage depending on the usage.

Meanwhile, the initial outcomes of the vertical drainage system revealed unfavorable results, with the phreatic groundwater level showing a rising rate of -0.36 meters between 2008 and 2009, and this is due to the fact that the vertical drainage system was in its beginning of its functioning to reduce the level of the water table that rose before the study period due to several natural and anthropogenic factors such as the natural topography and the absence of a natural outlet of the region, insufficient/weakness and miscoordination between different sectors that governs the water management in Oued Souf Valley that are represented by intensive exploitation of deep groundwater reservoirs which returns to the shallow aquifer, absence of sewage and drainage network, leakage from drinking water supply system.

However, over the course of the study, these adverse effects gradually

improved, and the drainage system started to yield more positive results. The implementation of the vertical drainage system in El Oued led to a progressive decline in groundwater levels over time, significantly reducing the contamination levels in the phreatic groundwater aquifer. The shift from septic tanks to the new drainage system played a crucial role in achieving this improvement. Moreover, the extension of the sewage network to connect most residential areas helped eliminate the previous practice of discharging large quantities of wastewater directly into the environment, which used to eventually find its way back to the phreatic aquifer. Approximately 27.5 million cubic meters per year of wastewater are now directed through the drainage system to the treatment station, as depicted in figure 22, with a discharge flow rate of 7.74 liters per second. This approach has contributed significantly to mitigating the contamination of the groundwater. However, despite the progress, there are concerns about the groundwater levels, particularly as indicated by the 2021 results, which have raised several questions and fears of a potential resurgence of the groundwater upwelling issue. Several factors might be contributing to the possible rise in groundwater levels in the study area. For instance, the inefficient drinking water supply network, plagued by significant water leakages, unaccounted withdrawals due to the lack of meters or measurement system failures, and illegal withdrawals (such as unauthorized connections and meter tampering) could all be influencing the groundwater situation. These factors require attention and corrective measures to avoid a recurrence of the groundwater upwelling crisis.

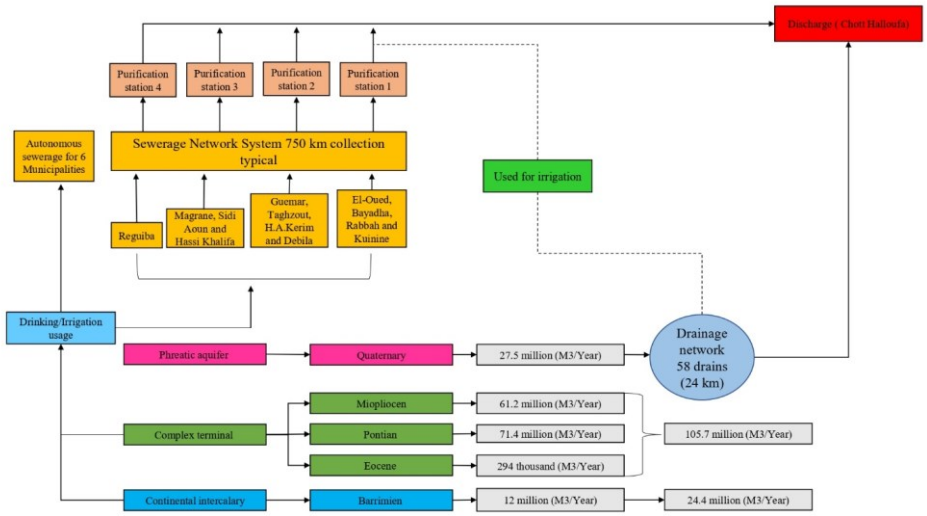

Figure 22. Groundwater exploitation, Sewerage, treatment of wastewater, evacuation, and drainage systems of the study area (source: The author).

Regarding the drinking water supply network in Oued Souf, there are several issues contributing to losses and inefficiencies. These include problems with defective joints in pipe connections and conduits made of various materials such

as steel, asbestos, concrete, and polyvinyl chloride. Additionally, leaking tanks and valves further exacerbate the situation. Moreover, there are problematic connections with other supply systems, and non-remunerated withdrawals, such as water usage for firefighting, inspection work, network maintenance, and pipe rinsing. The presence of water-intensive industries like gypsum production also significantly contributes to the high-water consumption.

In the drainage system, certain issues may lead to a resurgence in groundwater levels. Power outages can disrupt the pumping process, and regular maintenance is essential to keep the system functioning optimally. However, during the 2021 measurement period, several drains had not been operational since 2018, indicating a lack of proper maintenance. While it's worth mentioning another potential explanation, the non-homogeneity of the unconfined aquifer (phreatic aquifer) due to the presence of clay lenses at shallow depths that support the rise of groundwater, this aspect falls beyond the scope of this research and won't be further explored [340]. Additionally, the wastewater purification plant responsible for treating the collected wastewater faces various issues. Some of the problems include the breakdown of pumps, particularly in the Desander stage, primarily caused by the high level of wastewater in the grit trap, leading to the failure of two suction pumps and inadequate performance of the third pump. Consequently, the plant faces substantial pressure, resulting in a reduced volume of wastewater that can be properly purified. These challenges further compound the groundwater situation in the area.

4.1.2. Physicochemical and bacteriological characterization of the phreatic groundwater aquifer

4.1.2.1. Physico chemical charachterization of the phreatic aquifer

Table 11 presents a statistical overview of the physicochemical and bacteriological parameters analyzed in the groundwater samples obtained from the phreatic aquifer. The concentrations of these parameters were compared with the World Health Organization (WHO) limits for drinking purposes. This comparison aims to evaluate the quality of the phreatic aquifer for drinking, specifically under the conditions of the functioning of the vertical drainage system in the study area. The temperature of the groundwater within this aquifer exhibited a range between 25 and 31.40 °C. The groundwater temperature can have a negative impact on groundwater quality since it can lead to microbial proliferation and reduce the solubility of O_2^-, CO_2, N_2^+, and CH_4^+ [341].

Additionally, the pH values varied from 6.78 to 8.57, with most samples falling within the recommended pH limits for drinking water established by the World Health Organization (WHO). However, it was observed that six samples (S3, S20, S21, S22, and S23) which represent 21.43% of the total samples were classified as slightly alkaline groundwater. Meanwhile, one samples (S12) was classified as moderately alkaline groundwater. On the other hand, the rest of the samples (22 sample) were classified as slightly acidic to neutral groundwater.

The electrical conductivity (EC) is a crucial parameter for assessing the overall ionic concentration within groundwater, with elevated EC values indicating higher total dissolved solids in the groundwater [342]. Within the analyzed groundwater samples, EC ranged from 3100 to 7500 µs/cm, with a mean value of 4385.7 µs/cm. Additionally, 100% of the samples exceeded WHO limits for drinking purposes. According to [343], S13, S20, S21, S23, and S25 can be classified as waters with very high EC and of doubtful quality. The rest of the samples were categorized as waters with extensively high EC and poor quality. Similarly, except for S1, all TDS values exceeded the limits for drinking purposes, ranging from 500 to 5435 mg/l, with a mean value of 2350.07 mg/l.

The phreatic groundwater turbidity ranged from 0.36 to 71.60 NTU, with a mean value of 16.88 NTU. Fourteen samples did not exceed the WHO limits for drinking purposes, while the rest exceeded the limits. Using water classification based on water turbidity [344], S15 was of turbid water, S10 was of rather turbid water, S2, S16, S17, S18, S19, and S28 were of turbid waters, and the rest of the samples were of fairly turbid waters. This level of turbidity can impact the aesthetic quality of water and may require treatment, especially for drinking purposes.

The analytical outcomes pertaining to calcium (Ca^{2+}) content have revealed that all the analyzed samples exceeded the established guidelines prescribed by the World Health Organization (WHO) for potable water. The observed Ca^{2+} concentrations span a range from 440.88 to 1050.10 mg/l, with a computed arithmetic mean of 714.36 mg/l. Regarding magnesium (Mg) levels, the acquired results display a spectrum of values ranging from 36.44 to 705.05 mg/l, with an average concentration of 381.32 mg/l. It is imperative to emphasize that, barring a sole exception found in sample S26, all other samples exhibit Mg concentrations that exceed the WHO's recommended limits for potable water use. Sodium (Na^{+}) concentrations fluctuated from 232.15 to 582.15 mg/l with a mean value of 325.30 mg/l. All of the analyzed samples exceeded the WHO limits for drinking use in terms of Na^{+}.

In relation to potassium (K^{+}), S12, S16, S18, and S20 did not exceed the WHO limits for drinking purposes, while the remaining samples exceeded these limits. The concentrations of K^{+} ranged from 9.55 to 33.75 mg/l, with a mean concentration of 20.59 mg/l. Chloride (Cl^{-}) concentrations ranged from 124.25 to 914.69 mg/L, with a mean value of 378.92 mg/L. Only two samples, S11 and S16, did not exceed the limits for drinking purposes established by the WHO. The rest of the samples exceeded 250 mg/L.

Nitrate (NO_3^{-}), nitrite (NO_2^{-}), and ammonium (NH_4^{+}) are important indicators of groundwater contamination that can affect both human health and the environment. However, the ranges for NO_3, NO_2, and NH_4 were as follows: NO_3^{-} (min = 0.10 mg/l, max = 159.42 mg/l, mean = 27.67 mg/l), NO_2^{-} (min = 0 mg/l, max = 6 mg/l, mean = 0.88 mg/l), and NH_4^{+} (min = 0.08 mg/l, max = 4 mg/l, mean = 0.57 mg/l), respectively. Among the samples analyzed, it was observed that four samples (S24, S25, S26, and S27) exceeded WHO limits for drinking purposes, while the remaining samples complied with WHO guidelines. Moderate levels of contamination in groundwater, characterized by the presence of NO_3^{-}, NO_2^{-}, and NH_4^{+}, may be attributed to various sources, including agricultural runoff, septic

system leachate, or other localized pollution sources. Such contamination may necessitate monitoring and management to prevent further deterioration. On the other hand, high levels of contamination involving NO_3^-, NO_2^-, and NH_4^+ can pose significant risks to both human health and the environment. This heightened contamination often results from industrial discharges, intensive agriculture, or sewage contamination, and remediation efforts are typically required to reduce these contamination levels [345].

HCO_3^- concentrations ranged from 36.60 to 429.44 mg/l with 162.22 mg/l as the mean value. Fifteen samples exceeded the WHO limits for drinking water (S2, S4, S5, S8, S9, S10, S11, S15, S17, S19, S23, S25, S26, S27, and S28), representing 53.57% of the total samples. Regarding fluorine (F^-), ten samples exceeded the limits (S7, S13, S14, S15, S17, S19, S22, S24, S27, and S28), while the rest of the samples were within the WHO standards for drinking utilization. However, F^- concentrations ranged from 0.69 to 3.31 mg/l with 1.47 mg/l as the mean value. In terms of sulfate (SO_4^{2-}), the concentration ranged from 68.20 to 266.13 mg/l with 199.31 mg/l. Only two samples had a high concentration of SO_4^{2-} and exceeded the standards (S8, and S10), while the rest of the samples were under the limits. Phosphate (PO_4^{3-}) values of the analyzed samples varied from 0 to 6.92 mg/l, and the mean value was 0.67 mg/l. Furthermore, five samples exceeded the WHO limits for phosphate (S5, S8, S16, S21, and S22) [346].

Dissolved oxygen (DO), chemical oxygen demand (COD), and biochemical oxygen demand (BOD_5) are all important parameters used to assess the quality of water in terms of its oxygen content and pollution levels. DO values ranged from 0.02 to 0.83 mg O_2/l, with 0.25 mg O_2/l as the mean. COD values ranged from 184 to 291.05 mg O_2/l, with 276.86 mg O_2/l. Similarly, BOD_5 results ranged from 76.80 to 125.30 mg O_2/l, with 121.35 mg O_2/l as the mean value. The ratio of BOD_5/COD indicated that ten samples had a ratio higher than 0.5, indicating that a significant portion of the organic matter in the water is readily biodegradable, meaning that microorganisms can easily break it down, while the rest of the samples had a ratio less than 0.5, suggesting that a significant portion of the organic matter is refractory or non-biodegradable, which means it is more difficult for microorganisms to degrade [345,347,348].

Bacteriologically, based on the analyzed phreatic groundwater samples, the range of fecal coliforms fluctuated from 100 to 540 (UFC/100 ml), indicating that six analyzed groundwater samples (S5, S6, S7, S8, S26, and S27) are considered suitable for body contact and recreation, while the rest of the samples had a category of fishing and boating [349]. Meanwhile, total coliforms include a broader group of bacteria that are naturally present in the environment. Their presence suggests that the groundwater may be contaminated, although not necessarily with fecal matter. Moreover, the results of total coliforms in 28 phreatic groundwater samples ranged from 1290 to 2580 (UFC/100 ml), indicating a high level of contamination since all the values were higher than 100 CFU/100 ml [350].

Table 11. Statistical overview of the physicochemical and bacteriological parameters analyzed in the phreatic groundwater aquifer samples that were taken during October 2021.

Parameters	Mean	SD	Skewness	Kurtosis	Min	Median	Max	WHO
T(°C)	27.8	1.61	0.47	-0.18	25	27.8	31.4	-
pH	7.25	0.45	1.63	2.32	6.78	7.09	8.57	6.5–8.5
EC (µs/cm)	4386	1310	1.28	0.42	3100	3850	7500	1000
Turbidity (NTU)	16.9	21	1.17	0.08	0.36	5.52	71.6	5
TDS (mg/l)	2350	1089	0.66	1.66	500	1925	5435	500
Ca^{2+} (mg/l)	714.4	148.4	0.23	0.1	440.9	705.4	1050.1	75
Mg^{2+} (mg/l)	381.3	177.1	-0.25	-0.89	36.4	429.1	705.1	50
Na^{+} (mg/l)	325.3	91.0	1.45	1.52	232.2	290.5	582.2	200
K^{+} (mg/l)	20.6	6.28	-0.03	-0.81	9.55	21.7	33.8	12
Cl^{-} (mg/l)	378.9	157.3	2.01	4.69	124.3	337.3	914.7	250
NO_3^{-} (mg/l)	27.7	38.1	2.17	5.11	0.1	12.8	159.4	50
HCO_3^{-} (mg/l)	162.2	94.6	0.96	0.82	36.6	142.1	429.4	120
F^{-} (mg/l)	1.47	0.65	1.66	3.13	0.69	1.3	3.31	1.5
SO_4^{2-} (mg/l)	199.3	44.3	-0.98	1.2	68.2	204.2	266.1	250
PO_4^{3-} (mg/l)	0.67	1.36	3.93	17.4	0	0.19	6.92	1
DO (mgO_2/l)	0.25	0.26	0.89	-0.48	0.02	0.13	0.83	-
NH_4^{+} (mg/l)	0.57	0.8	3.25	12.6	0.08	0.26	4	-
NO_2^{-} (mg/l)	0.88	1.88	2.12	3.03	0	0.05	6	-
COD (mg/l)	276.9	70.1	-0.35	-1.77	184	291.1	352	-
BOD_5 (mg/l)	121.4	19.8	0.06	-0.66	76.8	118.9	152.3	-
Total coliforms (UFC/100 ml)	2041	406.8	-0.51	-0.83	1290	2123	2580	-
Fecal coliforms (UFC/100 ml)	320.5	120.8	-0.02	-0.51	100	311	540	-

4.1.2.2. Geostatistical analysis of the physicochemical parameters in the phreatic groundwater aquifer

For further statistical and geostatistical analysis of the hydrochemical parameters under consideration, normality for each parameter has been assessed based on skewness and kurtosis values. Additionally, the ordinary kriging interpolation method has been applied to generate spatial predictions for the distribution of each element using mean error (ME) and root mean square normalized error (RMSSE) as described by [208]. The results of the geostatistical modeling are presented in table 12 and figures 23, 24, and 25.

Based on the results, it was observed that there is significant variation in the strength structure of spatial dependency for each hydrochemical parameter in the study area.

Table 12. Best-fitted semi-variogram models and cross-validation for Ordinary kriging of groundwater quality parameters of the phreatic aquifer.

Hydro-chemical Parame-ters	Transfor-mation	Semivariogram model parameters					Prediction errors	
		Model	Nugget (C0)	Partial Sill (C)	(C0/ C0+C) *100 (%)	Spatial de pendence	Mean	Root-Mean-Square-Standard-ized
EC	Log trans-formation	Hole ef-fect	0.043	0	100	Weak	-83.959	1.208
Ca^{2+}	Original data	Stable	0.038	0.023	62.6	Moderate	7.091	1.013
Mg^{2+}	Original data	Rational quadratic	0.444	0.058	88.51	Weak	6.921	0.977
Na^{+}	Log trans-formation	Gaussian	0.047	0.053	46.92	Moderate	-5.643	1.154
K^{+}	Original data	Gaussian	0.08	0.069	53.7	Moderate	-0.332	1.023
Cl^{-}	Log trans-formation	Hole ef-fect	0.102	0.069	59.76	Moderate	-15.821	1.099
NO_3^{-}	Log trans-formation	Rational quadratic	3.201	1.396	69.63	Moderate	15.917	0.122
HCO_3^{-}	Original data	Pen-taspheri-cal	0	0.447	0	Strong	-0.009	0.9
F^{-}	Log trans-formation	Circular	0	0.2	0	Strong	-0.012	0.946
SO_4^{2-}	Log trans-formation	Spherical	0.081	0	100	Weak	0.893	0.756
PO_4^{3-}	Log trans-formation	K-Bessel	0.123	3.328	3.55	Strong	-0.009	1.184
DO	Original data	Tet-raspheri-cal	0.061	0	100	Weak	0.014	1.171
NH_4^{+}	Log trans-formation	Hole ef-fect	0.719	0.422	63.03	Moderate	0.04	0.881
NO_2^{-}	Log trans-formation	Circular	3.529	0	100	Weak	0.028	1
COD	Log trans-formation	Gaussian	0.022	0.081	21.37	Strong	-1.699	0.746
BOD_5	Original data	Stable	0.012	0.023	35.24	Moderate	-0.828	0.885

The spatial distribution map of electrical conductivity (EC) reveals that EC values increase from the south to the north of the study area. This pattern aligns with previous findings, which suggested a correlation with the groundwater flow direction in the phreatic aquifer [265,285]. Additionally, low EC values are observed in irrigated agricultural areas where groundwater originates from the complex terminal. Here, it comes into contact with the shallow aquifer, resulting in dilution. In contrast, the highest EC values are found in the northern part of the study area, near depression zones that are relatively close to Chotts and the discharge site. This proximity leads to high evaporation rates of shallow groundwater [245]. Calcium (Ca^{2+}) and magnesium (Mg^{2+}) exhibit a similar spatial

behavior, with low values in the agricultural areas, particularly in the northern east (Debila) and the western regions of the study area. These values increase from the north towards the south, reaching higher concentrations in urban areas such as El Oued and Bayadha municipalities.

The spatial distribution map of sodium (Na^+) reveals low concentrations in the extreme southern part of the study area (south of El Oued and Bayadha), as well as in the middle eastern section around S12, S20, and S22. Conversely, the highest Na values are concentrated in the middle of the study area, particularly around S23 (peri-urban area), S13 (northeast of the El Oued municipality), and in the northeastern and northwestern regions around S21 and S25, respectively. On the other hand, the spatial distribution of potassium (K^+) exhibits two different patterns. Low concentrations extend from the middle east of the study area towards the south (urban areas) and simultaneously towards the west via the north (peri-urban and agricultural areas). As for the high concentrations, these values are located in the south of the study area, covering the eastern part of the El Oued and all of Bayadha municipalities, as well as areas in the north of the study area that extend from the northwest to the northeast, and an area that also extends from the middle west to the central part of the study area, covering S23.

Regarding the spatial distribution of anionic content in the phreatic groundwater system, low concentrations of Cl^- covered almost the entire study area, including Bayadha, El Oued, and Guemar. Gradually, these concentrations increased towards the northeastern part of the study area around Debila. However, the spatial distribution of HCO_3^- exhibited different patterns. Areas with high concentrations of HCO_3^- were located to the north of Debila, south of Bayadha, east of El Oued, and in the western part of Guemar. Low concentrations were observed in the western part of Guemar, extending to the extreme west of the study area and the north of Bayadha.

High concentrations of NO_3^- were found in the northwestern part of the study area, covering Debila and the extreme eastern agricultural area. Concentrations then decreased on both sides, moving towards the urban areas. However, the elevated levels of NO_3^- suggest that the study area is experiencing pollution of urban and agricultural origins caused by human activities [351,352]. The distribution of PO_4^{3-} revealed a gradual increase from the south and east of the study area towards the northwestern part. In contrast, the spatial distribution of SO_4^{2-} concentrations increased gradually from the northeastern part of the study area (Debila) towards the rest of the study area.

For F^- distribution, high concentrations extended from the northern part of the study area, covering Debila, to the western part, encompassing Guemar, and also included the municipality of El Oued. Meanwhile, low concentrations were located in the eastern part of the study area, the western part of El Oued, and the southern part of Bayadha.

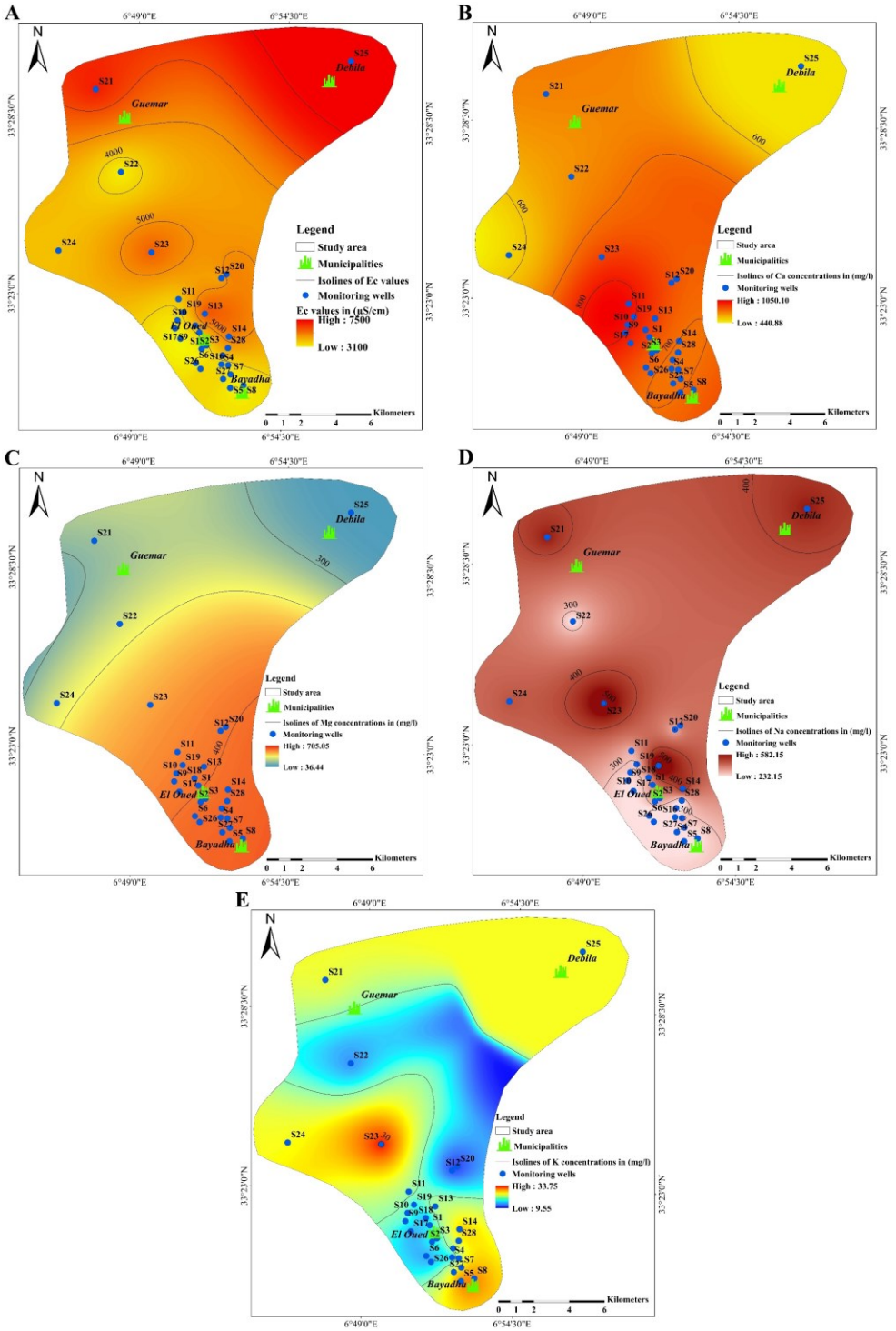

Figure 23. Spatial distribution of the chemical elements in the phreatic groundwater: (A). EC, (B). Ca^{2+}, (C). Mg^{2+}, (D). Na^{+}, (E). K^{+}.

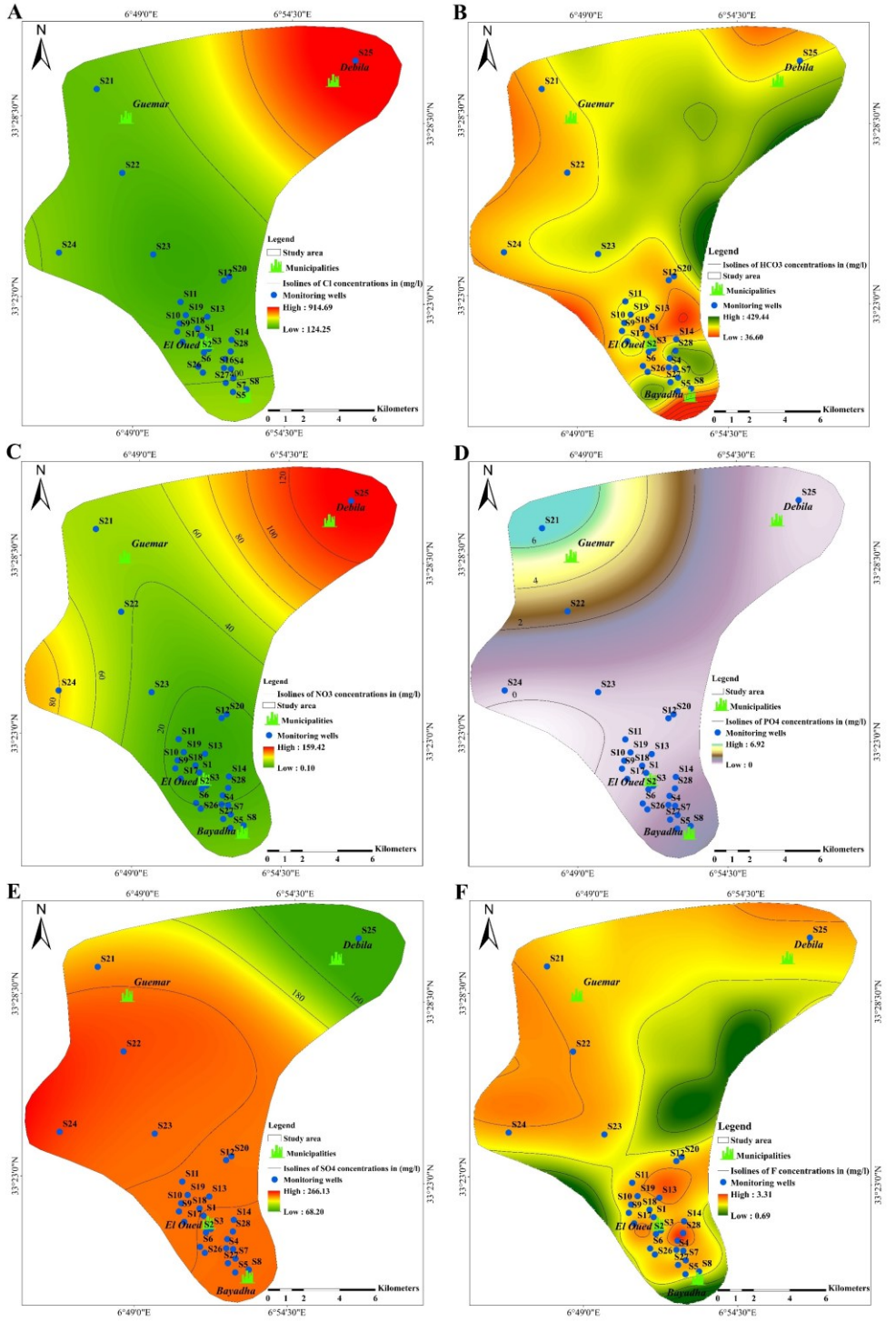

Figure 24. Spatial distribution of the chemical elements in the phreatic groundwater: (A). Cl^-, (B). HCO_3^-, (C). NO_3^-, (D). PO_4^{3-}, (E). SO_4^{2-}, (F). F^-.

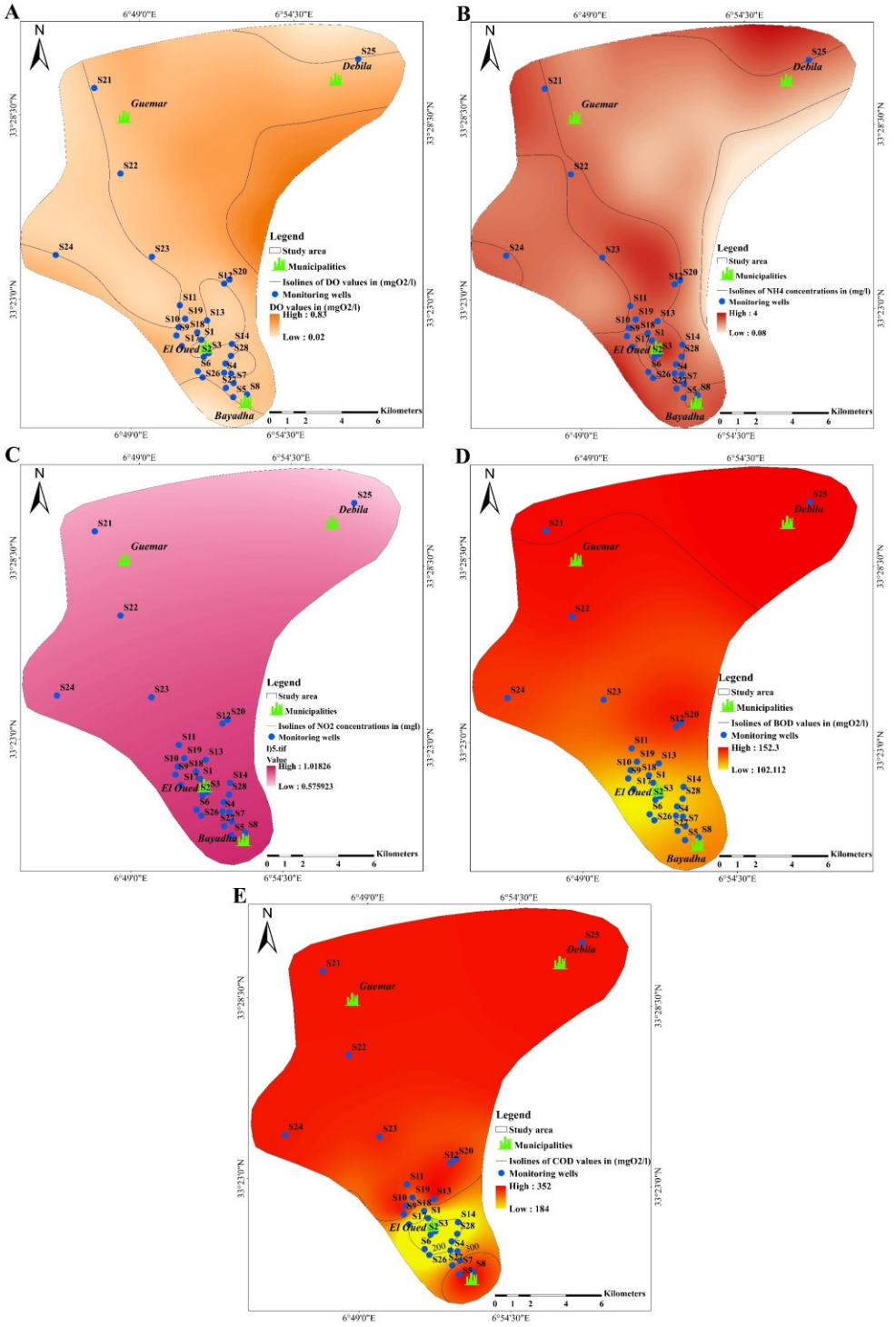

Figure 25. Spatial distribution of the chemical elements in the phreatic groundwater: (A) DO, (B) NH_4^+, (C) NO_2^-, (D) BOD, (E) COD.

BOD and COD exhibited similar spatial behavior, with low values located in the main city of El Oued, and the highest values extending toward the north and south of the study area. This shared spatial pattern may suggest a common source of pollution, including chemical and organic contaminants, possibly stemming from wastewater infiltration, especially from septic tanks. DO concentrations were high in the eastern part of the study area, while the rest of the study area had relatively low concentrations. Regarding NH_4^+, high concentrations were found in the north of Debila, west of Guemar, and east and west of El Oued, while the rest of the study area had low NH_4^+ concentrations. Concerning the spatial distribution of NO_2^-, the concentrations increased from the north of the study area towards the south (urban areas).

Analysis of the results revealed significant variations in the strength and structure of spatial dependency for each hydrochemical parameter within the study area. Hydrochemical parameters such as HCO_3^-, F^-, PO_4^{3-}, and COD demonstrated strong spatial dependency. This indicates a pronounced correlation among data points for each parameter, leading to distinct separation between distributed interpolated levels and the emergence of noticeable patterns or similarities across the spatial data, culminating in a high degree of spatial autocorrelation. Conversely, parameters like EC, Mg^{2+}, SO_4^{2-}, DO, and NO_2^- displayed weak spatial dependency, suggesting a lower correlation between data values for each parameter at varying locations relative to distance. This results in minimal separation between interpolated levels. The remaining hydrochemical parameters showed moderate spatial dependency, signifying a concentration of each element with a certain level of clustering, trending, or spatial continuity. The variability in data may stem from a mix of local and regional influences, imparting a moderate spatial dependence where data values not only relate to their immediate neighbors but also reflect variations due to wider-scale influences such as the problem of rising of phreatic groundwater level and its consequences on the water quality.

4.1.2.3. Assessment of the phreatic groundwater aquifer for drinking purposes

The assessment of the potential for utilizing phreatic groundwater from the aquifer for drinking water was conducted using the water quality index developed by [143]. Fourteen hydrochemical parameters were taken into consideration, along with their values based on the WHO limits established in 2011. These parameters encompassed Ca, Mg, Na, K, F, NO_3, HCO_3, Cl, turbidity, EC, TDS, SO_4, PO_4, and pH, which were analyzed across all 28 samples obtained from the studied aquifer. The findings revealed that 60.71% of the samples, representing the majority of the wells, were classified as having good water quality. Additionally, 7.14% were categorized as having excellent water quality, 10.71% exhibited poor water quality, 7.14% were found to have very poor water quality, and 10.71% were deemed unfit for drinking water utilization. These results are presented in table 13.

Table 13. WQI-based groundwater suitability for drinking.

Range	Classes	Number of wells	% Of samples (28 samples)
<50	Excellent water	S6, S26	7.14%
100.0-125.0	Good water	S1, S3, S4, S5, S7, S9, S10, S11, S12, S13, S14, S18, S20, S23, S24, S25, S27	60.71%
125.1-150.0	Poor water	S2, S8, S19	10.71%
150.1-175.0	Very poor water	S17, S22	7.14%
175.1-200.0	Unfit for drinking	S15, S16, S21, S28	10.71%

4.1.2.4. Assessment of the phreatic groundwater aquifer for irrigation purposes

The assessment of the 28 samples from the phreatic groundwater aquifer for irrigation suitability was performed using several indices depending on their intended use. The results are illustrated in table 14. The % Na values indicate that 67.85% of the samples are suitable for irrigation with excellent quality, while 32.14% present good quality. The SAR values range below class 10, indicating excellent water quality according to SAR, which can be used for most types of soil. Based on the TH (total hardness) values, 14.29% were classified as moderately hard water, and 78.57% of the analyzed samples (the majority of the samples) fell into the hard water category. At the same time, two samples were categorized as very hard water. On the other hand, MH results indicated that 64.29% of the samples were suitable for irrigation, while 35.71% of the 28 analyzed samples were unsuitable for irrigation. PI results indicated that all the samples were unsuitable for irrigation since their PI values were above 75. In contrast, based on Kr, ESP, RSC, and RBSC, all the samples were suitable, excellent, and satisfactory for irrigation. Meanwhile, all the analyzed samples of the phreatic groundwater aquifer were rated as Injurious to unsatisfactory based on the Ps index. Ka index results revealed that 14.29% of the samples were of permissible quality for irrigation, while the majority of the samples, representing 85.71%, had doubtful quality for irrigation. Furthermore, according to the K index, it was revealed that 35.71% of the phreatic samples were of excellent quality for irrigation, 28.57% of good quality, 17.85% of injurious quality, and 17.85% of the samples were of unsuitable quality for irrigation.

The apparent contradiction in the suitability of the wells in the Oued Souf Valley for drinking versus irrigation purposes is indeed explained by the differing criteria and thresholds used for assessing water quality for these two uses. For drinking water, the quality is primarily concerned with parameters that affect human health. This includes the presence of harmful chemicals, pathogens, and overall potability. The World Health Organization (WHO) sets guidelines for these parameters, focusing on aspects like turbidity, pH, and the presence of specific ions

such as (Ca^{2+}, Mg^{2+}, Na^{+}, K^{+}, F^{-}, NO_3^{-}, HCO_3^{-}, Cl^{-}, SO_4^{2-}, and PO_4^{3-}). These guidelines are strict because the direct consumption of water has immediate and potentially severe impacts on human health. In contrast, the suitability of water for irrigation depends on factors that can affect both the soil and the plants being irrigated. These parameters include salinity, sodium absorption ratio (SAR), magnesium hazard (MH), and permeability index (PI). High levels of certain elements like sodium or magnesium, which might not be harmful for drinking, can lead to soil degradation and negatively impact plant growth. This difference is crucial because plants and soil have different tolerances and requirements compared to human health. Thus, water can meet the standards for drinking but fail to meet agricultural standards, reflecting the distinct requirements and tolerances of human health and agricultural practices. Since the most effective index for evaluating irrigation water quality varies depending on specific soil types, crop requirements, and local environmental conditions, I considered multiple indices to gain a comprehensive understanding of water suitability for irrigation. However, I identified SAR (Sodium Adsorption Ratio), %Na (Percentage Sodium), and PI (Permeability Index) as the most critical indices. These indices are crucial because they directly relate to soil permeability and structure, which are essential for effective irrigation.

Table 14. Irrigation quality indices of the phreatic groundwater aquifer.

Range	Classes	Number of wells
Percent sodium (Na%)		
< 20	Excellent	S1, S2, S3, S4, S5, S6, S7, S8, S9, S10, S11, S12, S14, S15, S16, S17, S18, S20, S22
20–40	Good	S13, S19, S21, S23, S24, S25, S26, S27, S28
40–60	Permissible	-
60–80	Doubtful	-
> 80	Unsafe	-
Alkalinity hazard (SAR)		
< 10	Excellent	All the samples
10–18	Good	-
18–26	Doubtful	-
> 26	Unsuitable	-
Total hardness (TH)		
< 75	Soft	-
75–150	Moderately hard	S6, S19, S24, S26
150–300	Hard	S1, S2, S3, S5, S7, S8, S9, S10, S11, S12, S14, S15, S16, S17, S18, S20, S21, S22, S23, S25, S27, S28
> 300	Very hard	S4, S13
Magnesium hazard (MH)		
< 50	Suitable	S6, S7, S8, S9, S10, S11, S12, S18, S19, S20, S21, S22, S23, S24, S25, S26, S27, S28

> 50	Unsuitable	S1, S2, S3, S4, S5, S13, S14, S15, S16, S17
Permeability index (PI)		
< 25	Suitable	-
25–75	Moderate	-
> 75	Unsuitable	All the samples
Kelley ratio (KR)		
< 1	Suitable	All the samples
1–2	Moderate	-
> 2	Unsuitable	-
RSC		
<1.25	Acceptble	All the samples
1.25-2.5	Slightly adapted to irrigation	-
>2.5	Not suitible	-
Ps		
< 3	Excellent to good	-
> 3	Injurious to un-satisfactory	All the samples
RBSC		
< 5	Satisfactory	All the samples
5- 10	Marginal	-
> 10	Unsatisfactory	-
ESP		
< 20	Excellent	All the samples
20- 40	Good	-
40- 60	Permissible	-
60- 80	Doubtful	-
> 80	Unsuitable	-
Ka		
> 18	Excellent	-
6- 18	Permissible	S6, S15, S16, S18
1.2- 6	Doubtful	S1, S2, S3, S4, S5, S7, S8, S9, S10, S11, S12, S13, S14,S17, S19, S20, S21, S22, S23, S24, S25, S26, S27, S28
< 1.2	Unsuitable	-
Synthetic harmful coefficient (K)		
< 25	Excellent	S1, S3, S5, S6, S7, S8, S12, S15, S16, S22
26–36	Good	S2, S4, S9, S10, S11, S17, S18, S19
37–44	Injurious	S14, S24, S26, S27, S28
> 44	Unsuitable	S13, S20, S21, S23, S25

4.1.2.5. Assessment of the pollution level in phreatic groundwater aquifer

Three different indices, representative of the pollution level in any groundwater system, have been applied to evaluate pollution in the phreatic groundwater aquifer of the Oued Souf Valley. The applied indices include the National Sanitation Foundation Water Quality Index, Groundwater Pollution Index, and Nitrate Pollution Index. Table 15 reveals that, according to the National Sanitation Foundation method for water quality assessment [161], all the study areas fall into the poor category range, as all the values of NSFWQI range between 26 and 50. In contrast, 100% of the phreatic groundwater samples exhibit a very high pollution level according to the Groundwater Pollution Index. Regarding the Nitrate Pollution Index, it was found that 50% of the phreatic groundwater samples were clean in terms of nitrate contamination, 21.43% exhibited light nitrate pollution, 17.86% showed moderate nitrate pollution, 3.57% had significant nitrate pollution, and 7.14% were categorized as having very significant nitrate pollution.

The discrepancy in the assessment of the phreatic groundwater quality is related to the methodology used for calculating the Groundwater Pollution Index (GPI) and the Nitrate Pollution Index (NPI). The GPI is calculated by multiplying the weight parameter (WP) by the status of concentration (SC) for each parameter, and then summing up these values for all parameters in each water sample. This method considers various water quality parameters and their concentrations relative to the standards set by organizations like the World Health Organization. The NPI specifically assesses nitrate pollution, which is a key indicator of water pollution from human activities. The apparent contradiction in the obtained results could arise from the complex interplay of these different parameters and their varying concentrations in different samples. Whereas, the overall GPI is high due to certain parameters exceeding the limits, other aspects like nitrate levels might be within acceptable ranges, leading to the 7% excellent quality and 60% good quality drinking water assessments. This suggests a nuanced and heterogeneous pollution profile in the groundwater, where some contaminants may be at high levels while others remain within safe limits. However, in my point of view, the National Foundation Water Quality Index represents a comprehensive result since it is composed of the most important physicochemical and bacteriological parameters analyzed from the phreatic aquifer and is much more suitable for this case regarding the history of groundwater in Oued Souf Valley.

Table 15. The groundwater pollution indices classified the results of the phreatic groundwater samples.

Pollution index	Range	Classes	Number of wells	% of samples (28 samples)
National Sanitation Foundation Water Quality Index	91-100	Excellent	-	-
	71- 90	good	-	-
	51- 70	moderate	-	-
	26- 50	poor	All the samples	100%
	0- 25	very poor	-	-
Groundwater pollution index	< 1.0	Insignificant pollution	-	-
	1.0–1.5	Low pollution	-	-
	1.5–2.0	Moderate pollution	-	-
	2.0–2.5	High pollution	-	-
	> 2.5	Very high pollution	All the samples	100%
Nitrate pollution index	< 0	clean	S2, S3, S6, S7, S9, S10, S11, S12, S13, S14, S15, S17, S18, S28	50%
	0- 1	light pollution	S4, S5, S8, S16, S22, S23	21.43%
	1- 2	moderate pollution	S1, S19, S20, S21, S26	17.86%
	2- 3	significant pollution	S27	3.57%
	> 3	Very significant	S24, S25	7.14%

4.1.2.6. Application of hierarchical clustering approach for grouping the phreatic groundwater samples parameters

The normalized data, which included various parameters such as major ions of the analyzed phreatic groundwater samples (Ca^{2+}, Mg^{2+}, Na^{+}, K^{+}, Cl^{-}, SO_4^{2-}, HCO_3^{-}, F^{-}, and NO_3^{-}), electrical conductivity (EC), pH, and temperature, underwent hierarchical clustering analysis (HCA). The primary objective of this analysis was to identify potential hydro-chemical groups within the groundwater samples. To assess the similarity between water samples, the HCA process employed the Q-mode approach, Ward's linkage technique, and Euclidean distance. The outcomes were visualized as a spatial HCA dendrogram, as shown in figure 26. This dendrogram visually represents the clustering of groundwater samples based on their similarity in terms of the measured parameters. This analysis aids in comprehending the spatial distribution and variations in hydro-chemical properties across the study area, offering valuable insights for groundwater resource management and monitoring.

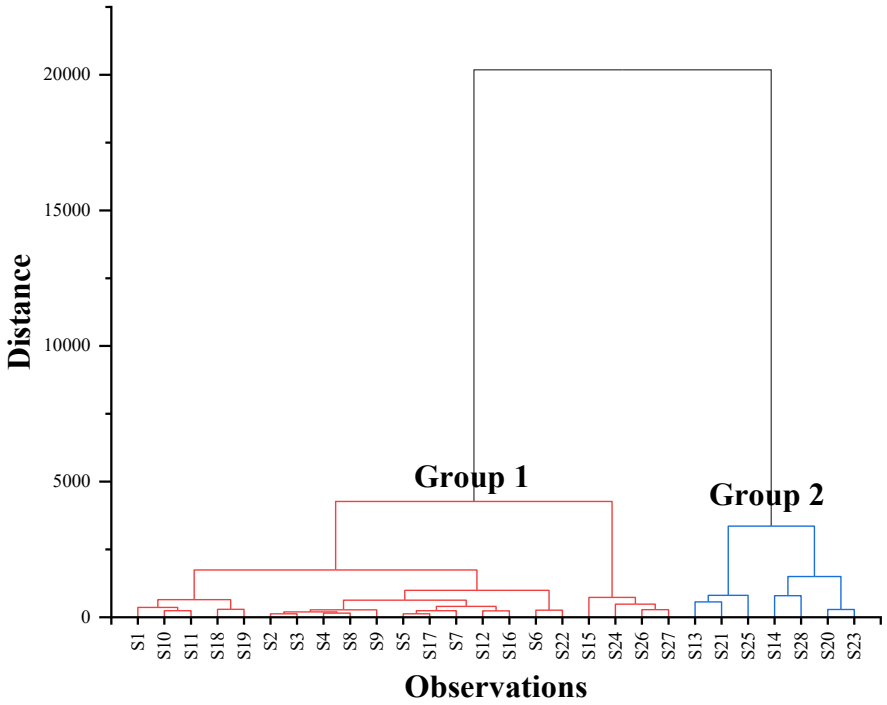

Figure 26. Hierarchical cluster dendrogram of the analyzed phreatic groundwater aquifer.

Two distinct groups of groundwater samples were established. The first group consists of twenty-one wells, and the second group consists of seven wells. The key factors distinguishing these groups appear to be Na^+, K^+, F^-, NO_3^-, HCO_3^-, Cl^-, and EC, as their concentrations exhibited a notable increase from the first group to the second, as depicted in table 16. While Na^+, K^+, HCO_3^-, Cl^-, and EC concentrations were elevated in both groups, they were notably lower when compared to the second group, with the exception of F^- and NO_3^-. The samples categorized in the first group did not exceed WHO limits for F^- and NO_3^- concentrations. Consequently, the samples in the first group indicated lower vulnerability concerning NO_3^- and F^- contamination. These samples represent a significant portion of the study area and are concentrated predominantly within the main municipality of El Oued. Conversely, the area housing the second group of samples exhibited higher vulnerability in terms of Na^+, K^+, F^-, NO_3^-, HCO_3^-, Cl^-, and EC . This area is situated on the outskirts of El Oued, Debila, and Guemar municipalities, in proximity to agricultural areas as shown in figure 27.

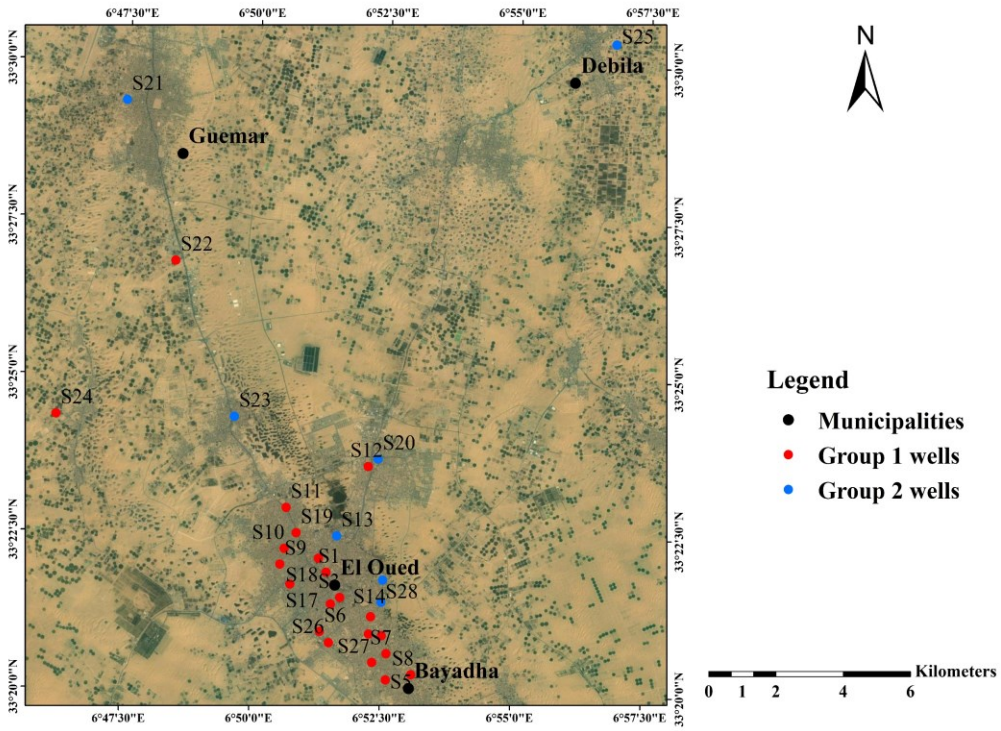

Figure 27. Map showing the spatial distribution of the generated clusters.

Table 16. A statistical summary of the selected hydrochemical parameters for the two groups generated by Hierarchical Cluster Analysis (HCA).

Groups	Group 1					Group 2				
Parameters	Mean	SD	Min	Median	Max	Mean	SD	Min	Median	Max
Ca^{2+} (mg/l)	725.5	158.7	440.9	697.4	1050	681.1	116.4	481	713.4	793.6
Mg^{2+} (mg/l)	382.1	175	36.4	449.8	627.3	378.9	197.4	145.8	313.6	705.1
Na^{+} (mg/l)	287.3	39.5	232.2	282.2	390.5	439.3	108.8	248.8	448.8	582.2
K^{+} (mg/l)	19.4	5.79	10	20.6	29.4	24.3	6.63	11.8	23.9	33.8
F^{-} (mg/l)	1.36	0.57	0.69	1.27	3.31	1.8	0.79	0.95	1.47	3.31
NO_3^{-} (mg/l)	23.5	31	0.1	4.6	120.3	40	55.8	1.93	20.5	159.4
HCO_3^{-} (mg/l)	154.4	83.3	36.6	146.4	312.3	185.8	127.6	80.5	115.9	429.4
Cl^{-} (mg/l)	353.5	120.3	124.3	337.3	702	455.1	232.4	301.8	337.3	914.7
Ph	7.2	0.41	6.78	7.08	8.57	7.39	0.55	6.9	7.1	8.31
EC (µs/cm)	3711	423.3	3100	3570	4560	6409	870.7	5170	6300	7500
T (°C)	27.9	1.8	25	27.8	31.4	27.7	0.91	26.3	28	28.8
SO_4^{2-} (mg/l)	202.6	45.9	68.2	212.9	266.1	189.5	41.1	146.2	199.5	241.5

4.1.2.7. Hydrochemical facies and controlling mechanism of the phreatic groundwater samples

Based on the stiff plot presented in figure 28, the major ion abundances in both of the generated groups in the phreatic groundwater aquifer followed an order of $Ca^{2+} > Mg^{2+} > Na^{+}+K^{+}$ and $Cl^{-} > SO_4^{2-} > HCO_3^{-}+CO_3^{2-}$. Furthermore, it was revealed that the hydrochemical facies in the phreatic groundwater aquifer exhibited slight differences between the first and the second group. The first group is characterized, according to the Piper plot shown in figure 29 (A), by the Ca^{2+}-Mg^{2+}-Cl^{-}-SO_4^{2-} type and the Ca^{2+}-Cl^{-} type. Three wells were identified as Ca type, two wells as Mg^{2+} type, and 20 wells as Cl^{-} type. C.

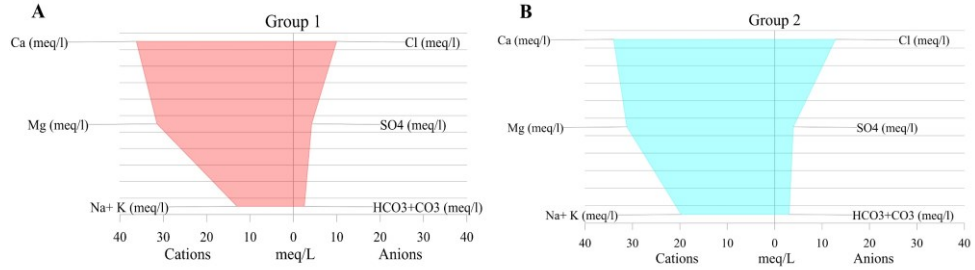

Figure 28. Stiff diagram for the two water groups, (A). group 1 and (B). group 2.

The Chadha plot of the phreatic groundwater samples in figure 29 (B) represents all the samples in both generated groups in the reverse ion-exchange Ca^{2+}- Mg^{2+}-Cl^{-} /SO_4^{2-} water type, revealing Ca^{2+}- Mg^{2+}- Cl^{-} type, Ca^{2+}- Mg^{2+} dominant Cl^{-} type, or Cl^{-}-dominant Ca^{2+}- Mg^{2+} type waters. This is characterized by alkaline earth ions (Ca^{2+} + Mg^{2+}) exceeding alkali metals (Na^{+} + K^{+}), and strong acidic anions (Cl^{-} + SO_4^{2-}) exceeding weak acidic anions (HCO_3^{-}).

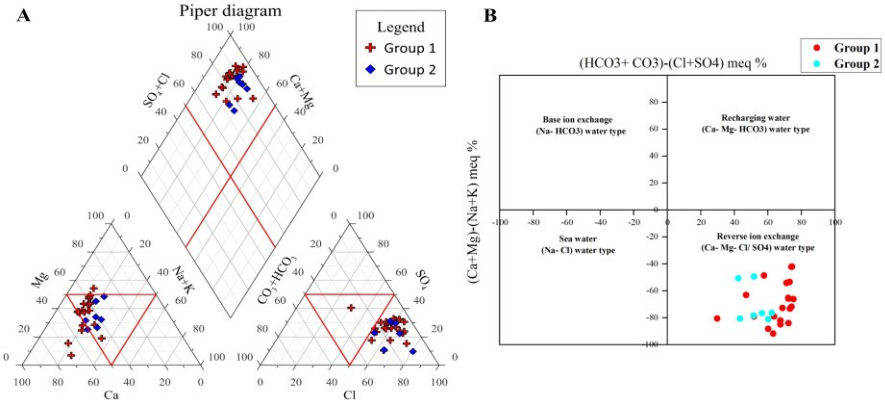

Figure 29. (A) Piper diagram for the phreatic groundwater samples, and (B) Chadha diagram of the phreatic groundwater samples.

As representations of the [Cl^{-}/(Cl^{-}/HCO_3^{-})] and [Na^{+}/(Na^{+}/Ca^{2+})] ratio fluctuations in relation to total dissolved solids (TDS), Gibbs diagrams serve as

visual illustrations of precipitation, rock, and evaporation processes. They aid in identifying the sources of dissolved chemical constituents in groundwater systems. As shown in figure 30, based on the cationic and anionic ratios versus the TDS values in both of the generated groups, the 22 phreatic groundwater samples were plotted in the evaporation-crystallization dominance (salinization) field, indicating that evaporation-crystallization has a significant influence on the majority of the total samples from the phreatic aquifer. On the other hand, two samples (S1, and S3) were plotted in rock-dominance weathering. At the same time, the chloro-alkaline indices (CAI-I, and CAI-II) that was used in this thesis for the identification of ion exchange reactions in the phreatic groundwater aquifer system. Furthermore, it was revealed that (S4, S5, S6, S7, S8, S9, S10, S12, S15, S17, S19, S22, S24, S25, S26, S27, and S28) have positive chloro- alkaline indices indicating the exchange of Na^+ and K^+ from the phreatic groundwater with Mg^{2+} and Ca^{2+} of the rocks (base-exchange reaction), while, the rest of the samples has a negative indices indicating that Mg^{2+} and Ca^{2+} from the water are exchanged with Na^+ and K^+ of the rocks as shown in figure 31.

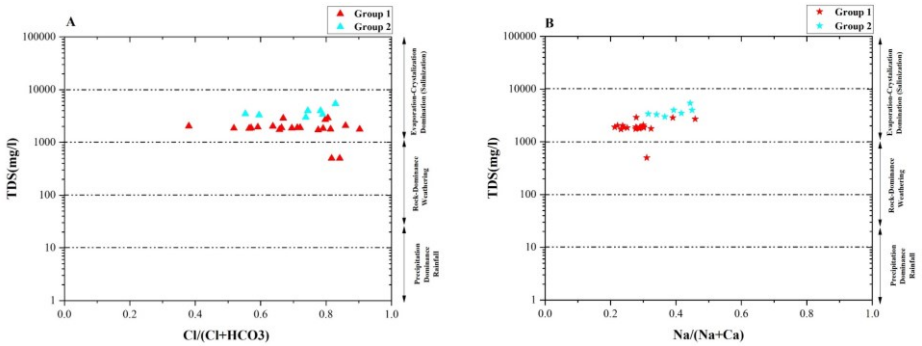

Figure 30. Gibbs diagrams of the phreatic groundwater samples.

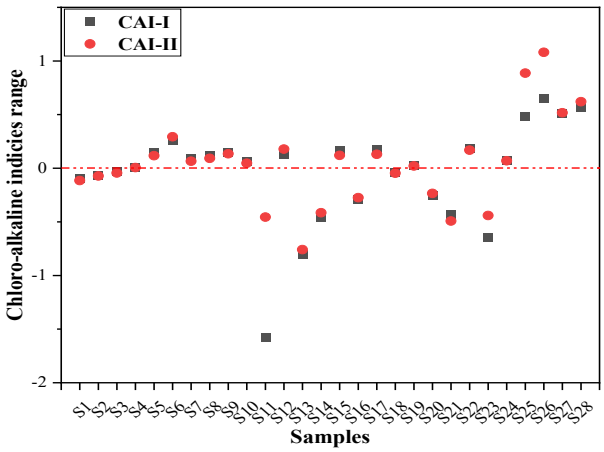

Figure 31. Chloro-alkaline indices for the two groups of the phreatic groundwater aquifer.

According to the normalized Na^+ graph of Ca^{2+} vs HCO_3^- and Ca^{2+} vs Mg^{2+}, it was illustrated that the phreatic groundwater samples from both generated groups exhibited a slight tendency towards silicate weathering and evaporate dissolution, as well as a slight tendency towards silicate weathering and carbonate dissolution, as shown in figures 32 (A), and (B).

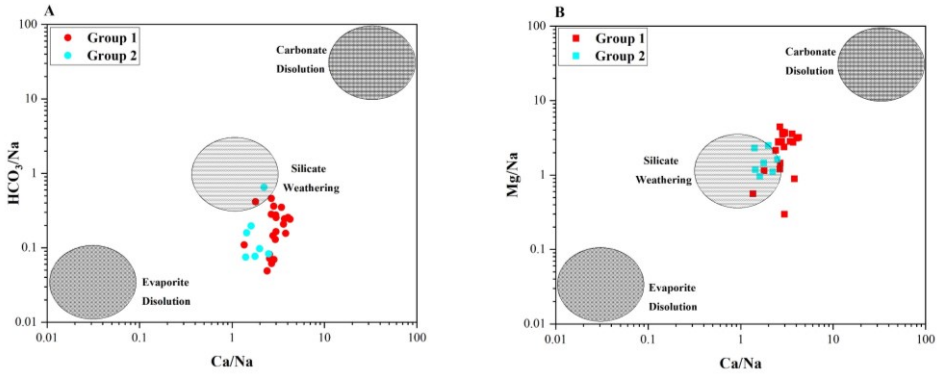

Figure 32. (A) Molar ratio in bivariate plots of Na^+ -normalized Ca^{2+} and HCO_3^-, and (B) Na^+ -normalized Ca^{2+} and Mg^{2+}.

4.1.2.8. Geochemical modelling of the phreatic groundwater aquifer

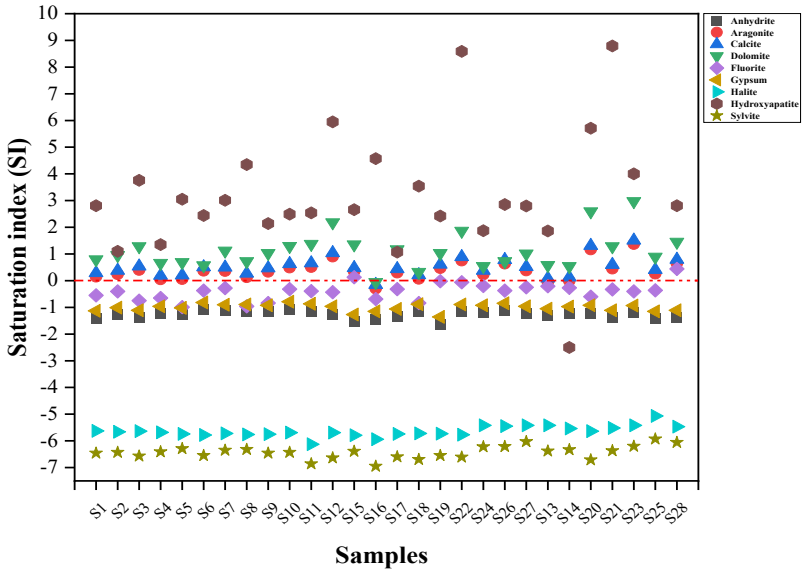

Figure 33. Saturation indices of the phreatic groundwater aquifer.

The primary influence on groundwater chemistry arises from the interplay between water and the geological formations of the aquifer. In this context, the saturation index was utilized to anticipate the potential mineral composition of the

subsurface without the need to physically collect solid-phase samples and perform mineralogical analyses on them [120]. Positive saturation index values indicate an excess of minerals in the water, potentially causing them to precipitate. Conversely, negative values suggest a deficiency, which could lead to mineral dissolution. When the saturation index falls within the range of -0.5 to +0.5, it signifies a state of equilibrium where minerals neither dissolve nor precipitate [353]. Based on the analysis of 28 samples and their resulting parameters, the computed saturation indices indicated that Anhydrite, gypsum, Halite, and Sylvite were completely dissolving since they were undersaturated (saturation index was negative). Meanwhile, Fluorite was dissolving in all the samples except S28. On the other hand, Aragonite was dissolving in S16, S13, and S14, as was Calcite in S16, and Dolomite in S16, along with Hydroxyapatite in S14. However, except for the samples characterized by the dissolution of Aragonite, Calcite, Dolomite, Fluorite, and Hydroxyapatite, the rest of the samples were characterized by the precipitation of Aragonite, Calcite, Dolomite, Fluorite, and Hydroxyapatite as shown in figure 33. Anyway, despite the precipitation and the dissolution of the specific minerals, several minerals were close to the equilibrium state in different wells.

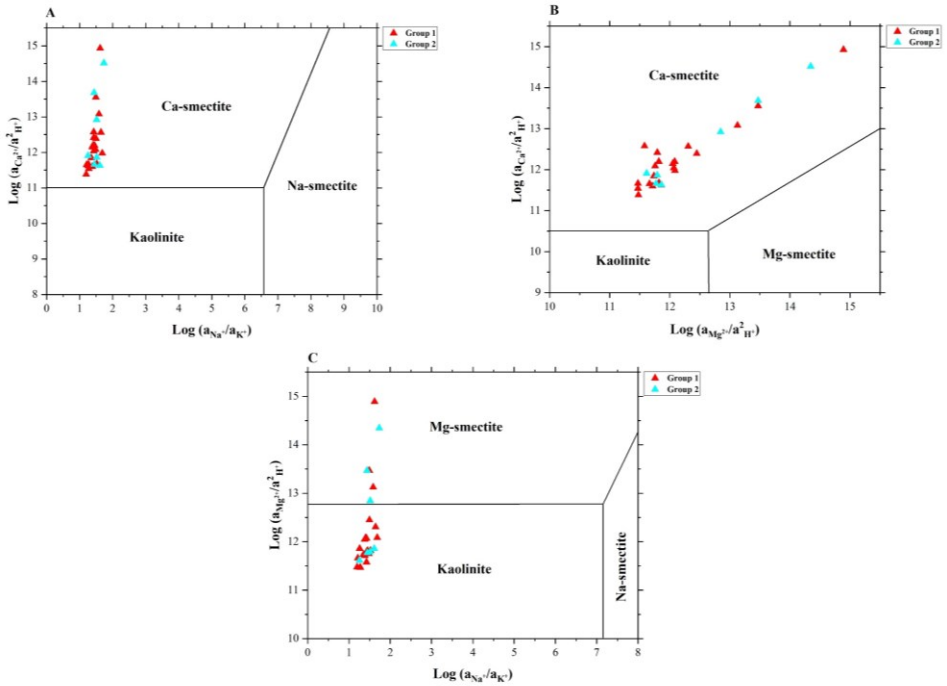

Figure 34. Mineral stability diagrams of the phreatic groundwater aquifer.

An alternative method for examining the suggested changes in water chemistry is to employ mineral stability diagrams, as suggested by [313]. Figure 34 signifies the four mineral stability fields for the $CaO–Na_2O–Al_2O_3–SiO_2–H_2O$, $CaO–MgO–Al_2O_3–SiO_2–H_2O$, and $MgO–Na_2O–Al_2O_3–SiO_2–H_2O$ systems at 25°C and 1 bar.

However, it was observed that all the samples fell within the Ca-smectite stability field, extending from the Mg-smectite field to concentrate in the Kaolinite field, indicating their role in the groundwater chemistry of the phreatic aquifer.

4.1.3. Assessment of metallic contamination in the Phreatic groundwater Aquifer

4.1.3.1. Metalic data of the phreatic groundwater aquifer

Table 17 presents the results of the statistical analysis applied to temperature, pH, and electrical conductivity, as well as the concentrations of the fifteen analyzed heavy metals. These metals are categorized into potentially toxic elements (Pb^{2+}, Cd^{2+}, Al^{3+}, Ba^{2+}, and Li^{+}), elements of probable physiological importance (Mn^{2+}, Ni^{2+}, and B^{3+}), and essential elements (Cr^{3+}, Cu^{2+}, Zn^{2+}, Fe^{2+}, and Co^{2+}). Additionally, Bi^{3+}, and Sr^{2+} were also analyzed. Cd, Co, and Li were not detectable, so they are indicated in the table as "less than the detection limit". To assess the significance of these results, all examined data were compared against the World Health Organization (WHO) standards of 2008, as no other suitable background information was available from previous studies.

Table 17. Statistical summary of the analyzed heavy metals from the phreatic groundwater aquifer of the Oued Souf Valley and its comparison with WHO standards.

Variables	Mean	SD	CV	Min	Median	Max	WHO 2008
T (°C)	27.850	1.720	0.062	25.000	27.800	31.400	-
pH	7.307	0.515	0.070	6.780	7.110	8.570	6.5–8.5
EC (µS/cm)	4035.714	858.018	0.213	3100	3725	6200	1000
Al^{3+} (mg/L)	0.309	0.083	0.269	0.220	0.290	0.520	0.2
Fe^{2+} (mg/L)	0.214	0.092	0.429	0.110	0.185	0.400	0.3
Mn^{2+} (mg/L)	0.440	0.111	0.253	0.300	0.400	0.710	0.5
B^{3+} (mg/L)	0.626	0.426	0.681	0.192	0.454	1.408	0.5
Ba^{2+} (mg/L)	0.015	0.009	0.628	0.004	0.011	0.034	0.7
Bi^{3+} (mg/L)	0.144	0.108	0.753	0.000	0.146	0.282	-
Cd^{2+} (mg/L)	<Lod	<Lod	<Lod	<Lod	<Lod	<Lod	0.003
Co^{2+} (mg/L)	<Lod	<Lod	<Lod	<Lod	<Lod	<Lod	-
Cr^{3+} (mg/L)	0.0081	0.010	1.231	0.000	0.000	0.023	0.05
Cu^{2+} (mg/L)	0.004	0.007	1.612	0.000	0.000	0.020	1
Li^{+} (mg/L)	<Lod	<Lod	<Lod	<Lod	<Lod	<Lod	-
Ni^{2+} (mg/L)	0.009	0.007	0.832	0.000	0.007	0.024	0.02
Pb^{2+} (mg/L)	0.005	0.013	2.711	0.000	0.000	0.045	0.01
Sr^{2+} (mg/L)	7.060	2.437	0.345	1.774	7.762	9.939	-
Zn^{2+} (mg/L)	0.0075	0.012	1.613	0.000	0.000	0.037	3

Although the electrical conductivity (EC) does not provide full information related to the ionic composition of the water, it is considered an important tool to indicate the salinity or the amount of total dissolved solids in the water. The EC results in the samples ranged from 3100 to 6200 µS/cm, with an average of 4035.71 µS/cm, exceeding WHO limits in all the samples. Therefore, based on [354] these waters can be classified as moderately saline waters. Nevertheless, it is crucial to

emphasize that elevated EC levels can impact the suitability of water for various purposes, including drinking and irrigation. In terms of pH values, which ranged from 6.78 to 8.57, with an average of 7.31, four samples (S3, S5, S11, and S12) exhibited acidic pH levels, which could potentially be attributed to the water's ability to dissolve metals. However, this acidity is not known to directly pose any health risks [355]. One sample, (S4), had a neutral pH, while the remaining samples had a basic pH. All of the samples fell within the range of WHO limits for drinking water, ensuring they meet the standards for human consumption.

4.1.3.2. Variations in Heavy Metals in the Phreatic Aquifer

Without considering Cd^{2+}, Co^{2+}, and Li^{+}, the other twelve analyzed heavy metals from the phreatic groundwater aquifer exhibited a dominance order as follows: $Sr^{2+} > B^{3+} > Mn^{2+} > Al^{3+} > Fe^{2+} > Bi^{3+} > Ba^{2+} > Ni^{2+} > Cr^{3+} > Zn^{2+} > Pb^{2+} > Cu^{2+}$. The differences in standard deviations, as highlighted in table 17, can be attributed to the variety of source strengths, and the geoenvironmental nature of the large and diverse sampling sites controlled by their physicochemical characteristics, larger variability, and human activities [356].

Fe^{2+} concentrations ranged from 0.110 to 0.40 mg/L, with three samples (S1, S8, and S14) surpassing the permissible limit set by the World Health Organization (WHO), while the rest of the samples remained below the acceptable threshold. The increased concentrations of Fe^{2+} in the study areas, particularly those that exceeded the WHO limits, can be attributed to several possible explanations related to natural and anthropogenic factors. However, the redox conditions of iron-bearing minerals in both rocks and soils may be the underlying cause of these variations [357]. At the same time, the corrosion of pump parts that equip the vertical drainage system of the study area might be listed as another reason for high Fe^{2+} concentrations [358]. Additionally, the dissolution of $FeCO_3$ at lower pH levels and the chemical reaction of oxidized Fe^{3+} minerals with organic matter can also raise the Fe^{2+} levels in aquatic systems [359]. The removal of dissolved oxygen by organic matter, which results in reduced conditions, may be another cause of high Fe^{2+} content which is reflected in the study area history (rising of groundwater level and the contact the septic tanks) [360]. Furthermore, Sewage also introduces a variety of microorganisms into the groundwater system, including those capable of reducing iron. These bacteria can facilitate the conversion of iron from its less soluble ferric form Fe^{3+} to the more soluble ferrous form Fe^{2+}.Under reducing conditions, the solubility of Fe^{2+}-bearing minerals increases, leading to the enrichment of dissolved iron in groundwater [361]. The obtained results indicated that the color of most samples changed from clear to red-brown, indicating the precipitation of FeO(OH). Several anthropogenic reasons might account for the elevated Fe concentrations in the groundwater. These include industrial waste leachates and activities from mechanic workshops [189]. Additionally, the oxidizing process of pipes in the water distribution system can also lead to the release of Fe^{2+} [357]. As for Mn^{2+} concentrations, they varied from 0.30 to 0.71 mg/L, with three samples (S1, S12, and S14) exceeding the limit, while the

remaining samples had concentrations below the limits. Similar to Fe^{2+}, Mn^{2+} is also one of the most prevalent metals in the earth's crust and is naturally present in the environment [358].

In the case of B^{3+}, the results ranged from 0.192 to 1.408 mg/L, with six samples (S9, S10, S11, S12, S13, and S14) that surpassed WHO limits, while the rest of the samples were under the allowable standards. In soils with a pH of 8.5, boron (B^{3+}) typically exists in the non-ionized form H_3BO_3, but at pH 8.5, it exists as the anion $B(OH)_4$ [362]. Industrial and home effluents emitted boron compounds into the water. Through the use of fertilizer, it may also be spread throughout the ecosystem. As all of the samples had pH values below 8.5, it seems that B^{3+} would appear as a non-ionized form. Long-term exposure to B^{3+} causes mild gastrointestinal irritation. Ba^{2+} concentrations from the analyzed samples did not exceed WHO limits since their range was from 0.004 to 0.034 mg/L. Ba^{2+} occurs usually as a complex of compounds in the crust of the earth and it can be used in different industrial activities. However, its presence in groundwater systems comes mainly from geogenic sources [363]. Ni^{2+} values ranged from 0 to 0.024 mg/L, and its concentration exceeded the WHO limit in S2, while S3, and S4 Ni^{2+} concentrations were within the permissible limits.

Zn^{2+} is a necessary trace element that may be found in almost every type of food and drink, either as salt or as organic complexes. However, metal smelters and mining operations are other environmental sources of zinc. When zinc is manufactured and utilized with other materials including brass, bronze, alloys, rubber, and paints, the metal may be ejected into the environment through several kinds of waste streams [364]. Zn^{2+} concentrations were below WHO guidelines and varied from 0 to 0.037 mg/L. As a trace metal, Cu^{2+} in high concentrations can have adverse effects on human health [365,366]. However, Cu^{2+} concentrations in the analyzed samples were below WHO guidelines and they varied from 0 to 0.020 mg/L. Superphosphate has the greatest impurity amounts of Cu^{2+}, with other metals such as Zn^{2+}, when compared to other fertilizers used on farmland, and its heavy metals may accumulate in soils in areas that have been used for agriculture for long periods [367,368].

Cr^{3+} had concentrations below the recommended limit, since their results ranged from 0 to 0.023 mg/L. The Pb^{2+} content in natural streams rises mostly as a result of human activity [369]. Paint, batteries, leaded gasoline and farmland diesel fuel use are some potential sources of lead in groundwater, and they were, and still are, used in the study area. Moreover, various insecticides include lead arsenate. In our study area, Pb^{2+} varied from 0 to 0.045 mg/L, and two samples (S13 and S14) exceeded the recommended limit of the WHO.

In another vision, Sr^{2+} has no limit since the WHO has not established a guideline for it. Based on the Federal-Provincial-Territorial Committee on Drinking Water [370], the allowable limit for drinking purposes was set to be 7 mg/L. However, Sr^{2+} levels oscillated from 1.774 to 9.939 mg/L, with eight samples exceeding the recommended guidelines (S1, S6, S7, S9, S10, S11, S12, and S13), while the remaining samples were within the limits. Agricultural activity produces an input of Sr^{2+} in huge amounts, suggesting that the source may be anthropogenic. To some extent, this is dependent on the amount of fertilizers,

carbonate additions, and manure from animals such as cattle and poultry [371]. The presence of strontium in the soil may also be attributed to the disposal of waste materials and industrial effluents. Water dissolves strontium in soil, allowing it to penetrate the earth more deeply and reach groundwater.

On the contrary, Al^{3+} concentrations in all fourteen samples ranged from 0.220 to 0.520 mg/L, surpassing the drinking water guidelines established by the WHO. Aluminum predominates in water with a neutral reaction as organic and hydroxide complexes, while fluoride and sulfate complexes are present in lesser amounts [372]. However, in relation with our results, aluminum and its organic complexes, as well as $Al(OH)_3$, appear to be harmless [373]. Another reason that might explain the high concentration of Al^{3+} is the six industrial factories processing aluminum in the Oued Souf region. In terms of Bi^{3+}, there are no guidelines for the recommended Bi^{3+} concentrations set by the WHO for drinking purposes. However, the Bi^{3+} concentrations in the analyzed phreatic groundwater samples ranged from 0 to 0.282 mg/L [374].

4.1.3.3. Spatial Patterns Detection

The accuracy evaluation of the IDW interpolation technique for the different examined heavy metals in the phreatic groundwater aquifer is summarized in table 18. According to the goodness-of-fit criterion, the model with the lowest RMSPE was the best fit for comprehending the spatial distribution patterns of the selected heavy metals. Figures 35 and, 36 represent the spatial distribution maps processed by the IDW method.

Table 18. Best-fitted interpolation models and cross-validation for IDW of heavy metals of the phreatic groundwater aquifer.

Parameters	Cross-Validation	K = 1	K = 2	K = 3	Optimized Errors	Optimized K Value
Al^{3+}	MPE	0.0015	0.0018	0.0031	0.0029	2.8692
	RMSPE	0.0835	0.0803	0.0795	0.0795	
Fe^{2+}	MPE	0.0011	−0.0009	−0.0016	−0.0002	1.5670
	RMSPE	0.1042	0.1039	0.1048	0.1038	
Mn^{2+}	MPE	0.0177	0.0232	0.0261	0.0177	1
	RMSPE	0.1278	0.1413	0.1527	0.1278	
B^{3+}	MPE	0.0356	0.0373	0.0310	0.0356	1
	RMSPE	0.5338	0.5667	0.5916	0.5338	
Ba^{2+}	MPE	−0.0002	−0.0006	−0.0009	−0.0002	1
	RMSPE	0.0115	0.0121	0.0127	0.0115	
Bi^{3+}	MPE	−0.0003	0.0020	0.0039	−0.0003	1
	RMSPE	0.1467	0.1580	0.1667	0.1467	
Cr^{3+}	MPE	0.0010	0.0018	0.0023	0.0010	1
	RMSPE	0.0118	0.0126	0.0134	0.0118	
Cu^{2+}	MPE	0.0006	0.0007	0.0007	0.0006	1
	RMSPE	0.0098	0.0102	0.0104	0.0098	
Ni^{2+}	MPE	0.0011	0.0019	0.0024	0.0011	1
	RMSPE	0.0079	0.0085	0.0091	0.0079	
Pb^{2+}	MPE	−0.0003	−0.0008	−0.0012	−0.0016	17.4658
	RMSPE	0.0181	0.0180	0.0180	0.0180	
Sr^{2+}	MPE	−0.0979	−0.2642	−0.3917	−0.0979	1
	RMSPE	2.7595	2.9281	3.0984	2.7595	
Zn^{2+}	MPE	0.0009	0.0018	0.0025	0.0017	1.7984
	RMSPE	0.0123	0.0120	0.0123	0.0120	

In comparison to the other areas, where Al^{3+} concentrations were high throughout the study area, there were low values represented by the first class (0.22–0.27 mg/L). These low values were observed from the north to the east of El Oued, covering S14 and S7 (Ourmes and El Oued) and even surrounding S13 in the south (El Oued). From these points, the concentrations gradually increased towards the north, east, and southwest, reaching almost the middle of the study site, encompassing the northern part of the investigated area.

Similarly, low concentrations of Fe^{2+} that did not exceed the WHO limits were found in the west of the Oued Souf Valley, specifically in an agricultural site (Kouinine, S6), in the east in peri-urban areas (El Oued, S7), and even in the south (between El Oued and Bayadha, S4, and S5). A similar pattern of spatial behavior was observed between the distribution of Fe^{2+} and Al^{3+} values, where Fe^{2+} values exceeded the limits in the north (Ouermes-S14), which is an agricultural site, and surrounded S8 and S1 in an area that approximately spreads from the middle west to the center of the study area, covering the northern part of El Oued municipality (see figure 35).

As well as the other elements that are related to each other, Mn^{2+} concentrations were increasing from the east of the study area toward the north and the south of the Oued Souf Valley. Furthermore, the high values that exceed the limits are located in the north (Ouermes municipality), which is an agricultural site, and S1 and S10 in El Oued (an urban area). Visually, it was also possible to observe a similar pattern between Mn^{2+}, Cu^{2+}, and Pb^{2+}, where the highest levels were found in the northern part of the Valley, which included the agricultural site (S14).

In connection to Mn^{2+}, low concentrations of B^{3+} are situated in almost the center of Oued Souf and extend from the west to the east, including S6, S7, and S8, and also in a small area surrounding S1, and the south including S3, S4, and S5. Then, the concentrations gradually increase toward the north to S14. Although Ba^{2+} and Cu^{2+} did not exceed the limit, another spatial similarity between them has been detected, where the highest values of Cu^{2+} and Ba^{2+} are located north of the study area covering S14. In contrast, an almost analogous spatial behavior can be noticed between Sr^{2+}, Bi^{3+}, Cr^{3+}, Ni^{2+}, and almost in the case of Zn^{2+}. However, the highest values are always found in the west of Oued Souf City, touching an agricultural site (S6), with some differences in the south (El Oued municipality) in various cases, such as Bi^{3+} (S8, and S5), Cr^{3+} (S3, S4, and S5), Ni^{2+} (S2, S3, S4, and S5), and Zn^{2+} (S3, and S4).

The consistent spatial patterns observed among the analyzed heavy metals in the study area are primarily governed by their respective origins and the direct and indirect interconnections they share with one another. These interrelationships are probably influenced by both natural (geogenic) and human-made (anthropogenic) sources. Geogenic sources include minerals and rocks susceptible to weathering, with heavy metals adsorbing onto specific mineral surface sites. Anthropogenic sources involve factors such as industrial discharge, household waste, and the use of various types of fertilizers. These combined factors contribute to the observed relationships among the heavy metals [362]. The septic source of the majority of these heavy metals is closely related to the study area's history, specifically when the phreatic groundwater aquifer rose to or was near the surface.

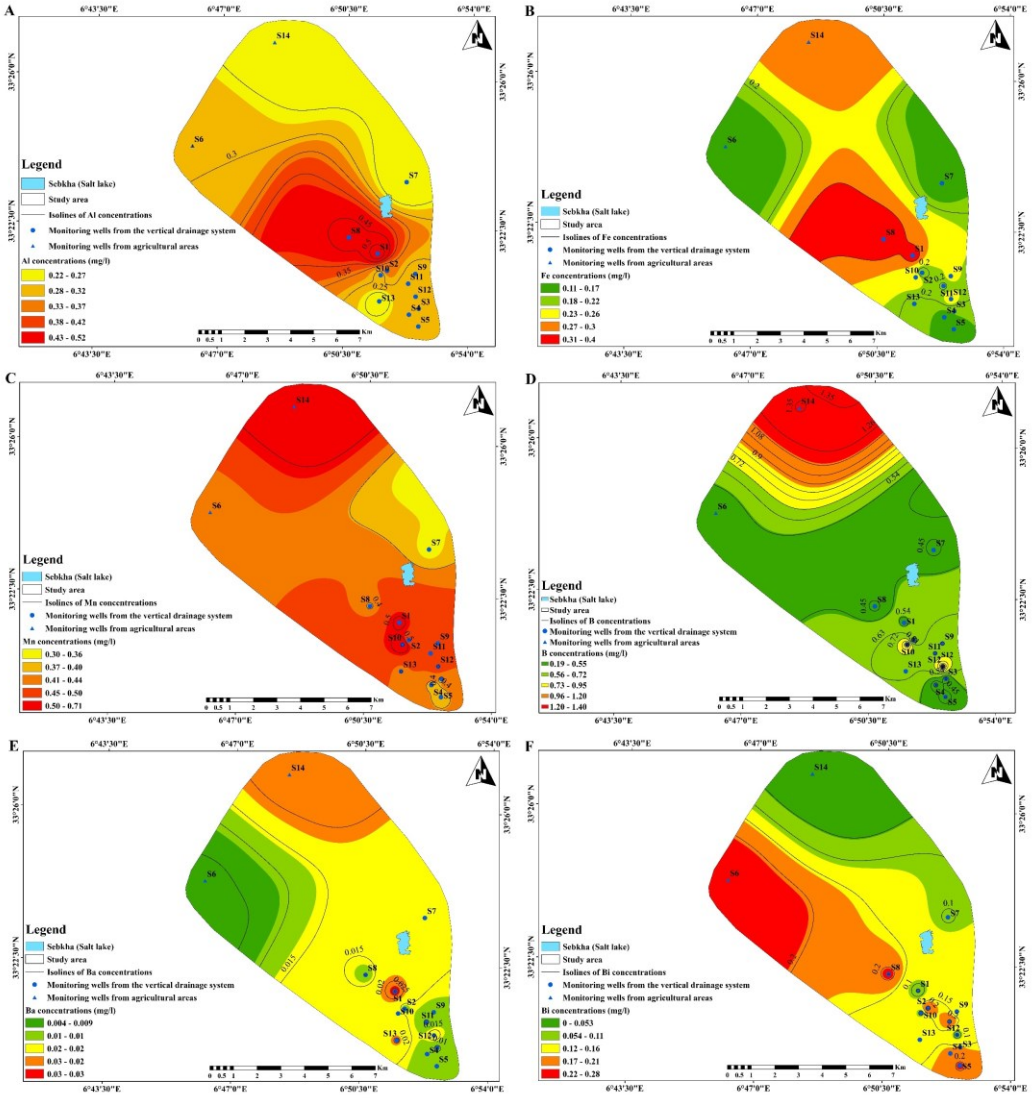

Figure 35. IDW spatial distribution maps of heavy metals concentration in the phreatic aquifer: (A). aluminum- Al^{3+}, (B). iron- Fe^{2+}, (C). manganese- Mn^{2+}, (D). boron- B^{3+}, (E). barium- Ba^{2+}, (F). bismuth- Bi^{3+}.

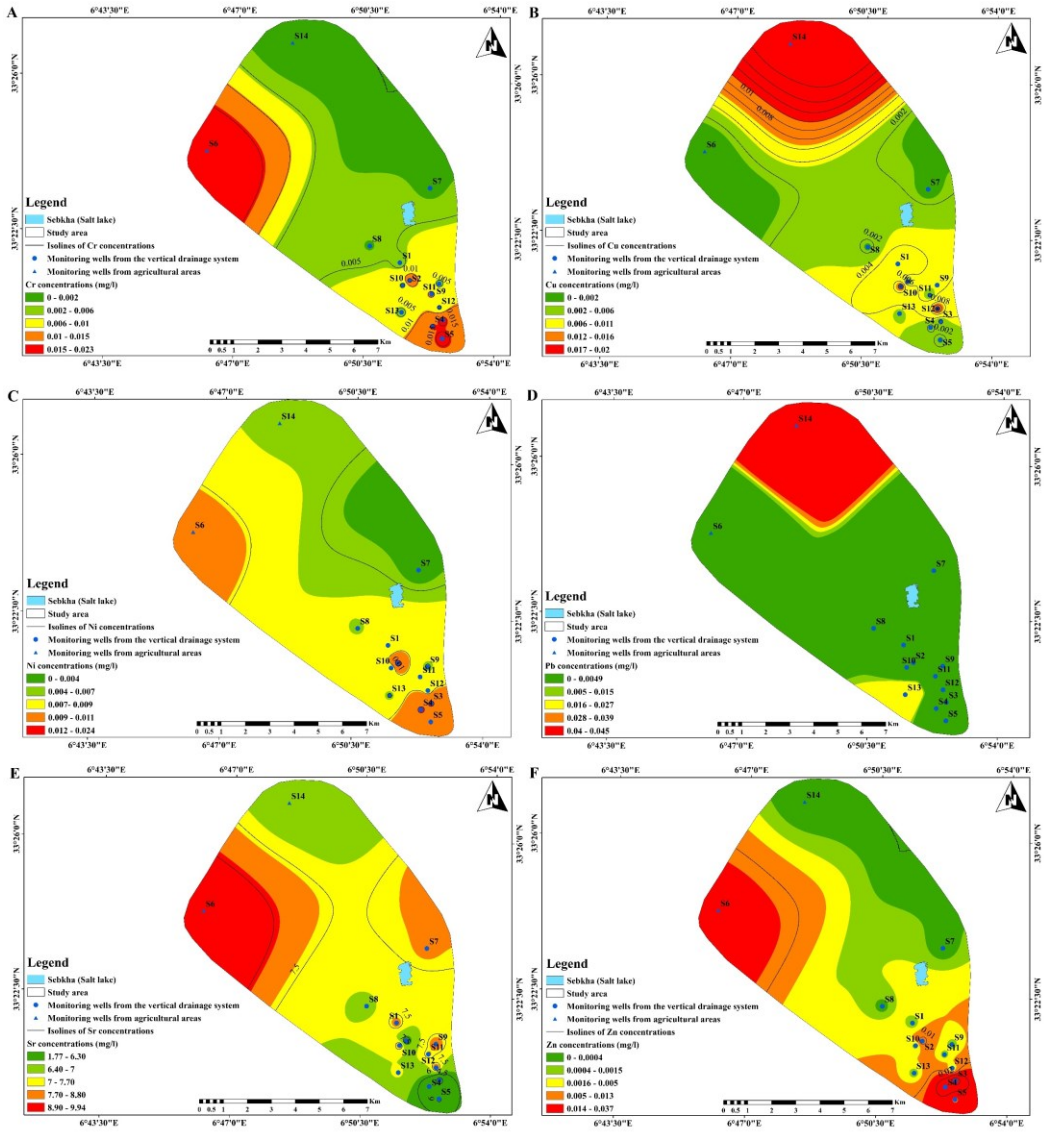

Figure 36. IWD spatial distribution maps of heavy metals concentration in the phreatic aquifer: (A). chromium- Cr^{3+}, (B). copper- Cu^{2+}, (C). nickel- Ni^{2+}, (D). lead- Pb^{2+}, (E). strontium- Sr^{2+}, (F). zinc- Zn^{2+}.

4.1.3.4. Cluster Analysis of the phreatic groundwater samples based on their metalic concentrations

The combined application of clustering analysis with Ward's linkage approach and Euclidean distance considered all the examined metals (Pb^{2+}, Al^{3+}, Ba^{2+}, Mn^{2+},

Ni^{2+}, B^{3+}, Cr^{3+}, Cu^{2+}, Zn^{2+}, Fe^{2+}, Bi^{3+}, and Sr^{2+}) on the normalized data to construct prospective groups present in the phreatic groundwater samples. Consequently, two groups have been plotted on the dendrogram (figure 37). Al^{3+}, Fe^{2+}, Mn^{2+}, B^{3+}, Ba^{2+}, Cu^{2+}, Pb^{2+}, and Sr^{2+} were considered key factors in the identification of the resulting groups through the HCA process, as shown in table 19.

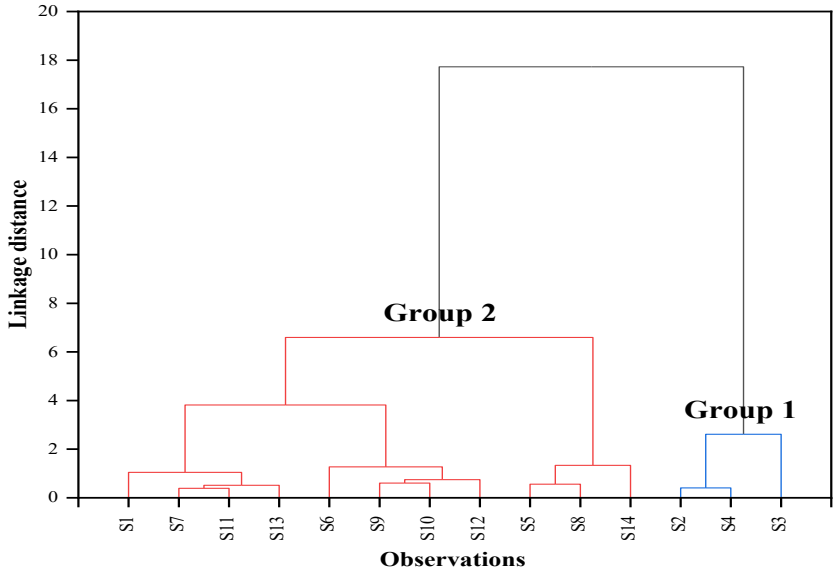

Figure 37. Dendrogram of hierarchical cluster analysis.

The samples in the first group reflected a lower risk of contamination in terms of heavy metals due to their lower concentrations compared to the second group. The area containing the second group samples was more vulnerable to heavy metals, which likely originated from urban, peri-urban, and even agricultural areas, as shown in figure 38.

Table 19. Statistical summary of the generated groups from HCA based on the analyzed phreatic groundwater samples.

Heavy Metals	**Group 1**				**Group 2**			
Parameters	**Mean**	**Median**	**Minimum**	**Maximum**	**Mean**	**Median**	**Minimum**	**Maximum**
Al^{3+}	0.30	0.3	0.28	0.33	0.31	0.29	0.22	0.52
Fe^{2+}	0.15	0.15	0.12	0.17	0.23	0.23	0.11	0.40
Mn^{2+}	0.37	0.37	0.35	0.38	0.46	0.42	0.30	0.71
B^{3+}	0.24	0.246	0.19	0.27	0.73	0.579	0.31	1.41
Ba^{2+}	0.01	0.008	0.01	0.01	0.02	0.016	0.00	0.03
Bi^{3+}	0.21	0.188	0.17	0.28	0.12	0.1	0.00	0.27
Cr^{3+}	0.02	0.022	0.02	0.02	0.00	0	0.00	0.02
Cu^{2+}	0.00	0	0.00	0.00	0.01	0.002	0.00	0.02
Ni^{2+}	0.02	0.019	0.02	0.02	0.01	0.006	0.00	0.01
Pb^{2+}	0.00	0	0.00	0.00	0.01	0	0.00	0.05
Sr^{2+}	3.15	3.642	1.77	4.02	8.13	8.158	6.19	9.94
Zn^{2+}	0.03	0.03	0.01	0.04	0.00	0.00	0.00	0.02

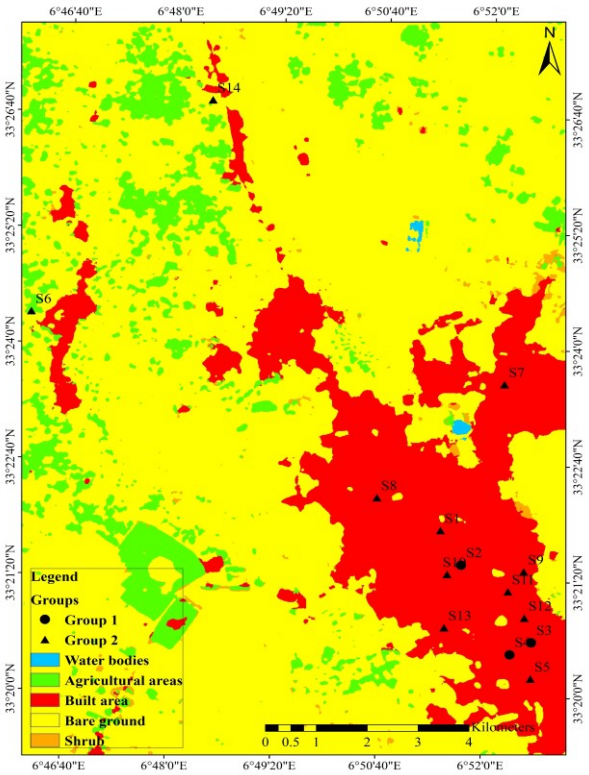

Figure 38. Cluster map of the clustered groups based on the phreatic groundwater samples.

4.1.3.5. Evaluation of the Heavy-Metal pollution in the Phreatic Aquifer

Figures 39- 41 illustrate the range of computed pollution indices based on the analyzed heavy metals from the phreatic groundwater aquifer. The presence of outliers in the contamination factor results for Al^{3+} and Pb^{2+} can probably be associated with the historical pollution event, which might still be affecting the data, along with the small number of samples. However, among the samples, 100% showed medium contamination from Al^{3+}, while 78% (eleven samples) exhibited low contamination, and 21.42% (three samples) had medium contamination of Fe^{2+}. Additionally, 50% of the samples showed both low and medium contamination with B^{3+}, whereas 100% of the samples were low in contamination with Ba^{2+}. As for Mn^{2+}, ten samples (71.43%) had a low contamination factor, and four samples (28.57%) were low in terms of Mn^{2+}. All samples showed low contamination factors for Cr^{3+}, Cu^{2+}, and Zn^{2+}. Regarding Sr^{2+}, Ni^{2+}, and Pb^{2+}, 42.86%, 78.57%, and 85.71% of the samples had low contamination factors, respectively, while 57.14%, 21.43%, and 14.29% of the samples had medium contamination factors.

The overall degree of contamination of the studied metals revealed that the majority of analyzed phreatic groundwater samples had a low degree of contamination, accounting for 78.57% of the samples. Only three samples (S10, S12, and S14) were characterized by a moderate degree of contamination.

Regarding the accumulations of heavy metals, whether anthropogenic or geological in nature, it was observed that Fe^{2+}, Mn^{2+}, Ba^{2+}, Cr^{3+}, Cu^{2+}, Ni^{2+}, Sr^{2+}, and Zn^{2+} did not reach contamination levels, indicating lower accumulations. However, in the case of B^{3+}, four samples (S9, S10, S12, and S14) showed values of the geoaccumulation index ranging from uncontaminated to moderately contaminated. The remaining samples were classified as uncontaminated in terms of B^{3+}.

The geoaccumulation index results indicated that S13 was uncontaminated to moderately contaminated, and S14 was moderately contaminated in relation to Pb^{2+}. Additionally, three samples (S1, S2, and S8) were classified as uncontaminated to moderately contaminated, while the rest of the samples did not reach the contamination level for the studied heavy metals.

In summary, the majority of the analyzed phreatic groundwater samples showed a low degree of contamination, with only a few samples exhibiting a moderate degree of contamination. The geoaccumulation index provided insights into the accumulations of different heavy metals, highlighting some samples with moderate contamination levels for certain elements.

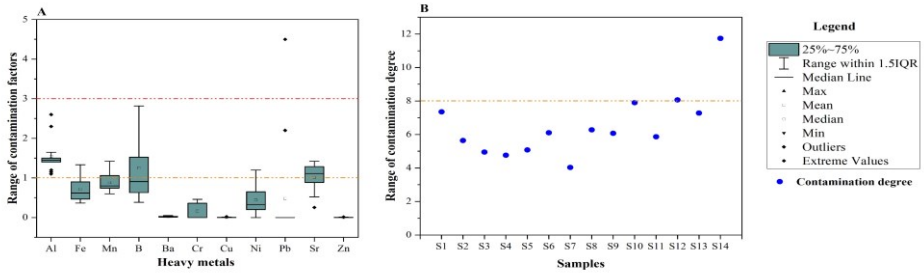

Figure 39. (A) Box plot of contamination factors. (B) Scatter plot of contamination degree.

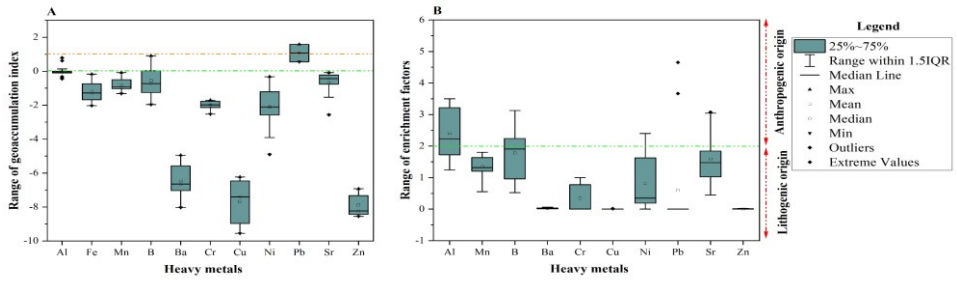

Figure 40. (A) Box plot of geoaccumulation index. (B) Box plot of enrichment factors.

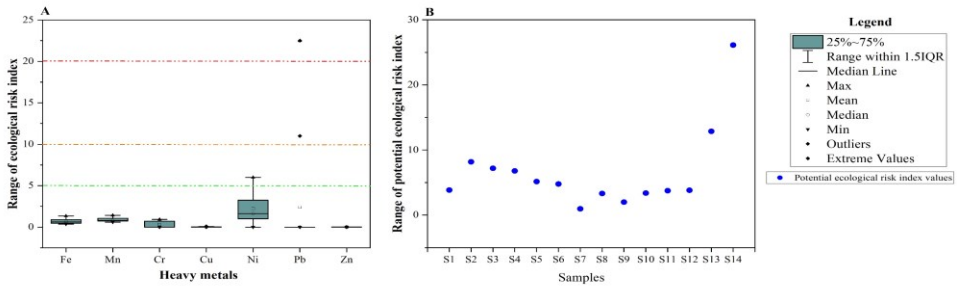

Figure 41. (A) Box plot of ecological risk index. (B) Scatter plot of the potential ecological index.

Regarding the enrichment of the studied metals in the phreatic aquifer, the analyzed metals had an enrichment trend of $Al^{3+} > B^{3+} > Sr^{2+} > Mn^{2+} > Ni^{2+} > Pb^{2+} > Cr^{3+} > Ba^{2+} > Cu^{2+} > Zn^{2+}$. Furthermore, all of the samples had minor enrichment in terms of Ba^{2+}, Cr^{3+}, Cu^{2+}, and Zn^{2+}, suggesting their geogenic source. In accordance with Al^{3+}, nine samples had a minor enrichment by Al^{3+} (S1, S3, S11, S8, S9, S10, S12, S13, and S14), while the other five samples had a moderate enrichment by Al^{3+}. Overall, the enrichment values of Al^{3+} suggested the anthropogenic source of Al^{3+} in the thirteen samples that cover almost all of the study area [327] Despite the minor enrichment by Mn^{2+} in all of the analyzed samples, S2, S4, S5, S6, S7, and S10 had enrichment factor values above 1.5, suggesting their anthropogenic source, which was reinforced by their being located mainly in El Oued (urban areas) and Kouinine (agricultural area). The possible anthropogenic source of Mn^{2+} in urban areas can be represented by wastewater, acid mine drainages [375], landfill leachates, and legal and illegal industries [376]. Meanwhile, the anthropogenic source of Mn^{2+} in rural areas can result from manganese-containing fertilizers such as manganese sulfate ($MnSO_4$), pesticides and herbicides, and livestock farming [377]. Furthermore, the enrichment by B^{3+} was minor in eight samples (S1, S2, S3, S4, S5, S8, S9, and S11), while the rest of the other samples reflect a moderate enrichment by B^{3+}. However, S6, S7, S10, S12, S13, and S14 had an enrichment suggesting the anthropogenic source of B^{3+}. In terms of Ni^{2+}, most of the phreatic groundwater samples showed minor enrichment, except for S2 and S4, which had moderate enrichment. Furthermore, four samples that were located in El Oued and Bayadha (S2, S3, S4, and S5) probably had an anthropogenic origin. In any case, S13 and S14 represented an anthropogenic moderate enrichment by Pb^{2+}, while the rest of the other samples were of minor enrichment. Correspondingly, three samples (S5, S6, and S7) were characterized by moderate enrichment by Sr, while the rest of the sample had minor enrichment by Sr^{2+}. Overall, six samples (S5, S6, S7, S11, S12, and S13) were of anthropogenic origin. Ecologically, all of the studied heavy metals represented no ecological risk, since their results were below 5, except for two samples: S13, which represents a considerable ecological risk, and S14, which represents a high ecological risk in terms of Pb^{2+}. Meanwhile, all of the samples reflected a low potential ecological risk concerning all of the metals.

4.1.3.6. Risk Evaluation of Human Health from the Heavy Metals of the Phreatic Aquifer

The presence of heavy metals with high concentrations in any groundwater system may generate a risk of adverse effects on human health, causing several serious effects that can vary from shortness of breath to several types of cancers in human beings (a significant threat to the normal performance of human body tissues) [326,378], reduced growth and development, organ damage, nervous system damage, and in extreme cases, death. The toxicity of heavy metals increases because of their non-metabolization and their accumulation in soft tissues [379,380]. Animal tissues have been found to have undergone morphological, histological, and biochemical changes after being exposed to environmental toxins such as heavy metals for an extended duration, even at very low concentrations [378]. Table 20 represents the results of the chronic daily intake (CDI) of the analyzed metals in this research. In figure 42, all of the obtained outcomes, including the hazard quotient (HQ) and hazard index (HI), are shown. For adults, the chronic daily intake (CDI) values with respect to all the analyzed metals were below the oral reference dose (RfD), leading to HQ values lower than 1 for all samples, indicating an acceptable level of non-concern. However, for eight samples (S1, S6, S9, S10, S11, S12, S13, and S14), the hazard index (HI) values were above 1, indicating a high long-term health risk and a non-negligible non-carcinogenic adverse effect in the case of adults. This high risk is attributed to the high presence of Al in most samples, and Fe^{2+}, Mn^{2+}, B^{3+}, Ni^{2+}, and Sr^{2+} in other wells. For children, the CDI values were below the RfD for Al^{3+}, Fe^{2+}, B^{3+}, Ba^{2+}, Cr^{3+}, Cu^{2+}, Ni^{2+}, Pb^{2+}, and Zn^{2+}. However, the CDI was above the RfD for Sr in S6 (CDI = 0.63537) and Mn^{2+} in S10 (CDI = 0.04538). Most of the analyzed heavy metals had HQ values less than 1 for children, except Mn^{2+} and Sr^{2+}. HQ values of Mn^{2+} exceeded 1 in nine samples (S1, S2, S6, S9, S10, S11, S12, S13, and S14), and the HQ of Sr^{2+} was high in two samples (S6 and S12).

Table 20. Statistical summary of the computed chronic daily intake (CDI) results for adults and children of Oued Souf.

Cases	Adults				Children			
Elements	**Mean**	**S.D**	**Min**	**Max**	**Mean**	**S.D**	**Min**	**Max**
Al^{3+}	0.0085	0.0023	0.006	0.0143	0.0198	0.0053	0.0141	0.0332
Fe^{2+}	0.0059	0.0025	0.003	0.011	0.0137	0.0059	0.007	0.0256
Mn^{2+}	0.0121	0.0031	0.0082	0.0195	0.0281	0.0071	0.0192	0.0454
B^{3+}	0.0171	0.0117	0.0053	0.0386	0.04	0.0273	0.0123	0.09
Ba^{2+}	0.0004	0.0003	0.0001	0.0009	0.0009	0.0006	0.0003	0.0022
Cr^{3+}	0.0002	0.0003	0	0.0006	0.0005	0.0006	0	0.0015
Cu^{2+}	0.0001	0.0002	0	0.0006	0.0003	0.0005	0	0.0013
Ni^{2+}	0.0002	0.0002	0	0.0007	0.0006	0.0005	0	0.0015
Pb^{2+}	0.0001	0.0004	0	0.0012	0.0003	0.0008	0	0.0029
Sr^{2+}	0.1934	0.0668	0.0486	0.2723	0.4513	0.1558	0.1134	0.6354
Zn^{2+}	0.0002	0.0003	0	0.001	0.0005	0.0008	0	0.0024

The current level of Fe^{2+}, Mn^{2+}, B^{3+}, Ni^{2+}, Pb^{2+}, Sr^{2+}, and Al^{3+} penetrating the digestive tract or causing skin contamination through the phreatic groundwater can have diverse effects on human health, since an excessive amount of iron in the body could raise concerns due to its potential link with various chronic illnesses such as heart disease [381,382] and diabetes [383,384]. High manganese exposure, often from contaminated drinking water, can cause neurotoxic effects, including tremors and cognitive impairment [385]. Furthermore, boron exposure may lead to gastrointestinal symptoms and, in chronic cases, kidney damage or developmental issues in children [386].

The buildup of nickel and its compounds within the body as a result of prolonged exposure could lead to a range of detrimental health effects in humans, including conditions such as lung fibrosis, kidney problems, cardiovascular diseases, and respiratory tract cancer [387,388]. Lead exposure, particularly in children, can result in developmental delays and cognitive problems, while adults may experience high blood pressure and fertility issues [389]. Strontium is less toxic than some other heavy metals, but excessive exposure can lead to bone problems, including changes in bone density [390]. Aluminum levels have been associated with neurological disorders such as Alzheimer's disease [391].

Consequently, the Hazard Index (HI) scores registered exceedingly elevated levels concerning children, encompassing all the wells within the research area. This indicates a substantial and enduring health hazard, along with a noteworthy non-cancer-related adverse impact. Elevated HI scores not only imply immediate dangers but also project into the foreseeable future. Prolonged exposure to these contaminants may result in persistent health issues, with the potential to impede the growth and development of children. Furthermore, children are inherently more susceptible to environmental pollutants than adults, given their ongoing physical development and their tendency to consume or breathe in a higher proportion of pollutants relative to their body weight.

Consequently, the elevated HI scores for children warrant special concern. Hence, it is imperative to involve pertinent authorities, including environmental agencies and public health departments, in formulating and executing strategies aimed at mitigating these risks and safeguarding the well-being of children in the affected region. Additionally, active community engagement and the dissemination of information about potential hazards and protective measures are essential steps to ensure the welfare of residents, particularly children.

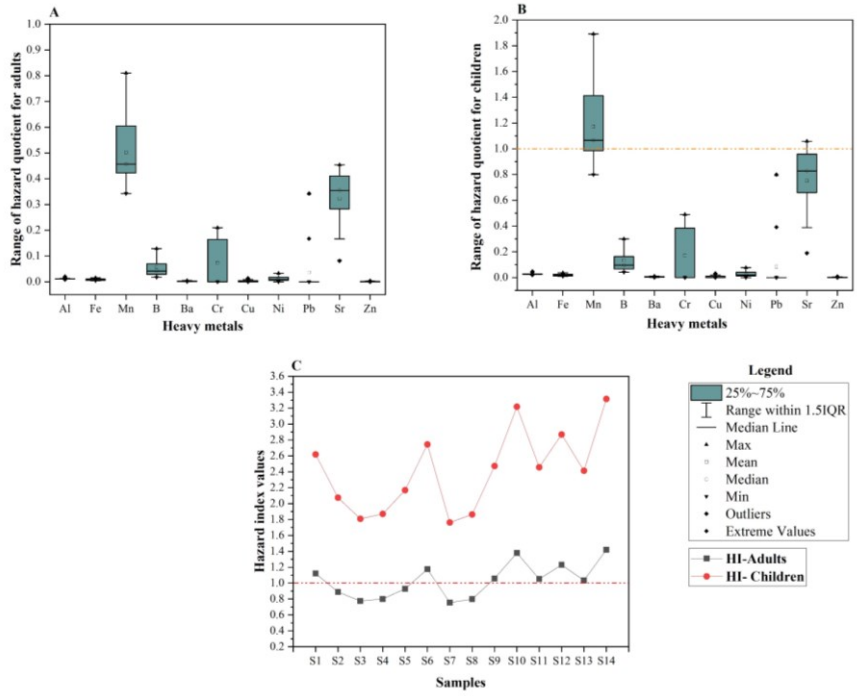

Figure 42. The results of health risk assessment: (A) Box plot of Hazard Quotients (HQs) of eleven heavy metals through ingestion exposure of adults. (B) Box plot of Hazard Quotients (HQs) of eleven heavy metals through ingestion exposure of children. (C) Hazard Index (HI) values of eleven heavy metals for both cases.

4.2. The Complex terminal groundwater aquifer analysis

4.2.1. Piezometry of the Complex terminal groundwater aquifer

Based on the data acquired from Agence Nationale des Ressources Hydrauliques (ANRH) in 2015-2016, the study area is intersected by a total of 49 wells. Among these, three wells are dedicated to irrigation purposes and are situated in El Oued's central city, while the remaining wells serve as sources for drinking water supply, distributed across the rest of the study area. Out of the 49 wells, 26 draw water from the Mio-Pliocene aquifer, and the remaining 23 wells are from the Pontian aquifer. The deepest well, reaching a depth of 398 meters, is located in Guemmar municipality and belongs to the Mio-Pliocene aquifer. Additionally, another well in the same municipality reaches a depth of 265 meters and is used for drinking water supply. The total water abstraction in the covered study area amounts to 67,820,480.64 cubic meters per year. On the other hand, the largest water extraction occurs in W25, situated in Guemmar, and is utilized for drinking water supply, drawing from the Pontian aquifer. According to the piezometric map depicted in figure 43, the overexploitation of the complex terminal aquifer is evidenced by a high groundwater level in various municipalities,

especially in the southern to the middle part of the study area, encompassing El Oued, Bayadha, Mih ouensa, Hassi khalfa, and Robbah. Conversely, the lowest groundwater levels are found in the northern part of the study area, specifically in Magrane, Debila, Reguiba, and Guemmar. The piezometric level indicates that the flow direction of groundwater is from the south (recharge area) to the north (discharge area), directing towards Chott Melrhir and Chott Merouane in the northern region of the study area.

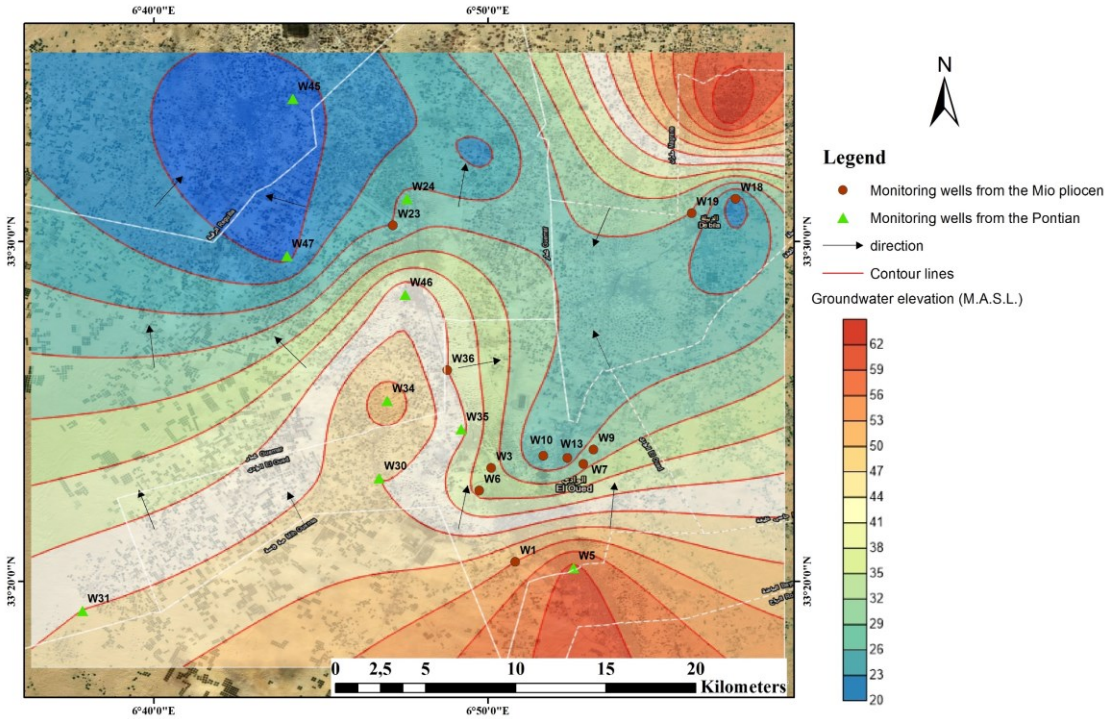

Figure 43. Piezometric map and groundwater flow of the complex terminal aquifer.

4.2.2. Physicochemical characterization of the complex terminal groundwater aquifer

Table 21 presents a statistical summary of the examined physicochemical parameters and the corresponding measurements obtained from groundwater samples. Furthermore, the analysis of the complex terminal groundwater aquifer indicates the absence of any microbiological contamination.

Table 21. List of the physicochemical parameters analyzed in the complex terminal groundwater aquifer samples.

Variables	Mean	S.D	Min	Max	WHO Standards
T ◦C	23.12	5.05	11.80	35.10	-
pH	7.49	0.15	7.23	7.84	6.5–8.5
EC (µs/cm)	4131.48	382.97	2760	4730	1000
Salinity (%)	2.64	0.26	1.80	3	-
TDS (mg/L)	2650.92	246.36	1766	3027	500
Turbidity (Ntu)	0.43	0.52	0.07	3.23	5
Dry Residue (mg/L)	3075.10	478.89	1900	3980	-
Total Alkalinity (mg/L)	138.87	27.17	83	189	-
Ca^{2+} (mg/L)	274.96	36.85	200.40	360.72	75
Mg^{2+} (mg/L)	122.74	30.19	63.12	184.72	50
Na^{+} (mg/L)	379.41	57.92557	137	600	200
K^{+} (mg/L)	33.34694	7.0113	15	50	12
Cl^{-} (mg/L)	888.59	144.18	457.34	1240.86	250
SO_4^{2-} (mg/L)	729.09	152.21	193.06	997.41	250
HCO_3^{-} (mg/L)	167.98	33.50	101.26	213.58	120
NO_3^{-} (mg/L)	22.39	6.62	1.91	34.90	50

The pH levels of the groundwater samples ranged from 7.23 to 7.84, with an average of 7.49. All the groundwater samples (100%) in the study area fell within the range of 7.2–8.5, indicating a low alkaline groundwater type. Importantly, all pH values were found to be within the acceptable range for drinking, as defined by the World Health Organization (WHO) in 2011.

Regarding the electrical conductivity, which reflects the presence of various dissolved salts in the groundwater samples, there were significant variations observed, ranging from 2760 to 4730 µs/cm. The average electrical conductivity was calculated to be 4131.48 µs/cm. It's worth noting that all recorded values (100% of the groundwater samples) exceeded the WHO standards established for drinking purposes. Similarly, the total dissolved solids (TDS) and salinity exhibited wide-ranging values. TDS in the study area ranged from 1766 to 3027 mg/L, with an average of 2650.918 mg/L. All of the groundwater samples (100%) exceeded the WHO standards for TDS in drinking water. TDS comprises various dissolved substances, including inorganic salts, organic matter, and dissolved gases, which contribute to its levels in the groundwater.

The analysis showed that 100% of the groundwater samples were categorized as slightly saline due to the TDS levels, and once again, all of them exceeded the WHO standards for drinking purposes. Additionally, the salinity values and dry residue showed variability, ranging from 1.8% to 3% and 1900 to 3980 mg/L, respectively. The average value for dry residue was calculated to be 3075.102 mg/L.

4.2.3. Application of hierarchical clustering approach for grouping the complex terminal groundwater samples parameters

The hierarchical clustering analysis (HCA) was performed on the normalized data of various parameters, including major ions (Ca^{2+}, Mg^{2+}, Na^{+}, K^{+}, Cl^{-}, SO_4^{2-}, HCO_3^{-}, and NO_3^{-}), electrical conductivity (EC), total dissolved solids (TDS), salinity, total hardness (TH), total alkalinity (TA), turbidity, temperature, and dry residue. The purpose of this analysis was to identify potential hydro-chemical groups present in the groundwater samples. The Q-mode approach was utilized for this analysis.

To assess the similarity between water samples, Ward's linkage technique and Euclidean distance were employed during the HCA process. The results were represented as a dendrogram of spatial HCA, which is displayed in figure 44. The dendrogram provides a visual representation of the clustering of groundwater samples based on their similarity in terms of the measured parameters. By using the Q-mode hierarchical clustering approach, different groups or clusters of groundwater samples with similar hydro-chemical characteristics can be identified and distinguished from each other. This analysis helps in understanding the spatial distribution and variations of hydro-chemical properties within the study area, which can be valuable for groundwater resource management and monitoring.

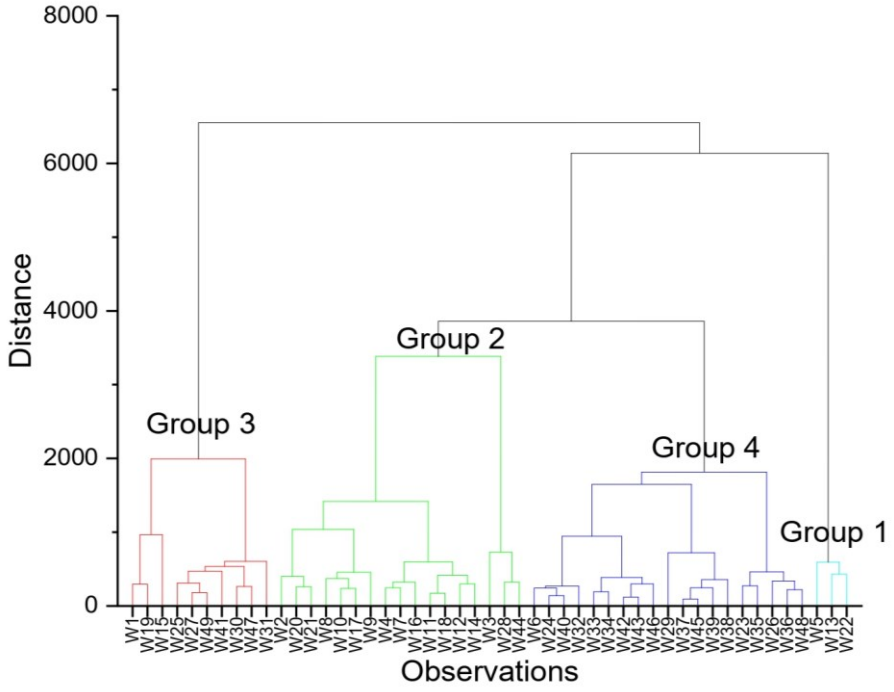

Figure 44. Hierarchical cluster dendrogram—Q mode based on the hydrochemical parameters of the Complex terminal groundwater samples.

Four distinct groups of groundwater samples were formed. The key differentiating factor among these groups appears to be the electrical conductivity (EC). EC shows a significant exponential increase from group 1 to group 4. In order to examine the geochemical evolution of water types, all these groups were plotted in a Piper plot. This plot helps in identifying the different geochemical characteristics of each water type. Furthermore, for assessing the suitability of these waters for drinking purposes, all the physicochemical parameters of the groundwater groups were compared to the World Health Organization (WHO) guidelines for drinking water in 2011. Statistical analyses were carried out to evaluate the compliance of these groundwater samples with the specified WHO standards.

The hydrochemistry of groundwater aquifers can be challenging to interpret in sedimentary environments due to the diverse and complex mineralogical and chemical properties of the studied area [392]. In group 1, which comprises wells W22, W13, and W5, the average electrical conductivity (EC) is measured at 3000 µs/cm, indicating significant mineralization and the presence of brackish water. Many of these wells are located in the recharge zone and are part of the Mio-Pliocene aquifer. The abundance of major ions in this group follows the order: $Na^+ + K^+ > Ca^{2+} > Mg^{2+}$ and $Cl^- > SO_4^{2-} > CO_3^{2-} + HCO_3^- > NO_3^-$, as illustrated in figure 45.

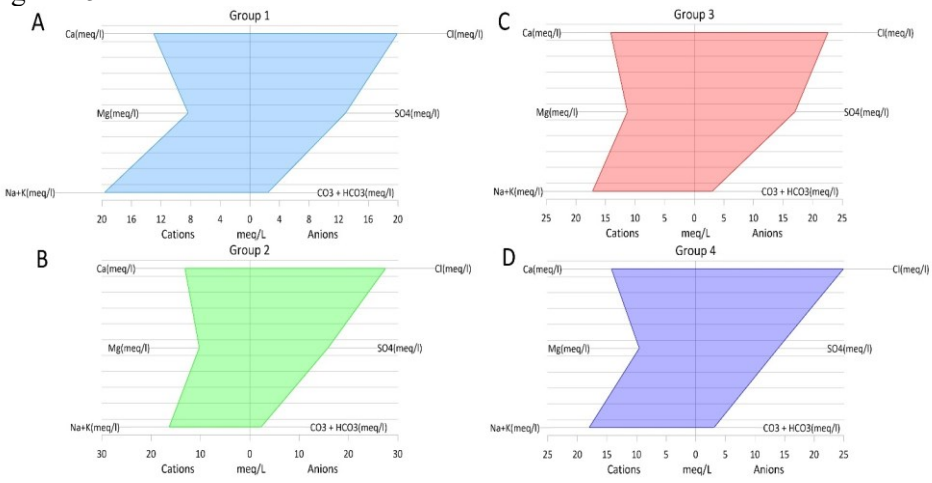

Figure 45. Stiff diagram for the four water groups, (A). group 1, (B). group 2, (C). group 3, (D). group 4.

The hydro-chemical facies identified in this group are primarily Ca^{2+}-Mg^{2+}-Cl^--SO_4^{2-} type, $Ca^{2+}Cl^-$ type, and chloride type, with one sample showing a magnesium type, as indicated in the Piper plot displayed in figure 46.

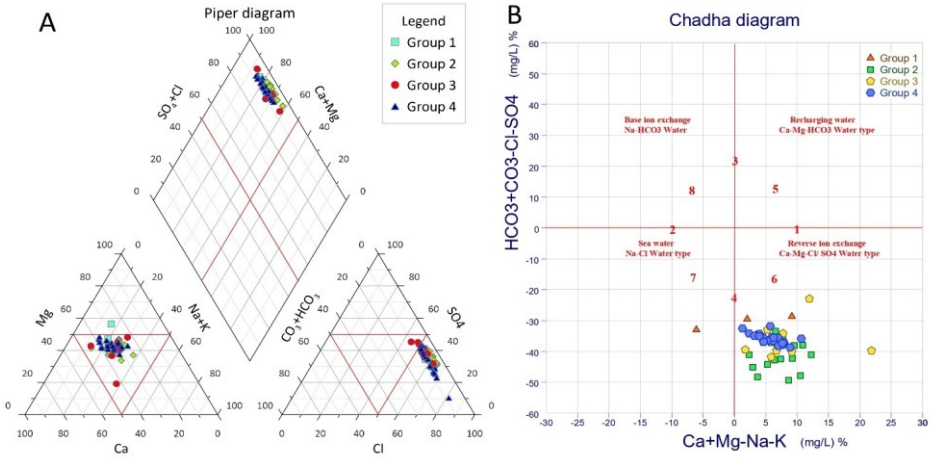

Figure 46. (A). Piper diagram for water samples, and (B). Chadha diagram of the groundwater samples.

In terms of concentration, chloride dominates this group (with minimum = 631.06 mg/L, maximum = 787.06 mg/L, and mean = 706.7 mg/L), followed by calcium (with minimum = 240.48 mg/L, maximum = 280.56 mg/L, and mean = 260.52 mg/L), magnesium (with minimum = 85.07 mg/L, maximum = 121.53 mg/L, and mean = 101.27 mg/L), and sulphates (with minimum = 568.33 mg/L, maximum = 654.02 mg/L, and mean = 621.57 mg/L). In contrast, the concentration of nitrate in this group is relatively lower when compared to the other elements, with values ranging from minimum = 1.911 mg/L, maximum = 34.9 mg/L, and mean = 22.39 mg/L. Anyway, it is important to note that chloride, calcium, magnesium, and sulphates in this group exceed the desirable WHO 2011 standards for drinking water, while nitrate concentrations remain within the acceptable limits according to the WHO guidelines.

Group 2 consists of a set of wells, numbered W2, W20, W21, W8, W10, W17, W9, W4, W7, W16, W11, W18, W12, W14, W3, W28, and W44. These wells collectively account for 34.69% of the water samples within the study area. Among these, 20.41% are situated in the El Oued municipality and belong to the Mio-Pliocene aquifer. These wells include numbers W2, W3, W4, W7, W8, W9, W10, W11, W12, and W14. Additionally, 10.20% of the water samples originate from Debila (wells W16, W17, W18, W20, and W21), which are also part of the Mio-Pliocene aquifer. However, a smaller portion, 2.04%, is divided between Guemar (W28) and Reguiba (W44), with the former belonging to the Mio-Pliocene aquifer and the latter to the Pontian aquifer. This group is notably characterized by extremely high salinity levels, ranging from 3650 to 4430 µS/cm, with a mean of 4005.44 µS/cm, indicating the presence of brackish water. The relative abundance of major ions in this group follows a similar pattern as observed in group 1 (figure 45). The hydro-chemical composition is predominantly of the Ca^{2+}-Mg^{2+}-Cl^{-}-SO_4^{2-} type, $Ca^{2+}Cl^{-}$ type, and chloride type (figure 46 (A)). Chloride stands out as the most dominant element within this group, with minimum, maximum, and mean

concentrations of 815.42 mg/L, 1240.86 mg/L, and 976.9 mg/L, respectively.

In this grouping, calcium and magnesium are the dominant ions, with minimum, maximum, and mean concentrations of 204.36 mg/L, 340.68 mg/L, and 263.24 mg/L for calcium, and 63.19 mg/L, 184.72 mg/L, and 124.26 mg/L for magnesium, respectively. Sulfate levels are also notably high, with minimum, maximum, and mean concentrations of 602.39 mg/L, 978.26 mg/L, and 764.12 mg/L. However, it's important to note that concentrations of chloride, calcium, magnesium, potassium, and sulfates exceed the recommended WHO 2011 standards for drinking water, while nitrate levels remain within acceptable limits.

Group 3 comprises ten wells (W1, W15, W19, W25, W27, W30, W31, W41, W47, and W49), collectively displaying an average electrical conductivity (EC) of 4272 µS/cm, which indicates the presence of brackish water. Among these wells, W1, W15, W19, and W27 are situated in El Oued, Debila, and Guemar, and they belong to the Mio-Pliocene aquifer. The remaining wells (W25, W30, W31, W41, W47, and W49) are associated with the Pontian aquifer and are distributed across Guemar, Reguba, and Taghzout. The relative abundance of major ions within this group follows the sequence $Na^+ + K^+ > Ca^{2+} > Mg^{2+}$, and $SO_4^{2-} > Cl^- > HCO_3^- > NO_3^-$ (figure 45). The hydro-chemical characteristics are predominantly of the Ca^{2+}-Mg^{2+}-Cl^--SO_4^{2-} type and $Ca^{2+}Cl^-$ type (figure 46 (A)). Within this group, sulfate and chloride ions dominate, with minimum, maximum, and mean concentrations of 630.25 mg/L, 997.41 mg/L, and 817.62 mg/L for sulfates, and 457.34 mg/L, 985.59 mg/L, and 800.88 mg/L for chloride, respectively. Calcium content varies between 200.4 and 360.72 mg/L, with an average of 282.96 mg/L, while magnesium concentrations range from 63.12 to 165.27 mg/L, with a mean of 137.32 mg/L. Nitrate levels fall within the range of min = 16.6 mg/L, max = 28.9 mg/L, and mean = 22.9 mg/L, while potassium and sodium concentrations span from 32 to 42 mg/L (mean = 36 mg/L) and 137 to 460 mg/L (mean = 373.9 mg/L) respectively. However, it's noteworthy that all the measured parameters exceed the standards set by the World Health Organization (WHO) for drinking water, with the exception of nitrate.

Group 4 consists of nineteen wells (W6, W24, W40, W32, W33, W34, W42, W43, W46, W29, W37, W45, W39, W38, W23, W35, W26, W36, and W48), collectively showing an average electrical conductivity (EC) of 4348.95 µs/cm, indicating the presence of brackish water. Among these wells, 21.05% are associated with the Mio-Pliocene aquifer (W6, W23, W36, and W37), located in El Oued, Guemar, and Kouinine. The remaining 78.95% are attributed to the Pontian aquifer and are distributed across Guemar, Ourmes, Kouinine, Reguiba, and Taghzout. The concentration order of major ions within this group is as follows: $Na^+ > Ca^{2+} > Mg^{2+}$, and $Cl^- > SO_4^{2-} > HCO_3^- > NO_3^-$ (figure 45). The hydro-chemical composition, as confirmed by the Piper plot, primarily represents the Ca^{2+}-Mg^{2+}-Cl^--SO_4^{2-} type, $Ca^{2+}Cl^-$ type, and chloride type (figure 46 (A)). Within this group, chloride and sulfate ions dominate, with minimum, maximum, and mean concentrations of 730.33 mg/L, 1127.41 mg/L, and 884.46 mg/L for chloride, and 193.06 mg/L, 923.19 mg/L, and 668.14 mg/L for sulfate, respectively. Calcium concentrations vary between 216.43 mg/L and 324.65 mg/L, with an average of 283.51 mg/L, while magnesium levels range from 65.62 mg/L

to 165.27 mg/L, with a mean of 117.11 mg/L. All ion concentrations meet the drinking water standards set by the World Health Organization (WHO) in 2011, except for nitrate which did not exceed the limits.

The diagram depicted in figure 46 (B) illustrates the Chadha plot, wherein a significant portion (97.96%) of the samples falls within the 6th category, denoting the reverse ion-exchange Ca^{2+}-Mg^{2+}-Cl^{-}/SO_4^{2-} water type. This grouping indicates the prevalence of waters characterized by a composition of Ca^{2+}-Mg^{2+}-Cl^{-}, Ca^{2+}-Mg^{2+}-dominant Cl^{-}, or Cl^{-}-dominant Ca^{2+}-Mg^{2+} types. In these water types, the concentration of alkaline earth metals (Ca^{2+} and Mg^{2+}) surpasses that of alkali metals (Na^{+} and K^{+}), while the presence of strong acidic anions (Cl^{-} and SO_4^{2-}) outweighs weak acidic anions (HCO_3^{-}), aligning with the conclusions drawn from the Piper diagram. Conversely, a smaller fraction (2.04%) is situated within the 7th category of the plot, corresponding to seawater Na-Cl characteristics. This subset signifies an abundance of alkali metals in comparison to alkaline earth metals and a prevalence of strong acidic anions over weak acidic anions. Notably, this group displays heightened levels of (Ca^{2+} + Mg^{2+}) and (Cl^{-} + SO_4^{2-}) compared to (HCO_3^{-}).

4.2.4. Assessment of the complex terminal groundwater aquifer for drinking purposes

In this research, a comparison was conducted between the calculated WQI values and the guidelines established by WHO (2011). The WQI computation for drinking water involved ten parameters: EC, pH, Ca^{2+}, Mg^{2+}, Na^{+}, K^{+}, Cl^{-}, SO_4^{2-}, HCO_3^{-}, and NO_3^{-}. All wells examined scored above 50 on the classification scale. However, wells with good water quality accounted for 10.20% (11.54% from Mio-Pliocene and 8.70% from the Pontian), while samples with poor quality constituted 24.49% (15.38% from Mio-Pliocene and 34.78% from the Pontian). Additionally, 55.10% exhibited very poor water quality (61.54% from Mio-Pliocene and 47.83% from the Pontian). Moreover, 4.08% were deemed unsuitable for drinking, including 7.69% from the Mio-Pliocene aquifer as shown in table 22.

Table 22. The results of WQI-based the complex terminal groundwater aquifer suitability for drinking and irrigation.

Range	Classes	Number of wells	% of samples (49 sample)	% of samples (Miopleocen sample)	% of samples (Pontian sample)
<50	Excellent water	-	-	-	-
100.0-125.0	Good water	W10, W4, W18, W24, W29.	10.20%	11.54%	8.70%
125.1-150.0	Poor water	W13, W21, W11, W28, W44, W30, W47, W40, W26, W38, W39, W48.	24.49%	15.38%	34.78%
150.1-175.0	Very poor water	W5, W22, W2, W20, W8, W17, W7, W16, W12, W14, W19, W15, W25, W27, W49, W41, W31, W6, W32, W33, W34, W42, W46, W23, W35, W36, W37.	55.10%	61.54%	47.83%
175.1-200.0	Unfit for drinking	W9, W3.	4.08%	7.69%	-

4.2.5. Assessment of the complex terminal groundwater aquifer for irrigation puposes

The evaluation of groundwater samples collected from the intricate that the complex terminal aquifer was carried out using various indices, and the presentation of the findings is outlined in table 23. Based on Total Hardness (TH) measurements, 44.90% of the samples were categorized as soft water (53.85% from the Mio-Pliocene and 34.78% from the Pontian), while 55.10% were moderately hard (50% from the Mio-Pliocene and 60.87% from the Pontian). Notably, no monitoring well fell within the hard to very hard range. The values of Sodium Adsorption Ratio (SAR) were above 10 indicating that these waters are not suitible for irrigation. While only one samples W41 had a good water quality for irrigation.

The Electrical Conductivity (EC) values of the complex terminal aquifer were divided into two groups: 2.04% (W5) and 4.35% from the Pontian displayed water quality of doubtful nature, while 97.96% exhibited unsuitable quality for irrigation, comprising 100% from the Mio-Pliocene and 95.65% from the Pontian. The percentage of Sodium (% Na) indicated that 81.63% of the samples were acceptable for irrigation (73.08% from the Mio-Pliocene and 91.30% from the Pontian), whereas 18.37% demonstrated good quality (26.92% from the Mio-Pliocene and 8.70% from the Pontian), with one sample classified as excellent quality.

Regarding the Magnesium Hazard Index, 85.71% of the samples were suitable for irrigation (80.77% from the Mio-Pliocene and 91.30% from the Pontian), while 14.29% were unsuitable (19.23% from the Mio-Pliocene and 8.70% from the Pontian). The Permeability Index (PI) indicated that 97.96% of the samples displayed moderate quality, except for W41 belonging to the Pontian aquifer, which was classified as suitable. The Kelley Ratio (KR) identified 97.96% of the samples as having suitable quality (100% from the Mio-Pliocene and 95.65% from the Pontian), with the exception of W5, attributed to the Pontian aquifer. In terms of Residual Sodium Carbonate (RSC), all samples, 100%, were considered acceptable for irrigation practices.

Table 23. Irrigation quality indices of the complex terminal aquifer.

Range	Classes	Number of wells
EC (µs/cm)		
< 250	Excellent	-
250–750	Good	-
750–2000	Permissible	-
2000–3000	Doubtful	W5
> 3000	Unsuitable	All the samples except W5
Percent sodium (Na%)		
< 20	Excellent	W41

20–40	Good	W22, W20, W8, W17,W7,18,15,41,46
40–60	Permissible	W5,W13,W2,W21,W10,W9,W4,W16,W11,W12,W14,W3,W28,W44,W1,W19,W25,W27,W49,W30,W47,W31,W6,W24,W32,W33,W34,W40,W42,W43,W23,W26,W29,W35,W36,W37,W38,W39,W45,W48
60–80	Doubtful	-
> 80	Unsafe	-
Alkalinity hazard (SAR)		
< 10	Excellent	-
10–18	Good	W41
18–26	Doubtful	-
> 26	Unsuitable	W5,W44,W25,W49, W30,W47,W31,W24,W32,W33,W34,W40,W46,W26,W29,W35,W38,W39,W45,W48, W13,W22,W2,W20,W21,W10,W17,W9,W4,W7,W16,W11,W12,W3,W28,W19,W15, W27,W6,W36,W37
Total hardness (TH)		
< 75	Soft	W36,W13,W2,W10,W4,W16,W11,W12,W14,W3,W28,W19,W6,W36,W38,W39,W29, W35,W40,W24,W30,W5
75–150	Moderately hard	W22,W20,W21,W8,W17,W9,W7,W18,W1,W15,W27,W23,W37,W44,W25,W49,W41, W47,W31,W33,W34,W42,W43,W46,W26,W45,W48
150–300	Hard	-
> 300	Very hard	-
Magnesium hazard (MH)		
< 50	Suitable	W5,W44,W25,W49,W41,W30,W47,W31,W24,W32,W33,W34,W40,W46,W26,W29, W35,W38,W39,W45,W48,W13,W22,W2,W20,W21,W10,W17,W9,W4,W7,W16,W11, W12,W3,W28,W19,W15,W27,W6,W36,W37
> 50	Unsuitable	
Permeability index PI		
< 25	Suitable	W41
25–75	Moderate	All the samples except W41
> 75	Unsuitable	-
Kelley ratio (KR)		
< 1	Suitable	All the samples except W5
1–2	Moderate	W5
> 2	Unsuitable	-
RSC		
<1.25	Acceptble	All the samples
1.25-2.5	Slightly adapted to irrigation	-
>2.5	Not suitible	-

4.2.6. Application of geostatistical modelling for the complex terminal hydro-chemical parameters

The primary hydro-chemical parameters of significance were fitted using the exponential semi-variogram model. These parameters included EC, Ca^{2+}, Mg^{2+}, K^{+}, Na^{+}, HCO_3^{-}, Cl^{-}, NO_3^{-}, and SO_4^{2-}. Among these, the rational quadratic model demonstrated the optimal fit for Na^{+} and NO_3^{-}, with the determination based on the

ratio of nugget variance to the sill. Furthermore, various classifications were employed to characterize the spatial interdependence of hydro-chemical groundwater parameters. In this thesis, three levels of spatial dependence were recognized: robust when the ratio falls below 25%, moderate when the ratio ranges between 25% and 75%, and weak when the ratio exceeds 75%, as detailed in table 24.

Table 24. Best-fitted semi-variogram models and cross-validation for Ordinary kriging of groundwater quality parameters.

Parameters	Transformation	Semi variogram model parameters						Prediction errors	
		Model	Nugget (C_0)	Partial Sill (C)	Sill (C_0+C)	(C_0/ C_0+C) *100 (%)	Spatial de-pend-ence	Mean	Root-Mean-Square Stand-ardized
EC	Original data	Expo-nential	0.028	0.098	0.126	22.35	Strong	0.228	1.090
Ca^{2+}	Original data	Expo-nential	0.744	0.677	1.421	52.37	Moder-ate	0.846	0.951
Mg^{2+}	Logarith-mic	Expo-nential	0.062	0.011	0.073	84.74	Weak	1.035	0.911
Na^{+}	Original data	Ra-tional Quad-ratic	0.112	0.167	0.279	40.19	Moder-ate	-1.865	1.235
K^{+}	Original data	Expo-nential	0.145	0.357	0.502	28.89	Moder-ate	0.224	1.131
HCO_3^{-}	Original data	Expo-nential	0.418	0.558	0.976	42.82	Moder-ate	-0.702	0.927
Cl^{-}	Logarith-mic	Expo-nential	0.027	0.005	0.0317	84.864	Weak	-0.515	0.905
SO_4^{2-}	Logarith-mic	Expo-nential	0.007	0.091	0.098	7.142	Strong	- 0,424	0.732
NO_3^{-}	Logarith-mic	Ra-tional Quad-ratic	0.054	0.316	0.369	14.54	Strong	0,993	1.117

In the designated research region, a distinct spatial correlation is observed among EC, SO_4^{2-}, and NO_3^{-}. On the other hand, Ca^{2+}, Na^{+}, K^{+}, and HCO_3^{-} exhibit a moderate level of spatial correlation, whereas Mg^{2+} and Cl^{-} display a relatively lower degree of spatial dependence. The spatial arrangement of EC (depicted in figure 47) illustrates an increase in mineralization from the eastern portion of the study zone towards the western and southwestern sectors. This phenomenon is attributed to both the geological composition of the local area and the problematic condition of specific wells within the complex terminal. These wells have breaches in their casing levels, facilitating direct interaction and connection with the phreatic aquifer, which is characterized by its elevated mineral content.

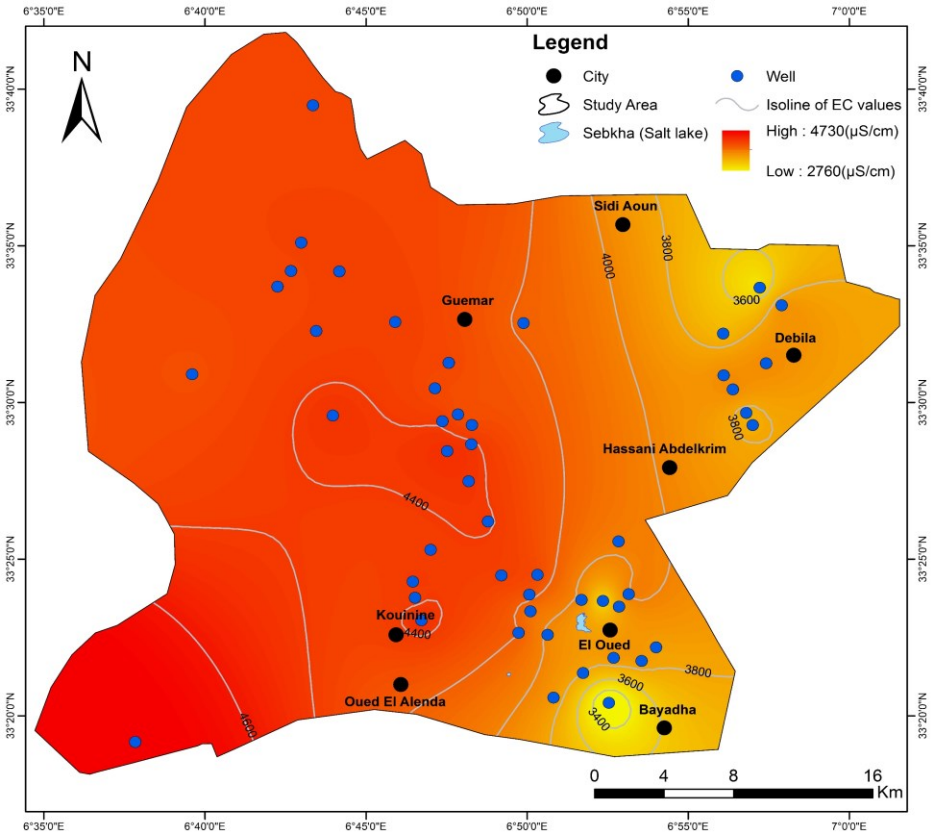

Figure 47. Spatial distribution of EC.

The spatial distribution of SO_4^{2-} and Mg^{2+} concentrations is predominantly influenced by the dissolution of evaporate formations, the leaching of clays, and the dissolution of gypsum and anhydrite. In the northern region of the research area encompassing Sidi Aoun and Guemar, diminished levels were detected, whereas the most elevated concentrations were witnessed in the southwestern part of the study zone. The least amounts of Mg^{2+} were situated in close proximity to Guemar, to the southwest of Debila, to the south of El Oued, and in the Kouinine vicinity. Additionally, a marked increase in value was also observed in the southwestern region, as depicted in figures 48 (B) and 49 (C).

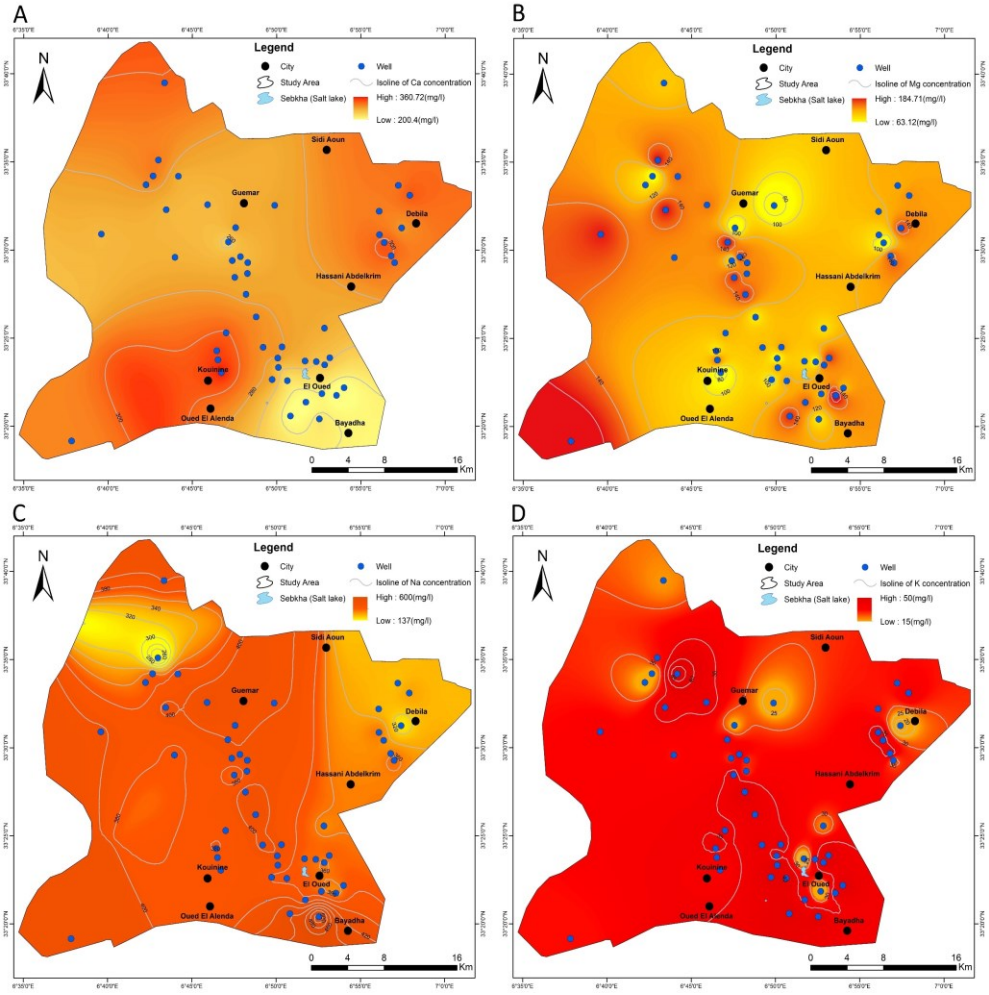

Figure 48. Spatial distribution of cations: (A). calcium (Ca^{2+}), (B). magnesium (Mg^{2+}), (C). sodium (Na^{+}), (D). potassium (K^{+}).

The spatial distribution maps for Ca^{2+}, HCO_3^{-}, Na^{+}, K^{+}, and Cl^{-} reveal significant heterogeneity attributed to both substantial geological variations across regions and varying well depths. To the south of El Oued, Ca^{2+} concentrations appear diminished, while elevated levels are evident in Debila, Sidi Aoun, and Kouinine. A rise in Ca^{2+} concentrations is observed in the southern expanse of the study area, particularly around Kouinine, as well as in the northwestern vicinity encompassing Debila and Sidi Aoun. Conversely, a decline in Ca^{2+} concentrations is noticeable when progressing from Guemar towards El Oued, extending until Bayadha. The presence of Ca^{2+} ions in groundwater is mainly linked to the dissolution of carbonate formations ($CaCO_3$) as well as gypsum formations ($CaSO_4 2H_2O$). The study geological and hydrogeological confirm this hypothesis where we find limestone and gypsum in the reservoir of the terminal complex (limestone layer), and limestone in the reservoir of the continental intercalary.

Furthermore, HCO_3^- concentrations exhibit an increase from the southeastern region around El Oued, extending towards the northwest and southwest, as depicted in figures 48 (A) and 49 (B). This observed pattern is attributed to the intricate interplay of geological diversity and well depths in the area.

The presence of sodium is fundamentally connected to the process of halite dissolution (evaporation). In fact, sodium, much like chlorides, exhibits significant and uneven concentrations within the waters of the complex terminal (CT). Sodium concentrations within the groundwater samples of the CT are reduced towards the northeast portion of the research area, in proximity to Debila, and towards the northwest. The graphical representations in figures 48 (C) and 49(A) indicate a rise in chloride levels from the western side to the eastern side.

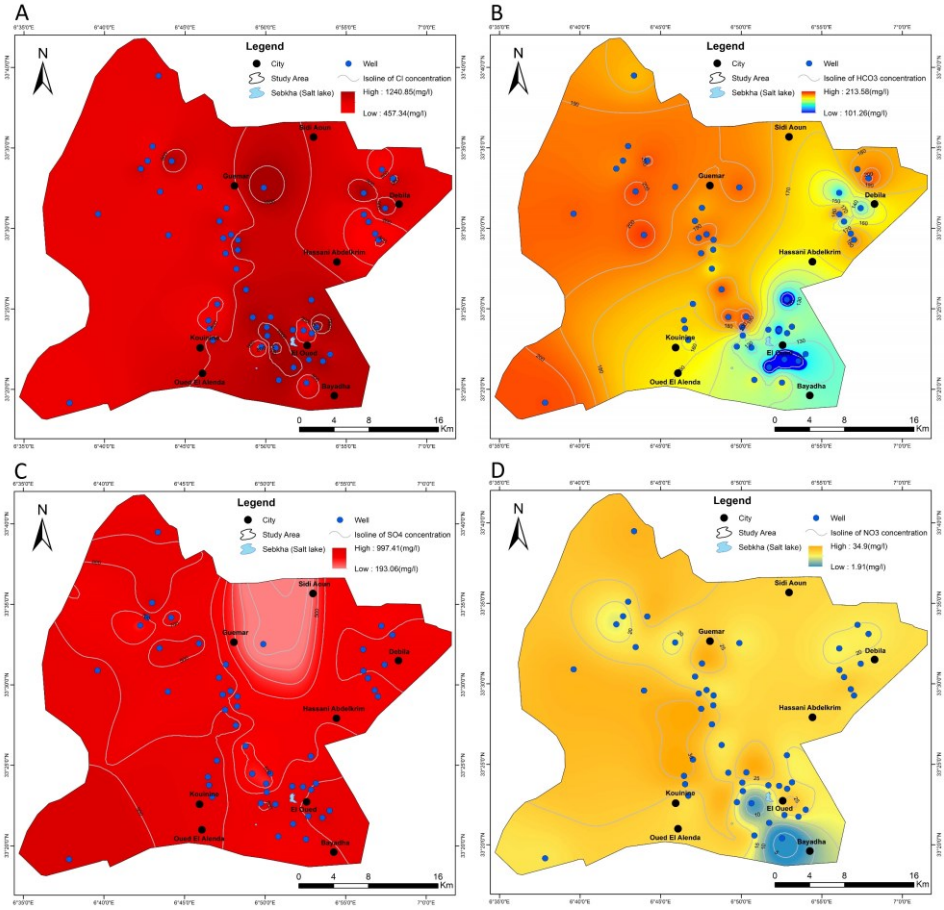

Figure 49. Spatial distribution of anions: (A). chloride (Cl^-), (B). bicarbonate (HCO_3^-), (C). sulfate (SO_4^{2-}), (D). nitrate (NO_3^-).

Potassium primarily originates from evaporites, specifically sylvite (KCl), or arises through the modification of potassium-rich clays within the phreatic aquifer and complex terminal aquifer. The study region is characterized by elevated potassium levels, with the exception of certain areas like Debila, Guemar, and El Oued, where potassium concentrations are notably low, as indicated in figure 48

(D). Nitrate contamination primarily stems from urban wastewater in metropolitan zones and agricultural fertilizer application in cultivated lands. Figure 49 (D) illustrates that elevated nitrate concentrations are observed in the northwestern and western sectors of the study area, north of Guemar, north of Kouinine, and in the eastern and northern parts of El Oued. The higher nitrate levels validate the blending of phreatic groundwater with complex terminal flows, leading to significant nitrate content in the complex terminal waters. Lower nitrate levels are recorded in the Ghouts covered by reeds, owing to their utilization for reed growth, and also near the El Oued discharge point, where nitrate denitrification provides the requisite oxygen for microorganism respiration.

4.2.7. Origin of Mineralization in the complex terminal aquifer

Lithology plays a significant role in shaping the mineral content of groundwater in arid and semi-arid regions [393]. However, the process of groundwater solute generation is influenced by three primary mechanisms: the dissolution of carbonates, evaporites, and silicates [128]. Notably, the dissolution rates of evaporites and carbonates surpass those of silicates by factors of up to 80 and 12 times, respectively. Consequently, even minor quantities of carbonates and evaporites can exert a substantial influence on water composition [394]. In figure 50 (A), it is evident that calcite dissolution is the predominant reaction in 40.81% of groundwater samples, with a ratio of 1 to 2. However, for 59.18% of samples, the ratio exceeds 2, indicating the presence of non-carbonate minerals that likely impact groundwater chemistry. This influence might be attributed to reverse cation exchange due to clay adsorption of calcium and magnesium in groundwater and/or the dissolution of gypsum [395]. The dissolution of carbonates (calcite and dolomite) is primarily driven by pH fluctuations and occurs mainly in the form of HCO_3^-.

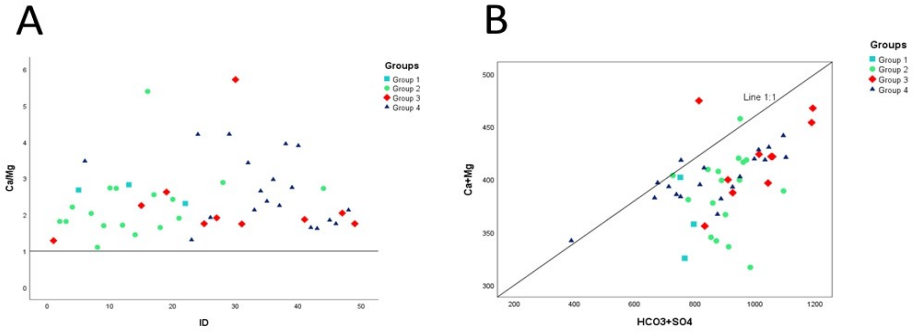

Figure 50. (A) Bivariate plots of a good number vs. Ca^{2+}/Mg^{2+}, and (B) bivariate plots of $Ca^{2+} + Mg^{2+}$ vs. $HCO_3^- + SO_4^{2-}$.

The majority of data points depicted in figure 50 (B) are concentrated on the right side, signifying that the dominance of ion exchange over reverse ion exchange results from an excess of ($SO_4^{2-} + HCO_3^-$). However, the data point corresponding to the 1:1 line is remarkably close to 47.37% for group 4 samples and 17.65% for

group 2 samples. This illustrates that calcite, dolomite, anhydrite, and gypsum are the predominant reactions within the system for this specific group. Group 1 contains only one sample that closely aligns with the 1:1 line [396,397].

In figure 51 (A) [398], a graph depicting Na^+-normalized Ca^{2+} against HCO_3^- reveals variations among the four group samples in their susceptibility to silicate weathering. Similarly, the Na^+-normalized versus Mg^{2+} plot in figure 51 (B) indicates that the four group samples exhibit a spectrum of responses to silicate weathering, ranging from a mild tendency toward dissolution of evaporates.

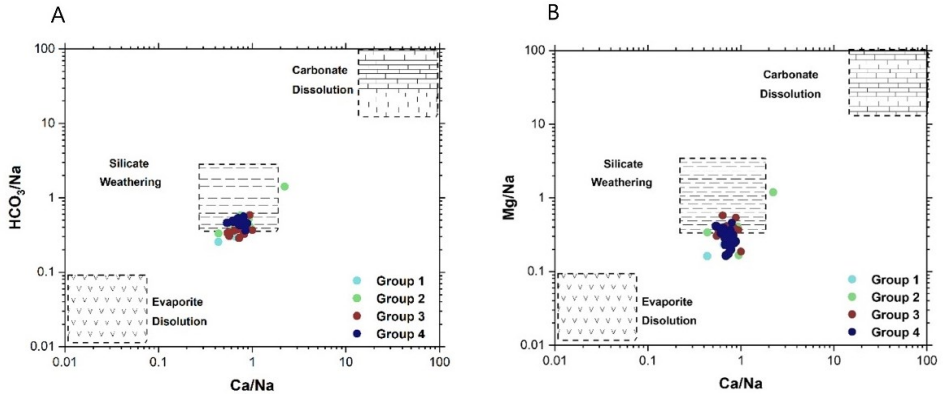

Figure 51. (A) Molar ratio in bivariate plots of Na^+ -normalized Ca^{2+} and HCO_3^-, and (B) Na^+ -normalized Ca^{2+} and Mg^{2+}.

4.2.8. Controlling Mechanisms of the complex terminal aquifer

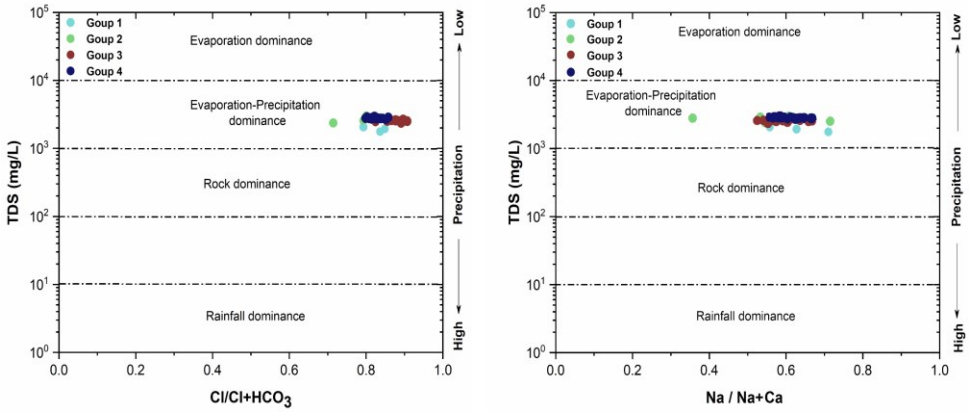

Figure 52. Gibbs diagrams of the complex terminal groundwater aquifer.

Gibbs diagrams are used to represent the changes in $[Cl^-/(Cl^-/HCO_3^-)]$ and $[Na^+/(Na^+/Ca^{2+})]$ ratios in relation to Total Dissolved Solids (TDS). These diagrams depict dominance through processes such as precipitation, rock interaction, and evaporation. They serve as visual aids in identifying the sources of dissolved chemical constituents. In figure 52, the cation and anion ratios are graphed against TDS for the four distinct groups. The data from all clustered groups

are situated in the evaporation-precipitation dominance section, indicating a significant impact of evaporation-precipitation on water quality.

For the evaluation of ion exchange reactions between groundwater and its geological host [314,399], the Chloro-Alkaline Indices (CAI) are commonly employed. These indices, CAI-I and CAI-II, provide a framework for interpreting ion exchange between groundwater and its surrounding environment. Whereas the positive values of the chloro-Alkaline Indices indicate the exchange of Na^+ and K^+ ions in water with Mg^{2+} and Ca^{2+} ions from rocks, signifying a base-exchange reaction. Conversely, negative chloro-Alkaline indices signify the exchange of Mg^{2+} and Ca^{2+} ions from water with Na^+ and K^+ ions from rocks. As depicted in figure 53, the majority of intricate terminal groundwater aquifers exhibit positive chloro-Alkaline Indices, attributed to the replacement of Ca^{2+} and Mg^{2+} ions in groundwater with Na^+ and K^+ ions in the aquifer system.

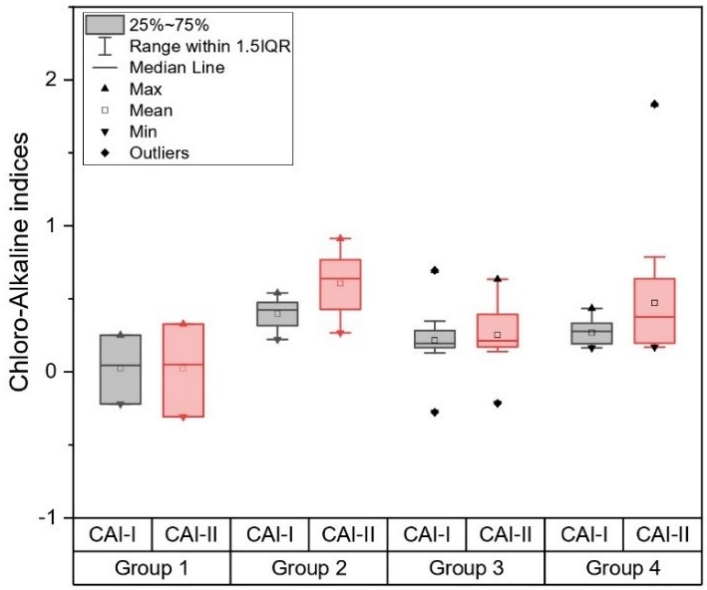

Figure 53. Chloro-Alkaline Indices for the four groups.

4.2.9. Geochemical Modeling of the complex terminal aquifer

Based on the computed saturation indices, Group 1 comprises anhydrite, gypsum, and halite, which are prone to dissolution, while aragonite, calcite, dolomite, and sylvite are in a state of supersaturation. Among these, aragonite, calcite, and dolomite in group 2 are undergoing precipitation, whereas anhydrite, gypsum, halite, and sylvite are undergoing dissolution. Meanwhile, Group 3 demonstrates the precipitation of aragonite, calcite, and dolomite, with anhydrite, gypsum, halite, and sylvite undergoing dissolution. A similar trend is observed in group 4, with minerals experiencing both precipitation and dissolution. Figure 54 illustrates that evaporated minerals (anhydrite, gypsum, and halite) consistently remain undersaturated across the groups due to the arid environment and minimal

precipitation in the study area. This results in significant evaporation in surface water, leading to heightened mineralization in the uppermost aquifer (the phreatic aquifer) compared to the more intricate terminal aquifer.

The undersaturation of evaporated minerals in groundwater samples indicates that their soluble elements (Na^+, Cl^-, Ca^{2+}, and SO_4^{2-}) are not constrained by mineral equilibrium. Table 25 provides the computed saturation indices for various minerals (anhydrite, aragonite, calcite, dolomite, gypsum, halite, and sylvite).

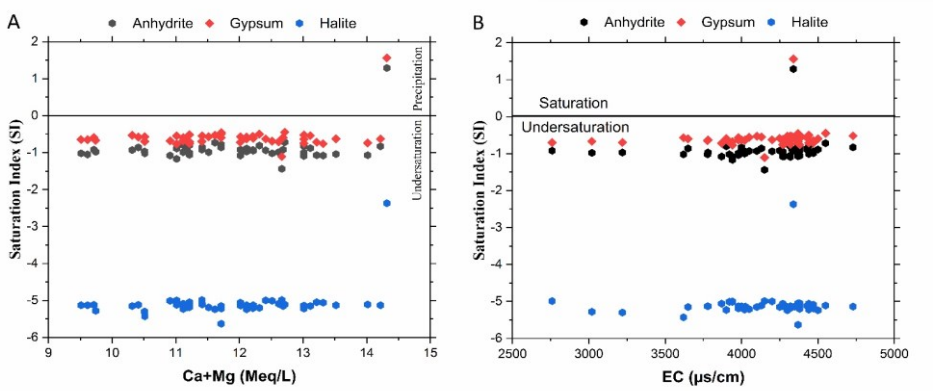

Figure 54. (A and B) Saturation indices of evaporate minerals.

Table 25. Saturation indices of minerals in groundwater with statistical summary using PHREEQC.

Groups	Minerals	N total	Mean	S. D	Min	Max
Group 1	Anhydrite	3	-0.95667	0.03215	-0.98	-0.92
	Aragonite	3	0.40333	0.34675	0.12	0.79
	Calcite	3	0.54333	0.34429	0.27	0.93
	Dolomite	3	1.04333	0.74895	0.41	1.87
	Gypsum	3	-0.69	0.01732	-0.7	-0.67
	Halite	3	-5.19	0.17349	-5.3	-4.99
	Sylvite	3	-5.84667	0.05859	-5.89	-5.78
Group 2	Anhydrite	17	-0.95588	0.08718	-1.08	-0.8
	Aragonite	17	0.18471	0.17288	-0.17	0.46
	Calcite	17	0.33235	0.16995	-0.02	0.59
	Dolomite	17	0.62647	0.37959	-0.05	1.28
	Gypsum	17	-0.62118	0.05243	-0.72	-0.53

	Halite	17	-5.12118	0.06855	-5.23	-5
	Sylvite	16	-5.75688	0.18062	-6.08	-5.51
Group 3	Anhydrite	10	-0.918	0.12541	-1.17	-0.72
	Aragonite	10	0.261	0.14798	0.05	0.49
	Calcite	10	0.409	0.14617	0.19	0.64
	Dolomite	10	0.779	0.36765	0.3	1.29
	Gypsum	10	-0.575	0.09192	-0.77	-0.45
	Halite	10	-5.208	0.1839	-5.63	-5
	Sylvite	10	-5.763	0.08957	-5.91	-5.57
Group 4	Anhydrite	19	-0.85263	0.54216	-1.44	1.29
	Aragonite	19	0.47579	0.56655	0.2	2.78
	Calcite	19	0.62	0.56805	0.34	2.93
	Dolomite	19	1.15684	1.04431	0.47	5.37
	Gypsum	19	-0.54368	0.52915	-1.11	1.56
	Halite	19	-4.98105	0.63605	-5.24	-2.37
	Sylvite	19	-5.62211	0.6585	-5.91	-2.93

4.2.10. Temporal changes of the complex terminal groundwater aquifer

The illustration of the temporal changes of the complex terminal groundwater aquifer data in several years using the same monitoring wells is shown in figure 55, 56, 57. pH values are stable, suggesting slightly alkaline water, with an increase in variability in 2019 and 2020. Electrical conductivity (EC) shows a downward trend, indicating less mineralized water, with earlier years displaying outliers. Turbidity is decreasing, suggesting clearer water since turbidity values aver the studied periods does not imply a significant variation and did not exceed the WHO limits for potability. Meanwhile total dissolved solids (TDS) also show a decline, aligning with EC readings. Based on the box plot of total hardness, a systematic change in groundwater hardness has been observed in 2017, and 2020. Anyway, the values of the total hardness in all the samples have exceeded 300 mg/l which indicate that these waters are very hard. Furthermore, as an important issue for monitoring pollution, the box plots show a decrease in chloride concentrations. Sodium levels slightly decrease with significant yearly variability. Potassium concentrations have notably increased in 2020, a potential of contamination. Nitrate levels show a significant rise in 2020, indicating possible agricultural runoff that can be related to communication with the shallow aquifer (drainage or

infiltration of the casings), as well as the clay roof, which fixes the nitrate ions and protects the groundwater table [400]. On the other hand, ammonium levels are generally low but with an increase in 2020, suggesting organic pollution. Phosphate levels are low and stable, which is positive for preventing eutrophication. calcium shows a decreasing trend with high variability represented by extreme values that might be related to a contamination event due to communication between the shallow aquifer and complex terminal aquifer, while magnesium levels are relatively stable with a slight decrease. Nitrite levels fluctuate, indicating possible nitrogen compound contamination. Sulfate concentrations decrease with a peak in 2017, suggesting variable geochemical processes. Bicarbonate levels are low and decreasing, affecting water buffering capacity. Iron concentration generally declines, with a notable outlier in 2019.

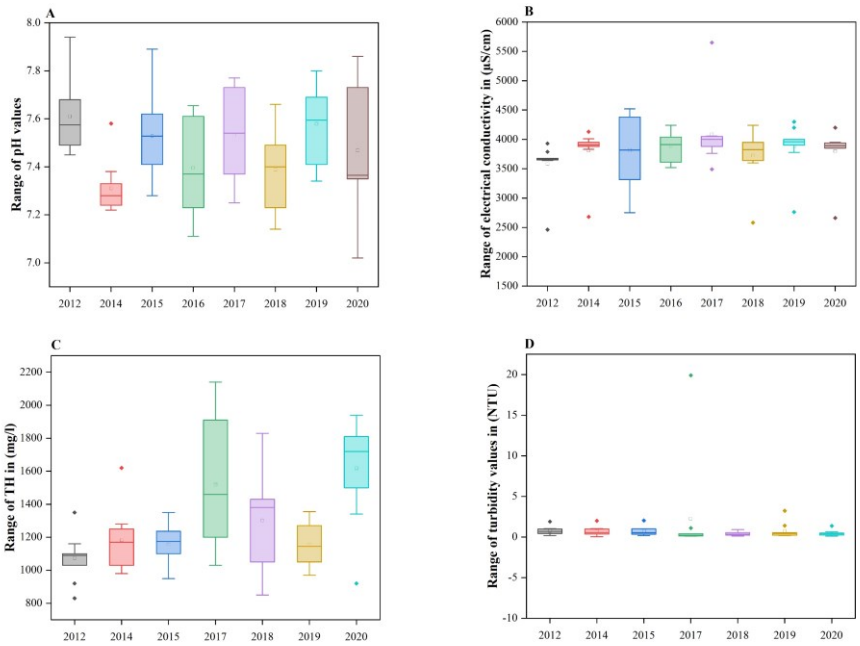

Figure 55. Box plots of complex terminal groundwater aquifer variation (A). pH, (B). EC, (C). TH, (D). Turbidity.

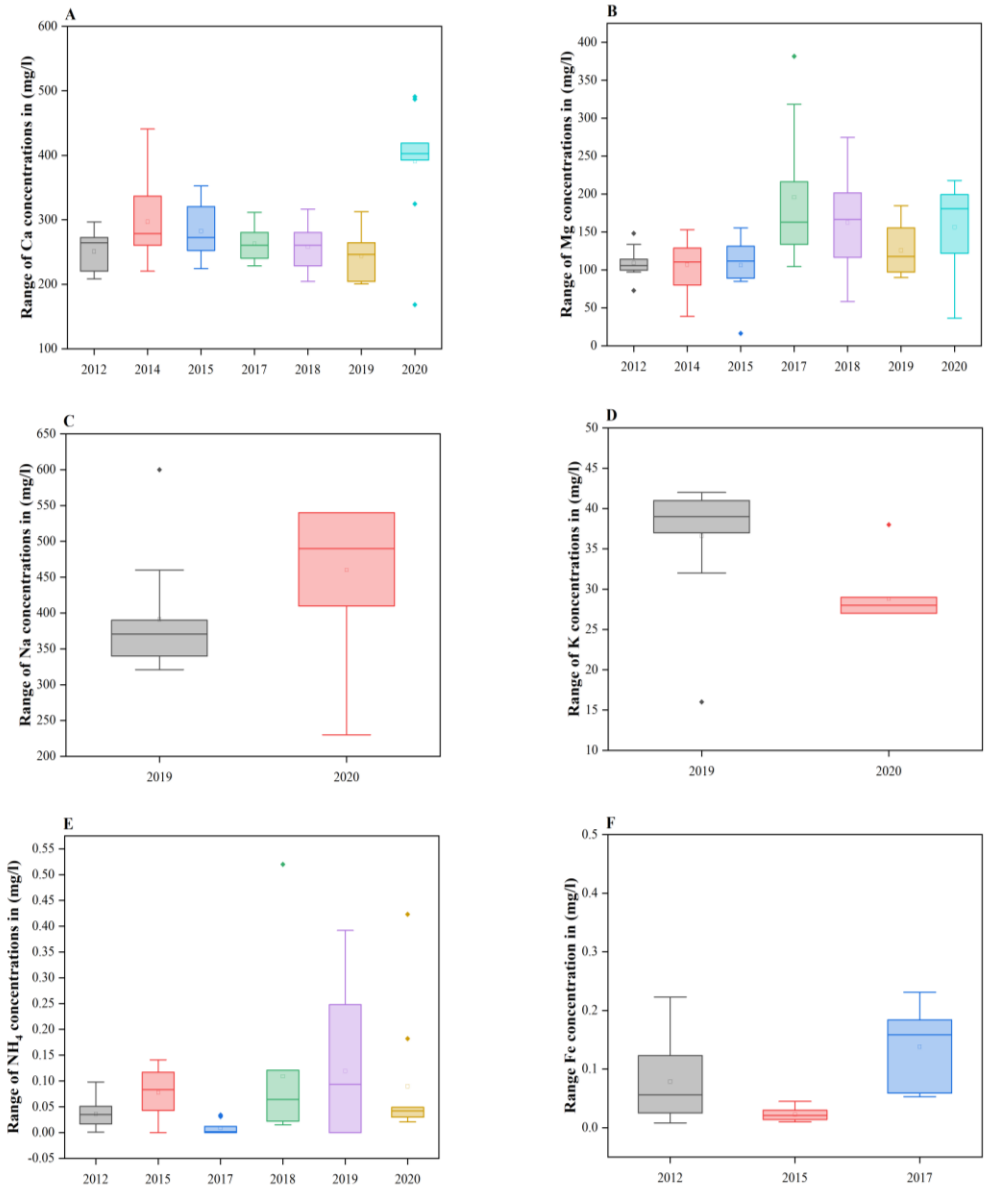

Figure 56. Box plots of complex terminal groundwater aquifer variation (A). Ca^{2+}, (B). Mg^{2+}, (C). Na^{+}, (D). K^{+}, €. NH_4^{+}, (F). Fe^{2+}.

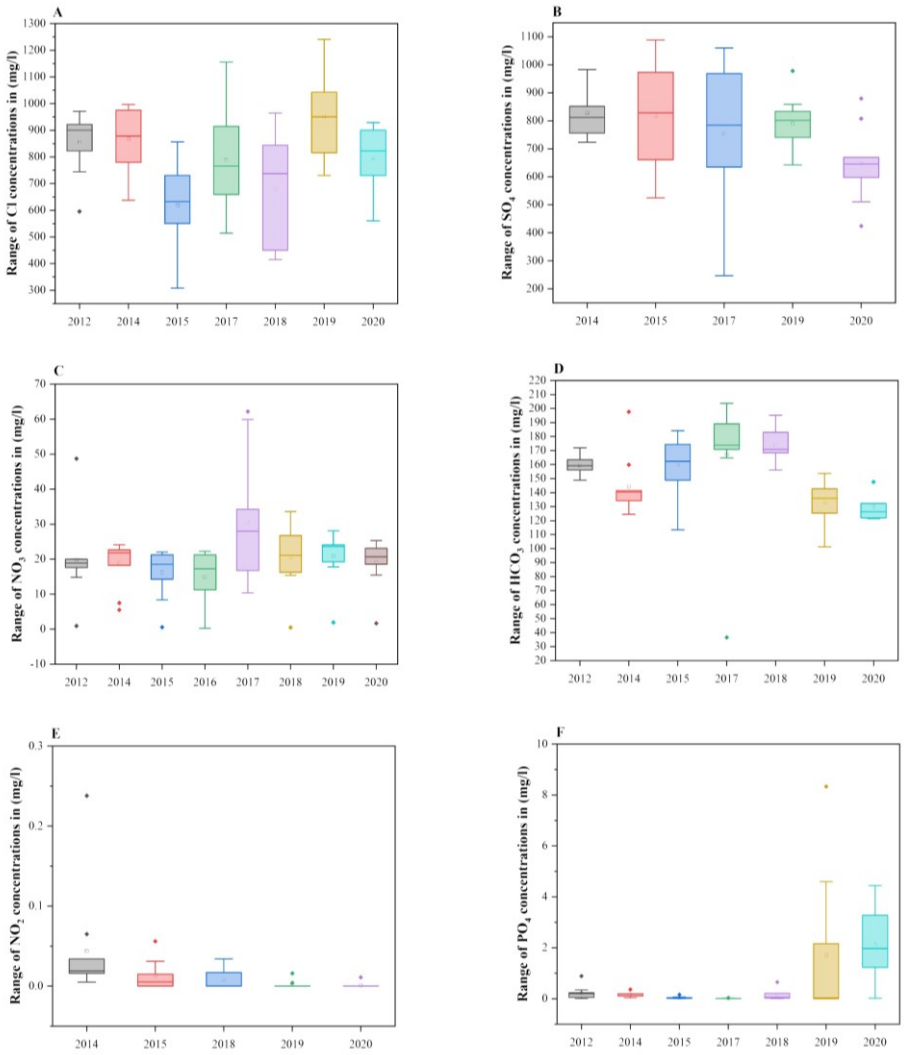

Figure 57. Box plots of complex terminal groundwater aquifer variation (A). Cl^-, (B). SO_4^{2-}, (C). NO_3^-, (D). HCO_3^-, (E). NO_2^-, (F). PO_4^{3-}.

4.3. The Continental intercalary groundwater aquifer analysis

4.3.1. Physicochemical Parameters of the continental intercalary groundwater aquifer

The continental intercalary groundwater aquifer in Oued Souf Valley was exploted throught five wells, but due to technical problems, two wells were abonded, and the remaining monitopring wells still connected and functioning. Furthermore, the depth of these three wells is ranging from 1842 to 1876 meters deep from the surface.

Anyway, based on the obtained data from ANRH and ADE that contains a yearly hydrochemical data from the continental intercalary, a comprehensive statistical analysis applied to a range of parameters, encompassing temperature, Ph, electrical conductivity, TDS, turbidity, Ca^{2+}, Mg^{2+}, Na^{+}, K^{+},SO_4^{2-} Cl^{-}, HCO_3^{-}, NO_3^{-}, NO_2^{-}, NH_4^{+}, PO_4^{3-}, and Fe as shown in table 26. The analysis of the continental intercalary groundwater aquifer reveals several key findings. The water is alkaline with pH values above 7, aligning with WHO standards. However, high mineralization is indicated by elevated electrical conductivity and TDS, surpassing WHO limits for safe drinking water. While turbidity and NO_3^{-} levels are generally acceptable, there are concerns with high concentrations of various ions (Ca^{2+}, Mg^{2+}, Na^{+}, K^{+}, Cl^{-}, SO_4^{2-}, HCO_3^{-}) and heavy metals like Fe^{2+} in some samples, exceeding WHO standards. This suggests a need for targeted water treatment to ensure safe drinking water quality.

Table 26. Statistical summary of the continental intercalary groundwater samples.

Parameters	N total	Mean	Standard Deviation	Minimum	Median	Maximum	WHO 2011
T°C	3	32.8	5.506	26.45	35.7	36.25	-
pH	3	7.193	0.086	7.1	7.21	7.27	6.5–8.5
EC (µS/cm)	3	2983.333	296.409	2795	2830	3325	1000
TDS (mg/l)	3	1909.333	189.69	1789	1811	2128	500
Turbidity (NTU)	3	2.807	2.224	0.88	2.3	5.24	5
Ca^{2+} (mg/l)	3	232.464	30.06	202.404	232.464	262.524	75
Mg^{2+} (mg/l)	3	100.866	21.293	80.207	99.651	122.74	50
Na^{+} (mg/l)	3	274.333	92.381	220	222	381	200
K^{+} (mg/l)	3	34.667	8.737	25	37	42	12
NH_4^{+} (mg/l)	3	0.31	0.081	0.216	0.354	0.359	-
Cl^{-} (mg/l)	3	652.335	30.907	631.063	638.154	687.788	250
SO_4^{2-} (mg/l)	3	604.493	108.901	541.214	542.025	730.24	250
HCO_3^{-} (mg/l)	3	153.72	14.992	142.74	147.62	170.8	120
NO_3^{-} (mg/l)	3	4.813	5.199	1.363	2.283	10.793	50
PO_4^{3-} (mg/l)	3	1.244	0.206	1.009	1.325	1.398	1
Fe^{2+} (mg/l)	3	0.538	0.613	0.165	0.203	1.245	0.3

4.3.2. Hydrochemical facies and controlling geochemical process of the continental intercalary

The abundance order of major ions is the same in CI-1 and CI-2, which is $Na^{+}+K^{+} > Ca^{2+} > Mg^{2+}$, and $Cl^{-} > SO_4^{2-} > HCO_3^{-} + CO_3^{2-} > NO_3^{-}$. However, CI-3 displays a different abundance order of its major ions: $Ca^{2+} > Na^{+}+K^{+} > Mg^{2+}$, and $Cl^{-} > SO_4^{2-} > HCO_3^{-} + CO_3^{2-} > NO_3^{-}$, as shown in figure 58. The hydrochemical facies of the continental intercalary groundwater samples exhibit distinct characteristics. CI-2 and CI-3 share the same facies, known as the Ca^{2+}-Mg^{2+}-Cl^{-}-SO_4^{2-} type, $Ca^{2+}Cl^{-}$ type, and chloride type. In contrast, CI-1 shows a mixed

$Ca^{2+}Mg^{2+}Cl^{-}$ water type based on the Piper plot in figure 59(A). The Chadha plot in figure 59 (B) reveals that all three samples display a reverse ion exchange pattern of Ca^{2+}-Mg^{2+}-Cl^{-}/SO_4^{2-}. This indicates an excess of alkaline earths (Ca^{2+} + Mg^{2+}) over alkali metals (Na^{+} + K^{+}) and a higher concentration of strong acidic anions (Cl^{-} + SO_4^{2-}) compared to weak acidic anions (HCO_3^{-}). This water type demonstrates permanent hardness and does not deposit residual sodium carbonate when used for irrigation. It corresponds to Ca^{2+}–Mg^{2+}–Cl^{-} type, Ca^{2+}–Mg^{2+} dominant Cl^{-} type, or Cl—dominant Ca^{2+}–Mg^{2+} type waters. Furthermore, the dissolution of calcite is the main reaction in the continental intercalary as the ratio of Ca^{2+}/ Mg^{2+} was between 1 and 2 as shown in figure 60.

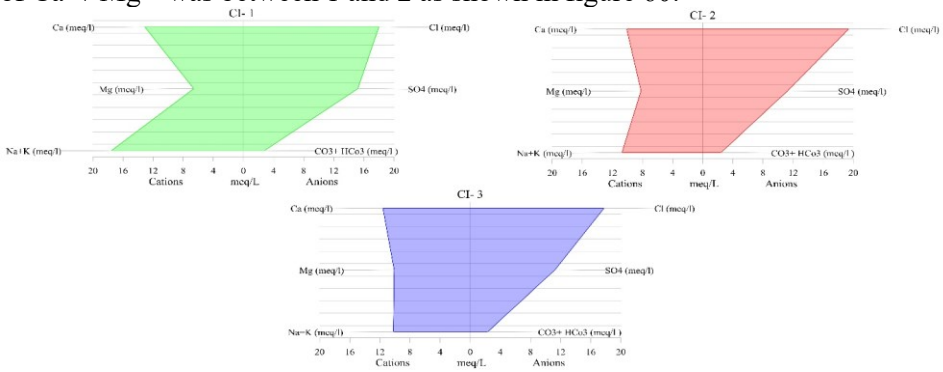

Figure 58. Stiff plot of the continental intercalary groundwater samples.

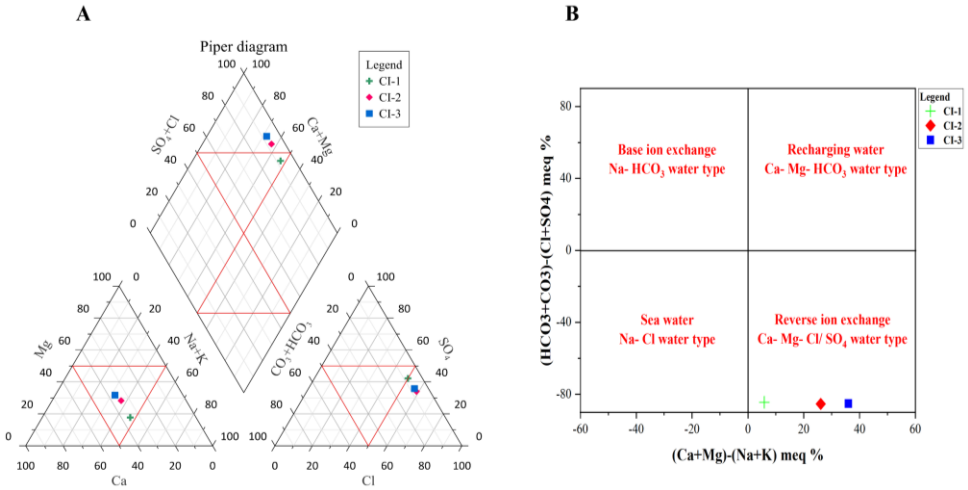

Figure 59. (A). Piper plot of the continental intercalary groundwater samples, (B). Chadha plot pf the continental intercalary groundwater samples.

The ion exchange reactions illustrated by the chloro-alkaline indices (CAI-I and CAI-II) in table 27 indicate that Ca^{2+} and Mg^{2+} are being replaced by Na^{+} and K^{+} in the studied aquifer system, as evidenced by their positive values in both CAI-I and CAI-II.

Table 27. Chloro-alkaline indices of the continental intercalary groundwater samples.

Samples	CAI-I	CAI-II
CI-1	0.345	0.241
CI-2	0.616	0.613
CI-3	0.612	0.563

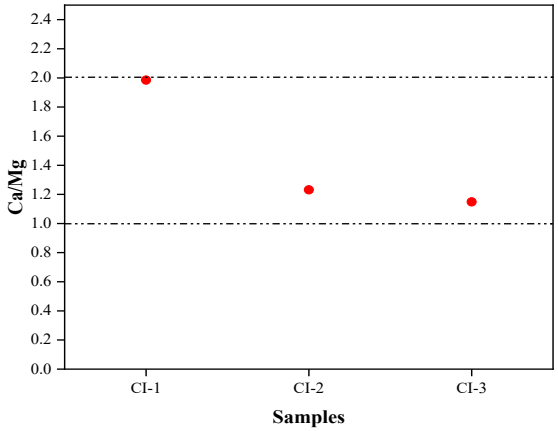

Figure 60. Bivariate plots of Ca^{2+}/Mg^{2+} vs samples.

In figure 61 (A), a Na-normalized graph of Ca^{2+} vs HCO_3^- illustrates that the three continental intercalary groundwater samples exhibited a strong sensitivity to silicate weathering. On the other hand, the Na-normalized graph of Ca^{2+} vs Mg^{2+} in figure 61 (B) indicates that the samples range from having a weak tendency affected by silicate weathering to the dissolution of evaporates.

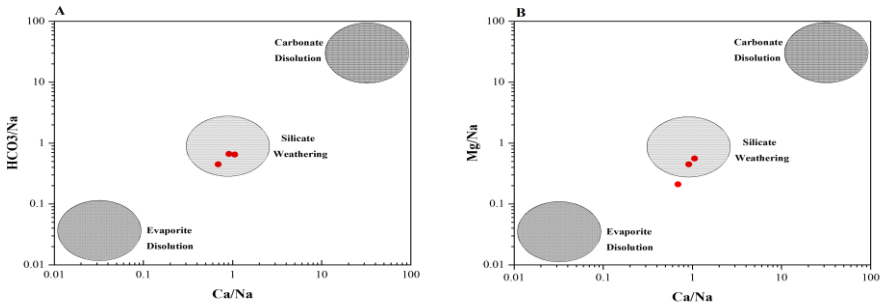

Figure 61.(A). Molar ratio in bivariate plots of Na^+ -normalized Ca^{2+} and HCO_3^-, and (B). Na^+ -normalized Ca^{2+} and Mg^{2+}.

Figure 62 (A) and (B), displays the Gibbs plots of cation and anion ratios against TDS for each sample. All the samples were plotted in the dominance of evaporation-crystallization (salinization), indicating the strong influence of

evaporation-precipitation on the water quality of the studied aquifer.

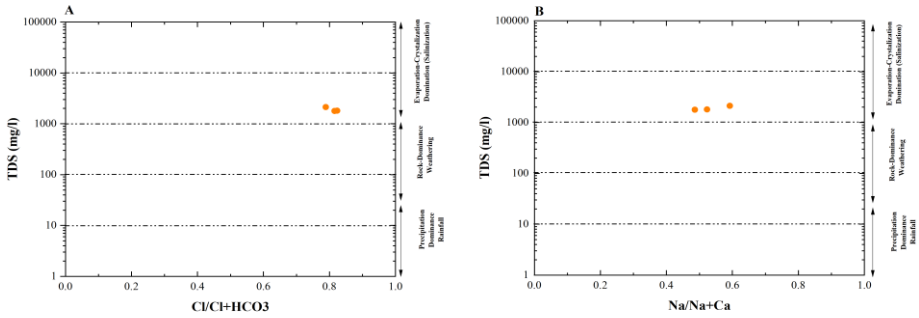

Figure 62. Gibbs diagrams of the continental intercalary groundwater aquifer.

4.3.3. Geochemical modelling of the continental intercalary groundwater samples

The results of the saturation index, as illustrated in figure 63, reveal noteworthy insights regarding the hydrogeochemical dynamics within the continental intercalary groundwater system. Evidently, evaporate minerals including Anhydrite, Gypsum, Halite, and Sylvite exhibit dissolution tendencies, underscoring the prevailing undersaturation of the evaluated groundwater samples with these specific minerals. In contrast, three carbonate minerals- Aragonite, Calcite, and Dolomite- manifest equilibrium states. It is noteworthy that Siderite within CI-1 attains equilibrium, while in CI-2 and CI-3, a discernible trend of Siderite dissolution is observed. Pertinently, the precipitation of oxide minerals, namely Goethite and Hematite, signifies the oversaturation of the analyzed samples. Additionally, phosphate minerals, typified by hydroxyapatite, demonstrate a predisposition for precipitation, juxtaposed with the dissolution tendencies exhibited by vivianite. In terms of sulfate minerals, Melanterite experiences dissolution within the continental intercalary groundwater sample. Notably, CI-1 registers an oversaturation state concerning Jarosite-K, whereas the remaining samples evince undersaturation in relation to Jarosite-K. These findings collectively illuminate the intricate mineralogical interplay and saturation dynamics characterizing the continental intercalary groundwater system.

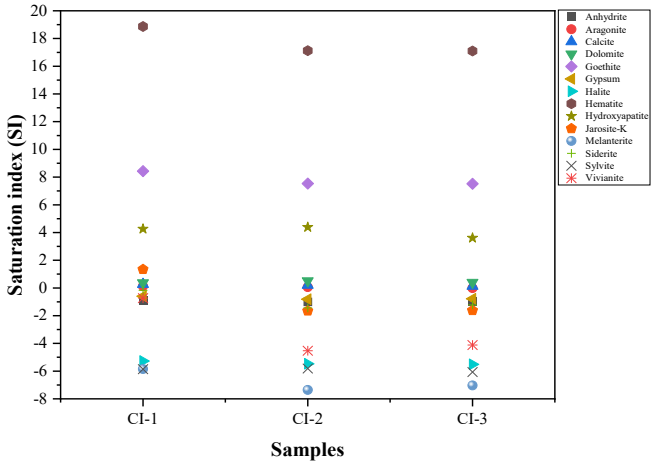

Figure 63. Saturation index results of the continental intercalary groundwater samples.

The mineral stability diagrams depicted in figure 64 reveal that all the samples have been positioned within the Ca-smectite and Kaolinite stability field. This positioning signifies that equilibrium with Ca-smectite and kaolinite is a pivotal controlling factor in the groundwater chemistry of the continental intercalary.

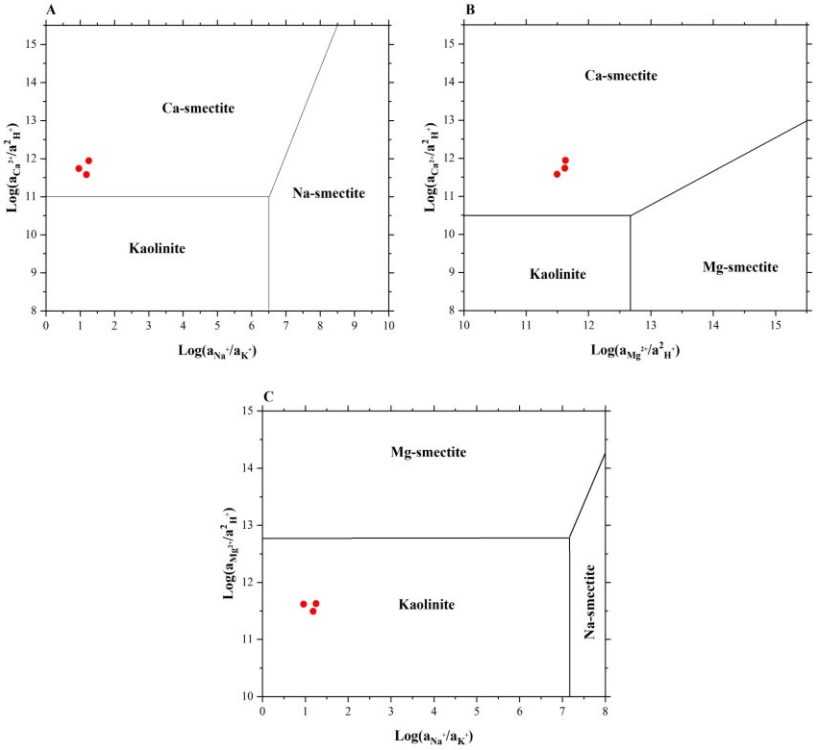

Figure 64. Mineral stability diagrams

4.3.4. Assessment of the continental intercalary groundwater aquifer for drinking and irrigation purposes.

The assessment of water quality in the continental intercalary for potable use has been facilitated through the utilization of various parameters, namely pH, electrical conductivity (EC), total dissolved solids (TDS), turbidity, calcium (Ca^{2+}), magnesium (Mg^{2+}), sodium (Na^{+}), potassium (K^{+}), chloride (Cl^{-}), sulfate (SO_4^{2-}), bicarbonate (HCO_3^{-}), nitrate (NO_3^{-}), and phosphate (PO_4^{3-}). These parameters were employed in accordance with the water quality index methodology outlined by [143]. The results of the water quality index analysis revealed a range of values spanning from 88.10 to 134.70. Notably, all three water samples assessed were found to fall within the classification of 'good' water quality, as delineated in table 28. The WQI classifies water with multiple exceeded parameters as 'good', this could indicate that the weighting or scaling of individual parameters within the index is not adequately reflecting the overall water quality. This highlights the need for careful evaluation and potential adjustment of the WQI methodology to ensure it accurately represents the water quality, especially in cases where multiple parameters exceed standard limits.

Table 28. WQI-based the continental intercalary groundwater aquifer suitability for drinking use.

Range	Classes	Number of Wells
< 50	Excellent water	-
100- 125	Good water	All the wells
125.1- 150	Poor water	-
150.1- 175	Very poor water	-
175.1- 200	Unfit for drinking	-

In the context of irrigation suitability, as depicted in table 29, the evaluation based on the percentage of sodium content (%Na) (ranging from 31.99 to 47.07) indicated that two samples, namely CI-2 and CI-3, exhibited good quality for irrigation purposes. Conversely, CI-1 demonstrated permissible quality for irrigation. The Sodium Adsorption Ratio (SAR) values (ranging from 4.11 to 7.47) revealed that all samples possessed excellent suitability for irrigation. Additionally, both the Magnesium Hazard (MH) (ranging from 33.51 to 46.55) and Kelly's Ratio (KR) (ranging from 0.44 to 0.84) measurements categorized all wells as suitable for irrigation. Furthermore, the Exchangeable Sodium Percentage (ESP) values (ranging from 4.58 to 8.89), Residual Bicarbonate (RBSC) values (ranging from -10.30 to -7.68), and Residual Sodium Carbonate (RSC) values (ranging from -19.36 to -15.88) collectively indicated that all three samples demonstrated excellent, satisfactory, and acceptable quality, respectively. Conversely, the Permeability Index (PI) (ranging from 35.50 to 50.30) classified the investigated

wells as possessing moderate quality for irrigation, while the Permeability Slope (PS) index (ranging from 23.42 to 25.59) categorized them as either injurious or unsatisfactory. The Kelly's Ratio (Ka) results (ranging from 3.25 to 3.57) suggested that all samples exhibited doubtful quality in terms of irrigation suitability. Moreover, based on the Electrical Conductivity (EC) classification, two samples (CI-2 and CI-3) demonstrated doubtful quality for irrigation, whereas one sample (CI-1) was deemed unsuitable for irrigation. Conversely, the Total Hardness (TH) results (ranging from 2470 to 3150 mg/L) indicated that all samples were characterized by a very hard water classification. Despite the fact that each used index has its own characteristics, used parameters, and overall categorization of the water quality, However, the variability of the irrigation suitability results of the continental intercalary groundwater aquifer samples is due to high salinity, sodium content, or other harmful dissolved ions that mainly affect soil structure, permeability, and overall plant health.

Under the absence of bacteriological parameters that were analyzed in ADE authority based on the three collected samples, water quality criteria for drinking and irrigation differ significantly due to the distinct impacts that certain water constituents have on human health compared to plant and soil health. For drinking purposes, the primary concern is the potential health risks associated with contaminants. Regulations are thus designed to ensure that water does not contain harmful levels of pathogens, toxic chemicals, or heavy metals that could lead to immediate or long-term health issues. In contrast, water quality for irrigation is predominantly assessed based on its effect on soil conditions and plant health. High salinity and elevated electrical conductivity (EC), which might be tolerable in drinking water within certain limits, can be detrimental for agricultural use. High salinity leads to the accumulation of salts in the soil, which can inhibit plant growth, alter soil structure, and reduce soil fertility. Similarly, high EC values indicate a high concentration of dissolved ions in water, which can lead to soil salinization, affecting the soil's ability to transmit water and nutrients. Therefore, managing water quality for irrigation not only involves maintaining nutrient levels that are conducive to plant growth but also involves managing the levels of salts and other minerals to prevent soil degradation and maintain agricultural productivity.

Table 29. Irrigation quality indices of the continental intercalary aquifer.

Index	Range	Classes	Number of Wells
EC	< 250	Excellent	-
	250- 750	Good	-
	750- 2000	Permissible	-
	2000- 3000	Doubtful	CI-2, CI-3
	> 3000	Unsuitable	CI-1
% Na	< 20	Excellent	-
	20- 40	Good	CI-2, CI-3
	40- 60	Permissible	CI-1

	60- 80	Doubtful	-
	> 80	Unsafe	-
SAR	< 10	Excellent	All the samples
	10-18	Good	-
	18- 26	Doubtful	-
	> 26	Unsuitable	-
TH	< 75	Unsuitable	-
	75- 150	Moderately Hard	-
	150- 300	Hard	-
	> 300	Very Hard	All the samples
MH	< 50	Suitable	All the samples
	> 50	Unsuitable	-
PI	< 25	Suitable	-
	25- 75	Moderate	All the samples
	> 75	Unsuitable	-
KR	< 1	Suitable	All the samples
	1-2	Moderate	-
	> 2	Unsuitable	-
RSC	< 1.25	Acceptable	All the samples
	1.25- 2.5	Slightly adopted to irrigation	-
	> 2.5	Not suitable	-
Ps	< 3	Excellent to good	-
	> 3	Injurious to unsatisfactory	All the samples
RBSC	< 5	Satisfactory	All the samples
	5-10	Marginal	-
	> 10	Unsatisfactory	-
ESP	< 20	Excellent	All the samples
	20- 40	Good	-
	40- 60	Permissible	-
	60- 80	Doubtful	-
	> 80	Unsuitable	-
Ka	> 18	Excellent	-
	6-18	Permissible	-
	1.2- 6	Doubtful	All the samples
	< 1.2	Unsuitable	-

Regarding the assessment of groundwater pollution and the nitrate pollution index, all the samples demonstrate water quality within the realm of cleanliness in relation to the contamination of this aquifer by nitrate, as the nitrate levels remain comfortably below the established World Health Organization (WHO) threshold

for potable water consumption. Notably, the groundwater from all samples has not approached the WHO's permissible limit for nitrate concentration, thus reflecting a favorable outcome in this aspect. On a global scale, it is observed that CI-2 and CI-3 showcase a moderate level of pollution, primarily attributed to elevated concentrations of Total Dissolved Solids (TDS), Total Hardness (TH), calcium (Ca^{2+}), magnesium (Mg^{2+}), sodium (Na^{+}), potassium (K^{+}), chloride (Cl^{-}), sulfate (SO_4^{2-}), and bicarbonate (HCO_3^{-}). These parameters were utilized in conjunction with Ph and nitrate (NO_3^{-}) content to compute the groundwater pollution index. However, it is noteworthy that CI-1 demonstrates a higher degree of pollution, as delineated in table 30.

Table 30. Groundwater pollution indices.

Pollution index	Range	Classes	Number of Wells
Nitrate pollution index	< 0	Clean	All the samples
	0-1	Light	
	1-2	Moderate	
	2-3	Significant	
	> 3	Very significant	
Pollution groundwater index	< 1	Insignificant pollution	
	1- 1.5	Low pollution	
	1.5- 2	Moderate pollution	CI-2, CI-3
	2- 2.5	High pollution	CI-1
	> 2.5	Very high pollution	

4.3.5. Temporal changes of the continental intercalary groundwater aquifer

Geogenic processes serve as the origin of all parameters within the continental intercalary groundwater aquifer due to water-rock interactions. Despite the limited comprehensive data from the source, a comparative study was conducted on specific hydrochemical parameters analyzed from three wells within the continental intercalary aquifer based on the obtained data in 2012, 2014, 2015, 2017, 2018, 2019, 2020, and 2021. The temporal variation of hydrochemical parameters analyzed in this aquifer was presented in box plots, as shown in figures 65, 66, and 67. Based on the pH box plot, a wide variation has been observed, indicating that the data points within the boxes are more dispersed or have a wider spread. However, the minimum pH value was observed in 2018 with 7.02, and the maximum pH value was observed in 2020 with 7.73. The minimum value of EC was recorded in 2021 with 2270 µS/cm, while the maximum value was observed in 2019 with 3325 µS/cm. All the values recorded over the study period exceeded WHO limits for drinking purposes, indicating that these waters have doubtful to unsuitable quality for utilization. Regarding turbidity, the highest value was recorded in 2018 with 11.1 NTU, and the lowest value was recorded in 2014 with 0.33 NTU. The values of turbidity exceeded WHO standards in 2017, 2018, 2019,

and 2020 in different wells. Regarding TH, the highest value recorded was 1550 mg/l in 2020, and the lowest value was 800 mg/l recorded in 2017. All the samples over the study period were categorized as very hard waters.

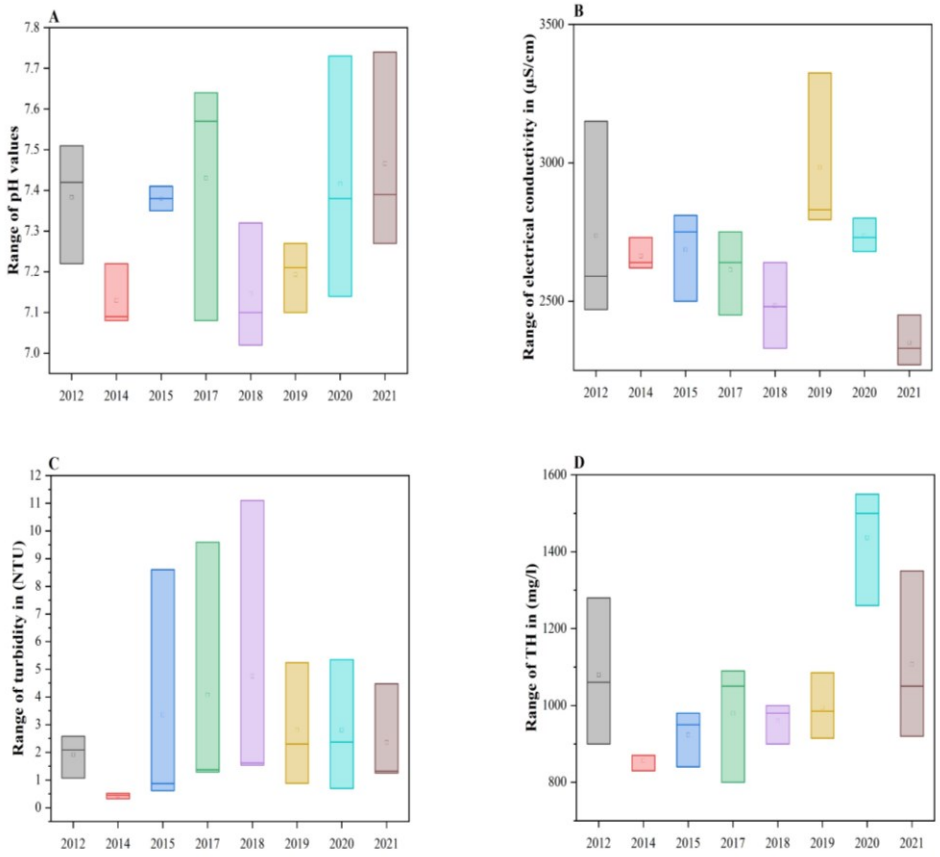

Figure 65. Box plots of continental intercalary groundwater aquifer variation (A). Ph, (B). EC, (C). Turbidity, (D). TH.

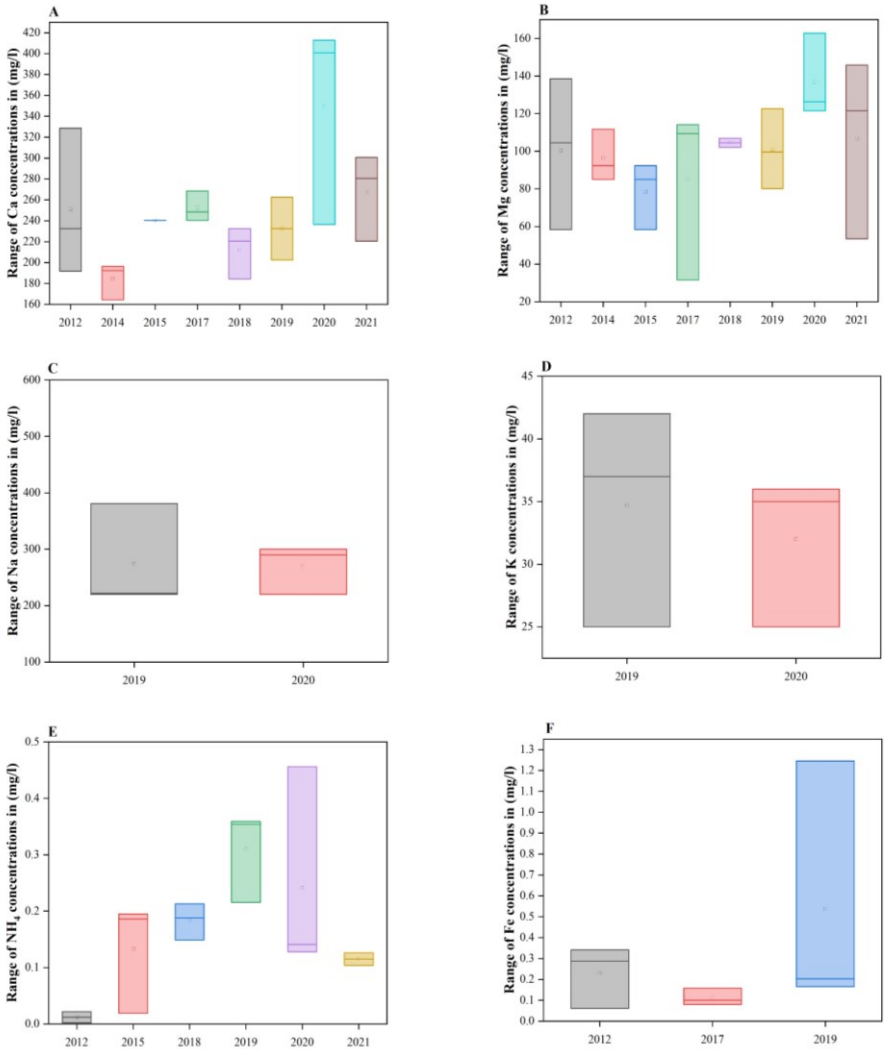

Figure 66. Box plots of continental intercalary groundwater aquifer variation (A). Ca^{2+}, (B). Mg^{2+}, (C). Na^{+}, (D). K^{+}, €. NH_4^{+}, (F). Fe^{2+}.

Based on the box plot of Ca^{2+} concentration over the studied period, it was noticed that there is a wide variation in Ca^{2+} concentrations. The minimum observed concentration of Ca^{2+} was in 2014 at 164.32 mg/l, and the maximum value was also observed in 2020 at 412.82 mg/l. The box plot of Mg^{2+} concentrations indicates a gradual decrease in Mg^{2+} concentrations from 2012 to 2015, then an increase in 2017, followed by a decrease until 2019, and then another increase in 2020 and a subsequent decrease in 2021. The minimum recorded concentration of Mg^{2+} was observed in 2017 at 31.60 mg/l, while the maximum value was noticed in 2020 at 162.84 mg/l. All the concentrations of Mg^{2+} throughout the studied period exceeded the WHO limits for drinking water use, except for one sample in 2017, which was within the limits for drinking purposes.

Due to the significant lack of data, it was only possible to analyze the changes in two years regarding Na^+ and K^+ concentrations. Furthermore, the maximum recorded values of Na^+ and K^+ were observed in 2019, at 381 mg/l and 42 mg/l, respectively, while the minimum values were also observed in 2019, at 220 mg/l and 25 mg/l, respectively. Similarly, for the temporal changes analysis of Na^+ and K^+, Fe^{2+} data had a significant shortage from the source, and it was only possible to analyze the changes in three years (2012, 2017, and 2019). The minimum recorded concentration of Fe^{2+} was observed in 2012 at 0.061 mg/l, while the maximum value was noticed in 2019 at 1.25 mg/l. CI-1 and CI-2 in 2017 exceeded the limits, and in 2019, CI-1 exceeded the limits, while the rest of the samples did not exceed the limits. On the other hand, NH_4^+ concentration over the studied period indicated slight variations in the concentrations. However, the minimum recorded values were observed in 2012 with 0.002 mg/l, while the highest concentration was noticed in 2020 at 0.456 mg/l.

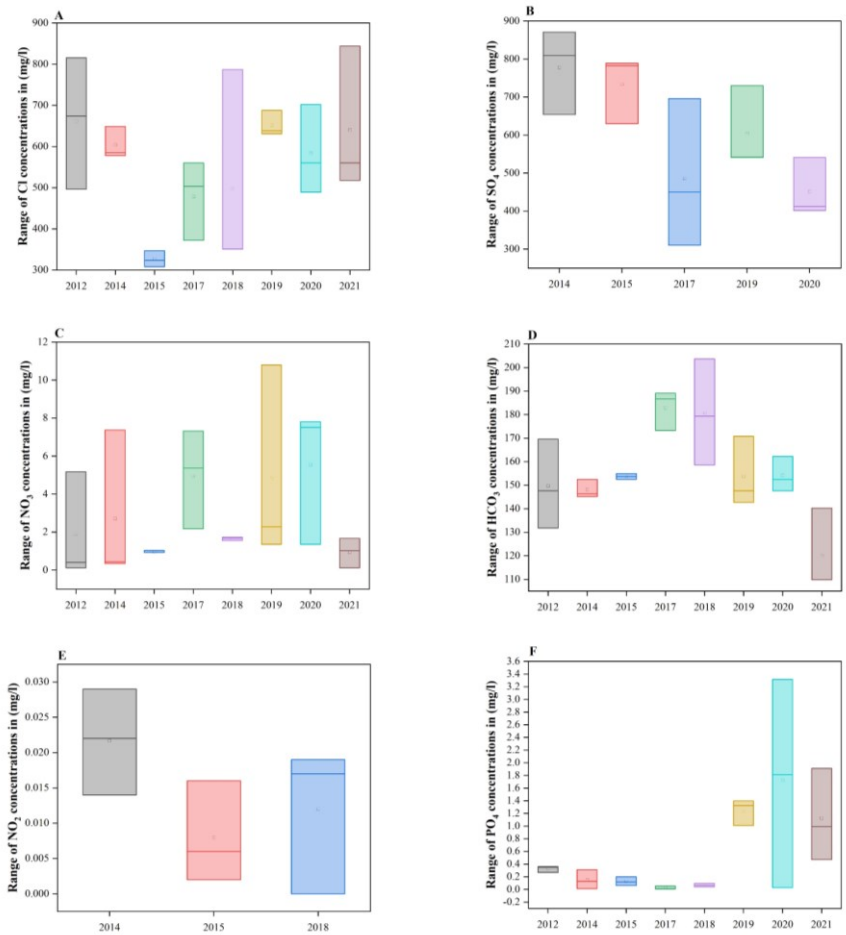

Figure 67. Box plots of continental intercalary groundwater aquifer variation (A). Cl^-, (B). SO_4^{2-}, (C). NO_3^-, (D). HCO_3^-, (E). NO_2^-, (F). PO_4^{3-}.

In relation to the temporal variation of anionic content in the continental intercalary groundwater aquifer, the minimum recorded concentration of Cl was 308.09 mg/l in 2015, while the maximum value was observed in 2021 at 843.78 mg/l. All the recorded values exceeded the WHO limits for drinking purposes. Regarding SO_4^{2-} variation, the minimum value was 310.41 mg/l recorded in 2017, and the maximum value was 871.35 mg/l in 2014. All the recorded values of SO_4^{2-} over the studied period exceeded the limits for drinking water use as they were higher than 250 mg/l. However, the minimum and maximum recorded values of HCO_3^- were observed in 2021 and 2018, at 109.8 mg/l and 203.74 mg/l, respectively. On the other hand, the minimum recorded value of NO_2^- in the continental intercalary groundwater aquifer was in 2018 at 0 mg/l, and the maximum value was 0.029 mg/l recorded in 2014. The minimum and maximum recorded values of PO_4^{3-} were observed in 2020, at 0.03 and 3.32 mg/l, respectively. In 2012, 2014, 2015, 2017, and 2018 data, PO_4^{3-} concentrations did not exceed the limits, while in 2019 all the samples exceeded the limits. In 2020, CI-1 and CI-2 exceeded the limits, and in 2021, CI-2 was the only sample that exceeded the limits. In relation to NO_3^- variations, the concentrations of NO_3^- over the studied period did not exceed the limits. However, the minimum recorded value was in 2021 at 0.126 mg/l, and the maximum value was 10.79 mg/l recorded in 2019.

5. *Summary*

Since the early 1980s, various regions in northern Algeria's Sahara have been grappling with rising groundwater levels. Among these regions, the Oued Souf Valley has been particularly affected by this phenomenon due to a combination of natural and anthropogenic factors, which have exacerbated the north west Sahara aquifer system pollution. In this thesis, I employed a comprehensive methodology structured around hydrogeochemical analysis, the application of water quality indices for drinking, irrigation, and pollution detection, multivariate statistical analysis, and spatial analysis. This approach aimed to investigate the Northwest Sahara Aquifer System both qualitatively and quantitatively by identifying pollutants within the aquifer, ensuring water safety for consumption and use, and assessing the phreatic groundwater aquifer's condition.

Consequently, in this dissertetion, an evaluation of the vertical drainage system performance and its impact on the phreatic groundwater level stabilization has been performed by mapping the water table of the phreatic groundwater level using geostatistical modelling using Ordinary kriging (OK) interpolation method, which has been applied to analyze the spatial and temporal structure of groundwater level fluctuation. Meanwhile, hierarchical cluster analysis (HCA) was applied for grouping the wells based on the groundwater fluctuations for 2008, 2009, 2014, 2016, 2018, and 2021. However, the vertical drainage system reflected a significant decline of groundwater from 2009 to 2018 due to the important drained volumes through it but another rising phenomenon might be threatening the region in the near future, and this is what was indicated in the 2021 groundwater level data. Cluster analysis has generated four groups based on their fluctuation means that are increasing from the first group to the fourth group ascendingly. The first cluster grouped the drains that have a shallow depth (average mean of 5.91 mbgl) and declined over the clusters. The clusters are spatially combined with significant separation of the fourth cluster which represents the deepest group (12.89 mbgl). Based on this research, several factors are influencing the stability of the phreatic groundwater level and even the performance of the drainage system, the most important of which is the overexploitation from deep groundwater reservoirs such as complex terminal and continental intercalary (in drinking and irrigation) and even the illegal use of the phreatic groundwater with important quantities for irrigation and illegal industries.

On the other side, using complex hydrogeochemical and geostatistical methods on the collected phreatic groundwater samples, it was revealed that groundwater temperatures of the phreatic aquifer ranged between 25 and 31.40°C, potentially influencing quality through microbial proliferation and reduced gas solubility. The pH values fluctuated between 6.78 and 8.57. While most samples fell within the World Health Organization's (WHO) recommended limits, approximately 32% exhibited slightly acidic conditions. EC values extended from 3100 to 7500 µs/cm, surpassing the WHO's guidelines for potable water. Elevated EC suggests a high concentration of total dissolved solids, which similarly exceeded WHO standards in most samples. Turbidity levels exhibited substantial variation, compromising aesthetic quality and necessitating treatment prior to consumption. Some samples

were identified as turbid or relatively turbid. The concentrations of Ca, Mg, Na, K, and Cl were predominantly high, frequently exceeding WHO's drinking water thresholds. Specific samples demonstrated varying compliance with these standards. Moreover, numerous samples surpassed WHO limits for NO_3, NO_2, and NH_4, suggesting potential contamination from agricultural runoff, sewage, or industrial effluents. Concentrations of F, SO_4, and PO_4 exceeded WHO guidelines in certain samples, whereas sulfate levels were generally within acceptable limits. DO, COD, and BOD varied among samples, reflecting differing degrees of biodegradability and pollution. Fecal and total coliform levels were elevated in some samples, indicating significant contamination.

Employing various indices such as the National Sanitation Foundation Water Quality Index, Groundwater Pollution Index, and Nitrate Pollution Index, the study revealed poor water quality, substantial groundwater pollution, and diverse levels of nitrate contamination. Furthermore, fourteen hydrochemical parameters were analyzed from phreatic groundwater samples to compute the water quality index for drinking suitability analysis. These parameters, evaluated against the WHO limits established in 2011, included Ca, Mg, Na, K, F, NO_3, HCO_3, Cl, turbidity, EC, TDS, SO_4, PO_4, and pH. Across all 28 samples obtained from the studied aquifer, the findings revealed that the majority of the samples were classified as having good water quality. Additionally, two samples were categorized as excellent, three as poor, two as very poor, and four as unfit for drinking water utilization.

The assessment of twenty-eight groundwater samples from a phreatic aquifer for irrigation suitability used various indices. Of these, nineteen were excellent for irrigation, and nine were good, based on the percentage of sodium (% Na) values. All twenty-eight samples were rated excellent according to the Sodium Adsorption Ratio (SAR), suitable for most soil types. Regarding total hardness (TH), four samples were moderately hard, twenty-two were hard, and two were very hard. The Magnesium Hazard (MH) index showed eighteen samples as suitable for irrigation, while ten were unsuitable. The Permeability Index (PI) indicated that all twenty-eight samples were unsuitable for irrigation. However, other indices like Kelley's Ratio (KR), Exchangeable Sodium Percentage (ESP), Residual Sodium Carbonate (RSC), and Relative Bicarbonate Sodium Concentration (RBSC) classified all samples as suitable. According to the Ps index, all samples were rated as injurious to unsatisfactory. The Ka index revealed four samples with permissible quality and twenty-four with doubtful quality for irrigation. Finally, the K index results showed ten samples of excellent quality, eight of good quality, five of injurious quality, and five as unsuitable for irrigation. On the other hand, two distinct groups of groundwater samples were identified based on HCA. The first group included twenty-one wells, while the second group consisted of seven wells. The key distinguishing factors between these groups appeared to be the concentrations of Na, K, F, NO_3, HCO_3, Cl, and EC, which exhibited a notable increase from the first group to the second. Notably, the samples in the first group did not exceed WHO limits for F and NO_3 concentrations, indicating lower vulnerability to NO_3 and F contamination. These samples were concentrated primarily within the main municipality of El Oued. Conversely, the second group of samples exhibited higher

vulnerability in terms of Na, K, F, NO_3, HCO_3, Cl, and EC. This area was situated on the outskirts of El Oued, Debila, and Guemar municipalities, near agricultural areas. This analysis provides valuable insights into the spatial distribution and variations in hydro-chemical properties across the study area, offering important information for groundwater resource management and monitoring, especially in relation to potential contamination sources and vulnerability. Furthermore, the applied spatial analysis identified and emphasized on the existence of three typical spatial patterns within the parameters under study. Through applied spatial analysis, it was observed that peri-urban and agricultural areas are characterized by elevated levels of EC, Na, K, Cl, HCO_3, PO_4, and DO. In contrast, higher concentrations of Ca, Mg, F, NO_2, and NH_4 were discovered predominantly in urban areas. Additionally, NO_3, SO_4, BOD, and COD exhibited high levels in both agricultural and urban regions.

The hydro-chemical analysis of phreatic groundwater samples revealed several key findings: Major Ion Abundances: The major ion abundances in both generated groups of phreatic groundwater samples followed an order of Ca > Mg > Na+K and Cl > SO_4 > HCO_3+ CO_3. The hydrochemical facies in the phreatic groundwater exhibited slight differences between the first and the second group. The first group was characterized by Ca-Mg-Cl-SO_4 type and Ca-Cl type waters, while the second group included Ca-Mg-Cl-SO_4, mixed Ca-Na-HCO_3, and Cl type waters. The Chadha plot revealed that all the samples in both groups belonged to the reverse ion-exchange Ca-Mg-Cl/SO_4 water type, indicating Ca-Mg-Cl type, Ca-Mg dominant Cl type, or Cl-dominant Ca-Mg type waters. Gibbs diagrams illustrated that the majority of the total samples from the phreatic aquifer were in the evaporation-crystallization dominance (salinization) field, suggesting a significant influence of evaporation-crystallization processes. However, two samples were in the rock-dominance weathering field. The chloro-alkaline indices revealed that some samples exhibited positive values, indicating the exchange of Na^+ and K^+ from the groundwater with Mg^{2+} and Ca^{2+} of the rocks (base-exchange reaction), while others had negative indices, indicating the opposite exchange. The normalized Na graphs suggested a slight tendency towards silicate weathering and evaporate dissolution, as well as a slight tendency towards silicate weathering and carbonate dissolution in the phreatic groundwater samples. The saturation indices indicated that Anhydrite, gypsum, Halite, and Sylvite were completely dissolving, while Fluorite was dissolving in all samples except one. Aragonite, Calcite, Dolomite, and Hydroxyapatite were found to be dissolving in some samples, while other samples were characterized by the precipitation of these minerals. Mineral stability diagrams revealed that all samples fell within the Ca-smectite stability field, with a concentration in the Kaolinite field, indicating the role of these minerals in the groundwater chemistry of the phreatic aquifer.

Also, as a one of the major parts of this thesis, contamination levels and the spatial pattern identification, as well as human and environmental health risk assessments of the heavy metals in the phreatic groundwater aquifer of the Oued Souf Valley were investigated for the first time. The applied methodology comprised a combination of heavy-metal pollution indices, inverse distance weighting, and human health risk assessment through water ingestion on samples

collected from fourteen monitoring wells. The contamination trend in the phreatic aquifer showed Al > B > Sr > Mn > Fe > Pb > Ni > Cr > Ba > Cu > Zn. Similarly, the enrichment trend was Al > B > Sr > Mn > Ni > Pb > Cr > Ba > Cu > Zn. Ecologically, most of the analyzed metals reflected a low potential ecological risk, except for two wells, S13 and S14, which represented a considerable and high ecological risk in terms of Pb. According to the applied grouping method, the samples in the first group indicated a lower risk of contamination in terms of heavy metals due to their lower concentration compared to the second group. This makes the area containing the second group's samples more vulnerable in terms of heavy metals, which could affect urban, peri-urban, and even agricultural areas. All of the samples (100%) indicated the possibility of potential health risks in the case of children. While six samples showed that the non-cancer toxicity risk is considered low, the rest of the samples had high Hazard Index (HI) values, indicating the possibility of health risks occurring in the case of adults. The constructed vertical drainage system is acting as a supporter and accelerator of the pollution levels in the shallow groundwater aquifer. This is due to its contribution to the penetration of different pollutants into this aquifer system, depending on the residence time of the water, which appears to be long within the drainage system.

In terms of deep aquifers, a comprehensive study has been conducted to assess the hydrogeochemical evolution of the deep groundwater aquifers such as the complex terminal groundwater aquifer in Oued souf valley for drinking and irrigation purposes. To achieve this, 49 groundwater samples from the complex terminal were examined and treated concurrently with multivariate statistical methods, geostatistical modeling and the WQI (water quality index). Focusing on the physico-chemical parameters, Q mode clustering analysis detected four major water groups, where the mineralization augmented from group 1 to group 4. The hydro-chemical type was the same, Ca-Mg-Cl-SO_4 for all the groups. Calcite, dolomite, anhydrite, and gypsum would be the dominant reactions with the undersaturation of evaporates minerals, based on geochemical modeling, while the carbonate minerals are precipitating. Geostatistical analysis using ordinary Kriging demonstrated the exponential semi-variogram model fitted for EC, Ca, Mg, K, HCO_3, Cl, and SO_4. At the same time, the rational quadratic model was the best-fitted semi-variogram model for Na and NO_3. EC, SO_4, and NO_3 have a strong spatial structure, while Ca, Na, K, and HCO_3 have a moderate spatial structure. Moreover, there was a weak spatial structure for Mg and Cl. The WQI shows that CT (complex terminal groundwater aquifers) in many of the wells have poor to very poor water quality (55.10%), with only a small fraction exhibiting good quality. Only two samples were deemed unfit for drinking and their quality for irrigation fluctuates from good to moderate quality although its high mineralization. Furthermore, temporal changes in a complex terminal groundwater aquifer have been analyzed, particularly focusing on various water quality parameters such as pH, Electrical Conductivity (EC), total hardness, turbidity, and the concentrations of different ions and elements. The analysis reveals fluctuations in pH values with potential seasonal patterns, as well as outliers that may result from factors like contamination events or measurement errors. EC values indicate variations and frequent exceedance of WHO limits for drinking and irrigation

purposes. Total hardness remains consistently high, while turbidity stays within WHO limits. Concentrations of Ca, Mg, Na, K, Fe, NH_4, Cl, SO_4, HCO_3, NO_2, PO_4, and NO_3 vary over the studied years, with some exceeding WHO limits. These variations may be linked to geological factors and potential communication with shallow aquifers.

The comprehensive hydrogeochemical analysis of groundwater samples from the continental intercalary aquifer revealed several key findings. The temperature and pH generally met the 2011 World Health Organization (WHO) standards for drinking water, but elevated EC, TDS, and turbidity levels indicated brackish water with mineralization. Major cations (Ca, Mg, Na, and K) and anions (Cl, SO_4, and HCO_3) exceeded WHO standards, while NO_3 levels were within acceptable limits. PO_4 levels surpassed WHO thresholds in all samples, and some samples exhibited elevated NH_4 levels. CI-1 showed elevated Fe levels exceeding WHO standards. Different major ion abundance orders indicated varying water types in the samples. Groundwater chemistry suggested the dissolution of calcite and ion exchange of Ca and Mg for Na and K. Saturation indices indicated mineral dissolution and precipitation. The water quality index classified all three samples as having "good" water quality for potable use, but irrigation suitability varied, with some samples being suitable and others doubtful or unsuitable. Nitrate levels remained below WHO standards, indicating a lack of nitrate pollution. CI-1 exhibited a higher degree of pollution compared to CI-2 and CI-3 based on the groundwater pollution index. Overall, the study provides insights into the hydrogeochemical dynamics and suitability of continental intercalary groundwater for various uses, highlighting variations in water quality and potential challenges for potable and irrigation purposes. The analysis of the temporal changes in the complex terminal groundwater quality over the years presents several noteworthy trends. The pH levels have remained relatively stable, indicating slightly alkaline water, with an uptick in variability in the last two years. EC has been on a decline, pointing towards a reduction in water mineralization, with the initial years showing greater extremes. Turbidity has decreased, suggesting the water is becoming clearer, a trend that is supported by the decline in total dissolved solids. Cl and Na concentrations have dropped, although Na levels exhibit considerable annual fluctuations. A worrying trend is observed with K and NO_3 levels, both of which have spiked in 2020, hinting at potential contamination issues. The rise in NO_3 could be linked to agricultural runoff or interaction with shallower aquifers. NH_4 levels are generally low but rose in 2020, potentially indicating organic pollution. PO_4 concentrations have been consistently low, which helps in preventing eutrophication. Ca shows a decreasing trend with considerable year-to-year variation, while Mg levels have been relatively stable with a marginal downward trend. NO_2 levels have been inconsistent, raising concerns about nitrogen compound contamination. SO_4 levels have varied, with a peak in 2017, reflecting changing geochemical processes. HCO_3 concentrations are low and on a downward trajectory, which could impact the water's buffering capacity. Lastly, Fe concentration has generally decreased, except for a significant outlier in 2019. These findings collectively suggest that while some aspects of water quality are improving, there are emerging concerns, particularly related to potential

contamination from agricultural and organic sources. On the other hand, the analysis of the continental intercalary aquifer's hydrochemistry from 2012-2021 reveals fluctuations in pH and consistently high TH, indicating poor water quality for consumption. EC and turbidity levels often exceeded WHO standards. Variability was observed in Ca and Mg levels, with Mg exceeding WHO limits in most years. Data gaps limited the analysis of Na, K, and Fe. Cl and SO_4 concentrations were consistently above drinking water standards, while NO_3 remained within safe levels. PO_4 levels varied, occasionally surpassing safe limits.

The present dissertation discusses highly important results obtained from the analysis conducted on several horizons of the aquifer system in the Oued Souf Valley, which represents a part of the Northwest Sahara Aquifer System. The results obtained and discussed throughout this dissertation can contribute to drawing attention and increasing the awareness of water experts, both locally and globally, about the consequences of inadequate water management and the negligence in implementing integrated water resource management, especially in arid regions with substantial groundwater resources such as the Oued Souf Valley.

While this thesis provides significant insights into groundwater resources in arid regions, it is important to acknowledge several limitations. The number of samples collected for hydrogeochemical analysis of the Phreatic, Complex terminal, and Continental Intercalary groundwater aquifers was insufficient to study the temporal changes in their quality. This necessitates continuous analysis of these aquifers in the future. A larger sample size is required to understand and confirm the origins of mineralization and pollutants (physicochemical, bacteriological, and heavy metals), which will be achieved by employing additional methods not utilized in this research.

As a further step for future research, extensive investigations must be conducted on the three groundwater aquifers to more thoroughly assess their quality, with a focus on the phreatic groundwater aquifer, including its vertical drainage system. Additionally, the introduction of new and modern techniques such as deep and machine learning techniques (Support Vector Machines (SVMs), Gradient Boosting Machine, and M5 and M5-cubist Convolutional Neural Networks) will be essential. These will be used alongside several modified DRASTIC methods to estimate pollution levels and identify areas most vulnerable to pollution. An assessment of soil contamination resulting from rising phreatic groundwater levels will represent a completely novel research axis for my future work.

6. References

1. Goonetilleke, A.; An, L.; Ted, G. “Urban Stormwater Reuse: An Agenda for Sustainable Development.” Global Sustainable Development Report; 2016.

2. Carroll, S.; Liu, A.; Dawes, L.; Hargreaves, M.; Goonetilleke, A. Role of Land Use and Seasonal Factors in Water Quality Degradations. Water Resour. Manag. 2013, 27, 3433–3440, doi:10.1007/s11269-013-0356-6.

3. McDonald, R.I.; Weber, K.; Padowski, J.; Flörke, M.; Schneider, C.; Green, P.A.; Gleeson, T.; Eckman, S.; Lehner, B.; Balk, D.; et al. Water on an Urban Planet: Urbanization and the Reach of Urban Water Infrastructure. Glob. Environ. Chang. 2014, 27, 96–105, doi:10.1016/j.gloenvcha.2014.04.022.

4. United Nations Transforming Our World: The 2030 Agenda for Sustainable Development; New York, 2015.

5. Intergovernmental Panel on Climate Change (IPCC) Climate Change 2021: The Physical Science Basis. Contribution of Working Group I to the Sixth Assessment Report of the Intergovernmental Panel on Climate Change; 2021;

6. (WRI), W.R.I. Aqueduct Water Risk Atlas; 2020.

7. Táany, R.A.; Tahboub, A.B.; Saffarini, G.A. Geostatistical Analysis of Spatiotemporal Variability of Groundwater Level Fluctuations in Amman-Zarqa Basin, Jordan: A Case Study. Environ. Geol. 2009, 57, 525–535, doi:10.1007/s00254-008-1322-0.

8. UNWWDR The United Nations World Water Development Report.; 2015.

9. Panda, U.C.; Sundaray, S.K.; Rath, P.; Nayak, B.B.; Bhatta, D. Application of Factor and Cluster Analysis for Characterization of River and Estuarine Water Systems - A Case Study: Mahanadi River (India). J. Hydrol. 2006, 331, 434–445, doi:10.1016/j.jhydrol.2006.05.029.

10. Tatawat, R.K.; Chandel, C.P.S. A Hydrochemical Profile for Assessing the Groundwater Quality of Jaipur City. Environ. Monit. Assess. 2008, 143, 337–343, doi:10.1007/s10661-007-9936-3.

11. Kumar, V.; Remadevi, V. Kriging of Groundwater Levels-A Case Study. J. Spat. Hydrol. 2006, 6, 81–94.

12. Ravikumar, P.; Somashekar, R.K.; Angami, M. Hydrochemistry and Evaluation of Groundwater Suitability for Irrigation and Drinking Purposes in the Markandeya River Basin, Belgaum District, Karnataka State, India. Environ. Monit. Assess. 2011, 173, 459–487, doi:10.1007/s10661-010-1399-2.

13. Luna, M.C.M. d. M.; Parteli, E.J.R.; Herrmann, H.J. Model for a Dune Field

with an Exposed Water Table. Geomorphology 2012, 159–160, 169–177, doi:10.1016/j.geomorph.2012.03.021.

14. Jha, M.K.; Chowdhury, A.; Chowdary, V.M.; Peiffer, S. Groundwater Management and Development by Integrated Remote Sensing and Geographic Information Systems: Prospects and Constraints. Water Resour. Manag. 2007, 21, 427–467, doi:10.1007/s11269-006-9024-4.

15. Momodu, M.A.; Anyakora, C.A. Heavy Metal Contamination of Ground Water: The Surulere Case Study. Res. J. Environ. Earth Sci. 2010, 2, 39–43.

16. Velis, M.; Conti, K.I.; Biermann, F. Groundwater and Human Development: Synergies and Trade-Offs within the Context of the Sustainable Development Goals. Sustain. Sci. 2017, 12, 1007–1017, doi:10.1007/s11625-017-0490-9.

17. Srivastava, S.; Singh, J.; Shirsath, P.B. Sustainability of Groundwater Resources at the Subnational Level in the Context of Sustainable Development Goals. Agric. Econ. Res. Rev. 2018, 31, 79, doi:10.5958/0974-0279.2018.00024.1.

18. Zamani, M.G.; Moridi, A.; Yazdi, J. Groundwater Management in Arid and Semi-Arid Regions. Arab. J. Geosci. 2022, 15, doi:10.1007/s12517-022-09546-w.

19. ANRH Ressources En Eau et En Sols de l'Algérie; Rapport Technique; Alger; Algeria, 1986.

20. CDTN Etude Hydrochimique et Isotopique Des Eaux Souterraines de La Cuvette de Ouargla; 1992.

21. Kadri, S.R.; Chaouche, S. La Remontée Des Eaux Dans La Région Du Souf : Une Menace Sur Un Écosystème Oasien. Les Cah. d'EMAM 2018, 30, doi:https://doi.org/10.4000/emam.1554.

22. Côte, M. Dynamique Urbaine Au Sahara. Rev. algérienne d'anthropologie Sci. Soc. 1998, 5, 85–92, doi:https://doi.org/10.4000/insaniyat.11818.

23. Bouzegag, C.; Bouzid-Lagha, S.; Djelal, N. Forecasting the Upwelling Phenomenon Using an Artificial Neural Network. Polish J. Soil Sci. 2020, 53, 245–259, doi:10.17951/pjss/2020.53.2.245.

24. Khezzani, B.; Bouchemal, S. Variations in Groundwater Levels and Quality Due to Agricultural Over-Exploitation in an Arid Environment: The Phreatic Aquifer of the Souf Oasis (Algerian Sahara). Environ. Earth Sci. 2018, 77, 1–18, doi:10.1007/s12665-018-7329-2.

25. Nayak, P.C.; Satyaji Rao, Y.R.; Sudheer, K.P. Groundwater Level Forecasting in a Shallow Aquifer Using Artificial Neural Network Approach. Water Resour. Manag. 2006, 20, 77–90, doi:10.1007/s11269-006-4007-z.

26. Morris, B.L.; Seddique, A.A.; Ahmed, K.M. Response of the Dupi Tila Aquifer to Intensive Pumping in Dhaka, Bangladesh. Hydrogeol. J. 2003, 11, 496–503, doi:10.1007/s10040-003-0274-4.

27. Government of Canada Groundwater Contamination Available online: https://www.canada.ca/en/environment-climate-change/services/water-overview/pollution-causes-effects/groundwater-contamination.html (accessed on 11 November 2023).

28. Gibson, J.M.; Kavanaugh, M.C. Restoring Contaminated Groundwater: An Achievable Goal? Environ. Sci. Technol. 2008, 28, 362A-8A.

29. Chakraborti, D.; Rahman, M.M.; Mukherjee, A.; Alauddin, M.; Hassan, M.; Dutta, R.N.; Pati, S.; Mukherjee, S.C.; Roy, S.; Quamruzzman, Q.; et al. Groundwater Arsenic Contamination in Bangladesh-21 Years of Research. J. Trace Elem. Med. Biol. 2015, 31, 237–248, doi:10.1016/j.jtemb.2015.01.003.

30. Su, Z.; Wu, J.; He, X.; Elumalai, V. Temporal Changes of Groundwater Quality within the Groundwater Depression Cone and Prediction of Confined Groundwater Salinity Using Grey Markov Model in Yinchuan Area of Northwest China. Expo. Heal. 2020, 12, 447–468, doi:10.1007/s12403-020-00355-8.

31. Wang, D.; Wu, J.; Wang, Y.; Ji, Y. Finding High-Quality Groundwater Resources to Reduce the Hydatidosis Incidence in the Shiqu County of Sichuan Province, China: Analysis, Assessment, and Management. Expo. Heal. 2020, 12, 307–322, doi:10.1007/s12403-019-00314-y.

32. Tatti, F.; Petrangeli Papini, M.; Torretta, V.; Mancini, G.; Boni, M.R.; Viotti, P. Experimental and Numerical Evaluation of Groundwater Circulation Wells as a Remediation Technology for Persistent, Low Permeability Contaminant Source Zones. J. Contam. Hydrol. 2019, 222, 89–100, doi:10.1016/j.jconhyd.2019.03.001.

33. Li, P.; Karunanidhi, D.; Subramani, T.; Srinivasamoorthy, K. Sources and Consequences of Groundwater Contamination. Arch. Environ. Contam. Toxicol. 2021, 80, 1–10, doi:10.1007/s00244-020-00805-z.

34. Elumalai, V.; Nethononda, V.G.; Manivannan, V.; Rajmohan, N.; Li, P.; Elango, L. Groundwater Quality Assessment and Application of Multivariate Statistical Analysis in Luvuvhu Catchment, Limpopo, South Africa. J. African Earth Sci. 2020, 171, 103967, doi:10.1016/j.jafrearsci.2020.103967.

35. Wu, J.; Li, P.; Qian, H. Hydrochemical Characterization of Drinking Groundwater with Special Reference to Fluoride in an Arid Area of China and the Control of Aquifer Leakage on Its Concentrations. Environ. Earth Sci. 2015, 73, 8575–8588, doi:10.1007/s12665-015-4018-2.

36. Amirabdollahian, M.; Datta, B. Identification of Contaminant Source

Characteristics and Monitoring Network Design in Groundwater Aquifers: An Overview. J. Environ. Prot. (Irvine,. Calif). 2013, 04, 26–41, doi:10.4236/jep.2013.45a004.

37. Wang, F.; Song, K.; He, X.; Peng, Y.; Liu, D.; Liu, J. Identification of Groundwater Pollution Characteristics and Health Risk Assessment of a Landfill in a Low Permeability Area. Int. J. Environ. Res. Public Health 2021, 18, doi:10.3390/ijerph18147690.

38. Soveri, J. Acidifying Effects on Groundwater. Stud. Environ. Sci. 1992, 50, 135–143, doi:10.1016/S0166-1116(08)70108-0.

39. Appleyard, S.; Wong, S.; Willis-Jones, B.; Angeloni, J.; Watkins, R. Groundwater Acidification Caused by Urban Development in Perth, Western Australia: Source, Distribution, and Implications for Management. Aust. J. Soil Res. 2004, 42, 579–585, doi:10.1071/sr03074.

40. Ford, M.; Tellam, J.H.; Hughes, M. Pollution-Related Acidification in the Urban Aquifer, Birmingham, UK. J. Hydrol. 1992, 140, 297–312, doi:10.1016/0022-1694(92)90245-Q.

41. Pacheco, F.; Van Der Weijden, C.H. Contributions of Water-Rock Interactions to the Composition of Groundwater in Areas with a Sizeable Anthropogenic Input: A Case Study of the Waters of the Fundäo Area, Central Portugal. Water Resour. Res. 1996, 32, 3553–3570, doi:10.1029/96WR01683.

42. Nordstrom, D.K.; Ball, J.W.; Donahoe, R.J.; Whittemore, D. Groundwater Chemistry and Water-Rock Interactions at Stripa. Geochim. Cosmochim. Acta 1989, 53, 1727–1740, doi:10.1016/0016-7037(89)90294-9.

43. Morán-Ramírez, J.; Ledesma-Ruiz, R.; Mahlknecht, J.; Ramos-Leal, J.A. Rock-Water Interactions and Pollution Processes in the Volcanic Aquifer System of Guadalajara, Mexico, Using Inverse Geochemical Modeling. Appl. Geochemistry 2016, 68, 79–94, doi:10.1016/j.apgeochem.2016.03.008.

44. Mohammed Barzinji, D.A.; Ganjo, G.A. Water Pollution, Limnological Investigations in Kurdistan Region and Other Part of Iraq. 2014, 3, 776–799.

45. Hansen, B.; Thorling, L.; Schullehner, J.; Termansen, M.; Dalgaard, T. Groundwater Nitrate Response to Sustainable Nitrogen Management. Sci. Rep. 2017, 7, 1–12, doi:10.1038/s41598-017-07147-2.

46. He, S.; Wu, J. Hydrogeochemical Characteristics, Groundwater Quality, and Health Risks from Hexavalent Chromium and Nitrate in Groundwater of Huanhe Formation in Wuqi County, Northwest China. Expo. Heal. 2019, 11, 125–137, doi:10.1007/s12403-018-0289-7.

47. Karunanidhi, D.; Aravinthasamy, P.; Subramani, T.; Wu, J.; Srinivasamoorthy, K. Potential Health Risk Assessment for Fluoride and

Nitrate Contamination in Hard Rock Aquifers of Shanmuganadhi River Basin, South India. Hum. Ecol. Risk Assess. 2019, 25, 250–270, doi:10.1080/10807039.2019.1568859.

48. Serio, F.; Miglietta, P.P.; Lamastra, L.; Ficocelli, S.; Intini, F.; De Leo, F.; De Donno, A. Groundwater Nitrate Contamination and Agricultural Land Use: A Grey Water Footprint Perspective in Southern Apulia Region (Italy). Sci. Total Environ. 2018, 645, 1425–1431, doi:10.1016/j.scitotenv.2018.07.241.

49. Zhang, Y.; Wu, J.; Xu, B. Human Health Risk Assessment of Groundwater Nitrogen Pollution in Jinghui Canal Irrigation Area of the Loess Region, Northwest China. Environ. Earth Sci. 2018, 77, 1–12, doi:10.1007/s12665-018-7456-9.

50. Li, P.; He, X.; Guo, W. Spatial Groundwater Quality and Potential Health Risks Due to Nitrate Ingestion through Drinking Water: A Case Study in Yan'an City on the Loess Plateau of Northwest China. Hum. Ecol. Risk Assess. 2019, 25, 11–31, doi:10.1080/10807039.2018.1553612.

51. He, X.; Wu, J.; He, S. Hydrochemical Characteristics and Quality Evaluation of Groundwater in Terms of Health Risks in Luohe Aquifer in Wuqi County of the Chinese Loess Plateau, Northwest China. Hum. Ecol. Risk Assess. 2019, 25, 32–51, doi:10.1080/10807039.2018.1531693.

52. Baird, C.; Cann, M. Environmental Chemistry; 3rd Editio.; W.H Freeman and Company press: USA, 2005.

53. Adimalla, N.; Wu, J. Groundwater Quality and Associated Health Risks in a Semi-Arid Region of South India: Implication to Sustainable Groundwater Management. Hum. Ecol. Risk Assess. 2019, 25, 191–216, doi:10.1080/10807039.2018.1546550.

54. Zamil Al-Sudani, H.I. A Review on Groundwater Pollution. Int. J. Recent Eng. Sci. 2019, 6, 13–21, doi:10.14445/23497157/ijres-v6i5p103.

55. Hashim, M.A.; Mukhopadhyay, S.; Sahu, J.N.; Sengupta, B. Remediation Technologies for Heavy Metal Contaminated Groundwater. J. Environ. Manage. 2011, 92, 2355–2388, doi:10.1016/j.jenvman.2011.06.009.

56. Suvarapu, L.N.; Baek, S.-O. Determination of Heavy Metals in the Ambient Atmosphere: A Review. Toxicol. Ind. Health 2017, 33, 79–96, doi:10.1177/0748233716654827.

57. Visnjic-Jeftic, Z.; Jaric, I.; Jovanovic, L.; Skoric, S.; Smederevac-Lalic, M.; Nikcevic, M.; Lenhardt, M. Heavy Metal and Trace Element Accumulation in Muscle, Liver and Gills of the Pontic Shad (Alosa Immaculata Bennet 1835) from the Danube River (Serbia). Microchem. J. 2010, 95, 341–344, doi:10.1016/j.microc.2010.02.004.

58. Cabral-Pinto, M.M.S.; Inácio, M.; Neves, O.; Almeida, A.A.; Pinto, E.;

Oliveiros, B.; Ferreira da Silva, E.A. Human Health Risk Assessment Due to Agricultural Activities and Crop Consumption in the Surroundings of an Industrial Area. Expo. Heal. 2020, 12, 629–640, doi:10.1007/s12403-019-00323-x.

59. He, X.; Li, P. Surface Water Pollution in the Middle Chinese Loess Plateau with Special Focus on Hexavalent Chromium (Cr6+): Occurrence, Sources and Health Risks. Expo. Heal. 2020, 12, 385–401, doi:10.1007/s12403-020-00344-x.

60. Abbas, G.; Murtaza, B.; Bibi, I.; Shahid, M.; Niazi, N.K.; Khan, M.I.; Amjad, M.; Hussain, M.; Natasha Arsenic Uptake, Toxicity, Detoxification, and Speciation in Plants: Physiological, Biochemical, and Molecular Aspects. Int. J. Environ. Res. Public Health 2018, 15, doi:10.3390/ijerph15010059.

61. Rebelo, F.M.; Caldas, E.D. Arsenic, Lead, Mercury and Cadmium: Toxicity, Levels in Breast Milk and the Risks for Breastfed Infants. Environ. Res. 2016, 151, 671–688, doi:10.1016/j.envres.2016.08.027.

62. Adeolu, A.O.; Ada, O. V; Gbenga, A.A.; Adebayo, O.A. Assessment of Groundwater Contamination by Leachate near a Municipal Solid Waste Landfill. African J. Environ. Sci. Technol. 2011, 5, 933–940, doi:10.5897/AJEST11.272.

63. Abiriga, D.; Vestgarden, L.S.; Klempe, H. Groundwater Contamination from a Municipal Landfill: Effect of Age, Landfill Closure, and Season on Groundwater Chemistry. Sci. Total Environ. 2020, 737, 140307, doi:10.1016/j.scitotenv.2020.140307.

64. Robinson, H.; Gronow, J.; Durrant, P.S.; Taylor, M.; Reeve, C.E.; Mackey, P.G.; Mull, R.; Dearlove, J.P.. Groundwater Protection in the UK - Assessment of the Landfill Leachate Source Term. J. Inst. Water Environ. Manag. 1992, 6, 229–236.

65. Singh, U.K.; Kumar, M.; Chauhan, R.; Jha, P.K.; Ramanathan, A.L.; Subramanian, V. Assessment of the Impact of Landfill on Groundwater Quality: A Case Study of the Pirana Site in Western India. Environ. Monit. Assess. 2008, 141, 309–321, doi:10.1007/s10661-007-9897-6.

66. Lesser, L.E.; Mora, A.; Moreau, C.; Mahlknecht, J.; Hernández-Antonio, A.; Ramírez, A.I.; Barrios-Piña, H. Survey of 218 Organic Contaminants in Groundwater Derived from the World's Largest Untreated Wastewater Irrigation System: Mezquital Valley, Mexico. Chemosphere 2018, 198, 510–521, doi:10.1016/j.chemosphere.2018.01.154.

67. Jurado, A.; Vàzquez-Suñé, E.; Carrera, J.; López de Alda, M.; Pujades, E.; Barceló, D. Emerging Organic Contaminants in Groundwater in Spain: A Review of Sources, Recent Occurrence and Fate in a European Context. Sci. Total Environ. 2012, 440, 82–94, doi:10.1016/j.scitotenv.2012.08.029.

68. Lapworth, D.J.; Baran, N.; Stuart, M.E.; Ward, R.S. Emerging Organic Contaminants in Groundwater: A Review of Sources, Fate and Occurrence. Environ. Pollut. 2012, 163, 287–303, doi:10.1016/j.envpol.2011.12.034.

69. Sorensen, J.P.R.; Lapworth, D.J.; Nkhuwa, D.C.W.; Stuart, M.E.; Gooddy, D.C.; Bell, R.A.; Chirwa, M.; Kabika, J.; Liemisa, M.; Chibesa, M.; et al. Emerging Contaminants in Urban Groundwater Sources in Africa. Water Res. 2015, 72, 51–63, doi:10.1016/j.watres.2014.08.002.

70. Lapworth, D.J.; Baran, N.; Stuart, M.E.; Manamsa, K.; Talbot, J. Persistent and Emerging Micro-Organic Contaminants in Chalk Groundwater of England and France. Environ. Pollut. 2015, 203, 214–225, doi:10.1016/j.envpol.2015.02.030.

71. Meffe, R.; de Bustamante, I. Emerging Organic Contaminants in Surface Water and Groundwater: A First Overview of the Situation in Italy. Sci. Total Environ. 2014, 481, 280–295, doi:10.1016/j.scitotenv.2014.02.053.

72. Kristanti, R.A.; Ngu, W.J.; Yuniarto, A.; Hadibarata, T. Rhizofiltration for Removal of Inorganic and Organic Pollutants in Groundwater: A Review. Biointerface Res. Appl. Chem. 2021, 11, 12326–12347, doi:10.33263/BRIAC114.1232612347.

73. Gwenzi, W.; Chaukura, N. Organic Contaminants in African Aquatic Systems: Current Knowledge, Health Risks, and Future Research Directions. Sci. Total Environ. 2018, 619–620, 1493–1514, doi:10.1016/j.scitotenv.2017.11.121.

74. Schulze, S.; Zahn, D.; Montes, R.; Rodil, R.; Quintana, J.B.; Knepper, T.P.; Reemtsma, T.; Berger, U. Occurrence of Emerging Persistent and Mobile Organic Contaminants in European Water Samples. Water Res. 2019, 153, 80–90, doi:10.1016/j.watres.2019.01.008.

75. Kurwadkar, S.; Kanel, S.R.; Nakarmi, A. Groundwater Pollution: Occurrence, Detection, and Remediation of Organic and Inorganic Pollutants. Water Environ. Res. 2020, 92, 1659–1668, doi:10.1002/wer.1415.

76. Makeig, K.S. Natural Buffers for Sludge Leachate Stabilization. Groundwater 1982, 20, 420–429.

77. Flemming, H.C.; Wuertz, S. Bacteria and Archaea on Earth and Their Abundance in Biofilms. Nat. Rev. Microbiol. 2019, 17, 247–260, doi:10.1038/s41579-019-0158-9.

78. Lam, T.P.; Lee, T.M.; Chen, C.Y.; Chang, J.S. Strategies to Control Biological Contaminants during Microalgal Cultivation in Open Ponds. Bioresour. Technol. 2018, 252, 180–187, doi:10.1016/j.biortech.2017.12.088.

79. Centers for Disease Control and Prevention Global COVID-19 Available online: https://www.cdc.gov/coronavirus/2019-ncov/global-covid-19/

(accessed on 23 November 2023).

80. Bhowmick, G.D.; Dhar, D.; Nath, D.; Ghangrekar, M.M.; Banerjee, R.; Das, S.; Chatterjee, J. Coronavirus Disease 2019 (COVID-19) Outbreak: Some Serious Consequences with Urban and Rural Water Cycle. npj Clean Water 2020, 3, doi:10.1038/s41545-020-0079-1.

81. Lokhandwala, S.; Gautam, P. Indirect Impact of COVID-19 on Environment: A Brief Study in Indian Context. Environ. Res. 2020, 188, 109807, doi:10.1016/j.envres.2020.109807.

82. Da'ana, D.A.; Zouari, N.; Ashfaq, M.Y.; Abu-Dieyeh, M.; Khraisheh, M.; Hijji, Y.M.; Al-Ghouti, M.A. Removal of Toxic Elements and Microbial Contaminants from Groundwater Using Low-Cost Treatment Options. Curr. Pollut. Reports 2021, 7, 300–324, doi:10.1007/s40726-021-00187-3.

83. Wu, J.; Zhang, Y.; Zhou, H. Groundwater Chemistry and Groundwater Quality Index Incorporating Health Risk Weighting in Dingbian County, Ordos Basin of Northwest China. Chemie der Erde 2020, 80, 125607, doi:10.1016/j.chemer.2020.125607.

84. Nelson, R.W. Evaluating the Environmental Consequences of Groundwater Contamination: 3. Obtaining Contaminant Arrival Distributions for Steady Flow in Heterogeneous Systems. Water Resour. Res. 1978, 14, 429–440, doi:10.1029/WR014i003p00429.

85. He, X.; Li, P.; Ji, Y.; Wang, Y.; Su, Z.; Elumalai, V. Groundwater Arsenic and Fluoride and Associated Arsenicosis and Fluorosis in China: Occurrence, Distribution and Management. Expo. Heal. 2020, 12, 355–368, doi:10.1007/s12403-020-00347-8.

86. Wu, J.; Sun, Z. Evaluation of Shallow Groundwater Contamination and Associated Human Health Risk in an Alluvial Plain Impacted by Agricultural and Industrial Activities, Mid-West China. Expo. Heal. 2016, 8, 311–329, doi:10.1007/s12403-015-0170-x.

87. Karunanidhi, D.; Aravinthasamy, P.; Deepali, M.; Subramani, T.; Bellows, B.C.; Li, P. Groundwater Quality Evolution Based on Geochemical Modeling and Aptness Testing for Ingestion Using Entropy Water Quality and Total Hazard Indexes in an Urban-Industrial Area (Tiruppur) of Southern India. Environ. Sci. Pollut. Res. 2021, 28, 18523–18538, doi:10.1007/s11356-020-10724-0.

88. Mthembu, P.P.; Elumalai, V.; Brindha, K.; Li, P. Hydrogeochemical Processes and Trace Metal Contamination in Groundwater: Impact on Human Health in the Maputaland Coastal Aquifer, South Africa. Expo. Heal. 2020, 12, 403–426, doi:10.1007/s12403-020-00369-2.

89. Ji, Y.; Wu, J.; Wang, Y.; Elumalai, V.; Subramani, T. Seasonal Variation of

Drinking Water Quality and Human Health Risk Assessment in Hancheng City of Guanzhong Plain, China. Expo. Heal. 2020, 12, 469–485, doi:10.1007/s12403-020-00357-6.

90. Subba Rao, N.; Ravindra, B.; Wu, J. Geochemical and Health Risk Evaluation of Fluoride Rich Groundwater in Sattenapalle Region, Guntur District, Andhra Pradesh, India. Hum. Ecol. Risk Assess. 2020, 26, 2316–2348, doi:10.1080/10807039.2020.1741338.

91. Zhou, Y.; Li, P.; Chen, M.; Dong, Z.; Lu, C. Groundwater Quality for Potable and Irrigation Uses and Associated Health Risk in Southern Part of Gu'an County, North China Plain. Environ. Geochem. Health 2021, 43, 813–835, doi:10.1007/s10653-020-00553-y.

92. Jenifer, M.A.; Jha, M.K. Comprehensive Risk Assessment of Groundwater Contamination in a Weathered Hard-Rock Aquifer System of India. J. Clean. Prod. 2018, 201, 853–868, doi:10.1016/j.jclepro.2018.08.005.

93. Yuan, Y.; Xiang, M.; Liu, C.; Theng, B.K.G. Chronic Impact of an Accidental Wastewater Spill from a Smelter, China: A Study of Health Risk of Heavy Metal(Loid)s via Vegetable Intake. Ecotoxicol. Environ. Saf. 2019, 182, 109401, doi:10.1016/j.ecoenv.2019.109401.

94. Njuguna, S.M.; Makokha, V.A.; Yan, X.; Gituru, R.W.; Wang, Q.; Wang, J. Health Risk Assessment by Consumption of Vegetables Irrigated with Reclaimed Waste Water: A Case Study in Thika (Kenya). J. Environ. Manage. 2019, 231, 576–581, doi:10.1016/j.jenvman.2018.10.088.

95. Wu, J.; Li, P.; Qian, H.; Fang, Y. Assessment of Soil Salinization Based on a Low-Cost Method and Its Influencing Factors in a Semi-Arid Agricultural Area, Northwest China. Environ. Earth Sci. 2014, 71, 3465–3475, doi:10.1007/s12665-013-2736-x.

96. Teng, Y.; Hu, B.; Zheng, J.; Wang, J.; Zhai, Y.; Zhu, C. Water Quality Responses to the Interaction between Surface Water and Groundwater along the Songhua River, NE China. Hydrogeol. J. 2018, 26, 1591–1607, doi:10.1007/s10040-018-1738-x.

97. Li, P.; Qian, H.; Zhou, W. Finding Harmony between the Environment and Humanity: An Introduction to the Thematic Issue of the Silk Road. Environ. Earth Sci. 2017, 76, 1–4, doi:10.1007/s12665-017-6428-9.

98. Schillinger, J.; Özerol, G.; Güven-Griemert, Ş.; Heldeweg, M. Water in War: Understanding the Impacts of Armed Conflict on Water Resources and Their Management. Wiley Interdiscip. Rev. Water 2020, 7, 1–19, doi:10.1002/wat2.1480.

99. Andrade, L.; O'Dwyer, J.; O'Neill, E.; Hynds, P. Surface Water Flooding, Groundwater Contamination, and Enteric Disease in Developed Countries: A

Scoping Review of Connections and Consequences. Environ. Pollut. 2018, 236, 540–549, doi:10.1016/j.envpol.2018.01.104.

100. Foster, S.S.D.; Chilton, P.J. Groundwater: The Processes and Global Significance of Aquifer Degradation. Philos. Trans. R. Soc. B Biol. Sci. 2003, 358, 1957–1972, doi:10.1098/rstb.2003.1380.

101. Fadlelmawla, A.A.; Dawoud, M.A. An Approach for Delineating Drinking Water Wellhead Protection Areas at the Nile Delta, Egypt. J. Environ. Manage. 2006, 79, 140–149, doi:10.1016/j.jenvman.2005.06.001.

102. Feng, S.; Huo, Z.; Kang, S.; Tang, Z.; Wang, F. Groundwater Simulation Using a Numerical Model under Different Water Resources Management Scenarios in an Arid Region of China. Environ. Earth Sci. 2011, 62, 961–971, doi:10.1007/s12665-010-0581-8.

103. Wang, X. Conceptual Design of a System for Selecting Appropriate Groundwater Models in Groundwater Protection Programs. Environ. Manage. 1997, 21, 607–615, doi:10.1007/s002679900053.

104. Zhou, W.; Beck, B.F.; Pettit, A.J.; Stephenson, B.J. A Groundwater Tracing Investigation as an Aid of Locating Groundwater Monitoring Stations on the Mitchell Plain of Southern Indiana. Environ. Geol. 2002, 41, 842–851, doi:10.1007/s00254-001-0464-0.

105. Allenby, G.; Margaret, M. World, Environment and People; Science Press: NSW, Australia, 1993.

106. Rice, J.; Viste, D. Major Sources of Groundwater Contamination Assessing the Extent of Point and Nonpoint Contamination in a Shallow Aquifer System. In Groundwater Contamination and Control; Zoller, U., Ed.; Marcel Dekker, Inc: New York, NY, 1994; pp. 21–35.

107. Khatri, N.; Tyagi, S. Influences of Natural and Anthropogenic Factors on Surface and Groundwater Quality in Rural and Urban Areas. Front. Life Sci. 2015, 8, 23–39, doi:10.1080/21553769.2014.933716.

108. Oun, A.; Kumar, A.; Harrigan, T.; Angelakis, A.; Xagoraraki, I. Effects of Biosolids and Manure Application on Microbial Water Quality in Rural Areas in the US. Water (Switzerland) 2014, 6, 3701–3723, doi:10.3390/w6123701.

109. Kulabako, N.R.; Nalubega, M.; Thunvik, R. Study of the Impact of Land Use and Hydrogeological Settings on the Shallow Groundwater Quality in a Peri-Urban Area of Kampala, Uganda. Sci. Total Environ. 2007, 381, 180–199, doi:10.1016/j.scitotenv.2007.03.035.

110. Burri, N.M.; Weatherl, R.; Moeck, C.; Schirmer, M. A Review of Threats to Groundwater Quality in the Anthropocene. Sci. Total Environ. 2019, 684, 136–154, doi:10.1016/j.scitotenv.2019.05.236.

111. Abdalla, F.; Khalil, R. Potential Effects of Groundwater and Surface Water Contamination in an Urban Area, Qus City, Upper Egypt. J. African Earth Sci. 2018, 141, 164–178, doi:10.1016/j.jafrearsci.2018.02.016.

112. Bashir, I.; Lone, F.A.; Bhat, R.A.; Mir, S.A.; Dar, Z.A.; Dar, S.A. Concerns and Threats of Contamination on Aquatic Ecosystems. In (eds) Bioremediation and Biotechnology; Springer, Cham, 2020; Vol. 3, pp. 15–23 ISBN 9783030460754.

113. Banach, J.L.; Van Der Fels-Klerx, H.J. Microbiological Reduction Strategies of Irrigation Water for Fresh Produce. J. Food Prot. 2020, 83, 1072–1087, doi:10.4315/JFP-19-466.

114. Kumar, A.; Kumar, A.; Cabral-Pinto, M.; Chaturvedi, A.K.; Shabnam, A.A.; Subrahmanyam, G.; Mondal, R.; Gupta, D.K.; Malyan, S.K.; Kumar, S.S.; et al. Lead Toxicity: Health Hazards, Influence on Food Chain, and Sustainable Remediation Approaches. Int. J. Environ. Res. Public Health 2020, 17, 2179, doi:10.3390/ijerph17072179.

115. Akankpo, O.; Igboekwe, M.U. Monitoring Groundwater Contamination Using Surface Electrical Resistivity and Geochemical Methods. J. Water Resour. Prot. 2011, 03, 318–324, doi:10.4236/jwarp.2011.35040.

116. Saibi, H.; Mesbah, M.; Moulla, A.S.; Guendouz, A.H.; Ehara, S. Principal Component, Chemical, Bacteriological, and Isotopic Analyses of Oued-Souf Groundwaters (Revised). Environ. Earth Sci. 2016, 75, 1–17, doi:10.1007/s12665-015-4878-5.

117. Belkhiri, L.; Boudoukha, A.; Mouni, L.; Baouz, T. Application of Multivariate Statistical Methods and Inverse Geochemical Modeling for Characterization of Groundwater - A Case Study: Ain Azel Plain (Algeria). Geoderma 2010, 159, 390–398, doi:10.1016/j.geoderma.2010.08.016.

118. Sako, A.; Sawadogo, S.; Nimi, M.; Ouédraogo, M. Hydrogeochemical and Pollution Characterization of a Shallow Glauconitic Sandstone Aquifer in a Peri-Urban Setting of Bobo-Dioulasso, Southwestern Burkina Faso. Environ. Earth Sci. 2020, 79, 1–18, doi:10.1007/s12665-020-09041-z.

119. Hwang, J.Y.; Park, S.; Kim, H.-K.; Kim, M.-S.; Jo, H.-J.; Kim, J.-I.; Lee, G.-M.; Shin, I.-K.; Kim, T.-S. Hydrochemistry for the Assessment of Groundwater Quality in Korea. J. Agric. Chem. Environ. 2017, 06, 1–29, doi:10.4236/jacen.2017.61001.

120. Bouteraa, O.; Mebarki, A.; Bouaicha, F.; Nouaceur, Z.; Laignel, B. Groundwater Quality Assessment Using Multivariate Analysis, Geostatistical Modeling, and Water Quality Index (WQI): A Case of Study in the Boumerzoug-El Khroub Valley of Northeast Algeria. Acta Geochim. 2019, 38, 796–814, doi:10.1007/s11631-019-00329-x.

121. Bahrami, M.; Zarei, A.R.; Rostami, F. Temporal and Spatial Assessment of Groundwater Contamination with Nitrate by Nitrate Pollution Index (NPI) and GIS (Case Study: Fasarud Plain, Southern Iran). Environ. Geochem. Health 2020, 42, 3119–3130, doi:10.1007/s10653-020-00546-x.

122. Parastar, S.; Jalilzadeh, A.; Poureshg, Y.; Hashemi, M.; Rezaee, A.; Hossini, H. Assessment of National Sanitation Foundation Water Quality Index and Other Quality Characterization of Mamloo Dam and Supporting Streams. Int. J. Environ. Health Eng. 2015, 4, 1–7, doi:10.4103/2277-9183.170711.

123. Keshavarzi, A.; Sarmadian, F. Mapping of Spatial Distribution of Soil Salinity and Alkalinity in a Semi-Arid Region. Ann. Warsaw Univ. Life Sci. - SGGW. L. Reclam. 2012, 44, 3–14, doi:10.2478/v10060-011-0057-x.

124. Kamaraj, J.; Sekar, S.; Roy, P.D.; Senapathi, V.; Chung, S.Y.; Perumal, M.; Nath, A. V. Groundwater Pollution Index (GPI) and GIS-Based Appraisal of Groundwater Quality for Drinking and Irrigation in Coastal Aquifers of Tiruchendur, South India. Environ. Sci. Pollut. Res. 2021, 28, 29056–29074, doi:10.1007/s11356-021-12702-6.

125. Kumar, M.; Ramanatahn, A.L.; Tripathi, R.; Farswan, S.; Kumar, D.; Bhattacharya, P. A Study of Trace Element Contamination Using Multivariate Statistical Techniques and Health Risk Assessment in Groundwater of Chhaprola Industrial Area, Gautam Buddha Nagar, Uttar Pradesh, India. Chemosphere 2017, 166, 135–145, doi:10.1016/j.chemosphere.2016.09.086.

126. Usman, U.N.; Mohd, E.T.; Hafizan, J.; Musa, G.A.; Ali, A.R.; Hamza, I. Assessment of Groundwater Quality Using Multivariate Statistical Techniques in Terengganu. Sci. Technol. 2014, 2014, 4, 42–49, doi:10.1007/978-3-031-04028-3_36.

127. Güler, C.; Thyne, G.D.; McCray, J.E.; Turner, A.K. Evaluation of Graphical and Multivariate Statistical Methods for Classification of Water Chemistry Data. Hydrogeol. J. 2002, 10, 455–474, doi:10.1007/s10040-002-0196-6.

128. Belkhiri, L.; Boudoukha, A.; Mouni, L.; Baouz, T. Multivariate Statistical Characterization of Groundwater Quality in Ain Azel Plain, Algeria. African J. Environ. Sci. Technol. 2010, 4, 526–534, doi:10.5897/AJEST10.003.

129. Bhuiyan, M.A.H.; Suruvi, N.I.; Dampare, S.B.; Islam, M.A.; Quraishi, S.B.; Ganyaglo, S.; Suzuki, S. Investigation of the Possible Sources of Heavy Metal Contamination in Lagoon and Canal Water in the Tannery Industrial Area in Dhaka, Bangladesh. Environ. Monit. Assess. 2011, 175, 633–649, doi:10.1007/s10661-010-1557-6.

130. Bouaicha, F.; Dib, H.; Belkhiri, L.; Manchar, N.; Chabour, N. Hydrogeochemistry and Geothermometry of Thermal Springs from the Guelma Region, Algeria. J. Geol. Soc. India 2017, 90, 226–232, doi:10.1007/s12594-017-0703-y.

131. Emenike, P.G.C.; Nnaji, C.C.; Tenebe, I.T. Assessment of Geospatial and Hydrochemical Interactions of Groundwater Quality, Southwestern Nigeria. Environ. Monit. Assess. 2018, 190, doi:10.1007/s10661-018-6799-8.

132. Li, J.; Shi, Z.; Liu, M.; Wang, G.; Liu, F.; Wang, Y. Identifying Anthropogenic Sources of Groundwater Contamination by Natural Background Levels and Stable Isotope Application in Pinggu Basin, China. J. Hydrol. 2021, 596, 126092, doi:10.1016/j.jhydrol.2021.126092.

133. Stiff, H.A. The Interpretation of Chemical Water Analysis by Means of Patterns. J. Pet. Technol. 1951, 3, 15–3, doi:10.2118/951376-g.

134. Piper, A.M. A Graphic Procedure in the Geochemical Interpretation of Water-analyses. Eos, Trans. Am. Geophys. Union 1944, 25, 914–928.

135. Chadha D. Proposed New Diagram for Geochemical Classification of Natural Waters and Interpretation of Chemical Data. Hydrogeol. J. 1999, 7, 431–439.

136. Ronald J. Gibbs Mechanisms Controlling World Water Chemistry. Science (80-.). 1970, 170, 1088–1090.

137. Kumar, S.K.; Rammohan, V.; Sahayam, J.D.; Jeevanandam, M. Assessment of Groundwater Quality and Hydrogeochemistry of Manimuktha River Basin, Tamil Nadu, India. Environ. Monit. Assess. 2009, 159, 341–351, doi:10.1007/s10661-008-0633-7.

138. Ganvir, P.S. Hydro-Geochemical Plots : An Efficient Tool for the Elucidation of Groundwater Chemistry. Int. J. Innov. Sci. Res. Technol. 2023, 8, 95–100.

139. Zhao, Y.Y.; Pei, Y.S. Risk Evaluation of Groundwater Pollution by Pesticides in China: A Short Review. Procedia Environ. Sci. 2012, 13, 1739–1747, doi:10.1016/j.proenv.2012.01.167.

140. Aghazadeh, N.; Mogaddam, A.A. Assessment of Groundwater Quality and Its Suitability for Drinking and Agricultural Uses in the Oshnavieh Area, Northwest of Iran. J. Environ. Prot. (Irvine,. Calif). 2010, 01, 30–40, doi:10.4236/jep.2010.11005.

141. Vaiphei, S.P.; Kurakalva, R.M.; Sahadevan, D.K. Water Quality Index and GIS-Based Technique for Assessment of Groundwater Quality in Wanaparthy Watershed, Telangana, India. Environ. Sci. Pollut. Res. 2020, 27, 45041–45062, doi:10.1007/s11356-020-10345-7.

142. Gharbi, A.; Ali, Z.I.; Zairi, M. Groundwater Suitability for Drinking and Agriculture Purposes Using Irrigation Water Quality Index and Multivariate Analysis: Case of Sidi Bouzid Aquifer, Central Tunisia. Environ. Earth Sci. 2019, 78, 1–19, doi:10.1007/s12665-019-8733-y.

143. Brown, R..; McClelland, N..; Deininger, R..; O'Connor, M.. A Water Quality Index—Crashing the Psychological Barrier. Indic. Environ. Qual 1973, 173–

182, doi:10.1016/b978-0-08-017005-3.50067-0.

144. Ram, A.; Tiwari, S.K.; Pandey, H.K.; Chaurasia, A.K.; Singh, S.; Singh, Y. V. Groundwater Quality Assessment Using Water Quality Index (WQI) under GIS Framework. Appl. Water Sci. 2021, 11, 1–20, doi:10.1007/s13201-021-01376-7.

145. Rawat, K.S.; Singh, S.K.; Jacintha, T.G.A.; Nemčić-Jurec, J.; Tripathi, V.K. Appraisal of Long Term Groundwater Quality of Peninsular India Using Water Quality Index and Fractal Dimension. J. Earth Syst. Sci. 2017, 126, doi:10.1007/s12040-017-0895-y.

146. Chaurasia, A.K.; Pandey, H.K.; Tiwari, S.K.; Prakash, R.; Pandey, P.; Ram, A. Groundwater Quality Assessment Using Water Quality Index (WQI) in Parts of Varanasi District, Uttar Pradesh, India. J. Geol. Soc. India 2018, 92, 76–82, doi:10.1007/s12594-018-0955-1.

147. Nadikatla, S.K.; Mushini, V.S.R.; Mudumba, P.S.M.K. Water Quality Index Method in Assessing Groundwater Quality of Palakonda Mandal in Srikakulam District, Andhra Pradesh, India. Appl. Water Sci. 2020, 10, 1–14, doi:10.1007/s13201-019-1110-x.

148. Balamurugan, P.; Muniraj, K.; Karuppannan, S.; Paramasivam, S.K.; Nagavinothini, R.; Vicky, S. Appraisal of Groundwater Quality for Drinking and Irrigation Purpose Using GIS and Statistical Approach with Special Reference to Nitrate Contamination in a Semi-Arid Region : A Case Study. Authorea … 2020.

149. Tegegne, A.M.; Lohani, T.K.; Eshete, A.A. Evaluation of Groundwater Quality for Drinking and Irrigation Purposes Using Proxy Indices in the Gunabay Watershed, Upper Blue Nile Basin, Ethiopia. Heliyon 2023, 9, e15263, doi:10.1016/j.heliyon.2023.e15263.

150. El Bilali, A.; Taleb, A.; Brouziyne, Y. Groundwater Quality Forecasting Using Machine Learning Algorithms for Irrigation Purposes. Agric. Water Manag. 2021, 245, 106625, doi:10.1016/j.agwat.2020.106625.

151. Panneerselvam, B.; Muniraj, K.; Thomas, M.; Ravichandran, N.; Bidorn, B. Identifying Influencing Groundwater Parameter on Human Health Associate with Irrigation Indices Using the Automatic Linear Model (ALM) in a Semi-Arid Region in India. Environ. Res. 2021, 202, 111778, doi:10.1016/j.envres.2021.111778.

152. Richards, L.. Diagnosis and Improvement of Saline and Alkaline Soils; Riverside, California, 1947.

153. Todd, D.. Groundwater Hydrology; 2nd ed.; Wiley: New York, NY, USA, 1980.

154. Wilcox, L.. Classification and Use of Irrigation Water; US Department of

Agriculture: Washington, DC, USA, 1955.

155. Ragunath, H.. Groundwater; 2nd ed.; Wiley Eastern Ltd: New Delhi, India, 1987.

156. Doneen, L.. Notes on Water Quality in Agriculture; Water Science and Engineering Paper 4001: CA, USA, 1964.

157. Kelly, W.. Alkali Soils-Their Formation, Properties and Reclamation; Reinhold Publishing: New York, NY, USA, 1951.

158. Rawat, K.; Pradhan, S.; Tripathi, V.; Jeyakumar, L.; Singh, S.K. Statistical Approach to Evaluate Groundwater Contamination for Drinking and Irrigation Suitability. Groundw. Sustain. Dev. 2019, 9, 100251, doi:10.1016/j.gsd.2019.100251.

159. Amiri, N.; Nakhaei, M. Evaluating the Potential of Treated Municipal Wastewater Reuse in Irrigation and Groundwater Recharge; 5-Year Contaminant Transport Modeling. Int. J. Environ. Sci. Technol. 2023, doi:10.1007/s13762-023-05293-x.

160. Akharame, M.O.; Ajayi, M.A. Assessment of Groundwater Quality Using the National Sanitation Foundation Water Quality Index Within. 2022, 8, 162–173.

161. Brown, R.M.; McClelland, N.I.; Deininger, R.A.; Tozer, R.G. A-Water-Quality-Index-Do-We-Dare-BROWN-R-M-1970. Water Sew. Work. 1970, 10, 339–343.

162. Cude, C.G. OREGON WATER QUALITY INDEX A TOOL FOR EVALUATING WATER QUALITY MANAGEMENT EFFECTIVENESS. J. Am. Water Resour. Assoc. 2001, 37, 125–137.

163. Liou, S.M.; Lo, S.L.; Wang, S.H. A Generalized Water Quality Index for Taiwan. Environ. Monit. Assess. 2004, 96, 35–52, doi:10.1023/B:EMAS.0000031715.83752.a1.

164. Ocampo-Duque, W.; Schuhmacher, M.; Domingo, J.L. A Neural-Fuzzy Approach to Classify the Ecological Status in Surface Waters. Environ. Pollut. 2007, 148, 634–641, doi:10.1016/j.envpol.2006.11.027.

165. Vasanthavigar, M.; Srinivasamoorthy, K.; Vijayaragavan, K.; Rajiv Ganthi, R.; Chidambaram, S.; Anandhan, P.; Manivannan, R.; Vasudevan, S. Application of Water Quality Index for Groundwater Quality Assessment: Thirumanimuttar Sub-Basin, Tamilnadu, India. Environ. Monit. Assess. 2010, 171, 595–609, doi:10.1007/s10661-009-1302-1.

166. Mohebbi, M.R.; Saeedi, R.; Montazeri, A.; Azam Vaghefi, K.; Labbafi, S.; Oktaie, S.; Abtahi, M.; Mohagheghian, A. Assessment of Water Quality in Groundwater Resources of Iran Using a Modified Drinking Water Quality

Index (DWQI). Ecol. Indic. 2013, 30, 28–34, doi:10.1016/j.ecolind.2013.02.008.

167. Hoseinzadeh, E.; Khorsandi, H.; Wei, C.; Alipour, M. Evaluation of Aydughmush River Water Quality Using the National Sanitation Foundation Water Quality Index (NSFWQI), River Pollution Index (RPI), and Forestry Water Quality Index (FWQI). Desalin. Water Treat. 2015, 54, 2994–3002, doi:10.1080/19443994.2014.913206.

168. Sikder, M.T.; Tanaka, S.; Saito, T.; Hosokawa; Gumiri, S.; Ardianor; Uddin, M.K.; Tareq, S.M.; Shammi, M.; Kamal, A.K.I.; et al. Vulnerability Assessment of Surface Water Quality with an Innovative Integrated Multi-Parameter Water Quality Index (IMWQI). Pollution 2015, 1, 333–346.

169. Benouara, N.; Laraba, A.; Rachedi, L.H. Assessment of Groundwater Quality in the Seraidi Region (North-East of Algeria) Using NSF-WQI. Water Sci. Technol. Water Supply 2016, 16, 1132–1137, doi:10.2166/ws.2016.030.

170. Misaghi, F.; Delgosha, F.; Razzaghmanesh, M.; Myers, B. Introducing a Water Quality Index for Assessing Water for Irrigation Purposes: A Case Study of the Ghezel Ozan River. Sci. Total Environ. 2017, 589, 107–116, doi:10.1016/j.scitotenv.2017.02.226.

171. Alexakis, D.E. Meta-Evaluation of Water Quality Indices. Application into Groundwater Resources. Water (Switzerland) 2020, 12, doi:10.3390/w12071890.

172. N. Subba Rao PIG: A Numerical Index for Dissemination of Groundwater Contamination Zones. Hydrol. Process. 2012, 26, 3344–3350, doi:10.1002/hyp.

173. Egbueri, J.C. Groundwater Quality Assessment Using Pollution Index of Groundwater (PIG), Ecological Risk Index (ERI) and Hierarchical Cluster Analysis (HCA): A Case Study. Groundw. Sustain. Dev. 2020, 10, 100292, doi:10.1016/j.gsd.2019.100292.

174. El Mountassir, O.; Bahir, M.; Ouazar, D.; Chehbouni, A.; Carreira, P.M. Temporal and Spatial Assessment of Groundwater Contamination with Nitrate Using Nitrate Pollution Index (NPI), Groundwater Pollution Index (GPI), and GIS (Case Study: Essaouira Basin, Morocco). Environ. Sci. Pollut. Res. 2022, 29, 17132–17149, doi:10.1007/s11356-021-16922-8.

175. Subba Rao, N.; Sunitha, B.; Rambabu, R.; Rao, P.V.N.; Rao, P.S.; Spandana, B.D.; Sravanthi, M.; Marghade, D. Quality and Degree of Pollution of Groundwater, Using PIG from a Rural Part of Telangana State, India. Appl. Water Sci. 2018, 8, 1–13, doi:10.1007/s13201-018-0864-x.

176. Qian, H.; Chen, J.; Howard, K.W.F. Assessing Groundwater Pollution and Potential Remediation Processes in a Multi-Layer Aquifer System. Environ.

Pollut. 2020, 263, 114669, doi:10.1016/j.envpol.2020.114669.

177. Chen, J.; Qian, H.; Gao, Y.; Wang, H.; Zhang, M. Insights into Hydrological and Hydrochemical Processes in Response to Water Replenishment for Lakes in Arid Regions. J. Hydrol. 2020, 581, 124386, doi:10.1016/j.jhydrol.2019.124386.

178. Al-Aizari, H.S.; Aslaou, F.; Al-Aizari, A.R.; Al-Odayni, A.B.; Al-Aizari, A.J.M. Evaluation of Groundwater Quality and Contamination Using the Groundwater Pollution Index (GPI), Nitrate Pollution Index (NPI), and GIS. Water (Switzerland) 2023, 15, doi:10.3390/w15203701.

179. Arauzo, M. Vulnerability of Groundwater Resources to Nitrate Pollution: A Simple and Effective Procedure for Delimiting Nitrate Vulnerable Zones. Sci. Total Environ. 2017, 575, 799–812, doi:10.1016/j.scitotenv.2016.09.139.

180. Baghapour, M.A.; Nobandegani, A.F.; Talebbeydokhti, N.; Bagherzadeh, S.; Nadiri, A.A.; Gharekhani, M.; Chitsazan, N. Optimization of DRASTIC Method by Artificial Neural Network, Nitrate Vulnerability Index, and Composite DRASTIC Models to Assess Groundwater Vulnerability for Unconfined Aquifer of Shiraz Plain, Iran. J. Environ. Heal. Sci. Eng. 2016, 14, 1–16, doi:10.1186/s40201-016-0254-y.

181. Chen, J.; Wu, H.; Qian, H. Groundwater Nitrate Contamination and Associated Health Risk for the Rural Communities in an Agricultural Area of Ningxia, Northwest China. Expo. Heal. 2016, 8, 349–359, doi:10.1007/s12403-016-0208-8.

182. Kavcar, P.; Sofuoglu, A.; Sofuoglu, S.C. A Health Risk Assessment for Exposure to Trace Metals via Drinking Water Ingestion Pathway. Int. J. Hyg. Environ. Health 2009, 212, 216–227, doi:10.1016/j.ijheh.2008.05.002.

183. Rahman, M.A.T.M.T.; Paul, M.; Bhoumik, N.; Hassan, M.; Alam, M.K.; Aktar, Z. Heavy Metal Pollution Assessment in the Groundwater of the Meghna Ghat Industrial Area, Bangladesh, by Using Water Pollution Indices Approach. Appl. Water Sci. 2020, 10, 1–15, doi:10.1007/s13201-020-01266-4.

184. Wagh, V.M.; Panaskar, D.B.; Mukate, S.V.; Gaikwad, S.K.; Muley, A.A.; Varade, A.M. Health Risk Assessment of Heavy Metal Contamination in Groundwater of Kadava River Basin, Nashik, India. Model. Earth Syst. Environ. 2018, 4, 969–980, doi:10.1007/s40808-018-0496-z.

185. Backman, B.; Bodiš, D.; Lahermo, P.; Rapant, S.; Tarvainen, T. Application of a Groundwater Contamination Index in Finland and Slovakia. Environ. Geol. 1998, 36, 55–64, doi:10.1007/s002540050320.

186. Ahmed, S.; Khurshid, S.; Qureshi, F.; Hussain, A.; Bhattacharya, A. Heavy Metals and Geo-Accumulation Index Development for Groundwater of

Mathura City, Uttar Pradesh (Desalination and Water Treatment, (2019), 138, 291-300, 10.5004/Dwt.2019.23322). Desalin. Water Treat. 2019, 138, 291–300, doi:10.5004/dwt.2019.23923.

187. Singh, K.P.; Malik, A.; Sinha, S.; Singh, V.K.; Murthy, R.C. Estimation of Source of Heavy Metal Contamination in Sediments of Gomti River (India) Using Principal Component Analysis. Water. Air. Soil Pollut. 2005, 166, 321–341, doi:10.1007/s11270-005-5268-5.

188. Muller, G. Index of Geoaccumulation in Sediments of the Rhine River. GeoJournal 1969, 2, 108–118.

189. Egbueri, J.C.; Unigwe, C.O. Understanding the Extent of Heavy Metal Pollution in Drinking Water Supplies from Umunya, Nigeria: An Indexical and Statistical Assessment. Anal. Lett. 2020, 53, 2122–2144, doi:10.1080/00032719.2020.1731521.

190. Loska, K.; Wiechułła, D.; Korus, I. Metal Contamination of Farming Soils Affected by Industry. Environ. Int. 2004, 30, 159–165, doi:10.1016/S0160-4120(03)00157-0.

191. Olivares-Rieumont, S.; De La Rosa, D.; Lima, L.; Graham, D.W.; D'Alessandro, K.; Borroto, J.; Martínez, F.; Sánchez, J. Assessment of Heavy Metal Levels in Almendares River Sediments - Havana City, Cuba. Water Res. 2005, 39, 3945–3953, doi:10.1016/j.watres.2005.07.011.

192. Fei, J.C.; Min, X.B.; Wang, Z.X.; Pang, Z. hua; Liang, Y.J.; Ke, Y. Health and Ecological Risk Assessment of Heavy Metals Pollution in an Antimony Mining Region: A Case Study from South China. Environ. Sci. Pollut. Res. 2017, 24, 27573–27586, doi:10.1007/s11356-017-0310-x.

193. Arslan, H.; Ayyildiz Turan, N. Estimation of Spatial Distribution of Heavy Metals in Groundwater Using Interpolation Methods and Multivariate Statistical Techniques; Its Suitability for Drinking and Irrigation Purposes in the Middle Black Sea Region of Turkey. Environ. Monit. Assess. 2015, 187, doi:10.1007/s10661-015-4725-x.

194. Goovaerts, P. Geostatistics for Natural Resources Evaluation; Oxford University Press on Demand, 1997.

195. Isaaks, E.; Srivastava, R.M. An Introduction to Applied Geostatistics; Oxford University Press: New York, 1989.

196. Journel, A..; Huijbregts, C.. Mining Geostatistics; Academic Press: London, United Kingdom, 1978.

197. Seyedmohammadi, J.; Esmaeelnejad, L.; Shabanpour, M. Spatial Variation Modelling of Groundwater Electrical Conductivity Using Geostatistics and GIS. Model. Earth Syst. Environ. 2016, 2, 1–10, doi:10.1007/s40808-016-0226-3.

198. Venkatramanan, S.; Chung, S.Y.; Kim, T.H.; Kim, B.W.; Selvam, S. Geostatistical Techniques to Evaluate Groundwater Contamination and Its Sources in Miryang City, Korea. Environ. Earth Sci. 2016, 75, 1–14, doi:10.1007/s12665-016-5813-0.

199. Barkat, A.; Bouaicha, F.; Bouteraa, O.; Ata, B.; Balla, D.; Rahal, Z.; Szabó, G. Assessment of Complex Terminal Groundwater Aquifer for Different Use of Oued Souf Valley (Algeria) Using Multivariate Statistical Methods, Geostatistical Modeling, and Water Quality Index. Water 2021, 11, 1–26.

200. Knotters, M.; Bierkens, M.F.P. Predicting Water Table Depths in Space and Time Using a Regionalised Time Series Model. Geoderma 2001, 103, 51–77, doi:10.1016/S0016-7061(01)00069-6.

201. Desbarats, a J.; Logan, C.E.; Hinton, M.J.; Sharpe, D.R. EARTH SCIENCES SECTOR GENERAL INFORMATION PRODUCT 15 On the Kriging of Water Table Elevations Using Collateral Information from a Digital Elevation Model. J. Hydrol. 2002, 255, 25–38.

202. Theodossiou, N.; Latinopoulos, P. Evaluation and Optimisation of Groundwater Observation Networks Using the Kriging Methodology. Environ. Model. Softw. 2006, 21, 991–1000, doi:10.1016/j.envsoft.2005.05.001.

203. Gundogdu, K.S.; Guney, I. Spatial Analyses of Groundwater Levels Using Universal Kriging. J. Earth Syst. Sci. 2007, 116, 49–55, doi:10.1007/s12040-007-0006-6.

204. Uyan, M.; Cay, T. Spatial Analyses of Groundwater Level Differences Using Geostatistical Modeling. Environ. Ecol. Stat. 2013, 20, 633–646, doi:10.1007/s10651-013-0238-3.

205. Xiao, Y.; Gu, X.; Yin, S.; Shao, J.; Cui, Y.; Zhang, Q.; Niu, Y. Geostatistical Interpolation Model Selection Based on ArcGIS and Spatio-Temporal Variability Analysis of Groundwater Level in Piedmont Plains, Northwest China. Springerplus 2016, 5, doi:10.1186/s40064-016-2073-0.

206. Chen, L.; Feng, Q. Geostatistical Analysis of Temporal and Spatial Variations in Groundwater Levels and Quality in the Minqin Oasis, Northwest China. Environ. Earth Sci. 2013, 70, 1367–1378, doi:10.1007/s12665-013-2220-7.

207. Montero, J.; Fernández-Avilés, G.; Mateu, J. Spatial and Spatio-Temporal Geostatistical Modeling and Kriging; John Wiley & Sons, 2015.

208. Kumar, A.; Maroju, S.; Bhat, A. Application of ArcGIS Geostatistical Analyst for Interpolating Environmental Data from Observations. Environ. Prog. 2007, 26, 220–225, doi:10.1002/ep.10223.

209. Webster, R.; Oliver, M. Geostatistics for Environmental Scientists; John Wiley & Sons, 2007.

210. Philip, G.M.; Watson, D.F. CONTOURED SURFACES. APPEA J. 1982, 22, 205–212.

211. Esri An Overview of the Interpolation Toolset. 2012.

212. Fortin, M.; Dale, M. Spatial Analysis: A Guide for Ecologists; Cambridge University Press: Cambridge, 2005.

213. Gong, G.; Mattevada, S.; Bryant, S.E.O. Comparison of the Accuracy of Kriging and IDW Interpolations in Estimating Groundwater Arsenic Concentrations in Texas. Environ. Res. 2014, 130, 59–69, doi:10.1016/j.envres.2013.12.005.

214. Charizopoulos, N.; Zagana, E.; Psilovikos, A. Assessment of Natural and Anthropogenic Impacts in Groundwater , Utilizing Multivariate Statistical Analysis and Inverse Distance Weighted Interpolation Modeling : The Case of a Scopia Basin (Central Greece). Environ. Earth Sci. 2018, 77, 1–18, doi:10.1007/s12665-018-7564-6.

215. Gomes, V.A.; Pitombo, C.S.; Rocha, S.S.; Salgueiro, A.R. Kriging Geostatistical Methods for Travel Mode Choice: A Spatial Data Analysis to Travel Demand Forecasting. Open J. Stat. 2016, 06, 514–527, doi:10.4236/ojs.2016.63044.

216. Yao, L.; Huo, Z.; Feng, S.; Mao, X.; Kang, S.; Chen, J.; Xu, J.; Steenhuis, T.S. Evaluation of Spatial Interpolation Methods for Groundwater Level in an Arid Inland Oasis, Northwest China. Environ. Earth Sci. 2014, 71, 1911–1924, doi:10.1007/s12665-013-2595-5.

217. Li, J.; Heap, A.D. A Review of Comparative Studies of Spatial Interpolation Methods in Environmental Sciences: Performance and Impact Factors. Ecol. Inform. 2011, 6, 228–241, doi:10.1016/j.ecoinf.2010.12.003.

218. Scanlon, B.; Keese, K.; Flint, A.; Flint, L.; Gaye, C.; Edmunds, W.; Simmers, I. Global Synthesis of Groundwater Recharge in Semiarid Andaridregions. Hydrol. Process. An Int. Journal. 2006, 20, 3335–3370, doi:10.1002/hyp.

219. Kumar, R.; Singh, R.D. Water Resources of India. Curr. Sci. 2005, 89, 794–811.

220. Wheida, E.; Verhoeven, R. Impacts of Agricultural Practices on Groundwater Quality in Europe and North Africa. Water Policy 2007, 9, 119–132.

221. Almasri, M.N.; Kaluarachchi, J.J. Modeling Nitrate Contamination of Groundwater in Agricultural Watersheds. J. Hydrol. 2007, 343, 211–229, doi:10.1016/j.jhydrol.2007.06.016.

222. Li, X.; Zhong, S.; Qiu, J.; Bodrud-Doza, M.; Aithani, D.; Adimalla, N. Hydrogeochemical Characteristics and Evaluation of Groundwater Resources in Jilin Province, China. Front. Environ. Sci. 2020, 8.

223. Zhong, S.; Qiu, J.; Li, X.; Bodrud-Doza, M. Evaluating the Impacts of Hydrogeochemical Processes on Groundwater Quality in Arid Regions Using Multivariate Statistical Techniques. J. Hydrol. 2022, 126019.

224. Zeng, Z.; Cui, Y.; Zhou, X.; Pan, X.; Sun, F.; Liu, Y.; Tian, J.; He, M.; Zhang, Y.; Yan, Y.; et al. Hydrogeochemical Characteristics and Evaluation of Groundwater Resources of Jilin Province, China. Front. Water 2023, 5, doi:10.3389/frwa.2023.1315805.

225. Megahed, H.A. GIS-Based Assessment of Groundwater Quality and Suitability for Drinking and Irrigation Purposes in the Outlet and Central Parts of Wadi El-Assiuti, Assiut Governorate, Egypt. Bull. Natl. Res. Cent. 2020, 44, doi:10.1186/s42269-020-00428-3.

226. Elkhalki, S.; Hamed, R.; Jodeh, S.; Ghalit, M.; Elbarghmi, R.; Azzaoui, K.; Hanbali, G.; Ben Zhir, K.; Ait Taleb, B.; Zarrouk, A.; et al. Study of the Quality Index of Groundwater (GWQI) and Its Use for Irrigation Purposes Using the Techniques of the Geographic Information System (GIS) of the Plain Nekor-Ghiss (Morocco). Front. Environ. Sci. 2023, 11, 1–12, doi:10.3389/fenvs.2023.1179283.

227. Jari, A.; Bachaoui, E.M.; Hajaj, S.; Khaddari, A.; Khandouch, Y.; El Harti, A.; Jellouli, A.; Namous, M. Investigating Machine Learning and Ensemble Learning Models in Groundwater Potential Mapping in Arid Region: Case Study from Tan-Tan Water-Scarce Region, Morocco. Front. Water 2023, 5, doi:10.3389/frwa.2023.1305998.

228. Atta, H.S.; Omar, M.A.S.; Tawfik, A.M. Water Quality Index for Assessment of Drinking Groundwater Purpose Case Study: Area Surrounding Ismailia Canal, Egypt. J. Eng. Appl. Sci. 2022, 69, 1–17, doi:10.1186/s44147-022-00138-9.

229. Ahmed, A.K.A.; El-Rawy, M.; Ibraheem, A.M.; Al-Arifi, N.; Abd-Ellah, M.K. Forecasting of Groundwater Quality by Using Deep Learning Time Series Techniques in an Arid Region. Sustain. 2023, 15, doi:10.3390/su15086529.

230. Liu, X.; Liu, H.; Jing, J.; Liu, Y.; Xu, Z.; Cao, X.; Ma, L.; Zhuo, Y.; Wen, L.; Wang, L. How the Land Use/Cover Changes and Environmental Factors at Different Scales Affect Lake Water Quality in Arid and Semi-Arid Regions. Front. Ecol. Evol. 2023, 11, 1–11, doi:10.3389/fevo.2023.1188927.

231. El-Rawy, M.; Batelaan, O.; Al-Arifi, N.; Alotaibi, A.; Abdalla, F.; Gabr, M.E. Climate Change Impacts on Water Resources in Arid and Semi-Arid Regions: A Case Study in Saudi Arabia. Water (Switzerland) 2023, 15, doi:10.3390/w15030606.

232. Alfarrah, N.; Walraevens, K. Groundwater Overexploitation and Seawater Intrusion in Coastal Areas of Arid and Semi-Arid Regions. Water

(Switzerland) 2018, 10, doi:10.3390/w10020143.

233. Wang, J.; Xu, D.; Li, H. Constructing GRACE-Based 1 Km Resolution Groundwater Storage Anomalies in Arid Regions Using an Improved Machine Learning Downscaling Method: A Case Study in Alxa League, China. Remote Sens. 2023, 15, doi:10.3390/rs15112913.

234. Kinzelbach, W.; Brunner, P.; Von Boetticher, A.; Kgotlhang, L.; Milzow, C. Sustainable Water Management in Arid and Semi-Arid Regions. Int. Hydrol. Ser. Groundw. Model. Arid Semi-Arid Areas 2010, 119–130.

235. Drouiche, N.; Ghaffour, N.; Naceur, M.W.; Lounici, H.; Drouiche, M. Towards Sustainable Water Management in Algeria. Desalin. Water Treat. 2012, 50, 272–284, doi:10.1080/19443994.2012.719477.

236. Harrat, N.; Achour, S. Pollution Physico-Chimique Des Eaux de Barrage de La Région d'El Tarf. Impact Sur La Chloration. Larhyss J. 2010, 8, 47–54.

237. Sekkoum, K.; Fouzi Talhi, M.; Cheriti, A.; Bourmita, Y.; Belboukhari, N.; Boulenouar, N.; Taleb, S. Water in Algerian Sahara: Environmental and Health Impact. Adv. Desalin. 2012, doi:10.5772/50319.

238. (Ministère des ressources en eau) Ministry of Water Resources Available online: https://www.mre.gov.dz/?page_id=1991.

239. Abdous, B.; Besbes, M.; Fezzani, C.; Latrech, D.; Mamou, A. SYSTEME AQUIFERE DU SAHARA SEPTENTRIONAL : Gestion Commune d'un Bassin Transfrontière; Ouargla, 2005; Vol. 12; ISBN 9973856031.

240. Daoudi, A.; Lejars, C.; Benouniche, N. La Gouvernance de l'Eau Souterraine Dans Le Sahara Algérien: Enjeux, Cadre Légal et Pratiques Locales. Cah. Agric. 2017, 26, doi:10.1051/cagri/2017021.

241. Negm, A.; Omran, E.; Bouderbala, A.; Chenchouni, H.; Barcelo, D. Introduction to "Water Resources in Algeria: Assessment of Surface and Groundwater Resources". InWater Resources in Algeria-Part I; Springer, Cham, 2020; ISBN 978-3-030-57894-7.

242. Kerényi, A.; McIntosh, R. Sustainable Development in Changing Complex Earth Systems; 2020; ISBN 9783030216443.

243. Khechana, S.; Derradji, F.; Mega, N. Caractéristiques Hydrochimiques Des Eaux de La Nappe Phréatique Du Vallée d'Oued-Souf (SE Algérien). Eur. J. Sci. Res. 2011, 62, 207–215.

244. Messekher, I.; Menani, M. Evolution de La Piezometrie de La Ville d'Oued Souf (Entre 1993, 2002 et 2007): Perspectives de La Maitrise Du Phenomene de Remont e de La Nappe Phréatique. In Proceedings of the J Int Net Env Manag Conf; 2010; Vol. 1, pp. 259–266.

245. Meziani, A.; Dridi, H. The Aquifer System of the Souf Valley: Algerian Northern Sahara. Eur. J. Sci. Res. 2011, 65, 416–423.

246. Bataillon, C. Le Souf, Étude de Géographie Humaine., Université d'Alger, 1955.

247. Najah, A. Le Souf Des Oasis.; La Maison des livres, A., Ed.; 1970.

248. Voisin A.R Le Souf Monographie. Document Multigraphié, Tours; carte et graphiques, 1970.

249. Giersch, P. Remontée Des Eaux de La Nappe Phréatique à El Oued; Strasbourg, 1989.

250. BOUSELSAL Boualem Etude Hydrogéologique et Hydrochimique de l ' Aquifère Libre d ' El Oued Souf (SE Algérie), UNIVERSITE BADJI MOKHTAR-ANNABA, 2016.

251. Voisin A.R Les Souf Monographie; Edition El.; El Oued-Algérie, 2004;

252. Côte, M. Si Le Souf m'était Conté : Comment Se Fait et Se Défait Un Paysage; Hannachi, S., Ed.; Média-Plus: Constantine, 2006; ISBN 9961-922-42-5.

253. Messekher, I.; Chabour, N.; Menani, R. Remontée de La Nappe Phréatique Du Souf. Conséquences et Solutions Envisagées. Ann. Univ. Bucharest Geogr. Ser. 2012, LXI, 179–197.

254. Bel, F.; Demargne, F. F. Etude Géologique Du Continental Terminal; Rapport Technique; Algiers, Algeria, 1966.

255. BUSSON, G. Principes, Méthodes et Résultats d'une Étude Stratigraphique Du MésozoÏque Saharien, Paris, 1972, Vol. 26.

256. Cornet, A. Introduction à l'hydrogéologie Saharienne. Géorg. Phys. Géol. Dyn 1964, 6, 5–72.

257. Fabre, J. Introduction à La Géologie Du Sahara Algérien et Des Régions Voisines: La Couverture Phanérozoïque. Vol. 1; Société Nationale d'Édition et de Diffusion: Algiers, Algeria, 1976; ISBN 84-499-2264-X.

258. Bel, F.; Cuche, D. Etude Des Nappes Du Complexe Terminal Du Bas Sahara; Données Géologiques et Hydrogéologiques Pour La Construction Du Modèle Mathématique; Ouargla, Algeria, 1970.

259. Castany, G. Sedimentary Basin of the Northern Sahara (Algeria, Tunisia). Intercalary Continental and Terminal Complex Aquifers [Confined Groundwater, Multilevel System, Hydrodynamics, Management of Water Resources, and Environment. Bull. du Bur. Rech. Geol. Minieres Sect. 3 Hydrogeol. Geol. l'Ingenieur 1982, 2, 127–147.

260. Halassa, Y.; Zeddouri, A.; Mouhamadou, O.B.; Kechiched, R.; Benhamida,

A.S. Hydrogeological Study of the Aquifer System of the Northern Sahara in the Algero-Tunisian Border: A Case Study of Oued Souf Region. AIP Conf. Proc. 2018, 1968, doi:10.1063/1.5039197.

261. Tabouche, N. Achour, S. ETUDE DE LA QUALITE DES EAUX SOUTERRAINES DE LA REGION ORIENTALE DU SAHARA SEPTENTRIONAL ALGERIEN. Larhyss J. 2004, 99–113, doi:10.3406/tlgpa.2002.1000.

262. CHEBBAH, M.; ALLIA, Z. Geochemistry and Hydrogeochemical Process of Groundwater in the Souf Valley of Low Septentrional Sahara, Algeria. African J. Environ. Sci. Technol. 2015, 9, 261–273, doi:10.5897/ajest2014.1710.

263. Habes S; Djabri L; Bettahar A Qualite Des Eaux Dans Une Region a Climat Aride Cas : Des Nappes Du Complexe Terminal Et Continental Intercalaire. Sud-Est Algerien Water Quality in an Arid Weather Area, Case: Ground Water of Terminal Complex and Continental Intercalary. Algerian Southea. Larhyss J. 2016, 28, 55–63.

264. Saibi, H. Les Ressources En Eau de La Vallée Du Souf (Sahara Algérien); Éditions universitaires européennes, 2010; ISBN ISBN-10:6131505276 ;ISBN-13 :978-6131505270.

265. Saibi, H.; Semmar, A.; Mesbah, M.; Ehara, S. Variographic Analysis of Water Table Data from the Oued-Souf Phreatic Aquifer, Northeastern Part of the Algerian Sahara. Arab. J. Geosci. 2009, 2, 83–93, doi:10.1007/s12517-008-0021-1.

266. Slimani, R.; Guendouz, A.; Trolard, F.; Souffi Moulla, A.; Hamdi-Aïssa, B.; Bourrié, G. Identification of Dominant Hydrogeochemical Processes for Groundwaters in the Algerian Sahara Supported by Inverse Modeling of Chemical and Isotopic Data. Hydrol. Earth Syst. Sci. 2017, 21, 1669–1691, doi:10.5194/hess-21-1669-2017.

267. Guendouz, A.; Moulla, A.S.; Edmunds, W.M.; Zouari, K.; Shand, P.; Mamou, A. Hydrogeochemical and Isotopic Evolution of Water in the Complexe Terminal Aquifer in the Algerian Sahara. Hydrogeol. J. 2003, 11, 483–495, doi:10.1007/s10040-003-0263-7.

268. Moulla, A.S.; Guendouz, A. Étude Des Ressources En Eau Souterraines En Zones Arides (Sahara Algérien) Par Les Méthodes Isotopiques. Hydrol. Mediterr. Semiarid Reg. 2003, 35–42.

269. Khebizi, H.; Benlaoukli, B.; Bouaicha, F.; Adadzi, P.; Bouras, O. Salinization Origin of Souf Terminal Complex: Application of Statistical Modelling and WQI for Groundwater Management. Hydrol. Earth Syst. Sci. 2020, 1–16.

270. Zaiz, I.; Zine, B.; Boutoutaou, D.; Khechana, S. Contribution to the Study of

The. J. Fundam. Appl. Sci. 2017, 9, 1559–1568.

271. ZAIZ, I.; BOUTOUTAOU, D. Irrigation Water Impact on Soil Properties in Arid Oued-Souf Region, Southeast Algeria. Geosci. Eng. 2022, 68, 70–81, doi:10.35180/gse-2022-0070.

272. Mega, N.; Khechana, S. Groundwater Quality Assessment by Analytic Hierarchy Process (Geographic Information Systems-Based Model) in Souf Region (South-East of Algeria). Int. J. Environ. Sci. Technol. 2021, 18, 3459–3468, doi:10.1007/s13762-020-03080-6.

273. Bouchahm, N.; Achour, S. Hydrochimie Des Eaux Souterraines de La Région Orientale Du Sahara Septentrional Algérien – Identification d'un Risque de Fluorose Endémique. La houille blanche 2008, 76–82.

274. Mameri, N.; Yeddou, A.R.; Lounici, H.; Belhocine, D.; Grib, H.; Bariou, B. Defluoridation of Septentrional Sahara Water of North Africa By Electrocoagulation. Water Res. 1998, 32, 1604–1612.

275. Achour, S.; Youcef, L. Excès Des Fluorures Dans Les Eaux Du Sahara Septentrional Oriental et Possibilité de Traitement. EIN Int. 2001, 47–54.

276. Achour, S.; Youcef, L. Defluoruration Des Eaux Du Sahara Septentrional Algerien Par Adsorption Sur Des Bentonites Locales. Int. J. Environ. Stud. 2009, 66, 151–165, doi:10.1080/00207230902859747.

277. Ramdani Amina . Taleb Safia . Djellouli Hadja Mebarka Seasonal Changes Comparison Of Physico-Chemical And Bacteriological Characteristics Of Water In Some Regions Of Southern Algeria. Phytochem BioSub J. 2016, 10, 21–23.

278. Dubief, J. Le Climat Du Sahara. Ann. Georgr. 1965, 74, 360–361, doi:10.3406/geo.1935.10846.

279. Barkat, A.; Bouaicha, F.; Rahal, Z.; Mester, T.; Szabó, G. Evaluation of Climatic Conditions from 1978 to 2020 of Oued Souf Valley (Southern East of Algeria). Landsc. Environ. 2023, 17, 1–10, doi:10.21120/LE/17/1/1.

280. Remini, B.; Kechad, R. Impact of the Water Table Razing on the Degradation of El Oued Palm Plantation (Algeria) Mechanisms and Solutions. Geogr. Tech. 2011, 48–56.

281. Khechana, S.; Ghomri, A.; Miloudi, A.; Guedda, E.H.; Derradji, E. Échec Du Système de Drainage Vertical Installé Contre La Remontée Des Eaux Dans La Vallée d ' Oued-Souf : Causes et Solutions Proposées. 2016, 28–29.

282. Medareg Narou, B.H.; Farhi, A. Le Rôle Des Services et Des Investissements Dans l'hypertrophie de La Ville d'El Oued Au Bas Sahara Algérien. Environ. Urbain 2009, 3, c-1-c–18, doi:10.7202/044600ar.

283. Remini, B. LA DISPARITION DES GHOUTS DANS LA REGION Alg • Rie Biskra . Larhyss J. 2006, 5, 49–62.

284. Burri, J.; Burri, J. “Vallée Du Souf: Etudes d’assainissement Des Eaux Résiduaires, Pluviales et d’irrigation.” Mesures Complémentaires de Lutte Contre La Remontée de La Nappe Phréatique, Mission II; 2004.

285. Guendouz, A.; Michelot, J.L. Chlorine-36 Dating of Deep Groundwater from Northern Sahara. J. Hydrol. 2006, 328, 572–580, doi:10.1016/j.jhydrol.2006.01.002.

286. Dervierux, F. La Nappe Phréatique Du Souf (Région d’El Oued, Algérie)-Etude Du Renouvellement de La Nappe. Terres eaux OCRS 3trim 1957, 56, 12–39.

287. Ben Hamida, S. Iventaire Des Forages d’eau de La Wilaya d’El Oued; Ouargla, Algérie, 2005.

288. DRE Inventaire Des Puits Traditionnels de La Wilaya d’El-Oued; El Oued, 2015.

289. Kherici, N.; Zounini, D.; Kherici, H. Origine de La Remontee Des Eaux Dans La Nappe Superficielle de Souf (Nord-Est Du Sahara Septentrional Algerien). Hidrogeol. 1996, 12, 49–59.

290. Djennane, A. Constat de Situation Dans Des Zones Sud Des Oasis Algériennes. Dollé V. (ed.), Toutain G. (ed.). Les systèmes Agric. oasiens. Montpellier CIHEAM 1990, 11, 29–40.

291. UNESCO Etude Des Ressources En Eau de Sahara Septentrional; Paris, France, 1972; Vol. 7.

292. Sebaa, A.; Berroussi, S.; Bouhanna, M.; Benazzouz, M. UTILISATION DES METHODES TRADITIONNELLES DE LUTTE CONTRE L’ENSABLEMENT DANS LE BAS - SAHARA ALGERIEN: LE TAS DE REMBLAI. J. Algérien des Régions Arid. 2009, 8, 96–107.

293. Ballais, J.; Côte, M.; Bensaad, A. L’influence de La Géomorphologie Sur Le Comportement de La Nappe Phréatique Du Souf,PhD Diss; 2002.

294. Nesson, C. L’évolution Des Ressources Hydrauliques Dans Les Oasis Du Bas-Sahara Algérien. GéoProdig, portail d’information géographique 1975, 17, 7–99.

295. Giraud, R. Le Continental Terminal En Algérie; Ann. Fac. Sci.: Dakkar, 1978; Vol. 31.

296. Drouiche, A.; Chaab, S.; Khechana, S. Impact Du Deversement Direct Des Eaux Usees et de Drainage Dans La Nappe Libre de l’Oued Souf et Son Influence Sur La Qualite Des Eaux Souterraines. Synthèse Rev. des Sci. la

Technol. 2013, 27, 50–62.

297. DUTIL, P. Contribution à l'étude Des Sols et Paléosols Du Sahara, Strasbourg, 1971.

298. Briere, P.R. Playa, Playa Lake, Sabkha: Proposed Definitions for Old Terms. J. Arid Environ. 2000, 45, 1–7, doi:10.1006/jare.2000.0633.

299. Medjber Teguig, T. Etude de La Composition Floristique de La Région Du Souf (Sahara Septentrional Algérien). Alger. J. Arid Environ. 2014, 258, 1–14, doi:10.12816/0008911.

300. D'Information, D. des S.A. et des S. Statistique Agricole, Superficie et Production, Série "B", 2019; Alger, 2021.

301. Bensaâd, A. L'eau et Ses Enjeux Au Sahara; KARTHALA Editions: touggourt, 2011.

302. Miloudi, A.M.; Remini, B. The Ghout of Souf: An Original Hydroagricultural System. Geosci. Eng. 2019, 64, 30–37, doi:10.2478/gse-2018-0015.

303. REMINI; SOUACI, B.. Le Souf : Quand Le Forage Et Le Pivot Menacent Le Ghout ! Larhyss J. 2019, 37, 23–38.

304. Khouli, M.R.; Haouchine, A.; Banton, O. Deterioration of the Quality of Ground Water in Agricultural Region. Case Mitidja (Algeria). J. Fundam. Appl. Sci. 2021, 13, 172–184, doi:10.4314/jfas.v13i1.10.

305. Tsanakas, G.F.; Georgakopoulou-Voyiatzi, C.; Voyiatzis, D.G. Cultivating Greenhouse Cut Roses with Bending System. J. Appl. Hortic. 2017, 19, 175–179, doi:10.37855/jah.2017.v19i03.32.

306. Ouarekh, M.; Bouselsal, B.; Elksier, M.S.; Benaabidate, L. Water Quality Assessment and Hydrogeochemical Characterization of the Complex Terminal Aquifer in Souf Valley, Algeria. Arab. J. Geosci. 2021, 14, doi:10.1007/s12517-021-08498-x.

307. Abdallah, A.; Raoudha, D.; Zohra, K. The Impact of Using Natural Fertilizers on the Productivity and Sustainability of Potato Crops in the Region of Oued Souf in Algeria Econometric Study for the Period 2002-2018. Roa Iktissadia Rev. 2021, 11, 177–191.

308. ANIREF (Agence Nationale d'Intermédiation et de Régulation Foncière) Monographie Wilaya D'El Oued; El Oued-Algérie, 2020.

309. Rodier, J. L'analyse de l'eau, Eaux Naturelles, Eaux Résiduaires, Eau de Mer: Chimie, Physico-Chimie, Bactériologie, Biologie; 7ème.; Dunod: Paris, France, 1984.

310. Sajtos, Z.; Herman, P.; Harangi, S.; Baranyai, E. Elemental Analysis of Hungarian Honey Samples and Bee Products by MP-AES Method.

Microchem. J. 2019, 149, 103968, doi:10.1016/j.microc.2019.103968.

311. Mei, K.; Liao, L.; Zhu, Y.; Lu, P.; Wang, Z.; Dahlgren, R.A.; Zhang, M. Evaluation of Spatial-Temporal Variations and Trends in Surface Water Quality across a Rural-Suburban-Urban Interface. Environ. Sci. Pollut. Res. 2014, 21, 8036–8051, doi:10.1007/s11356-014-2716-z.

312. Parkhurst, D..; Apelo, C.A.. User's Guide to PHREEQC (Version 2)-A Computer Program for Speciation, Batch-Reaction, One-Dimensional Transport, and Inverse Geochemical Calculations.In Water Resources Investigations; Report 99-4259; Washington, DC, USA, 1999.

313. Drever, J.. The Geochemistry of Natural Waters; 2nd edn.; Prentice Hall: Englewood Cliffs, 1988.

314. Schoeller, H. La Classification Géochimique Des Eaux. IASH Publ. 1964, 46, 16–24.

315. Subba Rao, N.; Chaudhary, M. Hydrogeochemical Processes Regulating the Spatial Distribution of Groundwater Contamination, Using Pollution Index of Groundwater (PIG) and Hierarchical Cluster Analysis (HCA): A Case Study. Groundw. Sustain. Dev. 2019, 9, 100238, doi:10.1016/j.gsd.2019.100238.

316. Hakanson, L. An Ecological Risk Index for Aquatic Pollution Control.a Sedimentological Approach. Water Res. 1980, 14, 975–1001, doi:10.1016/0043-1354(80)90143-8.

317. Ukah, B.U.; Ameh, P.D.; Egbueri, J.C.; Unigwe, C.O.; Ubido, O.E. Impact of Effluent-Derived Heavy Metals on the Groundwater Quality in Ajao Industrial Area, Nigeria: An Assessment Using Entropy Water Quality Index (EWQI). Int. J. Energy Water Resour. 2020, 4, 231–244, doi:10.1007/s42108-020-00058-5.

318. Adimalla, N.; Wang, H. Distribution, Contamination, and Health Risk Assessment of Heavy Metals in Surface Soils from Northern Telangana, India. Arab. J. Geosci. 2018, 11, doi:10.1007/s12517-018-4028-y.

319. Sinex, S.A.; Helz, G.R. Regional Geochemistry of Trace Elements in Chesapeake Bay Sediments. Environ. Geol. 1981, 3, 315–323.

320. Bhutiani, R.; Kulkarni, D.B.; Khanna, D.R.; Gautam, A. Geochemical Distribution and Environmental Risk Assessment of Heavy Metals in Groundwater of an Industrial Area and Its Surroundings, Haridwar, India. Energy, Ecol. Environ. 2017, 2, 155–167, doi:10.1007/s40974-016-0019-6.

321. Hakima, Z.; Mohamed, M.; Aziza, M.; Mehdi, M.; Meryem, E.B.; Bendahhou, Z.; Jean-Francois, B. Environmental and Ecological Risk of Heavy Metals in the Marine Sediment from Dakhla Bay, Morocco. Environ. Sci. Pollut. Res. 2017, 24, 7970–7981, doi:10.1007/s11356-017-8367-0.

322. Zhang, J.; Liu, C.L. Riverine Composition and Estuarine Geochemistry of Particulate Metals in China - Weathering Features, Anthropogenic Impact and Chemical Fluxes. Estuar. Coast. Shelf Sci. 2002, 54, 1051–1070, doi:10.1006/ecss.2001.0879.

323. Fang, H.; Wang, X.; Xia, D.; Zhu, J.; Yu, W.; Su, Y.; Zeng, J.; Zhang, Y.; Lin, X.; Lei, Y.; et al. Improvement of Ecological Risk Considering Heavy Metal in Soil and Groundwater Surrounding Electroplating Factories. Processes 2022, 10, 1267, doi:10.3390/pr10071267.

324. Tomlinson, D.L.; Wilson, J.G.; Harris, C.R.; Jeffrey, D.W. Problems in the Assessment of Heavy-Metal Levels in Estuaries and the Formation of a Pollution Index. Helgoländer Meeresuntersuchungen 1980, 33, 566–575, doi:10.1007/BF02414780.

325. Lim, H.S.; Lee, J.S.; Chon, H.T.; Sager, M. Heavy Metal Contamination and Health Risk Assessment in the Vicinity of the Abandoned Songcheon Au-Ag Mine in Korea. J. Geochemical Explor. 2008, 96, 223–230, doi:10.1016/j.gexplo.2007.04.008.

326. Rezaei, H.; Zarei, A.; Kamarehie, B. Levels , Distributions and Health Risk Assessment of Lead , Cadmium and Arsenic Found in Drinking Groundwater of Dehgolan ' s Villages , Iran. Toxicol. Environ. Health Sci. 2019, 11, 54–62, doi:10.1007/s13530-019-0388-2.

327. Eyankware, M.O.; Akakuru, O.C. Appraisal of Groundwater to Risk Contamination near an Abandoned Limestone Quarry Pit in Nkalagu, Nigeria, Using Enrichment Factor and Statistical Approaches. Int. J. Energy Water Resour. 2022, doi:10.1007/s42108-022-00186-0.

328. Wu, B.; Zhang, Y.; Zhang, X.; Cheng, S. Health Risk from Exposure of Organic Pollutants through Drinking Water Consumption in Nanjing, China. Bull. Environ. Contam. Toxicol. 2010, 84, 46–50, doi:10.1007/s00128-009-9900-8.

329. USEPA (US Environmental Protection Agency) Risk Assessment Guidance for Superfund Volume 1. Human Health Evaluation Manual (Part E, Supplemental Guidance for Dermal Risk Assessment); EPA/540/R/99/005 Office of Superfund Remediation and Technology Innovation: Washington, DC, 2004.

330. USEPA (US Environmental Protection Agency) Guidelines for Carcinogenic Risk Assessment; Risk Assessment Forum: Washington, DC, 2006.

331. USEPA (US Environmental Protection Agency) Guidance for Performing Aggregate Exposure and Risk Assessments; Office of Pesticide Programs: Washington, DC, 1999.

332. Paustenbach, D.. Human and Ecological Risk Assessment: Theory and

Practice (Wiley Classics Library); John Wiley and Sons: New York, 2015; ISBN 0-471-14747-8.

333. Qiu, H.; Gui, H. Human and Ecological Risk Assessment : An International Heavy Metals Contamination in Shallow Groundwater of a Coal-Mining District and a Probabilistic Assessment of Its Human Health Risk. Hum. Ecol. Risk Assess. An Int. J. 2019, 0, 1–16, doi:10.1080/10807039.2018.1562883.

334. Murray, F.J. A Human Health Risk Assessment of Boron (Boric Acid and Borax) in Drinking Water. Regul. Toxicol. Pharmacol. 1995, 22, 221–230.

335. Ganiyu, S.A.; Oyadeyi, A.T.; Adeyemi, A.A. Assessment of Heavy Metals Contamination and Associated Risks in Shallow Groundwater Sources from Three Different Residential Areas within Ibadan Metropolis, Southwest Nigeria. Appl. Water Sci. 2021, 11, 1–20, doi:10.1007/s13201-021-01414-4.

336. Giri, S.; Singh, A.K. Human Health Risk Assessment via Drinking Water Pathway Due to Metal Contamination in the Groundwater of Subarnarekha River Basin, India. Environ. Monit. Assess. 2015, 187, doi:10.1007/s10661-015-4265-4.

337. Nematollahi, M.J.; Dehdaran, S.; Moore, F.; Keshavarzi, B. Potentially Toxic Elements and Polycyclic Aromatic Hydrocarbons in Street Dust of Yazd, a Central Capital City in Iran: Contamination Level, Source Identification, and Ecological–Health Risk Assessment; Springer Netherlands, 2021; Vol. 43; ISBN 0123456789.

338. Mehrjardi, R.T.; Jahromi, M.Z.; Heidari, A. Spatial Distribution of Groundwater Quality with Geostatistics (Case Study : Yazd-Ardakan Plain). Appl. Sci. 2008, 4, 09–17.

339. Cambardella, C.A.; Moorman, T.B.; Novak, J.M.; Parkin, T.B.; Karlen, D.L.; Turco, R.F.; Konopka, A.E. Field-Scale Variability of Soil Properties in Central Iowa Soils. Soil Sci. Soc. Am. J. 1994, 58, 1501–1511, doi:10.2136/sssaj1994.03615995005800050033x.

340. Khechana, S.; Miloudi, A.; Ghomri, A.; Guedda, E.H.; Derradji, E.F. Failure of a Vertical Drainage System Installed to Fight the Rise of Groundwater in El-Oued Valley (SE Algeria): Causes and Proposed Solutions. J. Fail. Anal. Prev. 2016, 16, 216–224, doi:10.1007/s11668-016-0071-8.

341. Yilmaz, E., Koc, C. Physically and Chemically Evaluation for the Water Quality Criteria in a Farm on Akcay. J. Water Resour. Prot. 2014, 6, 63–67.

342. Azhdarpoor, A.; Radfard, M.; Pakdel, M.; Abbasnia, A.; Badeenezhad, A.; Mohammadi, A.A.; Yousefi, M. Assessing Fluoride and Nitrate Contaminants in Drinking Water Resources and Their Health Risk Assessment in a Semiarid Region of Southwest Iran. Desalin. Water Treat. 2019, 149, 43–51, doi:10.5004/dwt.2019.23865.

343. Handa, B.. Description and Classification of Media for Hydro-Geochemical Investigations. In Symposium on Ground Water Studies in Arid and Semiarid Regions. Roorkee 1969, 20, 319.

344. Azis, A.; Yusuf, H.; Faisal, Z.; Suradi, M. Water Turbidity Impact on Discharge Decrease of Groundwater Recharge in Recharge Reservoir. Procedia Eng. 2015, 125, 199–206, doi:10.1016/j.proeng.2015.11.029.

345. Mounjid, J.; Cohen, N.; Fadlaoui, S.; Oubraim, S. Study of Physicochemical and Microbiological Quality of Oued Bouskoura : Peri-Urbain of Casablanca , Morocco. Int. Res. J. Environ. Sci 2014, 3, 60–66.

346. Gandhi, R.K.; Raina, A.K.; Sharma, N. Ion Chromatography of Major Anions in the Neeru Stream, Bhaderwah, J&K, India. Environ. Conserv. J. 2018, 19, 17–30, doi:10.36953/ecj.2018.19302.

347. Widyastuti, M.; Haryono, E. Water Quality Characteristics of Jonge Telaga (Doline Pond) as Water Resources for the People of Semanu District Gunungkidul Regency. Indones. J. Geogr. 2016, 48, 157–167, doi:10.22146/ijg.17595.

348. Bisimwa, A.M.; Kisuya, B.; Kazadi, Z.M.; Muhaya, B.B.; Kankonda, A.B. Monitoring Faecal Contamination and Relationship of Physicochemical Variables with Faecal Indicator Bacteria Numbers in Bukavu Surface Waters, Tributaries of Lake Kivu in Democratic Republic of Congo. Hyg. Environ. Heal. Adv. 2022, 3, 100012, doi:10.1016/j.heha.2022.100012.

349. Hannan, A.; Anmala, J. Classification and Prediction of Fecal Coliform in Stream. Water (Switzerland) 2021, 13, 2790.

350. Singh, A.K.; Das, S.; Singh, S.; Pradhan, N.; Gajamer, V.R.; Kumar, S.; Lepcha, Y.D.; Tiwari, H.K. Physicochemical Parameters and Alarming Coliform Count of the Potable Water of Eastern Himalayan State Sikkim: An Indication of Severe Fecal Contamination and Immediate Health Risk. Front. Cell Dev. Biol. 2019, 7, 174, doi:10.3389/fpubh.2019.00174.

351. Bekkoussa, B.; Jourde, H.; Batiot-Guilhe, C.; Meddi, M.; Khaldi, A.; Azzaz, H. Origine de La Salinité et Des Principaux Éléments Majeurs Des Eaux de La Nappe Phréatique de La Plaine de Ghriss, Nord-Ouest Algérien. Hydrol. Sci. J. 2013, 58, 1111–1127, doi:10.1080/02626667.2013.800639.

352. Kraiem, Z.; Zouari, K.; Bencheikh, N.; Agoun, A.; Abidi, B. Processus de Minéralisation de La Nappe Du Plio-Quaternaire Dans La Plaine de Segui-Zograta (Sud-Ouest Tunisien). Hydrol. Sci. J. 2014, 60, 534–548, doi:10.1080/02626667.2013.877587.

353. Appelo, C.A..; Postma, D. Geochemistry, Groundwater and Pollution; Balkema: Rotterdam, 1993.

354. Rusydi, A.F. Correlation between Conductivity and Total Dissolved Solid in

Various Type of Water: A Review. IOP Conf. Ser. Earth Environ. Sci. 2018, 118, 012019, doi:10.1088/1755-1315/118/1/012019.

355. Ahmedat, C.; Dabi, S.; Zahraoui, M.; El Hassani, I.E.E.A. Spatial Distribution of Stream Sediment Pollution by Toxic Trace Elements at Tourtit and Ichoumellal Abandoned Mining Areas (Central Morocco). Arab. J. Geosci. 2018, 11, doi:10.1007/s12517-018-3390-0.

356. Batayneh, A.T. Toxic (Aluminum, Beryllium, Boron, Chromium and Zinc) in Groundwater: Health Risk Assessment. Int. J. Environ. Sci. Technol. 2012, 9, 153–162, doi:10.1007/s13762-011-0009-3.

357. Mgbenu, C.N.; Egbueri, J.C. The Hydrogeochemical Signatures, Quality Indices and Health Risk Assessment of Water Resources in Umunya District, Southeast Nigeria. Appl. Water Sci. 2019, 9, 1–19, doi:10.1007/s13201-019-0900-5.

358. Khan, M.M.A.; Umar, R.; Lateh, H. Study of Trace Elements in Groundwater of Western Uttar Pradesh, India. Sci. Res. Essays 2010, 5, 3175–3182.

359. Mondal, N.C.; Singh, V.S.; Puranik, S.C.; Singh, V.P. Trace Element Concentration in Groundwater of Pesarlanka Island, Krishna Delta, India. Environ. Monit. Assess. 2010, 163, 215–227, doi:10.1007/s10661-009-0828-6.

360. Xia, X.; Teng, Y.; Zhai, Y. Biogeochemistry of Iron Enrichment in Groundwater : An Indicator of Environmental Pollution and Its Management. Sustain. 2022, 14, 1–14.

361. White, A.F.; Benson, S.M.; Yee, A.W.; Wollenberg Jr, H.A.; Flexser, S. Groundwater Contamination at the Kesterson Reservoir, California 2. Geochemical Parameters Influencing Selenium Mobility. WATER Resour. Res. 1991, 27, 1085–1098.

362. Miller, R.W.; Donahue, R.L. Soils in Our Environment. Prentice hall 1995.

363. World Health Organization Guidelines for Drinking-Water Quality: Volume 1: Recommendations.; World Health Organization., Ed.; Switzerland: Geneva, 1984.

364. USEPA (US Environmental Protection Agency) Guidelines for Carcinogen Risk Assessment.; Risk Assessment Forum: Washington, DC, 2005.

365. Zhou, M.; Wu, Q.; Wu, H.; Liu, J.; Ning, Y.; Xie, S.; Huang, W.; Bi, X. Enrichment of Trace Elements in Red Swamp Crayfish: Influences of Region and Production Method, and Human Health Risk Assessment. Aquaculture 2021, 535, 736366, doi:10.1016/j.aquaculture.2021.736366.

366. Jiang, Z.; Xu, N.; Liu, B.; Zhou, L.; Wang, J.; Wang, C.; Dai, B.; Xiong, W. Metal Concentrations and Risk Assessment in Water, Sediment and Economic

Fish Species with Various Habitat Preferences and Trophic Guilds from Lake Caizi, Southeast China. Ecotoxicol. Environ. Saf. 2018, 157, 1–8, doi:10.1016/j.ecoenv.2018.03.078.

367. Nouri, J.; Mahvi, A.H.; Jahed, G.R.; Babaei, A.A. Regional Distribution Pattern of Groundwater Heavy Metals Resulting from Agricultural Activities. Environ. Geol. 2008, 55, 1337–1343, doi:10.1007/s00254-007-1081-3.

368. Rattan, R.K.; Datta, S.P.; Chhonkar, P.K.; Suribabu, K.; Singh, A.K. Long-Term Impact of Irrigation with Sewage Effluents on Heavy Metal Content in Soils, Crops and Groundwater - A Case Study. Agric. Ecosyst. Environ. 2005, 109, 310–322, doi:10.1016/j.agee.2005.02.025.

369. Goel PK Water Pollution Causes Effect and Control; New Age International Publishers, 2006.

370. Government of Canada Water Talk - Strontium in Drinking Water Available online:https://www.canada.ca/en/health-canada/services/publications/healthy-living/water-talk-strontium.html.

371. Négrel, P.; Petelet-Giraud, E.; Widory, D. Strontium Isotope Geochemistry of Alluvial Groundwater: A Tracer for Groundwater Resources Characterisation. Hydrol. Earth Syst. Sci. 2004, 8, 959–972, doi:10.5194/hess-8-959-2004.

372. Frankowski, M.; Zioła-Frankowska, A.; Siepak, J. Speciation of Aluminium Fluoride Complexes and Al3+ in Soils from the Vicinity of an Aluminium Smelter Plant by Hyphenated High Performance Ion Chromatography Flame Atomic Absorption Spectrometry Technique. Microchem. J. 2010, 95, 366–372, doi:10.1016/j.microc.2010.02.019.

373. Frankowski, M. Simultaneous Determination of Aluminium, Aluminium Fluoride Complexes and Iron in Groundwater Samples by New HPLC-UVVIS Method. Microchem. J. 2012, 101, 80–86, doi:10.1016/j.microc.2011.11.002.

374. Fernández-Luqueño, F.; López-Valdez, F.; Gamero-Melo, P.; Luna-Suárez, S.; Aguilera-González, E.; Martínez, A.; García-Guillermo, M.; Hernández-Martínez, G.; Herrera-Mendoza, R.; Álvarez-Garza, M.; et al. Heavy Metal Pollution in Drinking Water - a Global Risk for Human Health: A Review. African J. Environ. Sci. Technol. 2013, 7, 567–584, doi:10.5897/AJEST12.197.

375. Shakerkhatibi, M.; Mosaferi, M.; Pourakbar, M.; Ahmadnejad, M.; Safavi, N.; Banitorab, F. Comprehensive Investigation of Groundwater Quality in the North-West of Iran: Physicochemical and Heavy Metal Analysis. Groundw. Sustain. Dev. 2019, 8, 156–168, doi:10.1016/j.gsd.2018.10.006.

376. Devic, G.; Djordjevic, D.; Sakan, S. Natural and Anthropogenic Factors Affecting the Groundwater Quality in Serbia. Sci. Total Environ. 2014, 468–

469, 933–942, doi:10.1016/j.scitotenv.2013.09.011.

377. L.W. Diamond, R.E.S. Sources of Manganese in the Environment. Environ. Geochem. Health 1989, 11, 17–27, doi:10.1007/BF01734020.

378. Kumar, A.; Cabral-Pinto, M.; Kumar, A.; Kumar, M.; Dinis, P.A. Estimation of Risk to the Eco-Environment and Human Health of Using Heavy Metals in the Uttarakhand Himalaya, India. Appl. Sci. 2020, 10, 1–18, doi:10.3390/app10207078.

379. Butterworth, R.F. Metal Toxicity, Liver Disease and Neurodegeneration. Neurotox. Res. 2010, 18, 100–105, doi:10.1007/s12640-010-9185-z.

380. Struzyńska, L. A Glutamatergic Component of Lead Toxicity in Adult Brain: The Role of Astrocytic Glutamate Transporters. Neurochem. Int. 2009, 55, 151–156, doi:10.1016/j.neuint.2009.01.025.

381. Salonen, J.T.; Nyyssönen, K.; Korpela, H.; Tuomilehto, J.; Seppänen, R.; Salonen, R. High Stored Iron Levels Are Associated with Excess Risk of Myocardial Infarction in Eastern Finnish Men. Circulation. 1992, 86, 803–811, doi:10.1161/01.CIR.86.3.803.

382. Tuomainen, T.P.; Punnonen, K.; Nyyssönen, K.; Salonen, J.T. Association between Body Iron Stores and the Risk of Acute Myocardial Infarction in Men. Circulation 1998, 97, 1461–1466, doi:10.1161/01.CIR.97.15.1461.

383. Salonen, J.T.; Tuomainen, T.P.; Nyyssönen, K.; Lakka, H.M.; Punnonen, K. Relation between Iron Stores and Non-Insulin Dependent Diabetes in Men: Case-Control Study. Br. Med. J. 1998, 317, 727, doi:10.1136/bmj.317.7160.727.

384. Tuomainen, T.; Nyyssônen, K.; Salonen, R.; Tervahauta, A.; Korpela, H.; Lakka, T.; Kaplan, G.; Salonen, J. Body Iron Stores Are Associated with Serum Insulin and Blood Glucose Concentrations. Diabetes Care20 1997, 20, 426–428.

385. Rahman, M.F.; Ali, M.A.; Chowdhury, A.I.A.; Ravenscroft, P. Manganese in Groundwater in South Asia Needs Attention. ACS ES T Water 2022, doi:10.1021/acsestwater.2c00442.

386. Li, L.; Wang, Y.; Gu, H.; Lu, L.; Li, L.; Pang, J.; Chen, F. The Genesis Mechanism and Health Risk Assessment of High Boron Water in the Zhaxikang Geothermal Area, South Tibet. Water (Switzerland) 2022, 14, 3243, doi:10.3390/w14203243.

387. McGregor, D.B.; Baan, R.A.; Partensky, C.; Rice, J.M.; Wilbourn, J.D. Evaluation of the Carcinogenic Risks to Humans Associated with Surgical Implants and Other Foreign Bodies - A Report of an IARC Monographs Programme Meeting. Eur. J. Cancer 2000, 36, 307–313, doi:10.1016/S0959-8049(99)00312-3.

388. Seilkop, S.K.; Oller, A.R. Respiratory Cancer Risks Associated with Low-Level Nickel Exposure: An Integrated Assessment Based on Animal, Epidemiological, and Mechanistic Data. Regul. Toxicol. Pharmacol. 2003, 37, 173–190, doi:10.1016/S0273-2300(02)00029-6.

389. Ren, Y.S.; Ilyas, M.; Xu, R.Z.; Ahmad, W.; Wang, R. Concentrations of Lead in Groundwater and Human Blood in the Population of Palosai, a Rural Area in Pakistan: Human Exposure and Risk Assessment. Adsorpt. Sci. Technol. 2022, 2022, doi:10.1155/2022/8341279.

390. Khandare, A.L.; Validandi, V.; Rajendran, A.; Singh, T.G.; Thingnganing, L.; Kurella, S.; Nagaraju, R.; Dheeravath, S.; Vaddi, N.; Kommu, S.; et al. Health Risk Assessment of Heavy Metals and Strontium in Groundwater Used for Drinking and Cooking in 58 Villages of Prakasam District, Andhra Pradesh, India. Environ. Geochem. Health 2020, 42, 3675–3701, doi:10.1007/s10653-020-00596-1.

391. Hart, K.A.; Kennedy, G.W.; Sterling, S.M. Groundwater in Nova Scotia , Canada. 2021, 13, 1578.

392. Cloutier, V.; Lefebvre, R.; Therrien, R.; Savard, M.M. Multivariate Statistical Analysis of Geochemical Data as Indicative of the Hydrogeochemical Evolution of Groundwater in a Sedimentary Rock Aquifer System. J. Hydrol. 2008, 353, 294–313, doi:10.1016/j.jhydrol.2008.02.015.

393. Chabour, N.; Dib, H.; Bouaicha, F.; Bechkit, M.A.; Messaoud Nacer, N. A Conceptual Framework of Groundwater Flowpath and Recharge in Ziban Aquifer: South of Algeria. Sustain. Water Resour. Manag. 2021, 7, 1–15, doi:10.1007/s40899-020-00483-8.

394. Meybeck, M. Global Chemical Weathering of Surficial Rocks Estimated from River Dissolved Loads. Am. J. Sci. 1987, 287, 401–428, doi:10.2475/ajs.287.5.401.

395. Mayo, A.L.; Loucks, M.D. Solute and Isotopic Geochemistry and Ground Water Flow in the Central Wasatch Range, Utah. J. Hydrol. 1995, 172, 31–59, doi:10.1016/0022-1694(95)02748-E.

396. Cerling, T.E.; Pederson, B.L.; Von Damm, K.L. Sodium-Calcium Ion Exchange in the Weathering of Shales: Implications for Global Weathering Budgets. Geology 1989, 17, 552–554, doi:10.1130/0091-7613(1989)017<0552:SCIEIT>2.3.CO;2.

397. Fisher, R.S.; Mullican, W.F. Hydrochemical Evolution of Sodium-Sulfate and Sodium-Chloride Groundwater beneath the Northern Chihuahuan Desert, Trans-Pecos, Texas, USA. Hydrogeol. J. 1997, 5, 4–16, doi:10.1007/s100400050102.

398. Gaillardet, J.; Dupre, B.; Louvat, P.; Allegre, C.J. Global Silicate Weathering

and CO2 Consumption Rates Deduced from the Chemistry of Large Rivers. Chem. Geol. 1999, 159, 3–30.

399. Stuyfzand, P.J. Base Exchange Indices as Indicators of Salinization or Freshening of (Coastal) Aquifers. In Proceedings of the 20th Salt Water Intrusion Meeting, Naples, Florida, USA; IFAS Research Gainesville: Naples, Florida, USA, 2008; pp. 262–265.

400. Miloudi, A. monem; Remini, B. Water Potentiality of Sustainable Management Challenges in the Oued Souf Region, South East Algeria. Int. J. Energ. 2016, 1, 36, doi:10.47238/ijeca.v1i1.7.